DISS. ETH NO. 22126

The Role of Mismatch Repair, Base Excision Repair and PARP-1 in the Processing of Oxidative DNA Damage

A thesis submitted to attain the degree of

DOCTOR OF SCIENCES of ETH ZURICH

(Dr. sc. ETH Zurich)

presented by

SIMONE REPMANN

M.Sc. Molecular Biotechnology, Technical University of Munich

born on *29.12.1984*

citizen of

Germany

accepted on the recommendation of

Prof. Josef Jiricny

Prof. Ruedi Aebersold

Dr. Margherita Bignami

2014

Author: Simone Repmann
Institute of Molecular Cancer Research
Department of Biology
ETH-Zurich, Switzerland
srepmann@imcr.uzh.ch

Supervisor Prof. Dr. Josef Jiricny
Institute of Molecular Cancer Research
Department of Biology
ETH-Zurich, Switzerland
jiricny@imcr.uzh.ch

Committee member Prof. Dr. Ruedi Aebersold
Institute of Molecular Systems Biology
Department of Biology
ETH Zurich, Switzerland
aebersold@imsb.biol.ethz.ch

Committee member Dr. Margherita Bignami
Section of Experimental Carcinogenesis
Instituto Superiore di Sanità
Rome, Italy
margherita.bignami@iss.it

Summary

Our DNA is constantly exposed to spontaneous oxidative stress, which results from metabolic byproducts and which represents a key threat to genomic stability. Oxidation of DNA results in accumulation of the mutagenic 8-hydroxy-2'-deoxyguanosine (G^O), which is mainly removed by the base excision repair (BER) pathway. G/C base pairs are oxidized to G^O/Cs, which are recognized by oxoguanine DNA glycosylase (OGG1) and corrected to G/Cs, with the assistance of the downstream BER machinery. During replication, G^O can mispair with adenine. G^O/A mispairs are addressed by MYH-initiated BER that removes the As and replaces them with Cs to generate G^O/Cs, which are substrates for OGG1-dependent BER. Dysfunction of MYH leads to G:C to T:A transversions and is linked to MYH-associated polyposis (MAP).

During the past decade, repair of oxidative DNA lesions such as G^O was shown to involve also the postreplicative mismatch repair system (MMR), but its role within this process remained obscure. G^O/A mispairs were known to be poor substrates for MMR, but we show here that, in an *in vitro* MMR assay based on circular lesion-containing plasmids and human cell extracts, the intermediates of G^O/A - but not G^O/C - processing by BER can serve as strand discrimination signals for MMR. These observations were not restricted to human cell extracts, but were observed also in extracts of *Xenopus laevis* eggs. During S-phase, G^O would be present predominantly in the parental DNA strand. Thus, "hijacking" of strand breaks arising during MYH-dependent G^O/A processing by BER would help direct the mismatch repair process correctly to the daughter strand. In contrast, OGG1-generated nicks at G^O/C sites would direct MMR erroneously to the parental strand. Our data thus show that BER-mediated processing of oxidative DNA damage is coordinated to help MMR improve replication fidelity.

In a complementary study, we set out to study the interactome of the mismatch recognition factor MutSα during oxidative DNA damage response. We had hoped that identification of interaction partners of these MMR proteins might help us understand the details of the interplay of the different pathways of DNA metabolism and DNA damage signaling in cells subjected to oxidative stress. I generated a novel set of expression vectors and cell lines that could be used for future mass spectrometric analysis of the interacting partners of MutSα. I also confirmed that MMR deficiency leads to a decreased cell survival and a prolonged G_2/M arrest during oxidative stress.

Poly(ADP-ribose) polymerase 1(PARP-1) is an enzyme that is extremely rapidly activated by single-strand breaks (SSBs), to which it binds with high affinity. This 'nick protector' enzyme has been assigned a role in BER that is currently ill-defined, however, it has recently acquired substantial clinical importance, because its inhibition effectively kills BRCA1/-2 deficient breast and ovarian cancer cells.

PARP inhibition is generally believed to give rise to toxic SSB/PARP-1 complexes that can only be repaired in the presence of BRCA1/-2, but the underlying causes of those SSBs are undefined yet. We wanted to learn whether these breaks might stem from the processing of spontaneous oxidative damage. Using cell survival assays with human BRCA1-deficient cell lines, we show that MYH knockdown attenuates the toxic effect of PARP inhibitors. These findings show that DNA oxidation is a source of lesions that contribute to the toxicity of PARP inhibition in BRCA-deficient cells and suggest that augmentation of oxidative damage processing might increase the efficacy of PARP inhibitors in the clinic.

Zusammenfassung

Die menschliche DNS ist fortwährend spontanem oxidativen Schaden ausgesetzt, der als Nebenprodukt des Stoffwechsels entsteht und somit eine große Gefahr für die genomische Stabilität darstellt. DNS Oxidation führt zur Anreicherung von mutagenem 8-hydroxy-2'-deoxyguanosin (G^O), das hauptsächlich durch Basen-Exzisionsreparatur (BER) repariert wird. G/C Basenpaare können zu G^O/C oxidiert werden. Diese werden von der DNS Glykosylase OGG1 erkannt und mit Hilfe der nachgeschalteten BER Enzyme zu G/C korrigiert. Während der Replikation kann G^O jedoch auch Fehlpaarungen mit Adenin (A) eingehen. Hierbei entstehende G^O/As werden von der DNS Glykosylase MYH adressiert und nachfolgend durch BER repariert. Dabei wird das A entfernt, durch C ersetzt und somit ein G^O/C Basenpaar generiert, welches erneut ein Substrat für OGG1-abhängige BER darstellt. Fehlfunktionen von MYH resultieren in G:C zu T:A Transversionen und stehen im Zusammenhang mit der Entstehung von MYH-assoziierter Polyposis (MAP).

In den letzten Jahren wurde gezeigt, dass auch postreplikative Fehlpaarungsreparatur (mismatch repair = MMR) in die Reparatur von oxidativen DNA Läsionen, wie z.B. G^O, involviert ist. Seine Rolle in diesem Prozess ist jedoch weitestgehend ungeklärt. Es ist bekannt, dass G^O/A Fehlpaarungen schlechte Substrate für MMR darstellen. Allerdings zeigen wir hier, dass Zwischenprodukte der G^O/A Prozessierung durch BER, nicht aber Zwischenprodukte der G^O/C Prozessierung, als Strangdiskriminierungssignal für MMR dienen können. Dies zeigten wir in humanen Zellextrakten anhand von zirkulären Plasmiden, die entsprechende Läsionen trugen. Wir machten diese Beobachtungen nicht nur in humanen Zellextrakten, sondern auch in Extrakten aus *Xenopus laevis* Eiern. Während der S-Phase liegt G^O vorwiegend im parentalen DNS-Strang vor. Daher würde MMR, das seinen Reparaturvorgang an Strangbrüchen (= 'nicks') initiiert, die während MYH-abhängiger G^O/A-Prozessierung durch BER auftreten, korrekterweise zum Tochterstrang dirigiert werden. Im Gegensatz dazu würden OGG1-generierte 'nicks' an G^O/C Stellen MMR fälschlicherweise zum parentalen Strang dirigieren. Unsere Daten zeigen somit, dass die Prozessierung von oxidativem DNS Schaden durch BER so koordiniert ist, dass sie gleichzeitig zu einer Erhöhung der Replikationsgenauigkeit durch MMR führt.

In einer ergänzenden Studie sollte das Interaktom des Fehlpaarungserkennungsfaktors MutSα während oxidativer DNS Schadensantwort bestimmt werden. Die Identifizierung von neuen Interaktionspartnern der MMR Proteine könnte genaueren Aufschluss darüber geben, wie das Zusammenspiel der verschiedenen Signalwege des DNS Metabolismus und der DNS Schadenssignalisierung in Zellen, die oxidativem Stress ausgesetzt sind, abläuft.

Hierzu generierten wir ein neuartiges Set an Expressionsvektoren und Zelllinien, die für zukünftige massenspektrometrische Analysen von MutSα Interaktionspartnern verwendet werden könnten. Weiterhin konnten wir bestätigen, dass MMR-Defizienz zu verringertem Zellüberleben sowie verlängertem G_2/M-Arrest führt.

Poly(ADP-ribose) Polymerase 1 (PARP-1) ist ein Enzym, das extrem schnell durch DNS Einzelstrangbrüche aktiviert wird und mit hoher Affinität an diese bindet. Dieses 'nick-Protektor' Enzym scheint eine bisher noch nicht abschließend geklärte Rolle während BER zu spielen. Dennoch erlangte PARP-1 kürzlich erhebliche klinische Bedeutung, denn seine Inhibierung führt zur erfolgreichen Abtötung von BRCA1/-2 defizienten Brust- und Ovarialkrebszellen. Generell nimmt man an, dass die Inhibierung von PARP-1 zu toxischen Einzelstrangbruch/PARP-1 Komplexen führt, die nur in der Anwesenheit von BRCA1/-2 repariert werden können. Allerdings sind die zugrundeliegenden Verursacher der Einzelstrangbrüche bisher undefiniert. Wir wollten daher herausfinden, ob die Brüche durch die Prozessierung spontaner oxidativer DNS Schäden entstehen könnten. Dazu führten wir Sensitivitätsstudien mit humanen BRCA1-defizienten Zelllinien durch und zeigten, dass MYH knockdown die toxische Wirkung von PARP-1 Inhibitoren verringerte. Die DNS Oxidation stellt somit eine Quelle für Schäden dar, die zur Toxizität von PARP Inhibitoren in BRCA-defizienten Zellen beitragen. In Bezug auf die klinische Anwendung zeigt dieses Ergebnis, dass eine Steigerung von oxidativer DNS Schadensprozessierung den Effekt von PARP Inhibitoren erhöhen könnte.

Acknowledgments

First and foremost, I would like to thank Prof. Josef Jiricny for giving me the opportunity to do my PhD in such a great lab at the IMCR. I am extremely grateful to his continued support, constructive suggestions and valuable discussions throughout the last years. Thanks to those and the projects he let me work on, I gained deep insights into the field of cancer research and DNA repair. Thanks for always having your door and ears open for your PhD students, organizing movie nights and BBQs for us and in general for being such great boss.

I would like to thank my PhD thesis committee members Dr. Margherita Bignami, Prof. Ruedi Aebersold and Prof. Michael Hottiger for their supportive guidance throughout my PhD. A special thanks to Dr. Margherita Bignami for regularly travelling a long way to visit my committee meetings in Zurich, as well as for her additional valuable inputs during conferences.

A heartfelt thanks to all my labmates for the good times we spent inside and outside the lab. A special thanks to Steffi and Javi for all the fruitful scientific discussions, to Mariela and Anja for their help in the lab whenever needed, and to Svenja, Steffi, Lia, Tine, Julia, Mariela and Martin for all the joyful lunch and coffee breaks.

Thanks to all people of the IMCR who make it such a pleasurable working place, especially to Farah Hamedi-Baccouche, Odete Pereira Alves and Peter Binz for their vital work in the background that makes life at the IMCR much easier.

Many thanks to my former Master student Isabel Wassing and for her tireless commitment and help to establish an *in vivo* MMR assay. I couldn't imagine a more motivated and refreshing student.

I would also like to thank Mark O'Connor for his constructive advice and discussions in the PARP-1 project.

Furthermore, I would like to acknowledge the Cancer Biology PhD program for support and giving us the possibility to organize our own and unforgettable social events such as student retreats, BBQs and 'Stammtische'.

Very special thanks to my family: to my parents who continuously support me in every phase of my life and who made the realization of my studies and this thesis possible; to my great brother and his lovely family who are always there for me; and to Mischa for his precious love that reaches to the moon and back.

Table of contents **page**

List of figures

List of tables page

Acronyms

A^O:	2-hydroxyadenine
AP-site:	apurinic site
BER:	base excision repair
CRC:	colorectal cancer
Dox:	doxycycline
ds:	double-stranded
DSB:	double-strand break
FAP:	familial adenomatous polyposis
G^O:	8-oxoG = 8-oxoguanine
HNPCC:	hereditary non-polyposis colorectal cancer
HR:	homologous recombination
ICL:	interstrand crosslink repair
LP-BER:	long-patch base excision repair
MAP:	MYH-associated polyposis
MEF:	mouse embryonic fibroblasts
MMR:	mismatch repair
MSI:	microsatellite instability
MTX:	methotrexate
NER:	nucleotide excision repair
NHEJ:	non-homologous end joining
PAR:	poly(ADP-ribose)
PARP:	poly(ADP-ribose) polymerase
PARPi:	PARP inhibitor/inhibition
ROS:	reactive oxygen species
SL:	synthetic lethality
SP-BER:	short-patch base excision repair
SSB:	single-strand break
ss:	single-stranded

1 Introduction

1.1 DNA damage & repair

The meaning of faithful replication

DNA is the carrier of our genetic information and encodes all proteins that are necessary for the metabolism and function of the cells. When Watson and Crick uncovered the molecular structure of DNA in 1953, its potential for replication and encoding information became evident for the first time. Nevertheless, their statement: "It has not escaped our notice that the specific pairing we have postulated immediately suggests a possible copying mechanism for the genetic material" [1], was a big understatement. Since DNA is continuously exposed to numerous DNA damaging agents, its faithful replication depends on multiple other factors too, like accurate polymerase activities and various DNA repair mechanisms. The absence of those factors can lead to gene mutations. Although mutations are indispensable for evolution, they become dangerous when affecting genes that are critical for the control of cell growth. In prokaryotes, the loss of essential genes leads to cell death, but this is not necessarily the case in higher eukaryotes. Here, cells can transform into a malignant cell population and lead to cancer.

Exogenous and endogenous sources of DNA damage

Although DNA is highly stable, it is a complex organic molecule that is susceptible to modifications by both exogenous and endogenous sources. The former derive from the environment, such as ultraviolet (UV) light, ionizing radiation (IR), chemicals or tobacco smoke [2, 3], whereas the three major forms of endogenous DNA damage are i) spontaneous depurination, ii) deamination and iii) reactive metabolites. Depurination occurs about 5000 times per cell per day and results in the loss of adenine or guanine by spontaneous hydrolysis of their N-glycosyl linkage to deoxyribose, resulting in abasic sites [4]. The most common spontaneous deamination, which occurs about 100 times per cell per day, converts cytosines to uracils, leading to U/G mispairs [4, 5]. Reactive metabolites occur in the form of reactive nitrogen (RNS) or oxygen species (ROS). The latter represent the greatest threat to genomic integrity; as many as 10'000 oxidations were estimated to take place per cell per day [6, 7].

DNA repair pathways

To overcome the deleterious effects of DNA lesions, nature evolved a large set of DNA repair mechanisms with broad and partially-overlapping substrate specificities [2]. They present three major groups i) direct DNA damage reversal, ii) DNA single-strand repair, including base excision repair (BER), mismatch repair (MMR) and nucleotide excision repair (NER), and iii) DNA double-strand repair, namely homologous recombination (HR), non-homologous end-joining (NHEJ) and interstrand crosslink (ICL) repair.

Overview of the following chapters

The different repair pathways will be the subject of the next chapters, followed by an introduction about the cellular sources of ROS and their effects on DNA.

Subsequently, I will provide a detailed overview of how BER and MMR are involved in the metabolism of oxidative DNA damage repair. This will be followed by a summary of the current knowledge about the protein PARP-1, with special regard to its involvement during BER.

1.2 Direct DNA damage reversal

Direct DNA damage reversal

The simplest and fastest way to deal with highly mutagenic and cytotoxic lesions is by direct chemical reversal of the DNA damage. This single-enzyme mechanism is essentially error-free, but targets only a limited substrate range. In contrast to most other repair mechanisms, it does not involve any incisions of the DNA sugar-phosphate backbone. There are essentially three main types of direct DNA damage reversal systems: the removal of alkylation damage by i) alkyltransferases or ii) dioxygenases as well as the ii) elimination of UV-light-generated lesions by photolyases [8].

Alkyltransferases

Alkylation damage derives from drugs like N-methyl-N'-nitro-N-nitroso-guanidine (MNNG), but may also arise from endogenous sources like the metabolite S-adenosylmethionine (SAM). Alkyltransferases have evolved to repair methylated guanines, such as the mutagenic product O^6-methylguanine (O^6-meG). In bacteria this is performed by the C-terminal part of the O^6-Agt protein, while in humans it is the O^6-meG-DNA methyltransferase (MGMT). MGMT flips the O^6-meG base out of the DNA duplex into its active site and removes the methyl group by irreversibly transferring it onto its cysteine residue [9]. MGMT is thus inactivated and is cleaved by ubiquitin-mediated proteasomal degradation [10].

Dioxygenases

The specific repair of two other methylation products 1-methyladenine and 3-methylcytosine is achieved by dioxygenases, namely AlkB in *E. coli* and ABH2/ABH3 in humans. This happens by iron-catalyzed oxidation and results in the release of the methyl-group as formaldehyde.

Photolyases

Covalently-linked pyrimidine dimers induced by UV-radiation can be repaired by photolyases. They have been identified in various organisms, but not in mammals. They contain chromophoric groups and use the photon energy of blue light (300-500 nm) in order to break the covalent bonds between the pyrimidines, thus regenerating the original bases [8, 11].

1.3 Single-strand repair

Single-strand repair

Single-strand repair occurs if only one strand of the DNA helix contains a lesion. Depending on the nature of the lesion and the cell cycle stage, one of three single-strand repair pathways will be deployed: base excision repair, mismatch repair or nucleotide excision repair. All use the second, intact DNA strand as template to correct the damaged strand.

1.3.1 Base excision repair

Base excision repair

Base excision repair (BER) is indispensable for the maintenance of genome integrity and protects against premature aging, cancer and neurodegenerative diseases. It is a key guardian against multiple DNA alterations that frequently occur in DNA through oxidation, alkylation and deamination. Those base lesions cause generally only small distortions of the structure of the DNA helix, but because they may be mutagenic, or because they may destabilize DNA through spontaneous base loss, they must be efficiently removed from the genome. To ensure their faithful recognition and repair, a number of different DNA glycosylases have evolved. The first DNA glycosylase was discovered by Thomas Lindahl in 1974. He described an enzyme, today known as uracil-DNA glycosylase (UNG), that released uracil from DNA by cleavage of the N-glycosidic bond. He furthermore observed concomitant cleavage of the phosphodiester bond, followed by repair steps involving an exonuclease, a DNA polymerase and a DNA ligase [12] and thus outlined the basic steps of BER: i) base recognition and excision by a DNA glycosylase ii) incision of the abasic (AP) site iii) end processing by an endonuclease or lyase activity and iiii) polymerase-mediated repair synthesis and ligation (Figure 1-1). Currently, eleven human DNA glycosylases that recognize a wide range of DNA base modifications are known (Table 1-1) and can be subdivided into four structurally distinct superfamilies; helix-hairpin-helix (HhH) glycosylases including OGG1 and MYH, uracil DNA glycosylases (UDGs), 3-methyl-purine glycosylases (MPG) and endonuclease VIII-like (NEIL) glycosylases. In terms of viability, fertility and mutation frequencies, single DNA glycosylase knockout mice display relatively mild phenotypes [14], with the exception of TDG, the inactivation of which is embryonic lethal in mice [15, 16]. Double or triple knockout mice display severe phenotypes, suggesting that some have overlapping functions in terms of substrate recognition. For instance, MYH/OGG1 double knockout mice have shortened life spans and are cancer prone [17]. Redundancy amongst the different DNA glycosylases allows backup repair mechanisms within the BER pathway and therefore leads to high repair accuracy.

Table 1-1: Mammalian DNA glycosylases.
Overview about the main substrates, modes of action and mutant phenotypes of the DNA glycosylases.

Type of base lesion	Name	Physiological substrates	Mono (M) / bi (B) functionality	Mouse knockout (ko)/ knockdown (kd) phenotype
Uracil in ssDNA & dsDNA	UNG	U, 5-FU, ss- and ds-DNA	M	ko: viable, B-cell lymphomas, disturbed antibody diversification
	SMUG	U, 5-hmU, 5-FU, ss- and ds-DNA	M	kd: moderate increase in mutation frequency (C ➔ T)
Pyrimidine derivates in mismatches	MBD4	T, U, 5-FU, εC, opposite G, ds-DNA	M	ko: viable, elevated mutation frequency (C ➔ T)
	TDG	T, U, 5-FU, εC, 5-hmU, 5-fC, 5-caC; opposite G, ds-DNA	M	ko: embryonic lethal, aberrant DNA methylation and imbalanced chromatin marks in CpG-rich promoters
Oxidative base damage	OGG1	8-oxoG, fapy, opposite C, ds-DNA	B	ko: viable, accumulation of 8-oxoG, elevated mutation frequency (G ➔ T)
	MYH	A opposite 8-oxoG, C or G, 2-hA opposite G, ds-DNA	M	ko: viable, see OGG1
Alkylated purines	MPG	3-meA, 7-meG, 3-meG, hypoxanthine, εA, ss- and ds-DNA	M	ko: viable, elevated levels of ethenoA and hypoxanthine
Oxidized, ring-fragmented or -saturated pyrimidines	NTHL1	Tg, fapy-G, 5-hC, 5-hU, ds-DNA	B	ko: viable
	NEIL1	Tg, fapy-G, fapy-A, 8-oxoG, 5-hU, 5-hC, ss- and ds-DNA	B	ko: metabolic syndrome, increased damage levels in mitochondrial DNA; kd: hypersensitive to γ-radiation
	NEIL2	As NTHL1 and NEIL1	B	unknown
	NEIL3	fapy-G, fapy-A, prefers ss-DNA	B	ko: normal

U, uracil; A, adenine; T, thymine; C, cytosine; G, guanine; ss, single-stranded; ds, double-stranded; 5-hm, 5-hydroxymethyl; 5-FU, 5-fluorouracil; ε, etheno; 5-fC, 5-formylcytosine; 5-caC, 5-carboxylcytosine; 8-oxoG, 8-oxo-7,8-dihydroguanine; Tg, thymine glycol; FaPy, 2-6-diamino-4-hydroxy-5-N-methylformamidopyrimidine; me, methyl; h, hydroxyl

Taken from [13].

Structure & function of DNA glycosylases

Although DNA glycosylases are highly specialized enzymes with different structures and substrate specificities, they all share a common mode of action. They flip aberrant bases out of the DNA helix in order to trap and subsequently excise them. The enzyme moves along the DNA helix and inserts an amino acid side

chain (in cases of OGG1: Phe 114, or MYH: Tyr 165) into the minor groove of the double helix to search for vulnerable sites. While normal Watson-Crick base pairs are not disturbed by this intercalation, abnormal base pairs are disrupted, which leads to extrusion of the aberrant base into the exo-site of the enzyme. If it is not the 'right' base, it will be released back into the DNA helix, otherwise it will be passed to the active-site pocket. Thus, the base will be fixed in a position that allows cleavage of its N-glycosidic bond [18]. There are three hypotheses how the DNA glycosylase efficiently finds its target while the latter two gained more and more importance. The first is that the enzyme flips out each base but only removes those that fit into its binding pocket. The second is that it additionally recognizes weakened Watson-Crick base pairs and only flips out specific bases. A third scenario suggests that 'breathing' of non Watson-Crick base pairs leads to transient extrusions of such bases, which only have to be trapped by the enzyme when they are extrahelical [19].

Monofunctional DNA glycosylases

In terms of their catalytic mechanism, DNA glycosylases are subdivided into monofunctional and bifunctional enzymes (Table 1-1). Both will initiate nucleotide removal that results in 3'-hydroxy (OH) and 5'-phosphate (P) termini that can subsequently be used by a polymerase and a ligase respectively to refill the gap and seal the nick. However, the mechanism of creating these termini differs. Monofunctional glycosylases, such as MYH, UNG, SMUG1, MBD4, TDG and MPG, excise the substrate base by using a deprotonated water molecule as a nucleophile to attack the sugar C1', resulting in cleavage of the N-glycosidic bond and thus a free base and an apurinic (AP) site [13]. Further processing by apurinic endonuclease 1 (APE1) creates a nick 5' of the AP-site thus generating a 3'-OH and 5'-deoxyribophosphate (dRP) termini. This is removed by the amino-terminal dRP lyase activity of polymerase-β [20], thus generating a single nucleotide gap containing 3'-OH and 5'-P termini (Figure 1-1).

Bifunctional DNA glycosylases

OGG1, NTH1, NEIL1, NEIL2 and NEIL3, which process oxidized bases, belong to the family of bifunctional glycosylases. They possess an additional AP-lyase activity that can further process the AP-site *via* β (e.g. OGG1, NTH1) or βδ (e.g. NEILs) elimination reaction. In the first case, the resultant 3'-phospho α,β-unsaturated aldehyde (3' PUA) will be cleaved by APE1, while, in the latter case, the resultant 3'-P group will be eliminated by polynucleotide kinase 3'-phosphatase (PNKP). Both cases result in 3'-OH and 5'-P DNA ends, which can be used by polymerases and ligases, respectively [13, 21]. This last step of repair synthesis can occur *via* either short- or long-patch base excision repair (Figure 1-1).

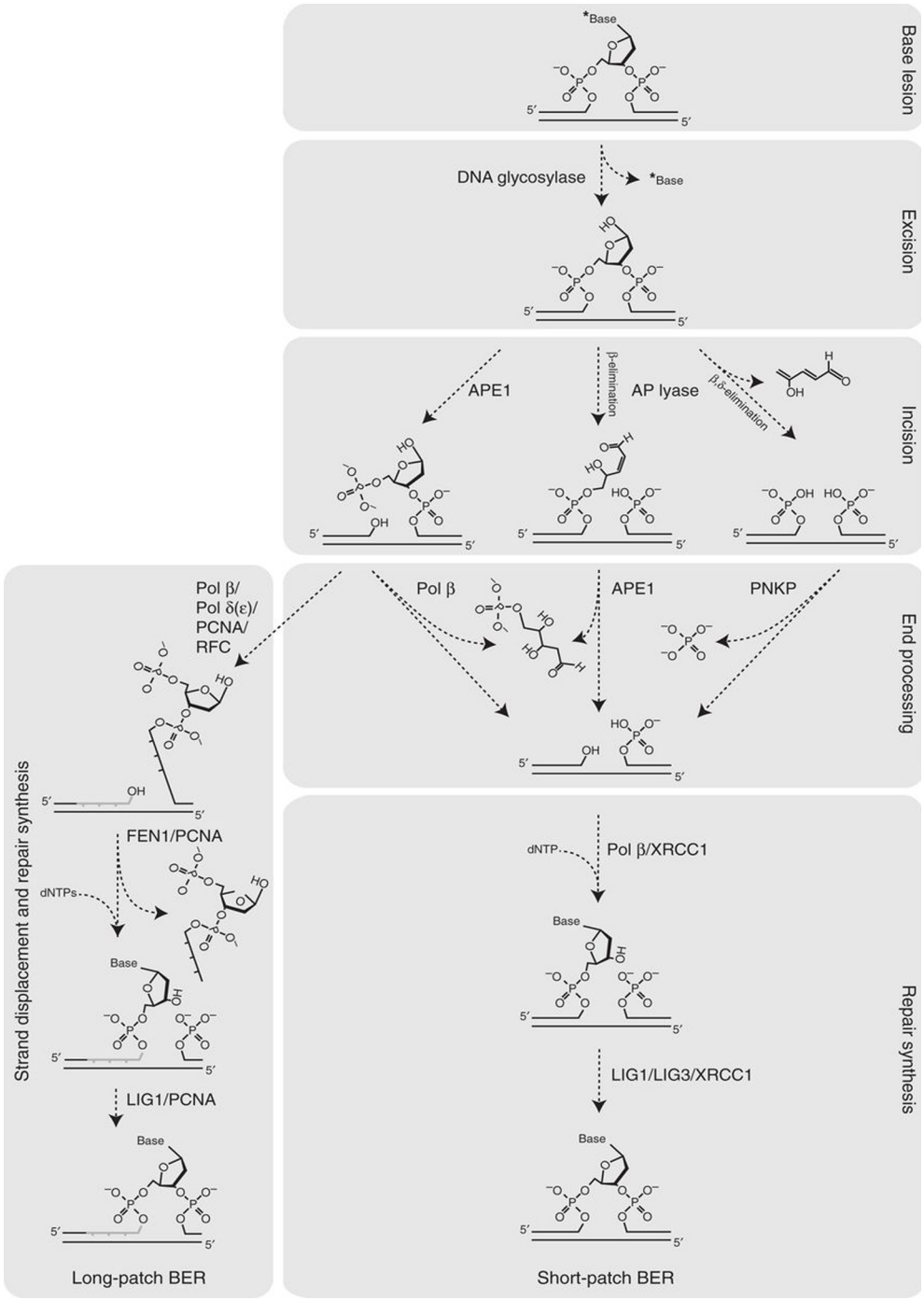

Figure 1-1: Subpathways in base excision repair.
BER is initiated by mono- or bifunctional DNA glycosylases and can occur as either short- (right panel) or long-patch (left panel) repair. A DNA glycosylase recognizes the base lesion and excises the base by cleavage of the N-glycosidic bond (excision step). The resultant AP-site gets excised by either APE1 (upon action of monofunctional glycosylases) or the AP lyase activity of bifunctional glycosylases (incision step). End processing occurs via the lyase activity of polymerase-β, APE1 or PNKP, respectively. The resultant 3'-OH group will be elongated by a polymerase and the remaining nick will be sealed by a ligase (repair synthesis step). Taken from [22].

Short-patch BER

Short-patch (SP) BER can appear in replicating as well as in non-replicating cells and leads to the replacement of only a single nucleotide. The single-strand break is recognized by X-ray repair cross-complementing 1 (XRCC1), which was described as a scaffold protein that coordinates the activities of its interacting partners such as polymerase-β and DNA ligase III (LIG III). [23-25]. The latter are responsible for gap filling and nick sealing (Figure 1-1).

Long-patch BER

In contrast, long-patch (LP) BER appears in replicating cells and displaces 2 to 10 nucleotides [26] by a process that uses proteins that are also involved in replication. While polymerase-β is likely to incorporate the first nucleotide in LP repair [27], the elongation step in this pathway is performed by a replicative polymerase such as -δ or -ε. Additional players required during this process are the polymerase's processivity factor proliferating cell nuclear antigen (PCNA) and its loading factor replication factor C (RFC). While flap endonuclease-1 (FEN-1) excises the displayed oligonucleotide, DNA ligase I (LIG I) is required for nick sealing [26, 28].

Switch between short- and long-patch BER

The choice between short- and long-patch BER depends on various factors, such as cell cycle stage, the type of lesion and the DNA glycosylase, ATP concentration or the structure of the 5' termini [29]. While ATP shortage was shown to result in XRCC1-promoted strand displacement by polymerase-β and LP-BER [30], efficient removal of 5'-dRP sites seemed to be important for the process of SP-BER [31], since otherwise the 5'-dRP site would make the nick refractory to ligation. However, the major role in pathway choice is played by the type of lesion and cell cycle stage. For example, the DNA glycosylases MYH and UNG were suggested to be involved mainly in LP-BER, since both enzymes preferentially locate within replication foci [32, 33]. Furthermore, MYH interacts with the replicating enzymes PCNA, RPA, APE1 and MSH6 [34, 35]. This hypothesis was further substantiated by a study showing that MYH-mediated repair of G^{O}/A mismatches in HeLa extracts was completely abolished by the polymerase-α/-δ/-ε inhibitor aphidicolin [36]. The involvement of MYH-initiated BER during S-phase makes sense, since G^{O}/A mismatches can only arise during replication and should be repaired immediately in order to prevent mutagenesis in the next round of replication. It was also hypothesized that NEIL1 and NEIL2, which preferentially excise lesions from DNA bubbles [37], which also occur at replication forks, might act during replication *via* LP-BER, while NTH1 that shares many substrates with NEILs, would act outside of S-phase *via* SP-BER [29]. OGG1 was also demonstrated to act *via* short-patch BER [38, 39]. However, there is no experimental evidence indicating in which cell cycle stage OGG1 might act.

1.3.2 Mismatch repair

Postreplicative MMR

Postreplicative Mismatch repair (MMR) is a key guardian of genomic integrity. It has evolved to improve the fidelity of replicative polymerases by several orders of magnitude [40, 41]. Those incorporate non-complementary nucleotides with a frequency of 1:10'000 to 1:100'000 [42]. These replication errors can be recognized and repaired by the polymerase's intrinsic proofreading exonuclease activity, thus increasing replication fidelity by approximately 2 orders of magnitude. This is when MMR comes into play and detects mismatches that escaped the polymerase's proofreading process, thus increasing replication fidelity by approximately another 3 to 4 orders of magnitude (Figure 1-2).

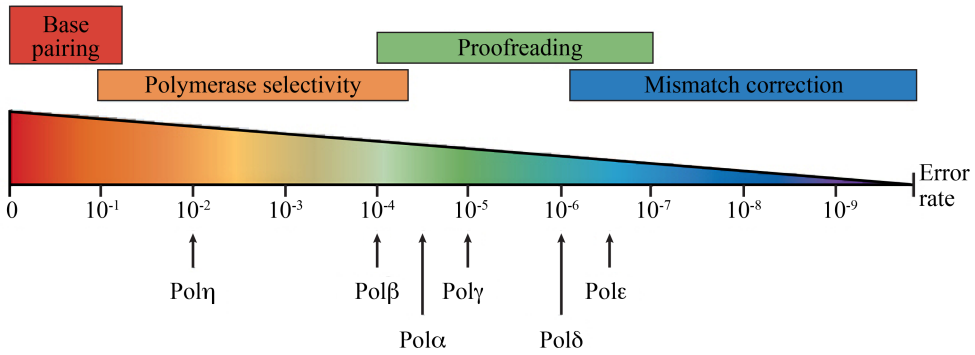

Figure 1-2: Determinants of replication fidelity.
Above the line: relative contribution of polymerases, their proofreading activity and mismatch repair to replication fidelity. Below the line: representative values for the rates of single-base substitutions by different DNA polymerases. Taken from [43].

Mismatches are defined as non-Watson-Crick base pairs or small loops of extrahelical nucleotides, also referred to as insertion/deletion loops (IDLs), that arise from slippage of the two strands during replication [44]. Mismatches hence consist of undamaged DNA and become 'invisible' for repair after the next round of replication. To ensure efficient mismatch correction, MMR has to satisfy three criteria [44]. First, it has to correct the error before the next round of replication. The recruitment of MMR proteins to replicating DNA is probably enabled by an interaction of the mismatch recognition factors with the replication fork [44-47]. Second, in order to repair a broad range of different mismatches with different structures, MMR must be able to recognize different distortions in the DNA helix. Third, since the parental strand carries - by definition - the correct genetic information, MMR has to distinguish the parental from the daughter strand in order to direct the repair to the error-containing, newly synthesized strand. How this is achieved in pro- and eukaryotes, will be discussed in detail in the following sections. Beforehand, an overview of proteins involved in MMR pathways of *E. coli* and eukaryotes is shown in Table 1-2.

Table 1-2: MMR factors in E. coli and eukaryotes and their functions.

E. coli	Eukaryotes	Function
MutS	MutSα (MSH2-6) MutSβ (MSH2-3)	Mismatch recognition
MutL	MutLα (MLH1-PMS2) MutLβ (MLH1-PMS1) MutLγ (MLH1-3)	Molecular matchmaker; strand-specific endonuclease, termination of excision
MutH		strand-specific endonuclease
UvrD (MutU)		DNA helicase
ExoI, ExoX		3'-5' Exonuclease; mismatch excision
ExoVII, RecJ	EXOI	5'-3' Exonuclease; mismatch excision
Pol III Holoenzyme	Pol	Repair synthesis
β clamp	PCNA	Molecular matchmaker; repair synthesis
γ Complex	RFC	β, respectively, PCNA loading; 3' nick-directed repair; activation of MutLα endonuclease
Ssb	RPA	Single-stranded DNA-binding protein; repair synthesis
	HMGB1	Accessory protein; stimulated excision
	PARP	Accessory protein; improved mismatch selectivity

Modified from [44].

1.3.2.1 MMR in prokaryotes

Mismatch repair in prokaryotes

The MMR system has been extensively studied in *E. coli*. In 1989 it has first been reconstituted *in vitro*, using the recombinant proteins MutH, MutL, MutS, DNA helicase II (UvrD), single stranded DNA binding protein (Ssb), DNA polymerase III holoenzyme, exonuclease I and DNA ligase [48]. In *E. coli*, the MutS homodimer recognizes and binds the biosynthetic error and subsequently recruits the MutL homodimer in an ATP-dependent manner. The resulting ternary complex activates MutH endonuclease that incises the erroneous strand. Strand discrimination occurs *via* methylation. Newly synthesized strands in *E. coli* are methylated at the N6 position of adenine in GATC sites by deoxyadenine methylase (Dam). Since Dam lags behind the replication fork, transiently hemi-methylated GATC sites are recognized by MutH and incised in the unmethylated strand [49, 50]. One of four exonucleases, together with UvrD helicase [51, 52], then degrades this strand towards and past the mismatch. Depending on the position of the nick relative to the mismatch, strand degradation will require either the 5'-3' exonucleases ExoVII or RecJ or the 3'-5' exonucleases ExoI or ExoX [53, 54]. The gap is then filled-in by DNA polymerase III and the remaining nick is sealed by DNA ligase.

1.3.2.2 MMR in eukaryotes

MutS and MutL heterodimers

In eukaryotes, the situation is more complex than in *E. coli*. The main players act in the form of heterodimers and have diversified into more substrate-specific proteins (Table 1-2). MutS homologue 2 (MSH2) dimerizes with MSH6 or MSH3 to form MutSα or MutSβ heterodimers, respectively [55]. MutSα is more abundant and recognizes base-base mismatches and IDLs of one or two extrahelical nucleotides [56], while MutSβ binds to larger IDLs. However, studies with MutS knockout mice suggest their functions to be partially redundant [57-59]. MutL homologue 1 (MLH1) dimerizes with post-meiotic segregation protein 2 (PMS2), PMS1 or MLH3 to form MutLα, MutLβ or MutLγ heterodimers, respectively [60]. Of the three, MutLα plays the most important role during MMR. The function of MutLβ is not defined yet, but might play a backup role for MutLα [40]. MutLγ is mainly involved in meiotic recombination, but may also play a role as MutLα backup [40, 61]. Several years ago, the minimal human MMR system has been reconstituted from purified recombinant proteins. It is composed of MutSα or MutSβ, replicating protein A (RPA), exonuclease I (EXOI), proliferating cell nuclear antigen (PCNA), replication factor C (RFC), polymerase-δ and DNA ligase I [62, 63].

Eukaryotic MMR

MMR is initiated by the binding of MutSα or MutSβ to the mismatch/IDL, followed by recruitment of MutLα. ATP hydrolysis causes a conformational change of MutSα, which converts it into a sliding clamp, enabling it to diffuse along the DNA backbone in either 5' or 3' direction, while searching for a strand discrimination signal [40]. This is where pro- and eukaryotes differ. Since eukaryotes lack d(GATC) methylation, MMR is targeted to the newly synthesized strand by strand discontinuities, such as preexisting termini [64]. Those might be gaps between Okazaki fragments on the lagging strand or 3' termini of the primer on the leading strand [40, 65] (Figure 1-3).

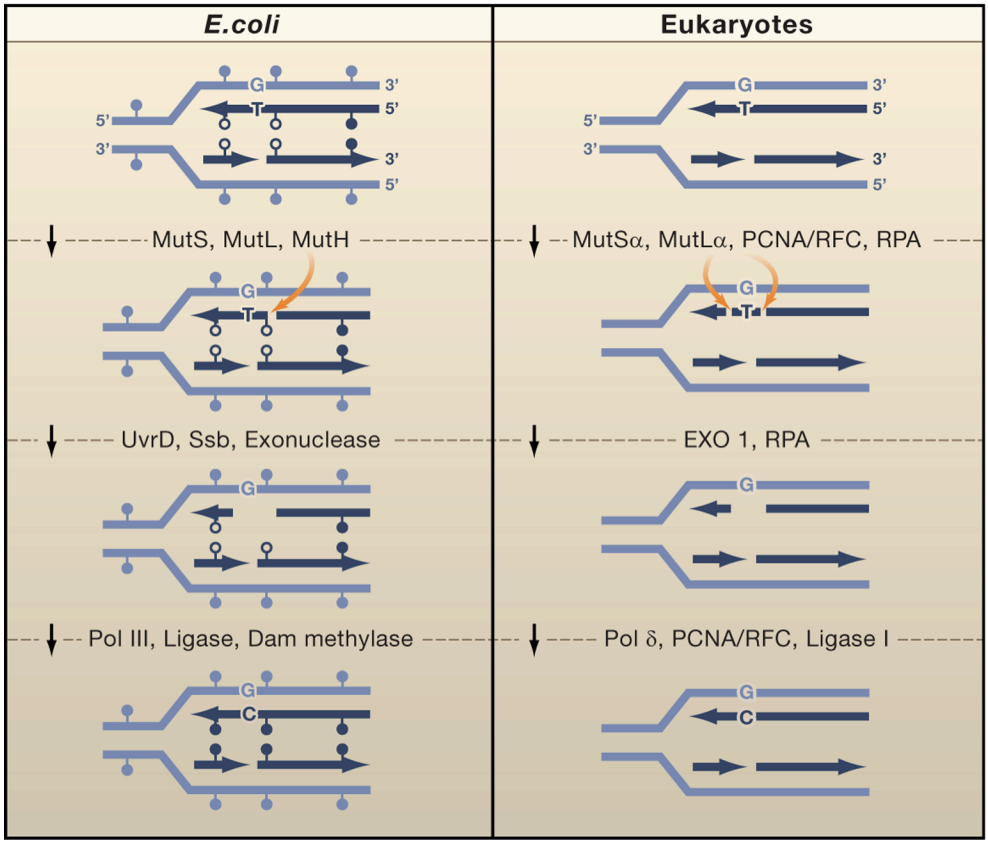

Figure 1-3: Strand discrimination signals in E. coli and eukaryotes.
Left: In E. coli, the newly synthesized strand (dark blue) is transiently unmethylated at GATC sites (empty circles) and can be incised by MutH either 5' or 3' to the mispair; filled circles, Dam methylated GATC sites. Right: In eukaryotes, the repairosome consisting of MutSα, MutLα, PCNA, RFC and RPA will identify the 3' terminus of the primer strand and MutLα will introduce random nicks at distal sites on the same strand (orange arrows). Taken from [65].

If the nick is 5' from the misincorporated nucleotide, MutSα/MutLα-stimulated EXOI will degrade the mismatch-containing strand in 5' to 3' direction. Once it has removed the mismatch, EXOI is no longer activated by MutSα, and is inhibited by MutLα and single-stranded DNA-bound RPA [66]. Since EXOI acts only in 5'-3' direction, an intrinsic endonucleolytic activity of the MutLα subunit PMS2, capable of inserting single-strand breaks in the vicinity of the mismatch, is required if the nick is 3' from the misincorporated nucleotide. In this case, MutLα endonuclease is activated in a MutSα-, RFC-, PCNA- and ATP-dependent manner [67, 68] and makes DNA incisions with a bias for the distal side of the mispair relative to the original strand break. Thereby it generates 5' nicks that serve as entry sites for MutSα/ MutLα -activated EXOI. Resynthesis is catalyzed by polymerase-δ and ligase I [40, 41] (Figure 1-4).

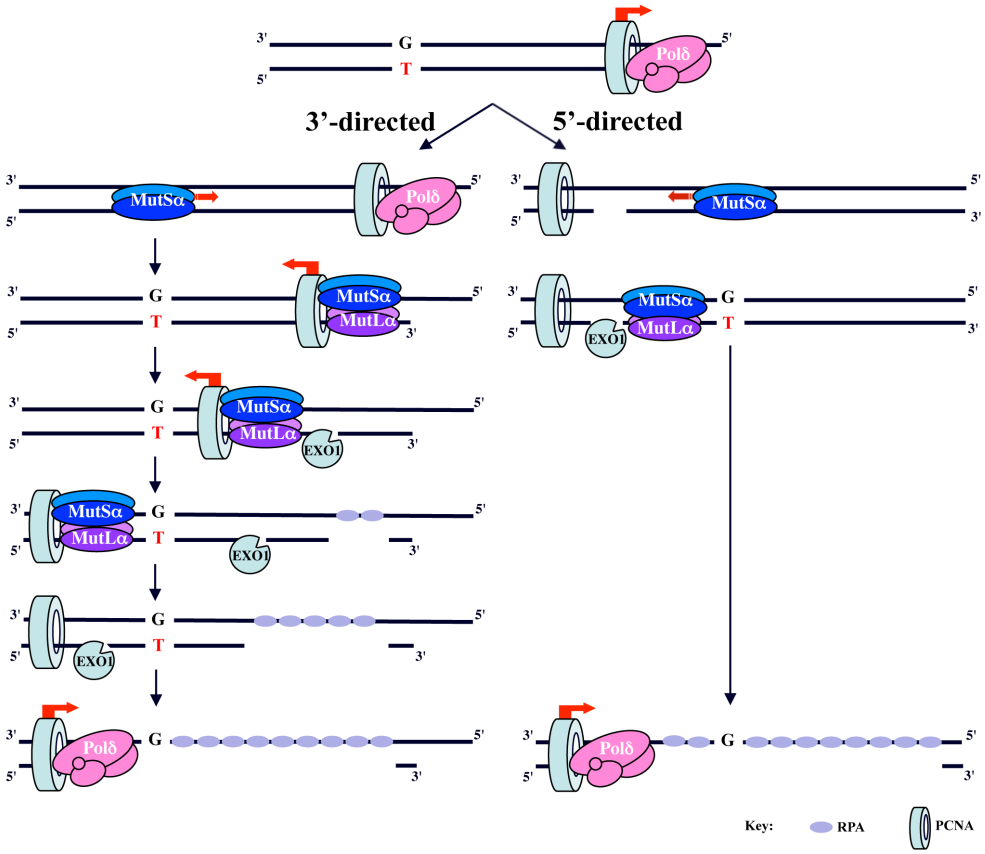

Figure 1-4: 5'- and 3'-directed mismatch repair in eukaryotes.
A G/T mismatch made by polymerase-δ is detected by MutSα, which slides along the DNA contour searching for strand discontinuities. Right panel: If it encounters a nick 5' of the mismatch, the 5'-3' exonuclease EXOI can immediately be loaded to perform strand degradation. Left panel: If the strand discontinuity is 3' of the mismatch, such as the terminus of the leading strand, MutSα could displace the polymerase from its complex with PCNA. Loading of MutLα and reversal of the direction of the travel of the protein complex would allow MutLα to introduce nicks in the leading strand, which can then be used for EXOI-catalyzed strand degradation. For details see text. Modified from [69].

MMR *in vivo*

While MMR has been extensively studied *in vitro*, less is known about its mechanism *in vivo*. This has been addressed in some recent studies. Discrimination between the parental and daughter strand in eukaryotes remains puzzling, due to the unequal incidence of preexisting nicks in the two strands. Elevated levels of ribonucleotide (rNMP) incorporation into the leading strand were reported [70, 71] and intermediate products of their processing were shown to serve as entry sites for MMR [72]. rNMP processing might thus contribute to MMR activity on the leading strand to a certain extent, however, the origin of other essential strand discrimination signals remains to be elucidated. Two other studies addressed the interplay between chromatin and MMR. One of those revealed the epigenetic histone mark H3K36me3 to be required for MutSα recruitment to the chromatin *in vivo*. This was shown to occur *via* direct interaction with the PWWP domain of

MSH6 [73]. Another study showed that the accessibility of mismatches in the chromatin for MMR proteins is facilitated by MSH6-mediated inhibition of nucleosome assembly by chromatin assembly factor 1 (CAF-1) [74]. This inhibition occurs *via* direct interaction of a PWWP-containing domain of MSH6 with CAF-1. Since MSH6 plays an important role during the initial steps of MMR, the next section will provide a closer look at the structure of MutSα, especially of MSH6.

Structure of MutSα

The MSH6 protein was first described in 1995 as a partner of MSH2 [56]. Both proteins consist of five conserved domains, while MSH6 contains an additional N-terminal disordered domain (Figure 1-5 A). All five domains of MSH6 and MSH2 dimerize as an asymmetric mirror image with each domain juxtaposed (Figure 1-5 B). Domain 1 allows DNA mismatch binding, which is conferred by the Phe-X-Glu motif of MSH6 and which is highly specific for the mismatched nucleotide [75]. This domain is connected *via* domain 2 to the lever, comprising domain 3. Domain 4, the clamp region, allows unspecific DNA binding, while domain 5 contains an ATPase activity [76-78]. The latter has been subject of extensive studies and though the precise mechanistic outcomes of ATP binding and hydrolysis are not yet completely understood, it is likely involved in altering MutSα DNA binding activity and structural conformation [44, 79]. However, also the N-terminal domain of MSH6 has sparked interest, as there is emerging evidence that it is involved in MMR-dependent DNA damage response and communication with other DNA repair pathways [79, 80]. Both could be mediated by posttranslational modifications. In fact, a poly(ADP-ribose) binding site [81] as well as 22 distinct phosphorylation sites of MSH6 were identified within its N-terminus [79, 80]. It is likely that alterations in phosphorylation patterns might regulate its role in repair and signaling processes. Indeed, within the described phosphorylation sites, four CDK2 and one ATM/ATR recognition motif have been identified, suggesting its association with cell cycle and/or DNA damage responses [79, 82]. A role of the N-terminal MSH6 PWWP domain in chromatin packaging and its recruitment to chromatin has been discussed in the previous section. Furthermore, the nuclear localization signal (NLS), which is not present in MSH2, is required for MSH6/MSH2 heterodimer transport into the nucleus [79]. The conserved and extreme N-terminal PIP motif (QXX(L/I)XXFF) (aa 4-11) allows interaction with PCNA. This is required, though not indispensable, for 5'-directed MMR [45] and furthermore assumed to be responsible for recruitment of MMR proteins to replicating DNA [46, 47, 83, 84]. Besides this, PCNA was shown to activate MutLα endonuclease [67].

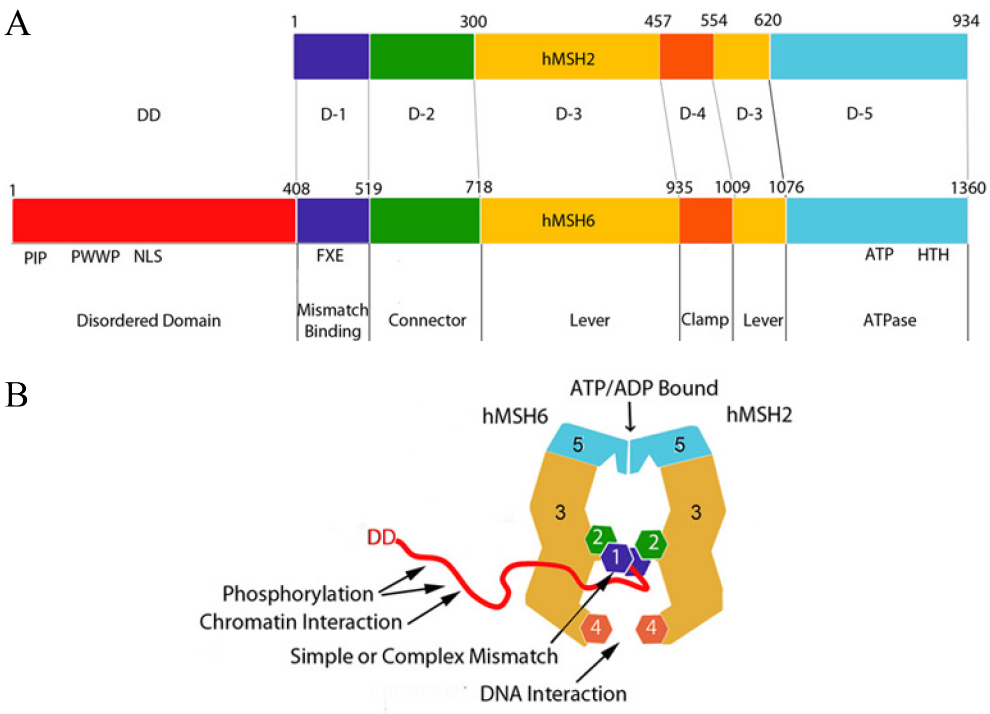

Figure 1-5: Structure of MutSα.
A) MSH2 (upper image) and MSH6 (lower image) domains in a comparative linear array. The domains (D) are abbreviated as follows. PIP: PCNA-interacting peptide, NLS: nuclear localization signal, FXE = Phe-X-Glu motif. Numbers of amino acids are indicated above the illustrated domains. B) MutSα in DNA binding configuration. Adapted from [79].

Role of MMR in other metabolic pathways

Beyond their function in the canonical mismatch repair pathway, MMR proteins are involved in a variety of other processes, such as meiotic and mitotic recombination, interstrand crosslink repair, DNA damage signaling and stability of trinucleotide repeats [85-93]. The role of MMR proteins in immunoglobulin class switching and somatic hypermutation, as well as in non-canonical MMR is interesting, since it is somehow counteracting their usual role in preventing mutagenesis [85, 94-97]. MMR has also been linked to oxidative DNA damage processing, however, its involvement in this process is still poorly understood and will be discussed in chapter 1.8.

1.3.3 Nucleotide excision repair

Nucleotide excision repair

Nucleotide excision repair (NER) is the most versatile repair pathway in terms of lesion recognition. It addresses an extraordinarily wide class of helix-distorting lesions that interfere with base-pairing or obstruct normal replication and transcription. These lesions mostly derive from exogenous sources such as chemicals or UV-light that induces the formation of cyclopyrimidine dimers (CPDs) or 6-4 photoproducts (6-4PPs) [98]. But also protein-DNA complexes can be recognized by NER [99]. Inborn defects in NER genes are associated with three

syndromes: *Xeroderma pigmentosum*, Cockayne syndrome and Trichothiodystrophy, all characterized by extreme sun sensitivity [100, 101]. The basic steps of NER are a) damage recognition, b) dual strand incision on either side of the lesion, c) release of the damage-containing oligomer, d) repair synthesis and e) ligation. The proteins involved in this reaction are not conserved amongst pro- and eukaryotes. While the former require only three proteins (UvrA, UvrB, UvrC), human NER comprises six core enzymes, namely RPA, XPA, XPC, TFIIH, XPG and XPF·ERCC1 [102-104]. In general, NER consists of two subpathways, global genome NER (GG-NER) and transcription-coupled NER (TC-NER). While GG-NER surveys the entire genome, TC-NER repairs lesions on transcribed strands that block the elongating RNA polymerase [98, 105]. The two subpathways are therefore initiated differently. In GG-NER, bulky DNA lesions are detected by the enzyme complex XPC-RAD23B (Figure 1-6, A-B). TFIIH that comprises the helicases XPB and XPD interacts with XPC-RAD23B and forms a complex (C). The helicases unwind the DNA in both directions, whereas stalling of XPD at the modification verifies the lesion (C). This leads to the recruitment of RPA, XPA and XPG (D). Subsequent recruitment of ERCC1-XPF leads to the incision of the modified DNA strand 5' to the lesion (E). Subsequent XPG-mediated 3' strand incision leads to the release of a ~30 nucleotides long oligomer in humans (F) [106]. The gap is then filled by polymerase δ/ε and its associated factors, and the remaining nick is sealed by DNA ligase IIIα/XRCC1 or DNA ligase I (G) [107]. TC-NER functions similarly, except that it does not require XPC-RAD23B for initiation, but rather stalling of the RNA polymerase and the factors CSA and CSB.

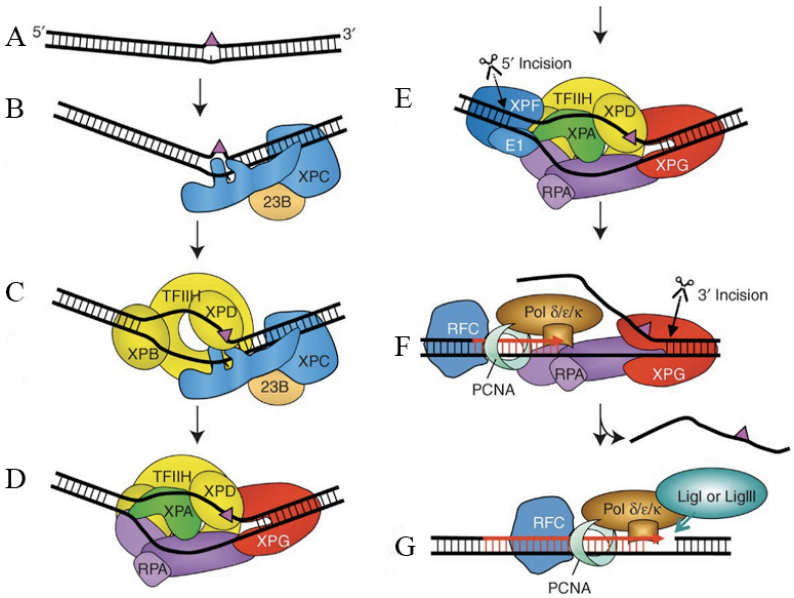

Figure 1-6: Global genome nucleotide excision repair.
Unwinding of the DNA is followed by excision of the lesion-containing oligomer. DNA synthesis and ligation complete the repair process. For details see text. Taken from [107].

1.4 Double-strand repair

Double-strand repair

As discussed in the beginning, if only one strand contains a lesion, it can be repaired with the help of the second strand that serves as template. In contrast, double-strand breaks (DSBs) are critical for the cell, since there is no template readily available for repair. DSBs can be induced by exogenous factors such as ionizing radiation (IR) or endogenous factors such as reactive oxygen species (ROS). In eukaryotes, two major pathways have evolved in order to repair DSBs, namely, homologous recombination (HR) and non-homologous end-joining (NHEJ). A third, minor pathway is single-strand annealing (SSA) repair. The choice of the repair pathway depends on the cell cycle phase. While NHEJ and SSA can act throughout the cell cycle, HR activity is restricted to S-phase [2, 108, 109]. HR is the preferred pathway during S-phase, since it is essentially error-free. In contrast, NHEJ and SSA represent faster repair mechanisms, but are error-prone, which can lead to the loss of genetic information.

1.4.1 Homologous recombination

Homologous recombination

Homologous recombination (HR) uses the sister chromatid as template for re-synthesis of the damaged strand. It takes place in three core steps: end resection, strand invasion and resolution (Figure 1-7, right panel). The initial step, end resection, involves the MRE11/RAD50/NBS1 (MRN) complex, BRCA1 and CtIP [110]. The endonuclease activity of MRE11 initiates the process by inserting a nick at a distance from the DSB [111]. This can be further processed in order to generate a single-stranded 3' overhang. The roles of BRCA1 and CtIP during end processing are less clear, but both were shown to promote HR [110, 112] and notably, BRCA1 interacts with both CtIP and MRN [113, 114]. The resultant 3' single-stranded DNA overhang is rapidly bound by RPA. RAD51 competes with RPA for binding to the DNA strand and will replace it with the help of its mediator BRCA2. In the absence of BRCA2, no RAD51 foci can be formed on the DSBs [115-117]. The RAD51 filament directs strand invasion to the homologous strand of the undamaged sister chromatid, thereby mediating the search for homologous sequences [118, 119]. A DNA polymerase will extend the 3' end using the homologous sequence as template. The resultant Holliday junctions can be resolved by e.g. MUS81/EME1 [120-122].

Single-strand annealing

A subpathway of HR is the single-strand annealing (SSA) mechanism. This does not require a sister chromatid, but uses sequence homologies of the complementary strand for strand annealing. The DSB is recognized by the MRN complex and processed until regions of homology on the two sides of the breaks are exposed. These regions are then paired and the overhangs are cropped off, so that the duplex ends can be ligated [99] (Figure 1-7, left panel).

BRCA1 & BRCA2 in HR and SSA

As both HR and SSA rely on DNA end resection, both depend on BRCA1. In contrast to HR, SSA does not rely on strand invasion and can therefore dispense with BRCA2. This becomes apparent from the observation that defects in BRCA1 lead to decreases in both HR and SSA, while loss of BRCA2 only decreases HR and, as a consequence, leads to stimulation of the alternative pathway SSA [123, 124]. Even though BRCA1 and BRCA2 act at different steps during HR, both are essential for this process and defects in either gene, lead to increased breast cancer susceptibility.

1.4.2 Non-homologous end-joining

Classical NHEJ

Since error-free HR is available during S-phase, non-homologous end-joining (NHEJ) occurs predominantly in G0- and G1-phases of the cell cycle when no sister chromatid is available. The fact that it is error-prone does not mean that it is just a poor alternative to HR. It is actually required during the processes of the immune response, such as V(D)J and class switch recombination (CSR). The core enzymes of classical NHEJ (c-NHEJ) are DNA-PK, XRCC4 and DNA ligase IV. DNA-PK consists of the DSB-binding heterodimer Ku70/80, as well as the DNA-PK catalytic subunit (DNA-PKcs) [125] that contains a kinase activity. Once activated, DNA-PK phosphorylates itself and other c-NHEJ proteins [126-128]. The actual repair process is initiated by Ku-binding to the DSB, which then recruits DNA-PKcs. The proteins bring the double-strand DNA ends into close proximity, which can then be rejoined by XRCC4/DNA ligase IV (Figure 1-7, middle panel). Before ligation, DNA ends might have to be processed to generate blunt ends. Several factors have been suggested to be involved in this processing, including MRN, Artemis, PNK and WRN [129].

Alternative NHEJ

In the absence of Ku70/80, a 20-fold less efficient alternative NHEJ (alt-NHEJ) pathway, also referred to as microhomology-mediated end-joining (MMEJ), has been observed [130]. Similar to SSA, it uses 3-16 base pair homologous sequences to align the broken strands and rejoin them by DNA ligase III [131].

Pathway choice

When it comes to pathway choice, end resection is a major determinant of whether HR or NHEJ is used for DSB repair. Both pathways seem to keep each other in check. Thus, while Ku promotes NHEJ, its absence results in increased HR [132, 133], suggesting that the presence of Ku at DNA ends blocks access to the end resection machinery. Also the proteins 53BP1 and RIF1 promote NHEJ, and four recent publications showed that this is because they prevent 5'-3' DNA end resection, as well as accumulation of BRCA1 at sites of DNA damage, specifically in G1 phase of the cell cycle [134-137]. In the absence of 53BP1, HR is increased [138] and, interestingly, the absence of 53BP1 or RIF1 even restored end-resection and HR in BRCA1-deficient cells [137, 139]. Conversely, HR might antagonize

NHEJ by clipping Ku from the DNA ends by MRN and CtIP, thus allowing end resection [109] .

Figure 1-7: Double-strand break repair.
Error-free repair during S- and G_2-phases of the cell cycle is mediated by homologous recombination (right panel). Error-prone repair during G0- and G1-phase is mediated by non-homologous end-joining (middle panel) or single-strand annealing (left panel). For details see text. Modified from [140].

1.4.3 Crosslink repair

Crosslink repair

DNA interstrand crosslinks (ICLs) are highly toxic to the cell since they prevent the unwinding of the DNA helix, which leads to the block of replication and transcription. Natural sources of ICLs are byproducts of lipid peroxidation [141]. Also many chemotherapeutic drugs induce ICLs such as platinum-containing drugs (e.g. cisplatin), nitrogen mustards (e.g. melphalan) or mitomycin C. *Fanconi anemia* (FA) proteins represent the hub of ICL repair. FANCM recognizes the damage, which leads to the recruitment of the FA core complex (FANCA, FANCB, FANC, FANCE, FANCF, FANCG, FANCL) to the stalled replication fork and FANCD2/FANCI monoubiquitylation [142-144]. The latter allows the recruitment of nucleases to the sites of DNA damage [145]. Unhooking of the crosslink by dual incision of the DNA strand is followed by translesion synthesis (TLS) (see chapter 1.5), NER and HR that mediate damage bypass, removal of the crosslink and recombination of the broken ends, respectively [146]. Also BRCA1 and -2 play a role during ICL repair since they are involved during the HR-step [147, 148], with BRCA1 participating also in the ubiquitylation of FANCD2 [149, 150]. Defects in one of the 13 *FA* genes lead to a rare autosomal-recessive or X-

chromosome-linked disease that involves chromosomal instability and high sensitivity to ICL-inducing agents.

1.5 DNA damage bypass

Translesion synthesis

Under certain circumstances, repair at replication forks could cause their collapse. In these cases, it is favorable for the cell to continue DNA replication and to repair it at a later time point. This can be achieved by translesion synthesis (TLS). TLS is conserved throughout evolution and relies on specialized polymerases that have more flexible base pairing properties than replicative polymerases. TLS polymerases are therefore characterized by low fidelity, a lack of proofreading activity, as well as relatively poor processivity. However, this allows them to temporarily take over DNA synthesis from polymerases-δ, -ε or -α in order to bypass certain lesions (see Table 1-3).

Table 1-3: TLS human DNA polymerases.

Polymerase name	Polymerase family	Proposed function
η (eta)	Y	Bypass UV lesions
ι (iota)	Y	Bypass UV lesions
κ (kappa)	Y	Bypass UV lesions
Rev1	Y	Incorporation of C opposite abasic sites
λ (lambda)	X	BER, NHEJ
μ (mu)	X	NHEJ
θ (theta)	A	DNA repair
ν (nu)	A	Unknown
ζ (zeta)	B	Bypass synthesis

Modified from [43].

For example, the TLS polymerase-η has a large active site, which enables it to accommodate both bases of UV-induced cyclobutane pyrimidine dimer (CBP) in such a manner that the linked thymidines can correctly pair with incoming adenines [151, 152]. Mutations in polymerase-η lead to the clinical syndrome *Xeroderma pigmentosum* variant (XPV) [153], which is, similarly to *XPA-XPG* mutation-associated disease, characterized by an increased risk of sunlight-induced skin cancer [154]. X-family polymerase members, such as polymerase-β and -λ, are involved in accurate bypass of the oxidative DNA lesion 8-oxoguanine, as discussed in chapters 1.6.4 and 1.7.1. On undamaged DNA, TLS polymerase activity would lead to mutations. Its access to DNA is therefore highly regulated by a polymerase switch. Both replication arrest and RPA-coated single-stranded DNA lead to monoubiquitylation of the proliferating cell nuclear antigen (PCNA) at lysine 164 by the E3 ubiquitin ligase RAD18 and the E2 ubiquitin conjugator RAD6 [155]. This allows a direct interaction of ubiquitin-PCNA with the ubiquitin-binding motif (UBM) or ubiquitin-binding zinc (UBZ) domain of Y-

family polymerases [156, 157]. Phosphorylation and ubiquitylation of TLS polymerases have also been observed, but how they might regulate TLS is still unclear [158-162]. The best understood example is polymerase-η. This was shown to be monoubiquitylated on its carboxyl-terminus, which in turn inhibits its interaction with PCNA [160]. This suggests that ubiquitylation could be another regulator of TLS and that polymerase-η has to be deubiquitylated before it can be recruited to stalled replication forks.

1.6 Cellular response to oxidative stress

Cellular response to oxidative stress

Life on earth has evolved in the presence of oxygen that allowed the evolution of aerobic creatures. However, their cellular respiration leads to the production of reactive oxygen species (ROS), which are a continuous threat to genome integrity and which led to the evolution of a battery of defense mechanisms. In the first instance, enzymatic as well as non-enzymatic antioxidants counter the accumulation of ROS in cellular compartments (see chapter 1.6.2). Remaining radicals can, however, oxidize the deoxynucleotide pool, which is in turn 'detoxified' by the enzyme MTH1 (see chapter 1.7.4). However, oxidized nucleotides can still be introduced into DNA. In order to counteract their mutagenic potential, sophisticated systems have evolved in order to correctly bypass (see chapter 1.6.4) or repair these lesions (see chapter 1.7.1). The defense mechanisms and ways to deal with threat of oxidative DNA damage are discussed in detail in this and the following chapters.

1.6.1 Sources of oxidative stress

Endogenous & exogenous sources of ROS

All aerobic organisms rely on mitochondrial respiration in order to generate energy in the form of ATP. This process strongly depends on the presence of oxygen that is converted into water molecules during this process. Nevertheless, normal cellular metabolism is also well established as a major source for endogenous ROS. During the electron transport of mitochondrial respiration, oxygen captures electrons and is thus transiently converted into ROS. Normally, its reaction with other molecules is prevented by the cytochrome oxidase complex that only releases the oxygen radical when paired with two hydrogen molecules, thus forming a non-reactive water molecule. However, this system is leaky and 1-5% of electrons escape from complexes of the electron transport chain and form superoxide anion radicals ($\bullet O_2^-$) in the presence of oxygen [163, 164]. Other endogenous sources of ROS are peroxisomes and inflammation [165]. The latter process involves phagocytes that, within a respiratory burst, release superoxide radicals and hydrogen peroxide (H_2O_2) that interact *via* the Haber-Weiss reaction to form highly reactive hydroxyl radicals ($\bullet OH$) [166] that destroy cells infected with bacteria or viruses. However, surrounding cells can also be affected. In addition, ROS can be generated by

exogenous sources such as ionizing or ultraviolet radiation, chemotherapeutic drugs or heavy metals [167-169].

Definition & types of ROS

ROS are oxygen-containing molecules that have an unpaired electron (Figure 1-8, shown in red) in its outermost shell of electrons and hence exhibit extremely high chemical reactivity. ROS include superoxide anions ($\bullet O_2^-$), peroxide ($\bullet O_2^{2-}$) and hydroxyl radicals ($\bullet OH$) while oxygen (O_2) and hydrogen peroxide (H_2O_2) represent reactive precursors. Although H_2O_2 is less reactive than some other ROS, it plays an important role during oxidative damage and carcinogenesis, since it is able to easily diffuse through biological membranes, which enables it to reach other cellular compartments, including the DNA-containing nucleus [170]).

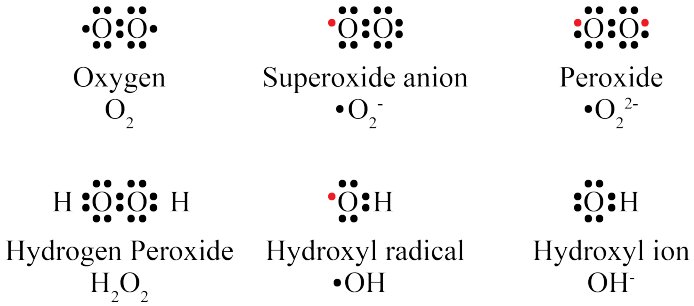

Figure 1-8: Electron structures of common reactive oxygen species (ROS).
Unpaired electrons are indicated in red. Hydroxyl ion is presented as comparison to the hydroxyl radical, but is not a ROS. Oxygen and hydrogen peroxide represent unstable, reactive molecules but are, per definition, not ROS, since they do not have any unpaired electrons. Adapted from www.biotek.com.

1.6.2 Antioxidants

Antioxidants

Reactive oxygen species can give rise to irreversible oxidation of cellular macromolecules such as lipids, proteins and DNA. However, the production of ROS during cellular metabolism is natural and living organisms have thus adapted by evolving a large number of antioxidant systems, which can be subdivided into two groups: enzymatic and non-enzymatic.

Enzymatic antioxidants

Amongst the enzymatic antioxidants, three groups of enzymes have evolved: superoxide dismutases (SOD), catalases and peroxidases (Table 1-4). **Superoxide dismutases** play an important role in converting superoxide anions ($\bullet O_2^-$) that are generated e.g. during the electron transport chain of cellular respiration, into less toxic hydrogen peroxide and oxygen [172]. The antioxidant activity of SODs derives from their metal cofactors: manganese (Mn), copper (Cu) or zinc (Zn) that are bound to the enzyme. While Mn SOD is primarily present in mitochondria, the other two SODs are found in the cytosol. Since H_2O_2 is unstable and reactive, it has to be further detoxified. This is where **catalases** and **peroxidases**, which are further subdivided into peroxiredoxins (PRXs) and glutathione peroxidases (GPXs), come

into play. Catalases are located in peroxisomes or in the cytosol and degrade H_2O_2 to water and oxygen, thereby finishing the detoxification reaction that was initiated by SOD [172]. **Glutathione peroxidases** can also reduce free hydrogen peroxide to water [172]. The reaction involves oxidation of the selenocysteine residue of two reduced monomeric glutathiones (GSH) by H_2O_2, which then results in a glutathione disulfide (GSSG) and two water molecules. Peroxiredoxin can also reduce H_2O_2 to a harmless water molecule.

Table 1-4: Enzymatic antioxidants, their cellular location, substrates and corresponding reactions.

Enzymatic antioxidant	Cellular location	Substrate	Reaction
Superoxide dismutase (Mn/Cu/Zn SOD)	Mitochondrial matrix (Mn SOD) Cytosol (Cu/Zn SOD)	Superoxide ($\bullet O_2^-$)	$2\ \bullet O_2^- + 2\ H^+ \rightarrow H_2O_2 + O_2$
Catalase	Peroxisomes	Hydrogen peroxide (H_2O_2)	$2\ H_2O_2 \rightarrow O_2 + 2\ H_2O$
Glutathione peroxidase (Gpx)	Cytosol	Hydrogen peroxide (H_2O_2)	$H_2O_2 + 2\ GSH \rightarrow GSSG + 2\ H_2O$
Peroxiredoxin (Prx)	Cytosol	Hydrogen peroxide (H_2O_2)	$H_2O_2 + PrxS_2 \rightarrow Prx(SH)_2 + 2\ H_2O$

Modified from [171].

Non-enzymatic antioxidants

In addition to those three main players in anti-ROS metabolism, there are also a number of non-enzymatic antioxidants. They include vitamins (e.g. A, C, E), organosulfur compounds (e.g. glutathione), coenzyme Q10, enzyme-bound minerals (e.g. zinc, selenium), carotenoids, nitrogen compounds (e.g. uric acid), phenolic acids and flavonoids [173]. They differ in their mode of action and cellular localization and thus represent another effective defense system against ROS.

1.6.3 Oxidative damage on DNA

Oxidative DNA damage

If cellular ROS production exceeds the capacity of the natural defense mechanisms, cells undergo oxidative stress, which has been linked to aging, neurodegenerative diseases and also cancer. The latter is a consequence of DNA mutations that can be caused by ROS reaching the nucleus in the form of H_2O_2, since this small and uncharged chemical compound is able to easily diffuse through biological membranes and hence reach diverse cellular compartments [174]. Hydrogen peroxide spontaneously reduces to the highly-reactive hydroxyl radical ($\bullet OH$), which can then attack the DNA [168]. The electron-rich double bonds in the DNA bases, as for instance between N7-C8 of purines or C5-C6 of pyrimidines, as well as their labile hydrogens are especially vulnerable to radical attack [168]. However, more than 20 base lesions caused by reactive oxygen and free radical species have been identified (Figure 1-9).

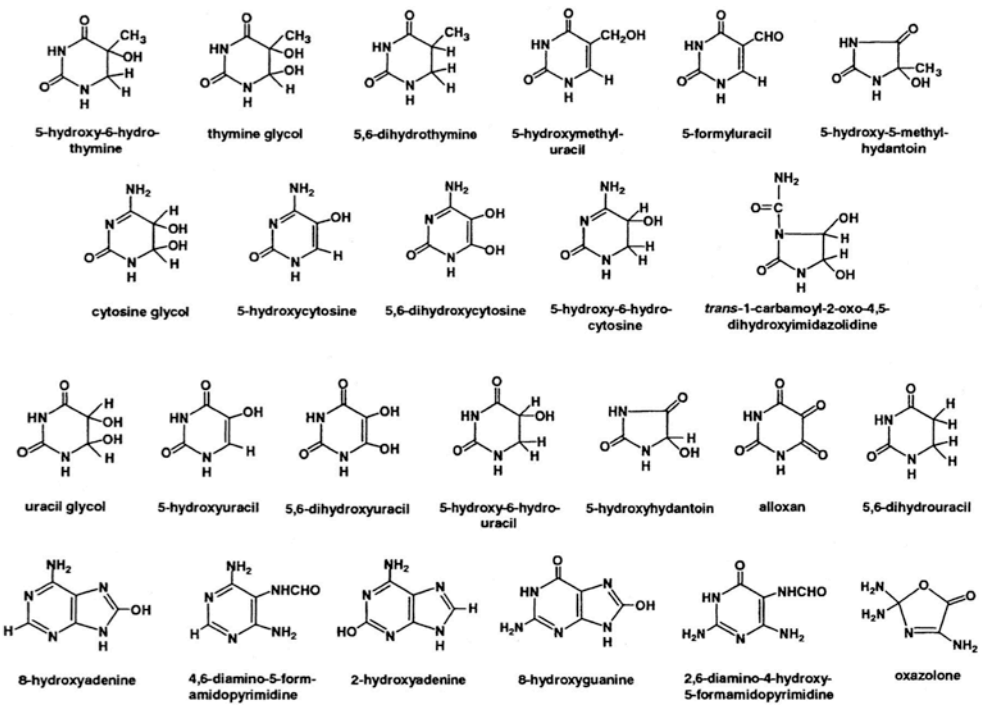

Figure 1-9: DNA base products of interaction with reactive oxygen and free radical species. Taken from [168].

Of the four DNA bases, guanine has the lowest redox potential and is thus particularly susceptible to oxidation [18, 175]. The main products of guanine oxidation are 7,8-dihydro-8-oxo-guanine (8-oxoguanine, G^O) and 2,6-diamino-4-hydroxy-5-formamidopyrimidine (fapy-G). Their generation and structures are represented in Figure 1-10.

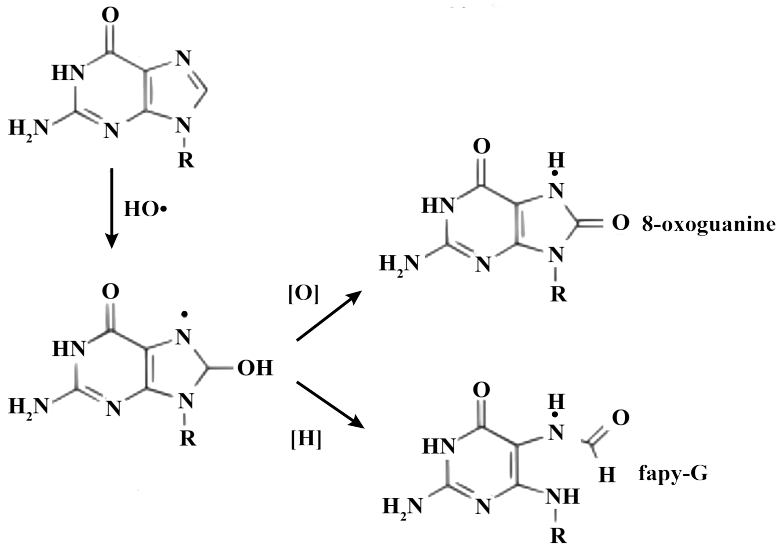

Figure 1-10: Formation and structures of 8-oxoguanine (G^O) and fapy-G. A hydroxyl radical attacks C8 of guanine thus forming either G^O or fapy-G. Modified from [176].

1.6.4 8-Oxoguanine

Incidence of G^O

8-Oxoguanine (G^O), is one of the most abundant and also best-investigated lesions created by ROS. Its steady state levels are estimated to be 10^3 lesions per cell per day in normal tissues and up to 10^5 lesions per cell per day in cancer tissues [170, 177, 178]. It is also used as a cellular biomarker to indicate the amount of oxidative stress [172].

Ambiguous base pairing properties of G^O

8-Oxoguanine endangers genomic integrity, since it does not only form Watson-Crick-like base pairs with cytosine, but also functionally mimics thymidine and can hence form a Hoogsteen mispair with adenine (Figure 1-11) [18]. Those are mutagenic if unrepaired, and lead to G to T transversions, as described in detail in chapter 1.7.1.

Watson-Crick versus Hoogsteen base pairing

In order to pair with adenine, G^O has to adopt a *syn* conformation as a prerequisite to form a G^O(*syn*):A(*anti*) mispair. Such *anti* - *syn* base pairs can only occur *via* Hoogsteen base pairing, which is mediated by the hydrogen atom on the N7 position as well as the oxo-group at the C6 position of the purine [18]. Such base pairs are rather rare; the majority of the DNA helix consists of Watson-Crick base pairs, in which the bases are in *anti* conformation (e.g. G/C and A/T) and purines form hydrogen bonds with their oxo-group at the carbon position 6 (C6), their NH group at N1 and their nitrogen group at carbon position 2 (C2).

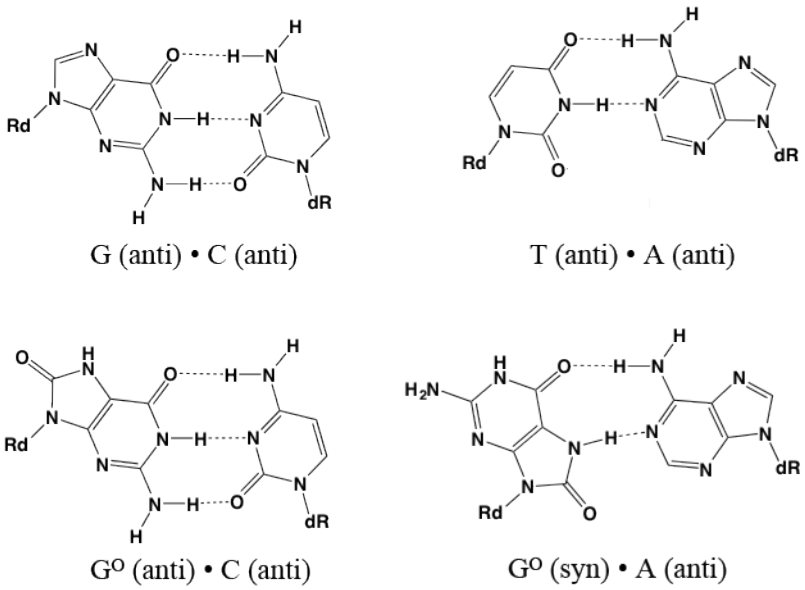

Figure 1-11: Structures of 8-oxoguanine-containing base pairs.
The structures of the Watson-Crick base pairs G(anti)/C(anti) and T(anti)/A(anti) are compared with G^O(anti)/C(anti) and the Hoogsteen mispair G^O(syn)/A(anti). Adapted from [18].

Bypass of 8-oxoguanine

In an ideal case, DNA polymerases should not generate G^O/A mispairs and even if they did, they should excise the mispaired nucleotide with the help of their proofreading activity. This is not the case; instead, G^Os are efficiently bypassed by replicative polymerases. This happens at the cost of mutations, since these enzymes preferentially incorporate A opposite G^O in the template strand [179-183]. This was clearly illustrated in a study by Hsu *et al*. [184]. Snapshots of X-ray crystal structures of *Bacillus stearothermophilus* (BF) DNA polymerase I fragment, which behaves analogously to replicative polymerases-α and -δ with respect to G^O replication, were taken during G^O/C and G^O/A replication. *Anti* G^O conformation in the template strand, a pre-requisite for pairing with C, lead to distortions in the template strand and also in the polymerase, as observed when polymerases encounter mismatches with their active site. This prevented the next template base from interaction with the pre-insertion site of the polymerase, explaining the polymerase's problem to elongate from G^O/C base pairs. In contrast, G^O(*syn*)/A(*anti*) mispairs did not lead to template or polymerase active site distortions. This is because the geometry of its minor groove, an area that the polymerase interacts with, is virtually identical to that of an A/T base pair and is therefore not recognized as a mismatch by the proofreading activity [184]. These data explain the more facile insertion of an A rather than a C opposite G^O, its lack of detection as well as its ease of elongation by replicative polymerases. However, bypass of G^O was shown to be correct in 80% of the cases *in vivo* [183], indicating that there must be other ways to bypass G^O correctly. This can happen *via* a polymerase switch, where stalling of a replicative DNA polymerase leads to PCNA monoubiquitination and subsequent recruitment of a translesion synthesis (TLS) polymerase to the site of DNA damage [185] (see chapter 1.5). Although both polymerase-η and -λ can correctly bypass G^O [186-188], it was shown that, in the presence of PCNA and RPA, polymerase-λ bypassed it more correctly. Its preference of C incorporation was 1200-fold higher than of A, while for polymerases-η it was only 68-fold [189]. Since polymerase-δ pauses at sites of G^O, it was suggested that the error-free bypass of G^O by polymerase-λ occurred *via* a polymerase switch [190]. This was not observed for polymerases-β and -η [190], supporting the observation that polymerase-λ is the most important and faithful polymerase during correct G^O bypass. However, it does not only play a crucial role during G^O replication, but also repair. Since every polymerase has a certain error-rate, also G^O replication will result in a certain percentage of A misincorporations. Those mutagenic mismatches are countered by MYH-initiated base excision repair. Also during this repair process, polymerase-λ seems to faithfully incorporate C opposite G^O, as described in the following chapter.

1.7 Base excision repair in oxidative stress & disease

1.7.1 The 'GO system' - Base Excision repair of 8-oxoguanine

BER of 8-oxoguanine

As previously described, base excision repair (BER) repairs a very diverse range of base modifications, amongst those, the major byproduct of oxidative DNA damage: 8-oxoguanine (G^O). Thereby it makes use of a highly coordinated process referred to as the 'GO system'. As described in the last chapter, G^O has ambiguous base pairing properties and can pair either with C or A [18]. While G^O/C base pairs do not endanger genomic integrity, G^O/A mispairs are mutagenic and result in G to T transversions if left unrepaired [191-194]. To counteract this, an ancient repair system has evolved, including the key players MutT, MutM and MutY [195]. In vertebrates, these proteins have orthologs: MTH1, OGG1 and MYH (= Mutyh, hMYH), respectively (Figure 1-12) [196]. The functions of the vertebrate orthologs are as follows. In the first instance, MTH1 counteracts incorporation of G^O by eliminating it from the nucleotide pool by hydrolyzing dG^OTP to dG^OMP [197]. However, if G^O arises in the template strand, thus leading to G^O/C base pairs, OGG1 will excise the G^O and subsequent processing by short-patch BER and polymerase-β will restore a G/C base pair [39, 198]. However, if G^O/C remains unrepaired, polymerases might incorporate an A opposite the G^O in the next round of replication [199]. In this case, MYH would remove the A from the G^O/A mispair, and further processing by BER would re-generate a G^O/C [200], which represents a substrate for OGG1. In order to prevent futile MYH-induced repair at G^O/A sites, the BER polymerase has to insert a C opposite the G^O rather than an A. Although polymerase-β and polymerases-δ/-ε are the main polymerases acting during short- and long-patch BER [27, 201-204], polymerase-λ was shown to accurately perform repair upon MYH-initiated BER. This occurs *via* long-patch BER (see chapter 1.3.1). In the presence of RPA and PCNA, polymerase-λ incorporates cytosine opposite G^O 145-fold more efficiently than polymerase-β and additionally elongates the primer by one nucleotide [200, 205]).

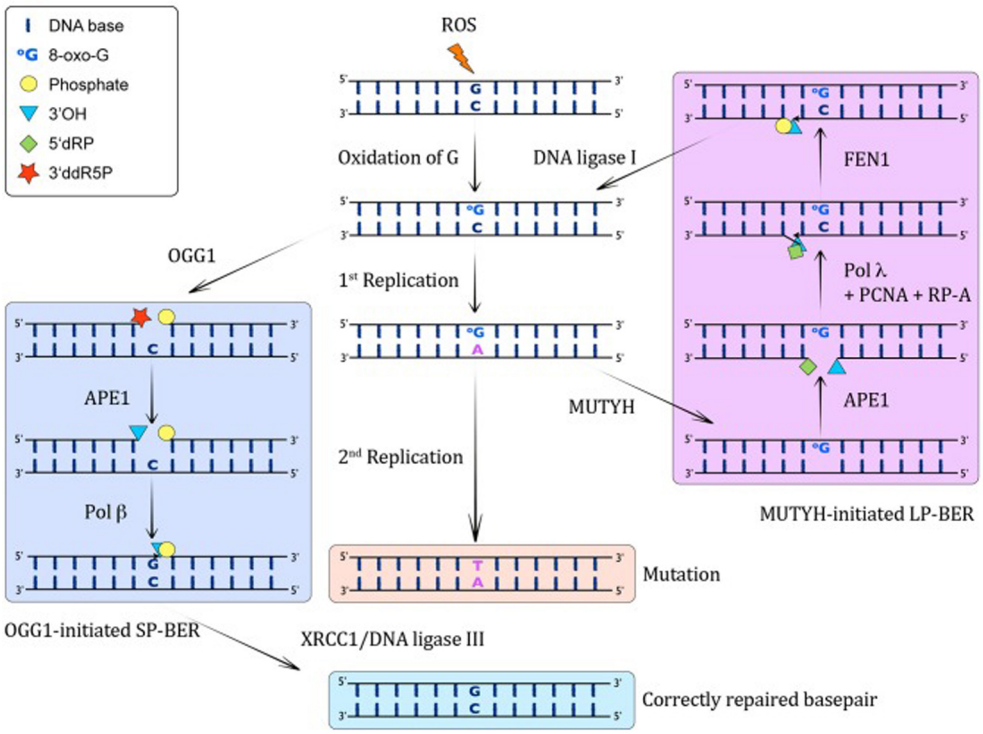

Figure 1-12: Base excision repair pathways of 8-oxoguanine (G^O).
G^0/C base pairs are addressed by OGG1-initiated short-patch BER that will remove G^0 and polymerase-β will incorporate a G. However if G^O was not repaired successfully, in the next round of replication, adenine can be incorporated opposite G^O, thus creating a target for MYH. It removes A from G^O/A mismatches via long-patch BER. The resultant gap will be filled with a C by polymerase-λ, thus resulting in a G^0/C base pair, which represents a target for OGG1 again. Unrepaired G^O/A lesions will result in G to T transversions. 5'dRP: 5' deoxyribophosphate, 3'ddR5P: 3' phospho α,β-unsaturated aldehyde. Taken from [206].

1.7.2 MYH

The effect of MYH deficiency in mice

Due to the frequent occurrence of G^O in the DNA, as well to the mutagenic potential of G^O/A mispairs, the absence of MYH would be expected to lead to increased spontaneous mutagenesis. Indeed, this is the case in MYH-deficient mouse embryonic stem cells and fibroblasts (MEFs) [207, 208]. In line with this, G^O levels were also increased in the livers of MYH knockout mice [209]. Based on these findings, an increased tumor incidence would be expected in these mice, but the available data are somewhat controversial [17, 210].

The history of MUTYH-associated polyposis (MAP)

This is not the case in humans. Twelve years ago, a new cancer type was discovered, today known as MYH-associated polyposis (MAP). This discovery was made by Al-Tassan and colleagues who studied a British family with three siblings suffering from multiple colorectal adenomas and carcinomas [191]. Sequencing of the *APC* gene in germline DNA samples excluded an inherited *APC* gene defect that is associated with familial adenomatous polyposis (FAP) and that leads to the described phenotype. Instead, colorectal tumors of the patients

exhibited unusually high proportions of somatic G:C to T:A transversions in their *APC* genes. Since MutY-deficient *E. coli* exhibit the same mutation footprint [194], the patients' *MYH* genes were analyzed and found to be mutated; the patients were compound heterozygotes for the missense variants Tyr179Cys and Gly396Asp (this nomenclature refers to the longest MYH transcript NM_001128425.1). Corresponding mutations in *E. coli* MutY caused a decreased activity of those mutants on G^O/A and G/A substrates [191]. Taken together, these findings indicated that MYH mutations were the cause of G to T transversions in the *APC* gene, which in turn led to a cancer phenotype similar to FAP.

Genotype of MAP

Although 303 unique MYH variants have been reported to date, in the LOVD database (www.lovd.nl/mutyh) in western European populations, the majority (up to 82%) was reported to be Y179C or G396D missense variants [211, 212]. Their location within the *MYH* gene is shown in Figure 1-13. Both regions are involved in G^O recognition [213], thus explaining the decreased MYH activity in these variants [191]. Many more MYH variants of MAP patients have been tested by the time and all were impaired in G^O/A repair [214-218] (see also chapter 1.8.1).

Phenotype of MAP

Germline mutations in *MYH* are inherited in an autosomal recessive manner and are associated with colorectal polyposis. Although also extracolonic tumors have been reported in MAP, they only account for a small minority. A possible explanation for the colorectal phenotype in MAP might be the exposure of the large bowel to high levels of oxidative stress [211]. Resultant *APC* and *KRAS* gene mutations in the colon can be explained by the fact that G:C to T:A mutations in MAP patients predominantly affect GAA sites [191, 192], of which the *APC* gene contains 211. Since G to T transversions in GAA sites generate a stop codon, it is not surprising that the *APC* tumor suppressor gene is specifically susceptible to inactivation in the absence of MYH. Since a germline defect in both the *APC* gene, the underlying cause for FAP, and the *MYH* gene results in *APC* mutations, it is obvious that the phenotype of MAP, exhibiting ten to a few hundred colonic adenomatous polyps [211], resembles the phenotype of attenuated FAP (10-100 adenomas) or FAP (100-1000 adenomas). In order to make the right diagnosis, analysis of the *APC* and *MYH* genes is therefore required.

MMR mutations in MAP

Apart from this, MAP caused carcinomas are near diploid and mostly microsatellite stable (MSS). The fact that microsatellite instability (MSI), a hallmark of MMR-deficient tumors, was absent in those cancers led to the assumption that defects in both BER and MMR were not compatible with cellular survival. This assumption was refuted by the description of six MAP patients that contained tumors with high MSI (MSI-H) [219, 220]. In three cases, the MSI could be attributed to loss of the MMR protein MLH1 [221-223]. In one of these cases, the lack of MLH1 expression could be traced back to biallelic methylation of the *MLH1* promoter [221] while in another case a G to T transversion in the *MLH1* gene led to complete

depletion of the MLH1 RNA levels [222]. While *MLH1* promoter methylation is rather unlikely to be a consequence of MYH malfunction, G to T transversions likely resulted from MYH dysfunction. Very recently, a seventh MAP patient with MSI-H tumors has been identified [224], Here, biallelic *MYH* mutations led to two somatic G to T mutations in the *MSH2* gene, resulting in its loss of expression, MSI and tumorigenesis [224]. Although such cases of coexistent MMR and MYH defects are rare and their biological relevance remains to be elucidated, the described studies show that both defects are not mutually exclusive as suggested [225]. Furthermore, they demonstrated that *MLH1* or *MSH2* genes can be affected by MYH deficiency [222, 224] and hence the latter can mimic Lynch syndrome and lead to a wrong diagnosis.

Posttranslational modifications of MYH

Although MYH dysfunction is mostly caused by the common Y179C and G396D missense mutations [211, 212], also its phosphorylation status seems to regulate its activity *in vitro* [226-228]. First hints were gained by Gu and Lu [226] who discovered that recombinant MYH purified from bacteria showed lower glycosylase and A/G binding activity than native MYH present in human cell extracts. Since bacterially-expressed recombinant MYH lacks posttranslational modifications (PTMs), its low activity was attributed to its phosphorylation status. Indeed, shrimp alkaline phosphatase (SAP) treatment of native MYH significantly decreased its activity [226], indicating that phosphorylation is needed for proper MYH function. This finding was confirmed by Parker *et al*. [228], who showed that protein kinase C or A (PKC or PKA) or casein kinase II treatment of human colorectal cancer cell extracts that lack *MYH* gene mutations but display defective G^O/A repair, increased their G^O/A repair capacity. At the same time, G^O/A repair did not change in extracts with functional MYH. This indicates that in proficient cells MYH is already phosphorylated to a certain extent [228]. While the corresponding phosphorylation sites on MYH were unknown at that time, Kundu *et al*. [227] discovered a Ser524 phosphorylation site, which is located in the G^O recognition domain within the PCNA binding region. This locus could explain the effect of phosphorylation on G^O/A repair. An overview about the different MYH domains is provided in Figure 1-13.

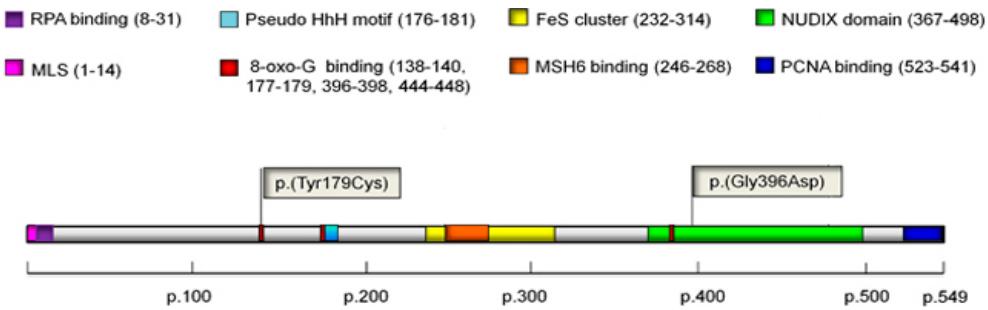

Figure 1-13: Schematic representation of the functional MYH domains.
The loci of the most common MYH variants Y179C and G396D are indicated. Modified from [216].

Although very little is known about PTMs of MYH, it was recently shown to also undergo ubiquitylation by the E3 ubiquitin ligase Mule [229]. While this modification occurs in the 475 to 535 amino acid region and is responsible for MYH degradation, non-ubiquitylated forms of MYH accumulated on the chromatin.

1.7.3 OGG1

OGG1 glycosylase/AP lyase

In contrast to MYH, OGG1 possesses not only a DNA glycosylase activity but also an AP lyase activity that allows the insertion of a nick into the DNA backbone *via* β-elimination. OGG1 is less well represented across phylogeny but present in most eukaryotic genomes. The enzyme was originally discovered in yeast in 1996, and one year later described in mammals [230-233]. It is the functional analog to the Fpg enzyme in bacteria [233, 234]. Both provide the major activity for removal of G^O opposite cytosine, but also excise other oxidized pyrimidines or ring-fragmented purines such as fapy-G [235, 236]. Many DNA glycosylases were shown to bind more strongly to the AP-sites they generated than to their substrates. This ensures protection of the noncoding and chemically unstable AP-site until cleavage of the phosphodiester bond allows processing by other BER enzymes and the release of the DNA glycosylase. Its release from the AP-site is therefore rate limiting and determines the turnover rate of the enzyme [237-241]. Surprisingly, the turnover rate of OGG1 was shown to be very slow, which was attributed to its weak lyase activity that cleaved AP-sites at half the rate of the glycosylase activity [240, 242]. However, addition of APE1 substantially increased the activity of OGG1 [240].

Posttranslational modifications on OGG1

It remains to be elucidated whether its weak lyase activity is only an *in vitro* effect of OGG1 that was purified from bacteria [240, 242], or whether this is the same *in vivo*. The former assumption would be supported by the finding of Hu *et al*. [243] who showed that OGG1 is phosphorylated by the protein kinase Cdk4 and that this modification increases its incision activity on G^O/C sites. Since proteins purified from bacteria lack proper posttranslational modifications, they would also miss such activating phosphorylation. Apart from Cdk4, two other kinases acting on OGG1 were described: c-ABL and PKC. But they failed to change OGG1 activity [243, 244]. Instead, protein fractionation of HeLa cells revealed that serine-phosphorylated OGG1 was exclusively found on the chromatin [244]. This suggests that this modification affects the localization of OGG1.

The role of OGG1 in cancer

The fact that inactivation of OGG1 in *S. cerevisiae* leads to G to T transversions suggests a role for OGG1 in cancer prevention. Although OGG1 null mice exhibit abnormal levels of G^O in their genome, the spontaneous mutation rate is only moderately increased and the mice do not develop malignancies [245, 246]. This can probably be explained by the function of MYH that acts as 'backup' pathway

and avoids G to T transversion mutations, but cannot remove the G^Os from the genome. Although *OGG1* gene defects have been observed in human lung and kidney cancer [247-251], it is currently not known to what extent they contributed to the cancer development. Overall, *OGG1* mutations may have a limited impact in the development of tumors, due to the guardian function of MYH that counteracts the mutagenic potential of G^O.

1.7.4 MTH1

MTH1

Although research mainly focuses on the damage in double stranded DNA, the free dNTP precursor pool is also susceptible to DNA damage, hence also to reactive oxygen species (ROS). To counter the incorporation of damaged dNTPs and NTPs into DNA or RNA, an enzyme, MTH1, the human analog of bacterial MutT, has evolved in order to sanitize the (d)NTP pool. To do so, it efficiently hydrolyzes oxidized purine nucleoside triphosphates, such as 8-oxo-dGTP, 8-oxo-GTP, 2-hydroxy(OH)-dATP and 8-oxo-dATP [197, 252] to monophosphates. Although seven different splice variants of MTH1 were identified, most of them encode an 18 kDa variant [253], which is mostly localized in the cytoplasm and only to a low extent in mitochondria [254]. Defects in the bacterial *mutT* gene lead to a 100 to 10'000 fold increase of A:T to C:G transversions [255], confirming its essential role in the removal of oxidized dATPs. Although MTH1 also removes oxidized dGTPs, the lack of G:C to T:A transversions can be explained by the activity of MutM/OGG1 and MutY/MYH (see chapter 1.7.1). The accumulation of transversion mutations in the absence of MTH1 suggests a role of this enzyme in cancer prevention. However, no report has described a link to human cancers to date.

Inhibition of MTH1 as novel cancer therapy

In contrast, inhibition of MTH1 was very recently described to selectively eradicate cancer cells but not normal cells, implicating that the latter can dispense with MTH1 [256, 257]. Due to this cancer-specific effect, MTH1 inhibition was suggested as a future therapeutic approach for cancer treatment [256, 257]. Gad *et al*. describe MTH1 as a 'non-oncogene addiction' target, since it is not a typical oncogene, but is indispensable for the survival of cancer cells. Hence its inhibition is suggested to cause lesser side effects in normal tissues than chemotherapeutic agents. MTH1 inhibitors could thus be more broadly applicable, irrespectively of the cancer genotype. This would also allow treatment of heterogeneous cancer tissues, as well as cancers without targetable mutations. The principle of this novel form of therapy was also described as 'cancer phenotypic lethality' [256]. However, both this and 'synthetic lethality' approaches (see chapter 1.9.4.1) have pros and cons, and the clinical applicability of 'non-oncogene addiction' target inhibition remains to be tested in future.

1.8 Mismatch repair in oxidative stress & disease

1.8.1 Mismatch repair in oxidative DNA damage response

MMR in oxidative DNA damage response

Although it is well established that 8-oxoguanine (G^O) is predominantly repaired by base excision repair (BER) (see chapter 1.7.1), several lines of evidence indicate that mismatch repair (MMR) is also involved in the processing of such lesions.

G^O/A repair in yeast

In *Saccharomyces cerevisiae*, which lacks the BER enzyme MYH, MMR was linked to oxidized DNA metabolism. Earley and Crouse described a substantial increase in G to T transversion mutations in MSH2- or MSH6-deficient strains, which was decreased under anaerobic conditions [258]. They explained the high mutation rate with adenine misincorporations opposite G^O, which would normally be prevented by MMR. This assumption was confirmed by genetic studies of Ni *et al*., showing that mutation rates and G:C to T:A transversions were synergistically increased in MutSα and OGG1 mutant strains [259]. Hence, this study proved that MutSα-dependent MMR is the major mechanism in *S. cerevisiae* by which G^O/A is repaired.

G^O repair in mice

This is different in most pro- and eukaryotes. They possess MYH glycosylase, which initiates G^O/A repair. Still, MMR-deficient cells exhibit sensitivity and prolonged G_2/M arrest upon H_2O_2 treatment [260], suggesting a role of MMR during oxidative DNA lesion processing. Though its precise role is still poorly understood, it has been substantiated in various studies. Thus, G^O levels were increased in the DNA of MSH2-deficient mouse embryonic fibroblasts (MEFs) [246], as well as in several organs of MSH2 knockout mice [208]. Studies in MMR-deficient MEFs showed that overexpression of MTH1, which eliminates dG^OTP from the nucleotide pool, reduced steady-state and H_2O_2-induced G^O levels [246], as well as mutation rates and microsatellite instability (MSI) at the *hprt*-locus [261]. Those data point towards a replication-coupled role of MMR in the removal of G^O from the newly-synthesized DNA strand [246, 261].

G^O repair *in vitro*

However, *in vitro* data revealed that G^O/A and G^O/C base pairs were inefficiently recognized by MutSα [262], unless they were located in certain sequence contexts that resembled frameshift intermediates in C or A repeats [263]. In line with this, Mazurek *et al*. [264] determined the binding efficiency of MutSα as well as its ADP to ATP exchange rate on G^O/C-containing oligos to be similar to homoduplex oligos. While both factors were increased on G^O/A oligos, they were still low compared to G/T, G^O/T or G^O/G oligos [264].

Common or distinct roles of MutSα and MYH in oxidative DNA lesion repair?

The discrepancy between the data gained *in vitro* and in mice can be explained by recent data from Gu *et al*. [35]. They demonstrated MutSα, in particular MSH6, to directly interact with MYH and to stimulate its binding and glycosylase activity on G^O/A sites, thereby raising the possibility that MYH and MutSα may act in the

same pathway. In this regard, Russo *et al*. [208] made some interesting observations. In MEFs, G^O levels increased similarly in the absence of MSH2, MYH or both proteins when compared to wild type, hence confirming a role of both proteins in the same pathway. The observations made in MEFs differed from those made in mouse organs. Several organs only showed increased G^O levels in $MSH2^{-/-}$, but not in $MYH^{-/-}$ knockout mice. A synergistic increase in G^O levels was observed in double-knockout mice, indicating independent functions of both proteins during oxidative DNA metabolism *in vivo*. This was confirmed by studies about life spans of mice, which were longer in $MSH2^{-/-}/MYH^{-/-}$ double knockout mice than in $MSH2^{-/-}$ knockout animals. This observation implies that the shorter life span of MSH2-deficient mice could be caused by MYH activity [208]. However, a completely novel role of MutSα during oxidative DNA damage repair was recently described by Zlatanou *et al.* [265]. They unraveled an alternative pathway in response to oxidative stress that is independent of BER, but that depends on MutSα-provoked PCNA monoubiquitylation and subsequent recruitment of polymerase-η. They suggest that MMR and BER might recognize different forms of oxidative DNA modifications and that their mutual interference could help in their successful repair, especially in clustered lesions. During this process, polymerase-η may enable DNA damage bypass [265].

Do MYH-MSH6 interactions play a role during MAP?

The observation about an interaction between MSH6 and MYH also attracted clinical interest. Several MYH mutations identified in MYH-associated polyposis (MAP) patients lie within or close to the MSH6 binding site, raising the question about a role of the disturbed MYH - MSH6 interaction during MAP progression. The phenotypes of different MYH variants were characterized in three studies [214-216]. All MYH mutants were strongly impaired or defective in G^O/A repair, irrespective of the location of the mutation. Studies of Bai *et al*. [214, 215] demonstrated that three MYH missense mutations R227W, V232F and R231L that lie within or adjacent to the putative MSH6 binding domain and are associated with MYH polyposis, do not affect the interaction of the mutant with MSH6. Thus, the question whether a disturbed MSH6 - MYH interaction would play a role during MAP progression, currently remains open.

1.8.2 The role of mismatch repair in cancer and drug resistance

HNPCC

Defects in MMR were linked to Lynch syndrome, also known as hereditary nonpolyposis colon cancer (HNPCC) and predispose to tumors of the colon, endometrium, ovary or other tissues [267]. Those tumors display a mutator phenotype known as microsatellite instability (MSI), which results from defective repair of insertion/deletion loops during replication. HNPCC accounts for approximately 3% of all colorectal cancer cases [267, 268]. It is mainly linked to defects in the MMR genes, which can be caused by hypermethylation of the *MLH1* promoter or germline mutations in the MMR genes *MLH1*, *MSH2*, *MSH6*, *PMS2*

and *PMS1* [268-270]. The majority of mutations affect *MLH1* (50%) and *MSH2* (40%), only to a minor extent *MSH6* (10%) and *PMS2/PMS1* genes [268]. Also knockouts of the MMR genes *MSH2*, *MSH3*, *MSH6*, *MLH1*, *PMS1*, *PMS2* and *EXOI* in mice brought about MSI and therewith linked tumor development, reflecting the known functions of MMR proteins in tumor suppression. The tumor phenotypes in mice are summarized in Table 1-5.

Table 1-5: Phenotypes of MMR-deficient knockout mice.

Gene	MSI	Tumor	Fertility
MSH2	Yes	Lymphoma, GI, skin, and other tumors	Yes
MSH3	Yes	Tumor free or GI tumors at a very late age	Yes
MSH6	Low MSI in dinucleotide repeats	Lymphoma, GI and other tumors	Yes
MLH1	Yes	Lymphoma, GI, skin, and other tumors	No
PMS1	Mononucleotide repeats only	None	Yes
PMS2	Yes	Lymphoma and sarcoma	Male infertile
MLH3	Yes	Not available	No
EXOI	Yes	Lymphoma	No

GI = gastrointestinal. Adapted from [271].

MYH mutations in HNPCC

Interestingly, it has been shown that some HNPCC patients with *MSH6* germline mutations also exhibited *MYH* mutations [225, 266], as described in the following two studies. Puijenbroek *et al*. identified a HNPCC patient with a *MSH6* germline mutation that was at the same time compound heterozygous for *MYH* [225]. The question whether *MYH* was mutated due to dysfunction of MSH6, could be excluded since nuclear MSH6 was still expressed and the tumor did not show microsatellite instability (MSI), a hallmark of MMR deficiency. It only exhibited G to T transversions [225], resulting from MYH-defects. A study of Niessen *et al*. [266] showed that colorectal and endometrial tumors with *MSH6* missense mutations showed significantly higher frequencies of coexisting monoallelic *MYH* mutations than MMR-proficient colorectal cancer patients. But again, *MYH* mutations were not caused by MSI and the link between MMR and *MYH* gene mutations in those cases remains unclear. It also remains to be elucidated whether such coexistence of BER and MMR mutations leads to faster progression of cancer [221].

MMR defects confer DNA damage tolerance

Since MMR is not only involved in repair but also in the detection of various kinds of DNA damage, MMR-deficient tumors show resistance to many drugs. Treatment of those cancers therefore represents a major challenge. Resistance has

been reported to methylating agents (MNNG, MNU, temozolomide, procarbazine), alkylating agents (busulfan), platinum-containing drugs (cisplatin, carboplatin), antimetabolites (6-thioguanine) and topoisomerase II inhibitors (etoposide, doxorubicin) [272]. For instance, S_N1 methylating agents such as MNNG, MNU or temozolomide, generate a variety of adducts, including the cytotoxic lesion O^6-methylguanine [273]. In MMR-proficient cells, ^{Me}G/C and ^{Me}G/T would be recognized by MutSα [274]. As ^{Me}G is in the template strand, MMR would repeatedly attempt to repair the lesion until the replication fork would arrest. This is known as the futile cycling model. In the absence of MMR, cells would not process the lesions and survive, at the cost of mutations [40, 275]. Interestingly, a PARP inhibitor AG14361 has been shown to restore temozolomide sensitivity in MMR-deficient cells, potentially due to impaired BER activity at other temozolomide-induced DNA lesions, such as N7-methylguanine or N3-methyladenine [276]. However, the futile cycling model could also explain resistance to other alkylating agents, platinum drugs and 6-thioguanine that form base pairs resembling non-Watson-Crick pairs, thus representing potential targets for MutSα. The mechanism for resistance to topoisomerase II inhibitors is less defined yet [272]. Other drugs were reported to be equally effective in MMR-deficient and -proficient tumors. An overview is provided in Table 1-6.

Table 1-6: The effect of loss of MMR on sensitivity to cytotoxic agents.

Resistance	No effect
Busulfan	BCNU [a]
Carboplatin	Melphalan
Cisplatin	Oxaliplatin
Doxorubicin	Paclitaxel
Etoposide	Perfosfamide
Mercaptopurine	Transplatin
MNNG	
MNU	
Procarbazine	
Temozolomide	
6-Thioguanine	

[a] BCNU, 1,3-bis(2-chloroethyl)-1-nitrosourea.

Adapted from [272].

For instance, the nitrogen mustard melphalan, a bifunctional S_N2 alkylator, is equally effective in MMR-proficient and -deficient cells [272, 277], possibly because it does not form DNA adducts, such as ^{Me}G [278]. Paclitaxel, a mitotic inhibitor, does not interfere with DNA and is therefore effective also in cells lacking MMR. While MMR-deficient cells are 2-fold resistant to Cisplatin [279, 280], sensitivity of cells to the platinum-containing drugs Oxaliplatin and Transplatin seems not to be affected by MMR status [272]. Interestingly,

interstrand crosslinking agents, such as 1-(2-chloroethyl)-3-cyclohexyl-nitrosourea (CCNU) or 1,3-bis(2-chloroethyl)-1-nitrosourea (BCNU) are the only agents described to date, that are more toxic to MMR-deficient than -proficient cells [281-283] and hence deserve to be examined in more detail. However, this difference is not large and has not been seen in all experimental systems [277]. In conclusion, since effective treatments of MMR-deficient tumors are still rare, drugs making use of MMR deficiency according to the concept of synthetic lethality (chapter 1.9.4.1), could be a promising alternative.

1.8.3 Synthetic lethality in MMR-deficient tumors

Synthetic lethality in MMR-deficient tumors

A body of data described sensitivity to oxidative stress and accumulation of 8-oxoguanine (G^O) in genomic DNA of MMR-deficient cells [208, 246, 260] (see chapter 1.8.1). Oxidative DNA damage thus represents an exception to the other drugs and might be a good target for exploiting the concept of synthetic lethality (SL) in MMR-deficient tumors. Indeed, some work in this field has been done by the research group of Alan Ashworth. A small molecule library screen identified the chemotherapy drug Methotrexate (MTX) to be specifically lethal to MSH2-deficient cells [284]. Further experiments revealed that treatment with this drug resulted in increased G^O levels in both MMR-proficient and -deficient cells. In MSH2-proficient cells, G^Os were rapidly cleared, while they remained in the DNA of MSH2-deficient cells, potentially explaining the biological effect of MTX in MutSα-deficient cells. The accumulation of G^O upon methotrexate treatment was attributed to the antimetabolite's property to inhibit dihydrofolate reductase (DHFR), which is involved in folic acid synthesis [284]. This in turn has antioxidant properties. This discovery resulted in a currently ongoing phase II clinical trial, testing the response of metastatic MSH2-deficient colorectal cancers to methotrexate [clinicalTrials.gov Identifier: NCT00952016]. Another study reported MSH2 to be synthetic lethal with polymerase-β (POLB), while MLH1 was synthetic lethal with polymerase-γ (POLG) [285]. Upon POLB/G knockdown, MMR-deficient cells exhibited lower survival than their MMR-proficient counterparts. In the absence of MSH2/POLB, nuclear G^O levels were increased, while MLH1/POLG synthetic lethality led to accumulation of G^O in mitochondria [285]. Those data suggested a BER-independent or BER-backup role for MMR in oxidative DNA damage response and proposed polymerase targeting as a therapeutic approach. A recent publication of the same research group uncovered PTEN-induced putative kinase 1 (PINK1) to be synthetic lethal with MSH2, MSH6 or MLH1 dysfunction [286]. PINK1 protects against oxidative stress-induced apoptosis by suppressing cytochrome c release from mitochondria [287]. Knockdown of PINK1 resulted in nuclear and mitochondrial accumulation of G^O in

both MutSα- and MutLα-deficient backgrounds. Thus, based on the principle of synthetic lethality, PINK1 was also proposed as therapeutic target in such tumors [286].

1.9 PARP-1 and PARP inhibition

1.9.1 PARP family

PARP family

In 1963, a NAD-dependent protein modification, today known as poly(ADP-ribosyl)ation (PAR), was described for the first time [288]. Since then, 17 enzymes containing an ADP-ribosyltransferase catalytic core have been identified and this family was named PARP, which stands for poly(ADP-ribose) polymerase. In fact, some of the PARP family members were shown to be mono- and not poly-ADP-ribosyltransferases. Hence, the name PARP does not fit to the catalyzed reactions and structural features of all of the PARP family members and a new nomenclature had therefore been proposed lately [289]: ARTD, an abbreviation for ADP-ribosyltransferase Diphteria toxin-like. However, the term PARP is still more conventional. Among all family members, the best characterized is poly(ADP-ribose) polymerase-1 (PARP-1). Its enzymatic activity and function, especially during DNA repair, will be discussed in detail in the following sections.

1.9.2 Structure & function of PARP-1

Structure of PARP-1

The PARP-1 protein consists of several structural and functional domains (Figure 1-14). The amino-terminal DNA binding domain contains three zinc finger motifs, of which are two involved in DNA binding. The BRCT domain can be auto-modified by PAR or mediate interactions with other proteins. While the function of the WGR (Trp-Gly-Arg) motif is as-yet unknown, the carboxyl-terminal catalytic domain is responsible for NAD^+ binding to the highly conserved signature (Sig) motif, which defines the PARP family of proteins. The PARP regulatory domain (PRD) within the catalytic domain interacts with the substrate-binding site and is thought to control branching of the PAR chain [290].

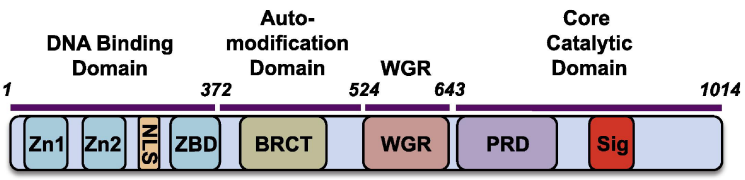

Figure 1-14: Structural and functional domains of PARP-1.
PARP-1 is a 116 kDa protein and contains the following domains. Zn1, Zn2 (amino acids 1-372): zinc finger motifs, ZBD: zinc binding domain, NLS: nuclear localization signal, BRCT: BRCA1 C-terminus motif within an auto-modification domain (amino acids 372-524) also serving as site for protein-protein interactions, WGR (amino acids 525-643): unknown function. The carboxy-terminal catalytic domain (amino acids 653-1014) contains a PARP regulatory domain (PRD) and a highly conserved signature motif (Sig). Taken from [290].

Enzymatic activity of PARP-1

PARP-1 can be activated by DNA breaks. Following its activation and binding to DNA breaks, the intrinsic enzymatic activity of PARP-1 catalyzes the transfer of ADP-ribose units from nicotinamide adenine dinucleotide (NAD^+) onto target proteins or onto itself. As the polymer is negatively charged, auto-modification of PARP-1 leads to its repulsion and dissociation from the DNA. The enzymatic actions of poly(ADP-ribose) glycohydrolase (PARG) and ADP-ribose hydrolase (ARH) allow recycling of the PAR polymers and the PARP-1 molecule itself (Figure 1-15).

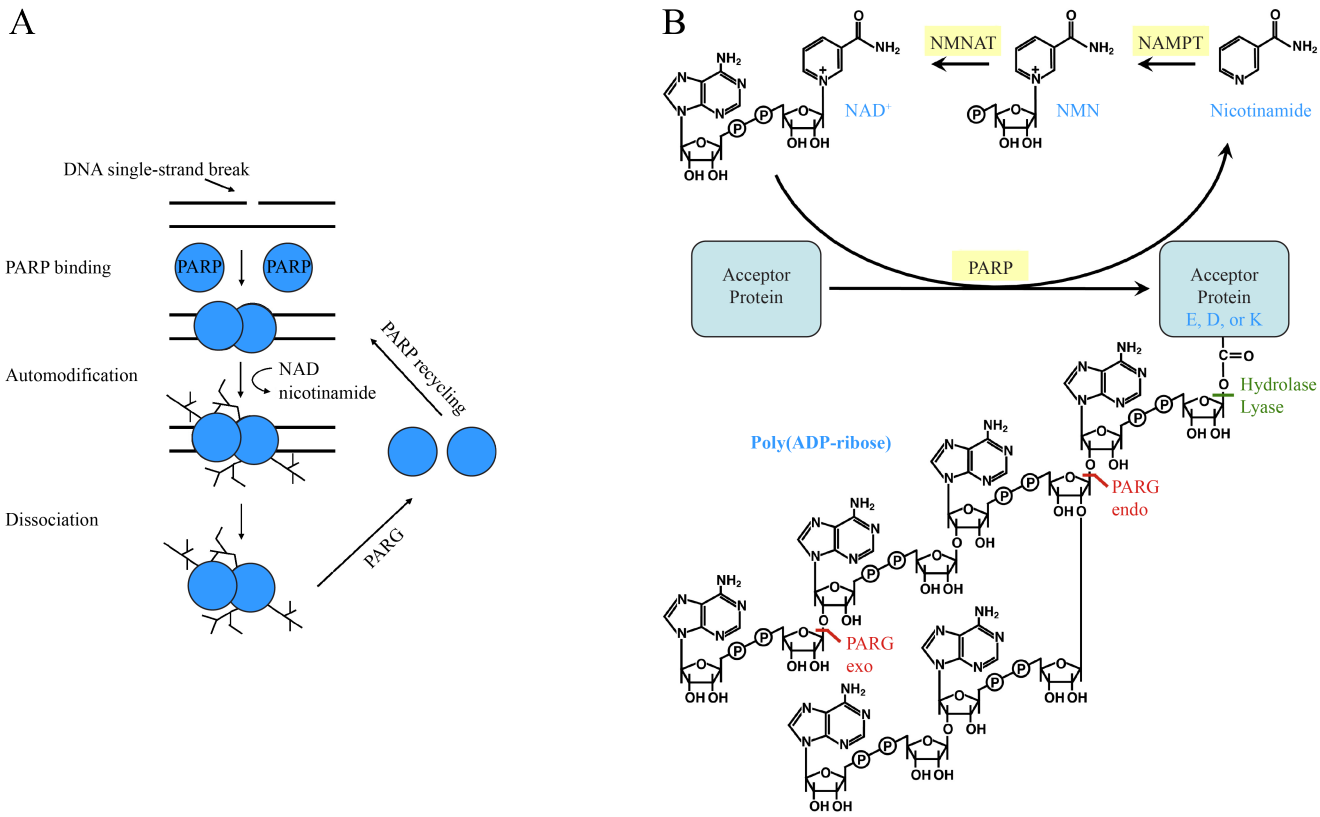

Figure 1-15: Enzymatic activities of PARP-1 and PARG.
(A) PARP-1 on DNA strand breaks. DNA binding and activation of PARP-1 results in auto-modification of the protein by PARylation. After dissociation of the enzyme from the DNA, poly(ADP-ribose)glycohydrolase (PARG) mediated PAR degradation allows recycling of the PAR polymers and PARP-1. Taken from [291]. (B) Biosynthesis of NAD^+ and PAR as well as degradation of PAR polymers. The latter is mediated by PARG, which hydrolyses glycosidic ribose-ribose bonds, and subsequently by ADP-ribose hydrolase (ARH), which removes the remaining mono-ADP-ribose from the protein. Taken from [292].

The different roles of PARP-1

PARP-1 is an abundant nuclear protein, playing a key role in the regulation of a variety of nuclear processes, including DNA repair and gene regulation such as chromatin remodeling and transcription [290]. PARP-1 operates *via* three main mechanisms: i) its intrinsic catalytic domain allows posttranslational modification of other target genes, which modulates their function. ii) Also auto-modification can change its interacting properties with other proteins. iii) Furthermore, its BRCT

domain allows PAR-independent interactions with a variety of other proteins. Here, PARP-1 might serve as a scaffold protein, recruiting and directing proteins to their place of action. Other posttranslational modifications on PARP-1, e.g. ubiquitylation, acetylation, phosphorylation and SUMOylation have also been reported [292], thus broadening the mode of action of PARP-1.

PARP-1 as chromatin remodeler

Remodeling of chromatin represents one of its major tasks. Thus, it was shown that PARP-1 activity on histone H1 [293], or other chromatin remodeling enzymes like ALC1 [294], leads to relaxation of the chromatin. Other data revealed PARP-1 to be involved in chromatin condensation by a mechanism in which the histone macroH2A1.1 senses PARP-1 activation and transiently compacts chromatin [295].

PARP-1 regulates gene expression

Furthermore, PARP-1 was shown to regulate gene expression by modulating the methylation status of DNA. This could be achieved through inhibition of Dnmt1 methyltransferase by polymers of ADP-ribose [296]. Other studies showed PARP-1 to stimulate or inhibit activators of transcription such as NF-κB [290].

1.9.3 PARP-1 in DNA repair

PARP-1 has also been linked to various DNA repair processes. The following sections will provide a detailed overview about current knowledge of its diverse roles during homologous recombination, non-homologous end-joining, mismatch repair and base excision repair, whereas its role during the latter is by far most intensively studied.

1.9.3.1 PARP-1 in homologous recombination

PARP-1 in homologous recombination

Several studies showed that loss of PARP-1 did not affect homologous recombination (HR) of endonuclease-induced DNA double strand breaks (DSBs) or gene targeting efficiency [297, 298]. In contrast, hydroxyurea (HU) treatment, which causes dNTP depletion and replication fork arrest, led to an increased number of Rad51 foci [297], elevated levels of sister chromatid exchanges (SCEs) [298] and hence a hypermutagenic phenotype in cells that lacked PARP-1. In line with this, overexpression of PARP-1 in hamster cells caused over-accumulation of poly(ADP-ribose) and suppression of alkylation-induced SCE [299]. Overall, those data suggest that PARP-1 prevents inappropriate DNA recombination during repair and reactivation of stalled replication forks, while being dispensable in HR of DSBs. Insights into how PARP-1 could control HR processes at stalled replication forks, were gained by Bryant and colleagues. They observed PARP-1 binding to and activation by stalled replication forks, followed by PARP-1- and Mre11-mediated replication fork restart. This was proposed to happen by PARP-1-mediated Mre11 recruitment to the fork and Mre11-promoted end resection [300].

1.9.3.2 PARP-1 in non-homologous end-joining

PARP-1 in c-NHEJ

To date, only a few studies have addressed a possible role of PARP-1 in classical non-homologous end-joining (c-NHEJ). Most of them point towards its involvement *via* interaction with DNA-PK. *In vitro* studies revealed a stimulatory effect of PARP-1 on the kinase activity of DNA-PK by PARylation. Indeed, DNA-PKcs has been identified as a PAR-associated protein [301], indicating that PARylated DNA-PK exists *in vivo*. Vice versa, DNA-PK can phosphorylate PARP. Although not well understood yet, this mutual interference of the two enzymes suggests a coordinated function of them during double-strand break repair [302]. Their interaction was recently confirmed *in vivo* by the purification of a PARP-1/DNA-PK complex. Electron microscopy of this complex revealed that PARP-1 caused major conformational changes in the DNA-PK synaptic dimer assembly [303]. However, further studies will be required for the better understanding of the role of PARP-1 during c-NHEJ.

PARP-1 in alt-NHEJ

If c-NHEJ is genetically impaired, a slowly acting backup pathway, identified as alternative NHEJ (alt-NHEJ), can still perform repair of a large number of double strand breaks (DSBs) [304] (see chapter 1.4.2). It is widely accepted that PARP-1 together with the XRCC1 - DNA ligase III complex is involved in alt-NHEJ. *In vitro* studies showed that those three enzymes promote end-joining, independent of the c-NHEJ complex DNA-PK/XRCC4-ligase IV [305]. The function of PARP-1 in this backup pathway was confirmed by the finding that its inhibition compromises rejoining of DNA DSBs in the absence of the c-NHEJ factor Ku70/80 [306]. The role of PARP-1/XRCC1/DNA ligase III as back-up pathway, can be explained by competition of PARP-1 and Ku70/80 for binding to DNA DSBs. Due to the higher binding affinity of Ku70/80 to irradiation-induced lesions, PARP-1 activity on such lesions is suppressed and becomes only apparent in the absence of Ku70/80 [306]. The involvement of PARP-1 in alt-NHEJ, could also explain the embryonic lethal phenotype of PARP-1/Ku80 double null mice [307].

1.9.3.3 PARP-1 in mismatch repair

MSH6 contains a PAR binding motif

A potential role of PARP-1 in mismatch repair (MMR) is also rather unexplored yet. The studies that have been done propose PARP-1 to be involved in this process. *In silico* studies suggested the MutSα component MSH6 to contain a poly(ADP-ribose)- (PAR-) binding sequence motif (see chapter 1.3.2.2), consisting of 20 amino acids that contain a cluster rich in basic amino acids and a pattern of hydrophobic amino acids interspersed with basic residues [81]. Polymer blot analysis confirmed PAR to interact with the 295-317 amino acid region of MSH6 [81], suggesting that PAR binding of MSH6 could interfere with the mismatch recognition step of MutSα.

MSH6 interacts with PARP-1

It was recently reported that MSH6 recruitment to the chromatin *in vivo* might be mediated by an interaction between the PWWP domain of MSH6 and the histone mark H3K36me3 [73]. Interestingly, unpublished data from our laboratory [370] revealed the PWWP domain of MSH6 to physically interact with PARP-1, which in turn is known to modulate chromatin. It would be interesting to elucidate whether PARP-1 is involved during the recruitment process of MSH6 to chromatin *in vivo*. The fact that MSH6 also contains a PAR binding site [81], would appear to support such an idea.

PARP-1 in MMR

Interestingly, the research group of Paul Modrich discovered that PARP-1 enhanced the mismatch-dependence of 5'-directed excision in human mismatch repair *in vitro* [308]. In other words, the effect that 5' nicked mismatch-containing plasmids are preferentially repaired over 5' nicked homoduplex substrates, was increased in the presence of PARP-1. Such an effect of PARP-1 was not observed in 3'-directed excision [308]. They further narrowed this effect of PARP-1 to its Zinc finger-containing DNA binding domain, as well as to its BRCT domain. The latter was shown to physically interact with MutSα, RPA, EXOI and RFC. The catalytic domain of PARP-1, responsible for NAD^+ binding, was not involved in this effect. Overall, they attributed the observed effect to a preferential suppression of EXOI by PARP-1 on 5' nicked homoduplex substrates than on 5' nicked heteroduplex substrates. Experiments suggested that a function of PARP-1 on the nick itself was rather unlikely. They hereby postulated PARP-1 to inhibit unspecific EXOI activities on 5' nicked homoduplex substrates. Since EXOI acts only in 5' to 3' direction, 3' nicked substrates are not affected by unspecific EXOI degradation, and therefore do not have to be protected by PARP-1-mediated EXOI suppression.

1.9.3.4 PARP-1 in base excision repair

PARP-1 in BER

Originally, base excision repair (BER) was described to follow a 'passing the baton' model [309], a well-coordinated process, in which single-strand break intermediates deriving from glycosylase and endonuclease/lyase activities, are passed from one enzyme to another and are inaccessible for other enzymes. This model was challenged by the discovery of PARP-1, which was shown to bind those 'inaccessible' nicks and thus being involved in BER. First hints about a role of PARP-1 in BER were gained with PARP-1 knockout mice. Those are viable and fertile and have no overt phenotype. Nevertheless, they are sensitive to monofunctional alkylating agents and γ-irradiation that cause a variety of lesions, including damage that is recognized by base excision repair (BER) [310, 311]. Other studies linked the roles of PARP-1 and poly(ADP-ribosyl)ation (PAR) to oxidative stress [312, 313], which also generates lesions that are addressed by BER. The involvement of PARP-1 in BER was further substantiated by various studies. Thus it was shown to physically and/or functionally interact with key

actors of the BER process like OGG1 [314], XRCC1 [315, 316], DNA ligase III and polymerase-β [317]. Also the processing of UNG- or OGG1-generated abasic (AP) -sites by BER was impaired in PARP-1-depleted extracts [316]. Moreover, PARP-1 was shown to bind to AP-sites *in vitro* and to be extensively modified by poly(ADP-ribosyl)ation upon APE1 activity at those sites [318].

Two-step BER model

These findings lead to a 'two-step' BER model [319] in which, upon generation of a nick by a glycosylase and endonuclease, PARP-1 detects and binds the strand break *via* its zinc finger domain (Figure 1-16). Thus, PARP-1 transiently protects the nick [320, 321] and simultaneously auto-modifies itself and other enzymes by PAR. It serves as a 'recruiting platform' for XRCC1, polymerase-β and DNA ligase III on the nick. Since the PAR modification on PARP-1 is negatively charged, this leads to a reduced affinity of the enzyme for DNA, it dissociates and allows access to the other repair proteins. However, although such model and other studies suggest that the presence of PARP-1 stimulates the BER process [316-318] and therefore accelerates single-strand break (SSB) repair [313], other studies show that PARP-1 is not absolutely required in these processes.

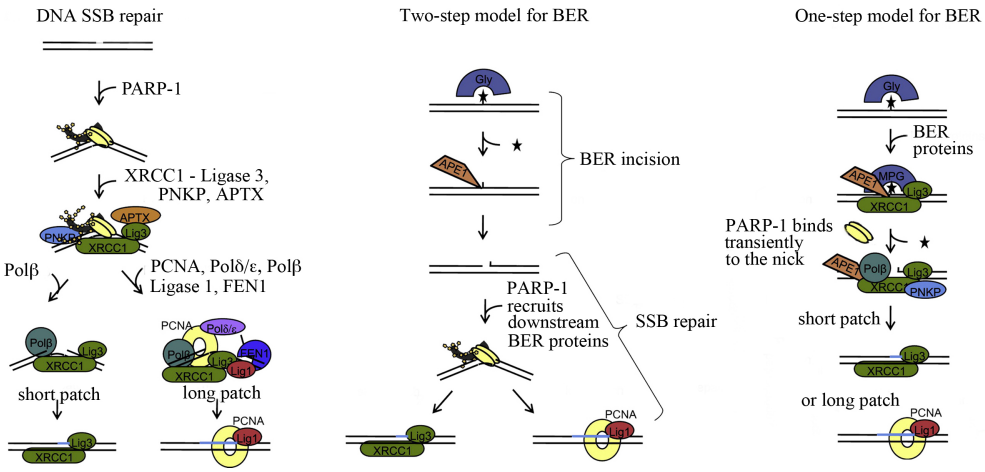

Figure 1-16: Illustration of DNA SSB repair, and two models of BER.
The 'two-step' BER model consists of strand incision by a glycosylase and endonuclease and subsequent single-strand break repair. The latter includes PARP-1 binding to the nick and auto-PARylation of PARP-1, which is required for the recruitment of the downstream BER enzymes. The 'one-step' BER model does not depend on PARP-1 activity. PARP-1 can bind transiently to the nick, but is not required for an efficient BER process. Modified from [319].

One-step BER model

While mice lacking the key BER enzymes APE1 [322], polymerase-β [323] or XRCC1 [324] are not viable, PARP-1 knockout mice are [310, 311], indicating that PARP-1 is not an essential factor of the BER machinery. Furthermore, studies of Satoh and Lindahl demonstrated that, in the presence of NAD^+, single-strand break-containing plasmids were repaired to the same extent when PARP-1 was present or absent in cell extracts [325]. Data from that time were supported by recent studies of Ström *et al.* [326], in which the absence of PARP-1 did not affect

alkylation-induced SSB repair. Those studies support the currently accepted 'one-step' BER model (Figure 1-16), in which the nick protector PARP-1 can transiently bind to DNA glycosylase-initiated nicks, but is not essential for the following BER process.

1.9.4 PARP inhibition

1.9.4.1 The principle of synthetic lethality

History of PARP inhibitors

PARP requires NAD^+ for its enzymatic activity. To inhibit PARP, the development of NAD^+-competitive nicotinamide mimics is therefore evident. Thus, the first PARP inhibitor (PARPi) which was described in 1971 was nicotinamide itself [327]. Since then, a multitude of PARP-inhibiting NAD^+ analogs have been developed (Figure 1-17). Optimization of potency of inhibition and substrate specificity of these compounds have been the biggest challenges and are, due to the high sequence similarities amongst the different PARP family members, still challenging today. Although the reason for PARP inhibitor-mediated cell death was not understood yet, first clinical studies with this drug for cancer therapy were already performed in 2003. However, first important observations about the specific effect of PARP inhibitors in certain tumor tissues were only made in 2005. BRCA1- or BRCA2-deficient tumors were shown to be specifically killed by PARP inhibitors [328, 329]. The use of a DNA repair enzyme inhibitor, which specifically kills a tumor holding a certain mutation, in the absence of any exogenous DNA damage, presented a novel kind of cancer treatment at this time [328]. This observation represents an example for the 'concept of synthetic lethality' and was probably the first example that attained clinical application.

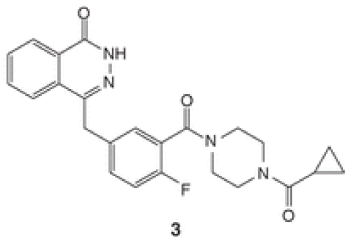

3
Olaparib

Figure 1-17: Chemical structure of the PARP inhibitor and NAD^+ analog Olaparib. Taken from [330].

Concept of synthetic lethality

The 'concept of synthetic lethality' is defined as a situation in which a defect in one of two genes individually has no implication on cell's fate, while a defect in both genes leads to cell death.

Original model

Synthetic lethality of BRCA1- or BRCA2 mutations with inhibition of PARP-1 was originally explained based on the 'two-step' BER model. Since in this model

PARP-1 is required for recruiting XRCC1, polymerase-β and DNA ligase III repair complex to glycosylase/endonuclease-induced nicks, it was assumed that inhibition of PARP-1 would interrupt the pathway and lead to an accumulation of single-strand breaks (SSBs). Unrepaired SSBs would collapse replication forks into double-strand breaks, which would normally be repaired by BRCA-dependent homologous recombination (HR) (see chapter 1.4.1). But in the absence of BRCA, cells would undergo apoptosis [328, 329]. Furthermore it was assumed that PARP inhibition would show the same effect as the absence of the PARP-1 enzyme itself.

Trapping model

Lately, this assumption was challenged by the following findings. The idea that PARP inhibition would lead to the same phenotype as the absence of PARP-1 was refuted by the observation that BRCA-defective cells were shown to be more sensitive to PARP inhibitors than to siRNA-mediated PARP-1 knockdown [328]. In line with this, depletion of PARP-1 did not affect alkylation-induced SSB repair, while the inhibition of PARP-1 lead to SSB accumulation [326]. Furthermore, already early *in vitro* studies done by Satoh and Lindahl demonstrated that, in the presence of NAD^+, single-strand break-containing plasmids were equally well repaired irrespectively of whether PARP-1 was present or absent, but less efficiently repaired upon PARP inhibition [325]. Also siRNA-mediated depletion of XRCC1, which should also interrupt BER repair and leave behind SSBs, did not sensitize human BRCA2-deficient ovarian cancer cell lines [331]. Since these data showed that the absence of neither BER enzymes nor PARP-1 was toxic to HR-deficient cells but only the inhibition of PARP-1, a new so-called 'trapping model' was proposed, which represents the currently accepted model. It suggests that PARP-1 transiently binds to SSBs. But since upon PARP-1 inhibition, PAR auto-modification would be inhibited by the PARP inhibitor, PARP-1 would be trapped on the lesion (Figure 1-18). This enzyme-DNA complex could then be converted to a more toxic lesion during replication [319], representing a substrate that can only be repaired in the presence of HR.

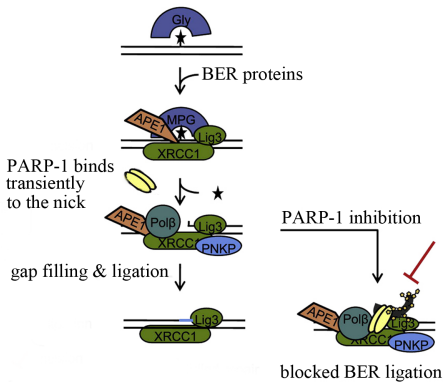

Figure 1-18: Trapping model of PARP-1 inhibition. Modified from [319].

NHEJ confers PARPi sensitivity in HR-deficient cells

One explanation of how PARP inhibition could lead to cell death of HR-deficient cells was delivered by Patel *et al*. [331], who showed that non-homologous end-joining (NHEJ) was stimulated specifically in HR-deficient cells upon PARP inhibition. Disabling of NHEJ by DNA-PK inhibition rescued sensitivity of these cells towards PARP inhibitors, suggesting that error-prone NHEJ might cause genomic instability in these cells.

Future perspective

The progresses that were made in understanding the effects of PARP inhibition are important for efficient clinical applications. While the 'original model' implicates that PARP inhibition is most effective in cells with low PARP-1 levels, the currently accepted 'trapping model' suggests the opposite. Such understanding is especially valuable in terms of personalized medicine.

1.9.4.2 Clinical applications of PARP inhibitors

Clinical application

While PARP inhibitors represent promising drugs for the treatment of cardiovascular diseases and diabetes [332], their widest and most advanced application concerns the treatment of cancer. First clinical trials with potent PARP inhibitors started in year 2003 [333]. Several different PARP inhibitors are currently tested in clinical trials [330]. One of the most advanced and promising inhibitors is Olaparib (AZD2281) (Figure 1-17), which is currently in phase III clinical trials. Within the clinical studies, two different treatment approaches are pursued. The small molecules can be either applied as single agents or as combination treatment.

Monotherapy

The potency of PARP inhibitors as monotherapy for cancer cells with defects in DNA repair genes was discovered in 2005 [328, 329]. This finding was evaluated by following phase I clinical studies. Amongst them, the PARP inhibitor Olaparib was successfully tested in BRCA1 or BRCA2 mutation carriers [334]. Since 2013, the drug is being further evaluated as monotherapy in patients with BRCA mutated ovarian cancers in a phase III clinical study [clinicalTrials.gov Identifier: NCT01844986]. In the last couple of years, an increasing amount of other gene mutations has been reported to be synthetic lethal with PARP inhibition, such as PTEN [335]. PTEN gene mutations have been encountered in several cancers like prostate, endometrial, melanoma or brain tumors [330] and have been reported to cause homologous recombination defects [335].

Monotherapy for MMR-deficient tumors

Also colorectal cancer types that display microsatellite instability (MSI), accounting for 15% of all colorectal cancers, were tested for response to PARP inhibition in a phase II trial [clinicalTrials.gov Identifier: NCT00912743]. These studies could be promising, since 80% of MSI tumors were shown to be mutated in MRE11 [336], a protein also being involved in homologous recombination. Since the MRE11 gene contains a poly(T)11 tract, it might be predisposed for secondary mutations caused by MSI. Indeed, experiments showed that MRE11 deficiency in

microsatellite unstable colorectal cancer cells resulted in increased sensitivity to PARP inhibition [337]. A similar observation was done in ATM-deficient mantle cell lymphoma cells [338].

Combination therapy

Other tumor types, which do not fulfill the prerequisite of synthetic lethality with PARP inhibitors, can be treated using combination therapy. Thus, additional exogenous DNA damage, which would normally be repaired in a PARP-dependent manner, will remain when PARP is inhibited. Another possibility is, that the HR-machinery would be saturated by the tremendous amounts of generated DNA lesion - PARP-1 complexes. Examples are combinations with alkylating agents, topoisomerase I inhibitors, platinum drugs, radiation, nucleoside analogs or antimetabolites. This multiplicity of combinations resulted in a large number of clinical trials.

Combination therapy for MMR-deficient tumors

Because of an increased tolerance to DNA damage, MMR-deficient tumors are resistant to some standard cancer chemotherapies such as platinum-based drugs, alkylating agents or inhibitors of topoisomerases, raising the need for more effective treatments. Interestingly, a study by Curtin *et al*. revealed that MMR-deficient colorectal carcinoma cells that were resistant to the alkylating agent Temozolomide could be sensitized by additional treatment with the PARP inhibitor AG14361 [276]. A similar observation was made with MMR-deficient leukemia cells using the PARP inhibitor Veliparib (ABT-888) [339]. In both studies this effect was more pronounced in MMR-deficient than in -proficient cells, and should therefore be further explored.

Resistance to PARP inhibitors

As is the case for many drugs, resistance towards PARP inhibitors has been reported in preclinical and clinical settings. Two main molecular mechanisms for this phenomenon have been observed. On the one hand it was shown that secondary mutations of BRCA1 or -2 genes could restore the proteins function. In particular in CAPAN1 cells, an intragenic deletion reconstituted the open reading frame of BRCA2, allowing expression of new functional isoforms [340]. On the other hand, upregulation of P-glycoproteins, key transporters involved in pumping xenobiotics out of cells, was described [341]. One explanation for that could be the role of PARP-1 as a 'master epigenetic regulator of gene expression', thereby also regulating P-glycoprotein promoter activity [342, 343]. Although drug resistance is a crucial issue, PARP inhibitors have tremendous therapeutic potential. New PARP inhibitors that should overcome resistance are currently being developed. One example is the inhibitor AZD2461, which is not targeted by P-glycoprotein.

2 Aims

This introduction described the various repair mechanisms that contribute to the maintenance of genomic integrity, with a particular focus on repair pathways and proteins that are involved in oxidative DNA damage repair. Since oxidative stress is the major endogenous source of DNA damage and therefore linked to cancer and aging, it attracted our particular interest and we set out to learn more about its effect on cellular repair metabolism. It is well established that base excision repair (BER) is the main repair pathway of oxidative DNA lesions, such as 8-oxoguanine (G^O). Here, the DNA glycosylases MYH and OGG1 are of unique importance, since they synergistically contribute to G^O removal from the DNA (see chapter 1.7.1). During the past years, experimental evidence implicated also postreplicative mismatch repair (MMR) in the processing of oxidative DNA damage, but the mode of its involvement is largely unknown (see chapter 1.8.1).

I set out to elucidate the above phenomenon. Given that MMR was reported to exert a stimulatory effect on BER of G^O, I decided to study how MMR and BER interact at sites of oxidative DNA damage. Within this project, I wanted to test whether BER processing of G^O affects MMR activity and fidelity.

An unbiased approach that might deliver additional insights into the largely unknown role of MMR in the metabolism of oxidative DNA damage is the characterization of the interactome of the main mismatch binding factor MutSα. A second aim of my PhD thesis was thus to generate expression vectors and cell lines that could be used for future mass spectrometric analysis of proteins interacting with MSH6 and/or MSH2.

The third aim of my work focused on the role of PARP-1 and PARP inhibition during BER of oxidative DNA lesions. PARP inhibitors efficiently kill BRCA-deficient breast and ovarian cancer cells. PARP inhibition leads to lethality, because single-strand break (SSB) - PARP-1 complexes that persist in the DNA upon PARP inhibition give rise to toxic lesions during replication that can only be repaired by homologous recombination (HR), which is defective in BRCA-deficient cells. However, the source of the SSBs is currently unknown. Since the toxic effect of PARP inhibition does not require any additional sources of exogenous DNA damage, we hypothesized that it might depend on the main source of spontaneous DNA damage: oxidative stress. This would be in line with earlier studies, in which PARP-1 was linked to oxidative DNA damage response. Additionally, PARP-1 is known to have a role during BER. We therefore set out to test whether BER-mediated processing of oxidative damage contributes to PARP inhibitor sensitivity of HR-deficient cells.

3 Results

3.1 Interdependence of base excision repair and mismatch repair during the processing of 8-oxoguanine in human cells

3.1.1 Manuscript

The following manuscript is in preparation and deals with the interdependence of base excision repair (BER) and mismatch repair (MMR) during the processing of oxidative DNA damage. We studied this phenomenon using substrates containing a single G^O/A mispair or G^O/C base pair in the close proximity of a G/T mismatch. Upon incubation with extracts of human cells or *Xenopus laevis* eggs, the G/T mispair is corrected to A/T or G/C, but only if a nick, which serves as a MMR initiation site, is introduced into the G or T strand, respectively. We showed that strand discontinuities arising during MYH-initiated BER of G^O/A can also serve as MMR initiation sites. Since G^O/A mispairs can only arise during replication through insertion of an A opposite G^O in the template strand, we suggest that higher eukaryotes may use G^O/A sites as additional strand discrimination signals for postreplicative MMR. This would lead to greater MMR efficiency and thus to an improved replication fidelity.

Not all DNA glycosylases would favorably influence MMR efficiency. OGG1-mediated processing of G^O/C sites would misdirect MMR to the G^O-containing template strand and lead to MMR-induced mutagenesis. Interestingly, we showed that G^O/C was not processed in our extracts and thus did not activate MMR. These findings suggest that the processing of oxidative damage by the different pathways of DNA metabolism is tightly regulated, thus resulting in a beneficial effect on MMR fidelity.

I contributed to this study by designing, performing and analyzing the experiments, as well as by drafting and editing the manuscript.

Interdependence of Base Excision Repair and Mismatch Repair during the Processing of 8-oxoguanine in Human Cells

Simone Repmann, Maite Olivera, Mariella Artola-Borán and Josef Jiricny*

Institute of Molecular Cancer Research of the University of Zurich and the ETH Zurich, Winterthurerstrasse 190, 8057 Zurich, Switzerland

Abstract: 200 words

Keywords: base excision repair, mismatch repair, oxidative DNA damage

* To whom correspondence should be addressed. Tel: +41 44 63 53450; Fax: +41 44 635 34 84; Email: jiricny@imcr.uzh.ch

Abstract

The major product of DNA oxidation, 8-oxoguanine (G^O), has ambiguous base-pairing properties and is thus highly mutagenic. Although DNA oxidation gives rise to G^O/C base pairs, G^O in the template strand can pair with either C or A during replication. Similarly, oxidation of nucleotide pools can lead to dG^OMP incorporation opposite template C or A. G^O/C pairs are repaired to G/Cs by base excision repair (BER), which is in eukaryotes initiated by OGG1 glycosylase/lyase. OGG1-initiated BER should not address G^O/A mispairs, because this would generate T/As instead of G/Cs. Instead, G^O/A repair is initiated by MYH glycosylase, which removes the A. BER then regenerates a G^O/C that can be re-addressed by OGG1. In *Saccharomyces cerevisiae*, which lacks MYH, G^O/A mispairs are processed by post-replicative mismatch repair (MMR), and this pathway has been linked to oxidized DNA metabolism also in mammals. We show here that the human MMR system does not address G^O/As *in vitro*, but that the intermediates of this MYH-dependent BER process act as MMR initiation sites in extracts of human cells or *Xenopus laevis* eggs. Unexpectedly, this was not the case for G^O/Cs. We postulate that MMR in higher eukaryotes adopted G^O/A processing intermediates as strand discrimination signals.

Introduction

Reactive oxygen species arising during cellular metabolism or through the action of external agents represent a constant threat to genomic integrity of all organisms. Although estimates vary, resting human cells harbor in their DNA between 1000 and 10'000 residues of 8-oxo-2'-deoxyguanosine, the predominant product of DNA oxidation [1-3]. This nucleoside has mutagenic potential, because the modified base, 8-oxoguanine (G^O), can adopt either *anti* or *syn* conformation about the glycosidic bond [4, 5]. In resting cells, most G^O residues are in G^O/C pairs, in which G^O is in the *anti* conformation. In eukaryotes, these lesions are addressed primarily by 8-oxoguanine DNA glycosylase (OGG1), a glycosylase/lyase that removes the oxidized base and cleaves the sugar-phosphate backbone to initiate a process of base excision repair (BER), which ultimately replaces the oxidized nucleotide with a dGMP [4].

Should G^O persist in the DNA until replication, however, the polymerases α, δ or ε will insert a C opposite *anti*-G^O to form a Watson-Crick-like G^O/C base pair, but an A opposite *syn*-G^O to form a Hoogsteen G^O/A mispair [6-8]. The former lesions can be repaired by OGG1-dependent BER to G/C, but OGG1 does not address G^O/A mispairs. Instead, they are recognized by the MutY homolog (MYH) glycosylase, which removes the mispaired A and thus initiates a BER process that generates a G^O/C, which can then be repaired to G/C by OGG1-dependent BER [9, 10].

The above scenario is further complicated by the fact that incorporation of a dG^OMP into the nascent DNA strand opposite C or A can give rise to C/G^O and A/G^O base pairs. These events should be rare, as dG^OTP in nucleotide pools is readily hydrolyzed to dG^OMP by the MutT homolog 1 (MTH1) protein [11-13]. However, when C/G^O or A/G^O do arise, they could present a problem to the repair machinery. Thus, although OGG1-dependent BER would eliminate the C/G^O pairs, MYH-mediated removal of an A in the template strand from an A/G^O mispair would give rise to an A➔C (T➔G in the opposite strand) transversion mutation. That the latter mutagenic events are rare can be inferred from the finding that DNA oxidation gives rise predominantly to G➔T rather than A➔C transversions [14-17]. This implies that the activity of MYH during replication is restricted to G^O/A rather than A/G^O mispairs. How might this be achieved? One possible scenario involves the participation of mismatch repair (MMR) [18-20].

By removing errors of DNA polymerases (primarily base-base mismatches and insertion-deletion loops) from the nascent strand, MMR improves replication fidelity by up to three orders of magnitude [21, 22]. Given the mispairing potential of G^O, it seemed logical to anticipate that MMR would be involved in the processing of oxidative DNA damage. Unexpectedly, G^O/A and G^O/C were shown

to be poor substrates for the human mismatch recognition protein MutSα (a heterodimer of MSH2 and MSH6) [23] and neither lesion was efficiently repaired in an *in vitro* MMR assay [23, 24]. However, *in vivo,* MMR deficiency was shown to lead to an extended G_2/M arrest and hypersensitivity to H_2O_2 treatment [25], which was accompanied by accumulation of G^O in genomic DNA [26, 27]. Overexpression of MTH1 decreased G^O levels as well as mutation rates at the *HPRT* locus of MMR-deficient cells, which implicated MMR in the removal of G^O from the nascent DNA strand [26, 28]. One explanation for this discrepancy might be that MMR is not directly involved in G^O processing, but rather that it might modulate BER efficiency, as suggested by the identification of a physical interaction between MYH and MutSα, which increased the binding affinity of MYH for G^O/A [19].

The likely interplay between BER and MMR in G^O processing requires further study. Recent description of a process activated by oxidative DNA damage that requires MMR but not BER proteins, and that involves MutSα-dependent PCNA monoubiquitylation and recruitment to chromatin of the translesion polymerase η [29] suggests that MMR might play additional roles in G^O metabolism. In this study, we studied the cross-talk between BER and MMR and show that the MMR excision machinery is activated by strand breaks arising after MYH-catalyzed removal of adenines from G^O/A mispairs in extracts of human cells or *Xenopus laevis* eggs. A similar stimulation was observed neither with G^O/C-containing substrates, nor with substrates containing 2-hydroxyadenine (A^O), another product of DNA oxidation [3], even though A^O/C and A^O/G mispairs were previously shown to be addressed by MYH [30, 31].

Results

G^O/A mispairs are not addressed by canonical MMR, but their processing by MYH is stimulated by MutSα

BER and MMR are mechanistically distinct biochemical pathways. They differ principally in their substrate specificity and in repair patch size. The specificity of BER is dictated by the enzymes that initiate the process, DNA glycoslases, which recognize and excise a limited number of substrates (mostly modifed bases) [32]. The repair process is thus initiated at the site of the modification and involves the replacement of a single (short-patch BER) [33] or only 2-6 (long-patch BER) nucleotides [34, 35]. MMR addresses non-Watson-Crick base pairs that arise during replication, but, in contrast to BER, the excision process initiates at a site distal to the mispair, at a strand discontinuity that denotes the nascent (and thus the error-containing) DNA strand. The repair tracts can thus be several hundred nucleotides long [36, 37]. Because we wished to study the potential interplay of BER and MMR in the processing of substrates that could conceivably be addressed by both systems, we first needed to find out whether both repair pathways were active in our cell extracts and to establish experimental conditions that would allow us to distinguish between the two processes. To this end, we generated covalently-closed circular phagemid substrates containing a single G/T, G^O/C or G^O/A base pair. We then incubated these heteroduplexes with extracts of human cells that were supplemented with radiolabelled nucleotides. Following recovery of the phagemids, restriction digest with *Not*I and *Bsa*I, and separation of the fragments on agarose gels, we anticipated that long-patch repair events (MMR) would give rise to heteroduplexes labeled in both fragments, whereas short-patch events (BER) would yield fragments containing only very limited amounts of radionucleotides and only in fragment **f** (Fig. 1A).

In the first experiment, we first introduced a nick into the Nt.*Bst*NBI site (Fig. 1A) and incubated the substrates with extracts of MutLα-deficient HCT116 cells (Fig. S1A) that were supplemented with purified recombinant MutLα and [a-^{32}P]dCTP. As shown in Fig. 1B, intense radiolabelling was seen only in the *bona fide* MMR substrate G/T (lane 4). That both fragments **f** and **g** were labeled with similar intensity indicates that the repair patch spanned at least the distance of 363 nucleotides between the nick and the mispair. Only background amounts of [a-^{32}P]dCMP were detected in the **f** and **g** fragments of the control homoduplex, G^O/C or G^O/A substrates (lanes 1-3), which confirms that the G^O/C and G^O/A pairs are not efficiently addressed by MMR [23, 24].

MYH-initiated BER of the G^O/A mispair should give rise to G^O/C. Thus, when the extracts are supplemented with [a-^{32}P]dCTP and when the substrate is unnicked, we should detect specific, albeit only limited, incorporation into the **f** fragment

(Fig. 1C). Moreover, this repair should be stimulated by MutSα, as reported previously [19].

When the substrates were incubated with HCT116 extracts that were additionally immunodepleted of MutSα with anti-MSH6 antibodies (Fig. S1B), we detected low levels of [a-^{32}P]dCMP incorporation into fragment **f**, which were approximately 1.5-fold higher in the extract containing MutSα (Fig. 1D).

MYH-dependent mismatch repair in human nuclear cell extracts

Having obtained preliminary evidence that both BER and MMR are active on our substrates in the extracts, we next wanted to learn whether there was a cross-talk between these processes. To address this question, we deployed a phagemid substrate containing a G/T mismatch within the unique *Sal*I restriction site (supercoiled or nicked with Nt.*Bst*NBI 376 nucleotides 3' from the mispaired T), a phagemid containing a single G^{O}/A mispair in addition to the G/T (G^{O}/A-G/T) and a control phagemid G^{O}/A-G/C. Upon incubation with the cell extracts, the recovered phagemids are digested with *Sal*I and *Dra*I to give rise to the pattern of bands shown in Fig. 2A. Successful repair of the G/T mismatch to G/C regenerates the *Sal*I site and the plasmid is cut into 4 instead of 3 fragments. This process should be dependent on the presence of a nick in the T strand, as MMR requires a strand discontinuity for initiation of the EXOI-dependent excision step [38, 39].

When the above substrates were incubated with MMR-deficient HCT116 nuclear cell extracts supplemented with [a-^{32}P]dATP, only background levels of repair and [a-^{32}P]dAMP incorporation were detected in the *bona fide* MMR substrate, nicked G/T (Fig. 2B, lane 2). However, the same substrate was repaired with high efficiency when the extracts were supplemented with purified recombinant MutLα (lane 3), particularly when compared to the unnicked control G/T (lane 1), which was processed to a limited extent by non-canonical MMR [40]. Strikingly, while only low levels of [α-^{32}P]dAMP incorporation were detected in this system when the supercoiled G^{O}/A-G/C control substrate was used (lanes 6-7), around 60% of the unnicked G^{O}/A-G/T phagemid were repaired in the extract supplemented with recombinant MutLα (lane 5). This result implies that A opposite G^{O} can serve as a cryptic strand discrimination signal for MMR.

We postulated that the MMR machinery might be hijacking intermediates of G^{O}/A processing for EXOI loading. We therefore set out to confirm that the above-described phenomenon was dependent on MYH, in the first instance by showing that MYH was active in the HCT116 extracts. When we incubated the homoduplex and the G^{O}/A substrates with HCT116 extracts supplemented with [α-^{32}P]dCTP, we observed substantial incorporation of [^{32}P]dCMP into fragment **f** of the G^{O}/A substrate (Fig. S3A), which contains the oxidized guanosine reside. We thus concluded that MYH was active at G^{O}/A sites in HCT116 nuclear cell extracts.

We then immunodepleted MYH from the extract (Fig. S2A) prior to incubation with the substrates. This reduced the MMR efficiency on the G^O/A-G/T substrate from 52% (Fig. 2C, lane 7) to ~20% (lane 8). The latter level was comparable to the efficiency of non-canonical MMR on the unnicked G/T substrates (~ 30%) (lanes 1-3). That the observed inhibition was due to MYH depletion was confirmed by complementation of the depleted extracts with purified, recombinant MYH, which restored the MMR efficiency on the G^O/A-G/T substrate to 43% (lane 9). As anticipated, MMR efficiencies on the G/T (lanes 1-3) and G/T nicked (lanes 4-6) substrates were unaffected by the amount of MYH in the extracts.

To confirm that processing of G^O/A intermediates by the BER machinery indeed generates DNA termini that can be utilized by EXOI in the strand degradation step of MMR, we pre-incubated the supercoiled G^O/A-G/T substrate with purified, recombinant MYH and apurinic endonuclease 1 (APE1), which cleaves the sugar-phosphate backbone at the MYH-generated abasic site. We then incubated the MYH/APE1-nicked substrate (Fig. S2B, upper panel) with HCT116 extracts supplemented with MutLα. As shown in Fig. S2B (lower panel), the MYH/APE1-generated nick in the G^O/A-G/T substrate was efficiently recognized by MMR factors. That the latter substrate was even more efficiently repaired than the Nt.*Bst*NBI-nicked G/T phagemid is most likely indicative of the substantially-shorter distance between the nick and the mispair in the G^O/A-G/T substrate than in the Nt.*Bst*NBI-nicked G/T phagemid.

2-Hydroxyadenine does not activate MMR in human nuclear cell extracts

MYH has been reported to excise the oxidation product of dATP, 2-hydroxy-2'-deoxyadenine (A^O), from base pairs with guanine or cytosine [30, 31]. We therefore wanted to test whether, analogously to G^O, A^O might also serve as a strand discrimination signal for MMR. We incubated the supercoiled homoduplex, G^O/A, A^O/G or A^O/C substrates with purified, recombinant MYH and APE1, and analyzed the extent of nicking (seen as conversion of supercoiled- to open-circular DNA) on agarose gels. As shown in Fig. 3A, the G^O/A phagemid was nicked very efficiently by MYH/APE1 (cf Fig. S3A). In contrast, only limited nicking was detected on the A^O/G and A^O/C substrates, with only 42% of the A^O/G and 38% of the A^O/C plasmids having been nicked after 8 hours. This is only slightly higher than that seen with the homoduplex (26%). Similarly, upon incubation of the A^O/C or A^O/G substrate with [α-^{32}P]dGTP- or [α-^{32}P]dCTP-supplemented HCT116 extracts, the amount of radionucleotide incorporated into the A^O-containing fragment **f** of both substrates was only slightly greater than that detected in the homoduplex substrate (Fig. S3).

We also carried out an *in vitro* MMR assay with substrates containing an A^O/G or an A^O/C pair in the vicinity of a T/G mismatch. These substrates differed from

those described above, inasmuch as the A^O residues were located within a *Pvu*I site (see Materials and Methods). Successful repair of the A^O/G to C/G or of the A^O/C to G/C by BER would restore the restriction site, such that *Pvu*I digestion of the recovered DNA would allow quantification of BER activity at the A^O sites (Figure 3B). As anticipated from data shown in Fig. 3A, incubation of the A^O/G-T/G and A^O/C-T/G substrates with MMR-proficient HCT116 extracts supplemented with recombinant MutLa yielded only 15% and 12% *Pvu*I-sensitive products respectively (Figure 3C, lanes 4-5), while the G/T phagemid was completely digested under identical conditions (lane 3). These results were reflected in MMR efficiency determined from the same assays by digestion of the recovered phagemids with *Sal*I/*Dra*I. Repair of the T/G mismatch in the A^O/G-T/G and A^O/C-T/G substrates was very inefficient (20% and 18%, respectively), while the G/T nicked (lane 3) and the G^O/A-G/T (lane 1) substrates were efficiently repaired to 93% and 59%, respectively. Taken together, these data show that A^O/G or A^O/C pairs are inefficiently processed by MYH in cell extracts and therefore fail to act as entry sites for mismatch-activated excision.

G^O/A, but not A^O/G and A^O/C, act as MMR initiation sites in *Xenopus laevis* egg extracts

Because G^O/A mispairs arise during replication, MYH should be able to act on newly-replicated DNA, and available experimental evidence shows that this glycosylase is indeed more abundant during S-phase [18]. In an attempt to learn whether MYH is also more efficient during S-phase, we decided to make use of *Xenopus laevis* (*X. laevis*) egg extracts, which are enriched in S-phase proteins [41].

In the first experiment, we wanted to learn whether the extracts are proficient in MYH-initiated BER. We decided to make use of the assay described above (Fig. 1C), in which the homoduplex or G^O/A closed-circular substrates were incubated with *X. laevis* egg extracts supplemented with [α-^{32}P]dCTP. Digestion of the recovered phagemid DNA with *Not*I/*Bsa*I revealed a three-fold greater incorporation of [^{32}P]dCMP into the G^O-containing fragment of the G^O/A substrate than into the corresponding fragment of the homoduplex phagemid (Fig. 4A). This demonstrated that MYH was active in the *X. laeavis* extracts.

We also had to show that the extracts supported nick-directed MMR, because an earlier report indicated that mismatch processing in *X. laevis* oocyte extracts was efficient, but not nick-directed [42]. We therefore incubated the covalently-closed and the nicked isoforms of the G/T phagemid with the extracts supplemented with [α-^{32}P]dATP, under conditions where DNA replication was inhibited. As shown in Fig. 4B, we were able to detect nick-directed MMR, with the G/T substrate

repaired to G/C (lane 2), whereas the covalently-closed phagemid was only inefficiently processed (lane 1).

Under these conditions, the covalently-closed G^O/A-G/T substrate (lane 3) was almost as efficiently repaired as the nicked G/T phagemid (lane 2). In contrast, the A^O/G-T/G and A^O/C-T/G substrates (lanes 4-5) were left largely unrepaired, which shows that, similarly to human extracts, 2-hydroxyadenine did not serve as a strand discrimination signal for MMR.

OGG1-dependent mismatch repair is inefficient in human nuclear cell extracts

Assuming that MTH1 functions with a 100% efficiency, all G^O residues in oxidized DNA should be in the template strand following replication, irrespective of whether they are paired with A or C. As discussed above, MYH-initiated BER of G^O/A would be directed to the A-strand that is also the nascent DNA strand. The observed interference of BER and MMR would therefore serve to improve the efficiency of MMR by providing this pathway with additional entry sites for EXOI. In contrast, BER-mediated repair of G^O/C pairs arising during replication would have the opposite effect on MMR. G^O/C repair is initiated by OGG1, a glycosylase/lyase that removes the G^O and concurrently cleaves the sugar-phosphate backbone of the DNA [43, 44]. Postreplicative BER-dependent processing of G^O/C pairs would therefore introduce breaks into the template DNA strand and thus provide MMR with the wrong strand bias.

We set out to test the above supposition by studying the effect on MMR efficiency and directionality of a G^O/C pair situated in the vicinity of a G/T mismatch. We generated a G^O/C-G/T substrate, in which the G^O was positioned 54 nucleotides 5' from the mispaired G. OGG1-initiated BER of the G^O would give rise to a break that should activate MMR to correct the G/T mismatch to A/T and thus regenerate an *Acl*I site in the substrate. This repair bias should be identical to that introduced by an Nt.Bst.NBI-generated nick in the G/T substrate (Fig. 5A).

When we incubated the G/T, nicked G/T, G^O/C-G/T or G^O/C-A/T phagemid substrates with HCT116 nuclear cell extracts supplemented with [α-^{32}P]dATP, no significant repair or [^{32}P]dAMP incorporation was observed (Fig. 5B, lanes 1, 3, 5, 7), but when the extract was supplemented with purified, recombinant MutLα, the Nt.*Bst*NBI-nicked G/T substrate was repaired (lane 4). In contrast to what was observed with the G^O/A-G/T substrate (Fig. 2B + 3C), only background levels of repair and [^{32}P]dAMP incorporation were detected with the G^O/C-G/T substrate (Fig. 5B, lane 6) and with the control, G/T phagemid (lane 2). Similar results were obtained also with MutSα-deficient LoVo extracts supplemented with purified recombinant MutSα (Fig. 5D, lane 2). Given that both extracts contained the key

MMR and BER factors as ascertained by western blotting (Fig. S1, S5A), these results indicated that G^O does not activate MMR in the G^O/C-G/T substrate.

The above result could be explained in several ways. The first possibility is that the MMR machinery was unable to use the BER intermediates generated during G^O processing as strand discrimination signals. We therefore treated the covalently-closed G^O/C-G/T substrate with purified recombinant OGG1 and showed that it was efficiently nicked (Fig. S5B). When this DNA was incubated with extracts of LoVo cells supplemented with purified recombinant MutSα, it was repaired with similar efficiency to the control, nicked G/T phagemid (Fig. 5C, cf lanes 2&4). This shows that MMR can use OGG1-generated strand breaks as initiation sites. The second possibility was that OGG1 in the tested cell extracts was inactive, or that it was present in insufficient amounts. We therefore incubated the G^O/C and homoduplex substrates with LoVo extracts supplemented with [α-^{32}P]dGTP. As shown in Fig. S5C only background levels of the radiolabeled nucleotide were incorporated into the phagemid heteroduplex, which suggested that G^O/C repair was indeed inefficient, despite the fact that the extracts contained readily-detectable amounts of OGG1 (Fig. S1A, S5A). Similar results were obtained with [^{32}P]-labeled G^O/C-containing oligomers, which were inefficiently nicked in LoVo extracts, while UNG/APE1-catalyzed processing of U/G-containing oligomers was very efficient (Fig. S5D). The reason underlying the low OGG1 activity in the extracts is currently unknown, but we were able to eliminate inappropriate salt concentration, lack of an activator protein, or short half-life of OGG1 as possible causes (Fig. S6). To test whether the extracts contained an inhibitor of OGG1, we supplemented them with purified recombinant OGG1 (Fig. 5D). Under these conditions, the G^O/C-G/T substrate (lane 3) was repaired with efficiency similar to the nicked G/T phagemid (lane 1). Importantly, this phenomenon was not limited to extracts of human cells, as identical results were obtained with the *X. laevis* MMR system (Fig. 6).

Discussion

The postreplicative mismatch repair system improves the fidelity of DNA replication by several orders of magnitude by removing from nascent DNA nucleotides that fail to form Watson-Crick base pairs. In order to fulfill this function, it has to satisfy two key criteria: it has to (i) recognize base-base mismatches and small insertion/deletion loops (IDLs) generated by the replicative polymerases during DNA synthesis and (ii) direct the repair process to the newly-synthesized DNA strand. How the major mismatch recognition factor MutSα recognizes the different helical distortions that are caused by purine/purine, purine/pyrimidine and pyrimidine/pyrimidine mispairs, as well as by IDLs, is still poorly understood, despite the fact that several structures of protein/DNA complexes have been described [45]. However, because MMR deficiency leads to transition, transversion and frameshift mutations, MutSα clearly has broad substrate specificity. Although this characteristic of MutSα is clearly beneficial as far as its role in the maintenance of replication fidelity is concerned, it might also be deleterious, should MutSα bind to lesions that should be processed by other repair systems. One such example are mispairs containing O^6-methylguanine; these lesions activate MMR, but because their processing does not lead to the removal of the modified nucleotide from the template strand, they trigger futile repair that eventually leads to cell death [21]. Processing of G^O/A mismatches arising through the incorporation of dAMP opposite G^O in the template strand might also trigger futile MMR, but the evidence for such a process is currently lacking. As discussed above, the MMR system does appear to influence the efficiency of A/G^O processing, either directly through removing from the nascent strand G^O misincorporated opposite template A, or indirectly, through increasing the efficiency of MYH-dependent BER. Thus, available experimental data argue that the broad substrate specificity of MutSα does not deleteriously affect BER efficiency. In the present study, we asked whether the reverse might be true, namely, whether BER-dependent processing of G^O could affect MMR efficiency, by for example interfering with its second key criterion: strand directionality.

In our earlier studies, we could show that the MMR system could use breaks generated during the BER-mediated processing of uracil residues [40, 46] or during the RNaseH2-mediated excision of ribonucleotides misincorporated into DNA during replication [47] for the purpose of strand discrimination. We postulated that MMR might also use breaks generated during the BER-dependent processing of oxidative damage, but the outcome of such interference would be positive only in the case that the breaks were generated in the nascent DNA strand. We show here that MYH-dependent processing of a G^O/A mispair in extracts of human cells or of *Xenopus laevis* eggs directs MMR to the A-strand (Figs. 2 + 4). *In vivo*, the ability of the MMR system to use breaks generated during the MYH-directed processing

of G^O/A mispairs arising through the incorporation of dAMP opposite G^O would direct mismatch correction to the nascent strand and thus possibly improve the fidelity of replication (Fig. 7). MYH-dependent BER and MMR would thus synergize during S-phase, as might have been anticipated based on their physical interaction [19].

Breaks introduced into the nascent DNA strand by OGG1 during the processing of C/G^O pairs arising through the incorporation of dG^OMP opposite template C would also help improve MMR efficiency and replication fidelity. However, due to the sanitization of dNTP pools by MTH1, dG^OTP concentrations should be extremely low, such that dG^OMP incorporation into nascent DNA during replication should be minimal. As a result, most G^O residues present in DNA during replication should be in the template strand. Incision of this strand by OGG1 behind the replication fork would misdirect MMR to the wrong strand (Fig. 7), and OGG1-catalyzed incision of DNA at G^O/C sites in front of the replication fork could cause its collapse. It would therefore appear logical that G^O/C processing should be completed prior to the onset of S-phase and that OGG1 should be inactivated during this cell cycle stage. Interestingly, we found that G^O/C processing in both *in vitro* systems was extremely inefficient and that the presence of a G^O/C pair in the heteroduplex substrate failed to activate MMR of the G/T mismatch (Figs. 5, 6, S5, S6), despite the fact that OGG1 was present in considerable quantities. Because addition of the recombinant polypeptide to the extracts resulted in both, efficient G^O/C processing and G^O-dependent G/T repair, we postulate that OGG1 present in the cell extracts is inactive, either as a result of post-translational modification, or through complexation with an inhibitor. We are currently attempting to identify the underlying cause of this inhibition, as well as carrying out a series of *in vivo* experiments that should show whether the observations described above correspond to the situation in living cells. Our current findings indicate that the repair of oxidative damage in vertebrate cells is highly regulated in order to prevent genomic instability and future experiments should show how this regulation is mediated at the molecular level.

Materials and methods

Human, nuclear cell extracts

Nuclei were isolated as previously described [48], resuspended in 1/3 of their packed volume in cold extraction buffer (25 mM HEPES-KOH pH 7.5, 292 mM sucrose, 1 mM PMSF, 0.5 mM DTT, 1 µg/ml leupeptine) and transferred to a small beaker fitted with a magnetic stirrer bar. NaCl was added dropwise to a final concentration of 150 mM and extraction continued for 1h at 4°C. The nuclei were pelleted by centrifugation at 14'500 x g for 20 min at 4°C in a tabletop centrifuge. The supernatant was transferred and dialyzed 2 x 1 h at 4°C against 1 liter of cold dialysis buffer (25 mM HEPES-KOH pH 7.5, 50 mM KCl, 0.1 mM EDTA, 231 mM sucrose, 1 mM PMSF, 2 mM DTT, 1 µg/ml leupeptine). The dialyzed extract was clarified by centrifugation at 20'000 x g for 15 min at 4°C. The supernatant was aliquoted, snap frozen in liquid nitrogen and stored at -80 °C. The protein concentration was determined with a Bradford assay and the salt concentration was measured using a conductivity meter.

Xenopus laevis egg extracts

S-phase extract was prepared as previously described [49]. Briefly, eggs were dejelled, activated with calcium ionophore (Sigma-Aldrich), rinsed with S-buffer (50 mM HEPES-KOH pH 7.5, 50 mM KCl, 2.5 mM $MgCl_2$ and 250 mM sucrose), transferred to 2 ml Eppendorf tubes and crushed by centrifugation for 12 min at 13'200 rpm. The cytoplasmic layer was removed and after addition of CytB (Sigma-Aldrich) cleared by centrifugation for 25 min at 70'000 rpm (Sorvall TL55 swinging bucket rotor). The extract was supplemented with 250 mg/ml cycloheximide, 25 mM phosphocreatine and 10 mg/ml creatine phosphokinase before use.

Cell culture, Western blot

HCT116 (MutLα-) and HCT116 + chromosome 3 (MutLα+) cells were obtained from Richard Boland [50] and were cultured in McCoy's 5a medium (GIBCO) supplemented with 10% fetal calf serum (GIBCO). The medium for the chromosome 3-complemented cell line was supplemented with 400 µg/ml G418. LoVo (MutSα-) cells were grown in DMEM (GIBCO) supplemented with 10% fetal calf serum (GIBCO). All media additionally contained 1% penicillin/streptomycin. Whole cell extracts of the cell lines were prepared using 2 x Lämmli buffer (120 mM Tris-HCl pH 6.8, 4% SDS, 20% glycerol). Upon determination of the protein concentration by Lowry assay, proteins were analyzed with SDS-PAGE and Western blot.

Antibodies

For western blot analysis, the MYH antibody (mouse monoclonal, Abcam, ab55551) was used at a dilution of 1:333, OGG1 (rabbit monoclonal, Abcam,

ab124741) at 1:10'000, MSH6 (mouse monoclonal, BD Transduction Laboratories, 610919) at 1:1000, MSH2 (mouse monoclonal, Calbiochem, NA-27) at 1:500, MLH1(mouse monoclonal, BD Transduction Laboratories, 554073) at 1:500, β-Tubulin (rabbit polyclonal, Abcam, ab6046) at 1:10'000 and TFIIH (rabbit polyclonal, Santa Cruz, sc-293) was used at a dilution of 1:1000. The anti-MTH1 antibody was a generous gift of Yusaku Nakabeppu and was used at a dilution of 1:250. Horseradish peroxidase (HRP)-coupled anti-mouse and anti-rabbit secondary antibodies (GE Healthcare) were used at a dilution of 1:5000.

Substrate production

The detailed procedure was described previously [51]. Briefly, hetero- and homoduplexes were constructed by primer extension using the oligonucleotides listed below as primers and the single-stranded phagemid DNA listed in brackets as template. The single-stranded DNA templates differed in position of the Nt.*Bst*NBI site, which was situated at nucleotide 2850 either in the viral (top) or complementary (bottom) strand. Incubation of the substrates with the nickase yielded substrates in which MMR occurred either 5′ to 3′, or 3’ to 5’, respectively. The mismatches were located within a *Sal*I and/or *Acl*I restriction site, that were restored upon repair. The desired supercoiled heteroduplex substrates were purified on cesium chloride gradients.

Primers: The G^O- or A^O-containing primers were obtained from Eurogentec (Seraing, Belgium). All other primers were obtained from Microsynth (Balgach, Switzerland). Where necessary, the *Sal*I (**GTCGAC**) and *Acl*I (AACGTT) restriction sites are highlighted in bold and grey, respectively. *Pvu*I restriction sites (CGATCG) are marked grey and mispaired residues are underlined. Primer sequences correspond to the outer strand sequence of the substrate.

- G/T (pRichi-2850top*Acl*I or pRichi-2850bot*Acl*I):
  5'-CCAGACGTCT**GTC**GACGTTGGGAAGCTTGAG-3'
- T/G (pRichi-2850top*Sal*I):
  5'-CCAGACGTCT**GTTGAC**GTTGGGAAGCTTGAG-3'
- G^O/A-G/T (pRichi-2850bot*Acl*I):
  5'-GAATTGTAAG^OACGAACACTATAGGGCGAATTGGCGGCCGCGATCT
  GATCAGATCCAGACGTCTGTCGACGTTGGGAAGCTTGAG-3';
- G^O/C-G/T (pRichi-2850top*Acl*I):
  5'-GAATTGTAATACG^OAACACTATAGGGCGAATTGGCGGCCGCGATCT
  GATCAGATCCAGACGTCTGTCGACGTTGGGAAGCTTGAG-3'
- A^O/G-T/G (pRichi-2850top*Sal*I):
  5'-GGGAAGGGCGATA^{O}GGTGCGGGCCTC-3'
  The T/G primer was used for T/G mismatch generation.

- A^O/C-T/G (pRichi-2850top*Sal*I):
  5'-GGGAAGGGCA^{O}ATCGGTGCGGGCCTC-3'
  The T/G primer was used for T/G mismatch generation.
- A/T (pRichi-2850top*Acl*I)
  5'-CCAGACGTCTGTCAACGTTGGGAAGCTTGAG-3'
- G/C (pRichi-2850top*Sal*I)
  5'-CCAGACGTCT**GTCGAC**GTTGGGAAGCTTGAG-3'

***In vitro* MMR assay in human nuclear cell extracts**

The MMR assays were described previously [22, 46, 51]. Unless otherwise specified, the reactions were carried out with 100 ng substrate and 100 µg nuclear cell extract in a total volume of 25 µl in a buffer containing 20 mM Tris-HCl pH 7.6, 5 mM $MgCl_2$, 1 mM glutathione, 50 µg/ml BSA, 0.1 mM dNTPs, 1.5 mM ATP and 80 mM KCl in experiments involving MYH substrates, or 110 mM KCl in experiments involving OGG1 substrates. 1.8 pmol of purified MutLα or MutSα were added where indicated. The reactions were incubated at 37°C for 1 hour. The reaction was stopped by adding an equal volume of STOP solution (50% Poteinase K, 1 mM EDTA, 3% SDS) and subsequent incubation for 1 hr at 50°C. Substrates were purified on MinElute Spin columns (Qiagen), subjected to *Sal*I/*Dra*I restriction digest and the DNA fragments were separated on 1% agarose gels stained with GelRed. The percentage of mismatch repair was quantified from the ratio of the repaired bands (**b+c**) to the total amount of DNA (**a+b+c**) using ImageQuantTL. The band intensities were corrected according to their respective DNA fragment sizes. Some assays were supplemented with 2 µCi [α-^{32}P]dATP. To monitor incorporation of the radiolabeled nucleotide, the agarose gels were vacuum dried, exposed to a PhosphoScreen and scanned with a Typhoon Scanner (FLA 9500, GE Healthcare).

***In vitro* MMR assay in *Xenopus laevis* egg extracts**

Briefly, the reaction mixture containing 150 ng substrate, 26 µl S-phase extracts and 2 µCi [α-^{32}P]dATP was incubated in a total volume of 30 µl at 23°C for 45 min. To inhibit replication, 500 nM geminin and 40 µg/ml p27 were added. The reaction was stopped by the addition of 70 µl STOP solution (76 mM EDTA, 1.5% SDS) and 40 µg RNase (Sigma-Aldrich) and incubated for 30 min at 37°C. Subsequently, 200 µg Proteinase K (AppliChem) were added and incubation continued at 37°C overnight. The substrates were purified on MinElute Spin columns (Qiagen) and subjected to *Sal*I/*Dra*I or *Acl*I restriction digest in the presence of RNase. The digested DNA was cleaned up again and analyzed on a 1% agarose gel stained with GelRed.

BER assay

To determine A^O/G to C/G or A^O/C to G/C repair by MYH, a MMR assay was performed. After the reaction, 50% of the purified, eluted substrate were digested

with *Sal*I/*Dra*I (MMR assay), while the other half of the purified substrate was used for *Pvu*I digestion.

MMR- or BER- dependent incorporation assay

This assay was used to test MMR or BER activities. It was performed similarly to the MMR assay, except for the following modifications: In order to track MMR-, MYH- or OGG1-dependent nucleotide incorporation, the reactions were supplemented with 2 µCi [α-^{32}P]dATP, [α-^{32}P]dCTP or [α-^{32}P]dGTP, respectively. Finally, the substrates were digested with *Not*I/*Bsa*I, and analyzed on a GelRed-stained 1% agarose gels. Repair tracts of up to 330 bp in Nt.*Bst*NBI nicked substrates, up to 29 bp in the G^{O}/A substrates and up to 22 bp in the G^{O}/C substrates are seen in the 1810 bp fragment **f**. Longer repair tracts appear in the 1387bp fragment **g** (see Figure 1 A+C). While MMR-dependent [^{32}P]dAMP incorporation gives rise to a strong radioactive signal in both bands, MYH-dependent [^{32}P]dCMP or OGG1-dependent [^{32}P]dGMP incorporation occurs only in DNA fragment **f**. Quantification of [^{32}P]dCMP or [α^{32}P]dGMP incorporation in MYH- or OGG1-induced BER was determined from the ratio between the band intensities of fragment **g** on the autoradiograph and the intensity of fragment **f** on the GelRed-stained agarose gel.

Immunodepletion

20 µl Protein A/G PLUS-agarose beads (sc-2003, SantaCruz) were washed twice with 750 µl binding buffer (30 mM HEPES-KOH [pH 7.6], 7 mM $MgCl_2$) and spun down at 2'700 g for 2 min at 4°C. The beads were resuspended in binding buffer and 1 µg anti-MYH (ab55551, Abcam) or anti-MSH6 (610919, BD Transduction Laboratories) antibody was added. The mixture was then incubated for 3 hr at 4°C, the beads were washed 3x with 750 µl binding buffer and subsequently used to immunodeplete 100 µg nuclear cell extracts for 30 min at 4°C. MMR assays were performed immediately after depletion. Mock-depleted nuclear cell extracts were obtained by incubation with beads only.

Nicking of substrates

MYH+APE1: 200 ng G^{O}/A-G/T substrate were incubated with 10 ng purified recombinant MYH-GST and 10 U of APE1 (New England Biolabs) in 1x MMR buffer (20 mM Tris-HCl pH 7.6, 40 mM KCl, 5 mM $MgCl_2$, 1 mM glutathione, 50 µg/ml BSA, 0.1 mM dNTPs) for 4 hr at 37°C. The reaction was stopped by heat inactivation and 50 ng of the pre-nicked substrate were analyzed on a 1% GelRed-stained agarose gel for nicking efficiency. The rest was purified on a MinElute Spin column (Qiagen) and subsequently used in a MMR assay.

OGG1: 1 µg G^{O}/C-G/T substrate was incubated with 0.8 µg purified recombinant OGG1 (a gift of Barbara van Loon) in 20mM Tris-HCl pH 8, 1mM DTT, 1mM EDTA and 0.1mg/ml BSA for 2.5 hours at 37°C and subsequently purified on a

MinElute Spin column (Qiagen). 100 ng of the pre-nicked substrate were used for a MMR assay.

Nt.BstNBI: Supercoiled DNA substrates (100ng) were incubated with 1 U of Nt.*Bst*NBI (New England Biolabs) according to the recommendations of the manufacturer.

***In vitro* MYH nicking assay**

100 ng of supercoiled G^O/A, A^O/G, A^O/C or homoduplex substrate were incubated with 10 ng purified recombinant MYH-GST, 10 U of APE1 (New England Biolabs) and 1.5 mM ATP in 1x MMR buffer (20 mM Tris-HCl pH 7.6, 40 mM KCl, 5 mM $MgCl_2$, 1 mM glutathione, 50 µg/ml BSA, 0.1 mM dNTPs) in a total volume of 10 µl. For time course experiments, 5 µl aliquots were withdrawn at the indicated time points. The reactions were stopped by the addition of 2 µl of 6x loading dye (37.5 mg/ml Ficoll 400, 23% glycerol, 0.03% bromophenol blue) and subsequent heat inactivation. The samples were separated on 1% agarose gels and visualized with GelRed. The nicking efficiency was quantified from the ratio of the amount of nicked DNA product to the total amount of DNA (supercoiled + nicked).

Restriction enzymes

All restriction enzymes were purchased from New England Biolabs.

MYH-GST purification, Recombinant proteins

GST-tagged human full-length MYH (isoform 5) was expressed from the pET41a-MUTYH expression vector (gift of Barbara van Loon) and partially purified using Glutathione Sepharose™ 4B beads (GE Healthcare) as described previously [52] (see SI text for details). Eluates were loaded on a HiTrap™ Heparin HP column (GE Healthcare), washed with 10 column volumes of washing buffer (30 mM Tris-HCl pH 8, 0.1 mM EDTA, 10% glycerol, 1 mM DTT, 50 mM NaCl) at a flow rate of 0.5 ml/min. Elution was performed using a salt gradient (50-600 mM NaCl). MYH-GST was eluted with 400-500 mM NaCl. The active fractions were identified using a MYH nicking assay, pooled, aliquoted and stored at -80°C. Recombinant APE1 was purchased from New England Biolabs. Recombinant MutLα and MutSα were expressed and purified in our laboratory.

Supplementary materials and methods

MYH-GST purification

GST-tagged MYH was expressed from the pET41a-MUTYH expression vector (gift of Barbara van Loon) and partially purified using Glutathione Sepharose beads (GE Healthcare) as described previously [52]. Briefly, Bl21 bacteria were transformed with 200 ng pET41a-MUTYH expression vector and 200 ng pRARE vector (a kind gift of Barbara van Loon). Transformed bacteria were grown in

kanamycin and chloramphenicol containing Luria-Bertani (LB) medium at 37 °C until an OD_{600} of 0.6 was reached. To induce MYH-GST expression, IPTG was added to a final concentration of 1 mM. Further expression was carried out at 20°C for 21 hr. Bacteria were pelleted at 4'000 rpm for 30 min at 4°C. All following steps were carried out at 4°C or in the cold room. Each pellet deriving from a 1 liter culture was resolved in 20 ml of lysis buffer [PBS containing 0.1% Triton X-100, 1 mM PMSF, 1 tablet protease inhibitor cocktail "Complete, EDTA-free" (Roche) per 66 ml, 1 µg/ml proteinase inhibitors (Leupeptin, Benzamide, Pepstatin)]. Subsequently, cells were mechanically disrupted in a French press (pressure: 1500 psi). Subsequently, the lysed cells were spun at 20,000 rpm for 2 hr in a Sorvall Lynx 6'000 centrifuge (Thermo Scientific) using a SS-34 rotor. 2 x 1 ml of packed GST- beads were washed 3 times with 15 ml of cold PBS and spun at 1'500 rpm for 30 sec. Half of the supernatant was added to 1 ml of washed GST beads in a 50 ml Falcon tube and the mixture was incubated on a horizontal roller mixer (RM5, CAT) overnight. Samples were then centrifuged at 2'000 rpm for 5 min. The flow through was removed and the beads were washed with 30 ml of washing buffer [PBS containing 0.2% Triton X-100, 1 mM PMSF, 1 tablet protease inhibitor cocktail "Complete, EDTA-free" (Roche) per 66 ml, 1 µg/ml proteinase inhibitors (Leupeptin, Benzamide, Pepstatin)] during a 10 min rotation. Beads were collected by centrifugation at 2'000 rpm for 5 min. The supernatant was removed, the beads of both tubes were pooled, transferred to a 15 ml Falcon tube, washed 3x with 10 ml of washing buffer and once with PBS as described for the previous washing step. Elution was carried out by washing once with 3 ml of elution buffer (30 mM Tris-HCl pH 8, 50 mM glutathione pH 8, 10% glycerol, 150 mM NaCl) and once with 2 ml. Each time, the protein in the supernatant was collected by a centrifugation step at 2'000 rpm for 2 min.

Nicking assay with G^O/C oligonucleotides

The oligo sequences were as follows:
G^O/C sense 5'-GCCAGTGAATTGTAATAC$\underline{G^O}$AACACTATAGGGCGA-3',
G^O/C antisense 5'-TCGCCCTATAGTGTT$\underline{C}$GTATTACAATTCACTGGC-3'.
U/G sense 5'-GCCAGTGAATTGTAATA$\underline{U}$GAACACTATAGGGCGA-3',
U/G antisense 5'-TCGCCCTATAGTGTTC$\underline{G}$TATTACAATTCACTGGC-3'.

The sense strands were labeled at their 5' termini with [γ-^{32}P]ATP and T4 polynucleotide kinase (New England Biolabs), and annealed to their complementary strands. 20 fmol annealed oligo and 100 µg LoVo nuclear cell extracts were incubated in a buffer containing 20 mM Tris-HCl pH 7.6, 80 mM KCl, 5 mM EDTA, 1 mM glutathione, 50 µg/ml BSA, 1.5% glycerol in a total volume of 10 µl at 37°C. At the indicated time points, reactions were stopped by addition of the same volume of stop solution (3% w/v SDS, 5 mg/ml Proteinase K, 1 mM EDTA) and incubation for 1 hour at 50°C. NaOH was then added to a final

concentration of 90 mM and the sample was heated at 95°C for 5 min. Reactions were purified on MinElute Spin columns (Qiagen). Samples were mixed with 80% formamide loading dye and heated for 5 min at 95°C immediately prior to loading onto a denaturing 20% polyacrylamide gel. The dried gel was analyzed with a Typhoon scanner (FL9500, GE Healthcare).

Purification of geminin and p27

hGeminin-pET28 and hp27-pET21 constructs were a kind gift of Yoshi Hashimoto/Vincenzo Costanzo. Briefly, protein expression was induced with 0.5 mM IPTG in BL21 cells (Invitrogen) grown at 37°C. The cell pellets were resuspended in 20 mM Tris-HCl pH 7.5, 500 mM KCl, 10% glycerol, 1 mM β-mercaptoethanol, 0.1% NP40 and PMSF for lysis. After cell disruption and centrifugation of cell debris and membranes, the soluble fraction containing 10 mM imidazole was loaded onto a nickel chelating column, which was then washed with 5-25 mM imidazole. The protein was eluted with a gradient of 50-300mM imidazole. Fractions were pooled and dialysed against EB (100mM KCl, 2.5mM $MgCl_2$ und 50mM Hepes-KOH pH 7.5)/10% glycerol.

References

1. Collins, A.R., *Oxidative DNA damage, antioxidants, and cancer.* Bioessays, 1999. **21**(3): p. 238-46.
2. Gedik, C.M., A. Collins, and Escodd, *Establishing the background level of base oxidation in human lymphocyte DNA: results of an interlaboratory validation study.* FASEB J, 2005. **19**(1): p. 82-4.
3. Burrows, C.J. and J.G. Muller, *Oxidative Nucleobase Modifications Leading to Strand Scission.* Chem Rev, 1998. **98**(3): p. 1109-1152.
4. David, S.S., V.L. O'Shea, and S. Kundu, *Base-excision repair of oxidative DNA damage.* Nature, 2007. **447**(7147): p. 941-50.
5. McAuley-Hecht, K.E., et al., *Crystal structure of a DNA duplex containing 8-hydroxydeoxyguanine-adenine base pairs.* Biochemistry, 1994. **33**(34): p. 10266-70.
6. Shibutani, S., M. Takeshita, and A.P. Grollman, *Insertion of specific bases during DNA synthesis past the oxidation-damaged base 8-oxodG.* Nature, 1991. **349**(6308): p. 431-4.
7. Avkin, S. and Z. Livneh, *Efficiency, specificity and DNA polymerase-dependence of translesion replication across the oxidative DNA lesion 8-oxoguanine in human cells.* Mutat Res, 2002. **510**(1-2): p. 81-90.
8. Einolf, H.J. and F.P. Guengerich, *Fidelity of nucleotide insertion at 8-oxo-7,8-dihydroguanine by mammalian DNA polymerase delta. Steady-state and pre-steady-state kinetic analysis.* J Biol Chem, 2001. **276**(6): p. 3764-71.
9. Michaels, M.L. and J.H. Miller, *The GO system protects organisms from the mutagenic effect of the spontaneous lesion 8-hydroxyguanine (7,8-dihydro-8-oxoguanine).* J Bacteriol, 1992. **174**(20): p. 6321-5.
10. Fortini, P., et al., *8-Oxoguanine DNA damage: at the crossroad of alternative repair pathways.* Mutat Res, 2003. **531**(1-2): p. 127-39.
11. Sakumi, K., et al., *Cloning and expression of cDNA for a human enzyme that hydrolyzes 8-oxo-dGTP, a mutagenic substrate for DNA synthesis.* J Biol Chem, 1993. **268**(31): p. 23524-30.
12. Maki, H. and M. Sekiguchi, *MutT protein specifically hydrolyses a potent mutagenic substrate for DNA synthesis.* Nature, 1992. **355**(6357): p. 273-5.
13. Mo, J.Y., H. Maki, and M. Sekiguchi, *Hydrolytic elimination of a mutagenic nucleotide, 8-oxodGTP, by human 18-kilodalton protein: sanitization of nucleotide pool.* Proc Natl Acad Sci U S A, 1992. **89**(22): p. 11021-5.
14. Al-Tassan, N., et al., *Inherited variants of MYH associated with somatic G:C-->T:A mutations in colorectal tumors.* Nat Genet, 2002. **30**(2): p. 227-32.
15. Jones, S., et al., *Biallelic germline mutations in MYH predispose to multiple colorectal adenoma and somatic G:C-->T:A mutations.* Hum Mol Genet, 2002. **11**(23): p. 2961-7.
16. Sieber, O.M., et al., *Multiple colorectal adenomas, classic adenomatous polyposis, and germ-line mutations in MYH.* N Engl J Med, 2003. **348**(9): p. 791-9.

17. Nghiem, Y., et al., *The mutY gene: a mutator locus in Escherichia coli that generates G.C----T.A transversions.* Proc Natl Acad Sci U S A, 1988. **85**(8): p. 2709-13.
18. Boldogh, I., et al., *hMYH cell cycle-dependent expression, subcellular localization and association with replication foci: evidence suggesting replication-coupled repair of adenine:8-oxoguanine mispairs.* Nucleic Acids Res, 2001. **29**(13): p. 2802-9.
19. Gu, Y., et al., *Human MutY homolog, a DNA glycosylase involved in base excision repair, physically and functionally interacts with mismatch repair proteins human MutS homolog 2/human MutS homolog 6.* J Biol Chem, 2002. **277**(13): p. 11135-42.
20. Parker, A., et al., *Human homolog of the MutY repair protein (hMYH) physically interacts with proteins involved in long patch DNA base excision repair.* J Biol Chem, 2001. **276**(8): p. 5547-55.
21. Jiricny, J., *The multifaceted mismatch-repair system.* Nat Rev Mol Cell Biol, 2006. **7**(5): p. 335-46.
22. Modrich, P., *Mechanisms in eukaryotic mismatch repair.* J Biol Chem, 2006. **281**(41): p. 30305-9.
23. Mazurek, A., M. Berardini, and R. Fishel, *Activation of human MutS homologs by 8-oxo-guanine DNA damage.* J Biol Chem, 2002. **277**(10): p. 8260-6.
24. Larson, E.D., K. Iams, and J.T. Drummond, *Strand-specific processing of 8-oxoguanine by the human mismatch repair pathway: inefficient removal of 8-oxoguanine paired with adenine or cytosine.* DNA Repair (Amst), 2003. **2**(11): p. 1199-210.
25. Chang, D.K., et al., *Effect of H(2)O(2) on cell cycle and survival in DNA mismatch repair-deficient and -proficient cell lines.* Cancer Lett, 2003. **195**(2): p. 243-51.
26. Colussi, C., et al., *The mammalian mismatch repair pathway removes DNA 8-oxodGMP incorporated from the oxidized dNTP pool.* Curr Biol, 2002. **12**(11): p. 912-8.
27. Russo, M.T., et al., *Role of MUTYH and MSH2 in the control of oxidative DNA damage, genetic instability, and tumorigenesis.* Cancer Res, 2009. **69**(10): p. 4372-9.
28. Russo, M.T., et al., *The oxidized deoxynucleoside triphosphate pool is a significant contributor to genetic instability in mismatch repair-deficient cells.* Mol Cell Biol, 2004. **24**(1): p. 465-74.
29. Zlatanou, A., et al., *The hMsh2-hMsh6 complex acts in concert with monoubiquitinated PCNA and Pol eta in response to oxidative DNA damage in human cells.* Mol Cell, 2011. **43**(4): p. 649-62.
30. Ohtsubo, T., et al., *Identification of human MutY homolog (hMYH) as a repair enzyme for 2-hydroxyadenine in DNA and detection of multiple forms of hMYH located in nuclei and mitochondria.* Nucleic Acids Res, 2000. **28**(6): p. 1355-64.
31. Ushijima, Y., et al., *A functional analysis of the DNA glycosylase activity of mouse MUTYH protein excising 2-hydroxyadenine opposite guanine in DNA.* Nucleic Acids Res, 2005. **33**(2): p. 672-82.

32. Jacobs, A.L. and P. Schar, *DNA glycosylases: in DNA repair and beyond.* Chromosoma, 2012. **121**(1): p. 1-20.
33. Dianov, G., A. Price, and T. Lindahl, *Generation of single-nucleotide repair patches following excision of uracil residues from DNA.* Mol Cell Biol, 1992. **12**(4): p. 1605-12.
34. Frosina, G., et al., *Two pathways for base excision repair in mammalian cells.* J Biol Chem, 1996. **271**(16): p. 9573-8.
35. Klungland, A. and T. Lindahl, *Second pathway for completion of human DNA base excision-repair: reconstitution with purified proteins and requirement for DNase IV (FEN1).* EMBO J, 1997. **16**(11): p. 3341-8.
36. Fang, W.H. and P. Modrich, *Human strand-specific mismatch repair occurs by a bidirectional mechanism similar to that of the bacterial reaction.* J Biol Chem, 1993. **268**(16): p. 11838-44.
37. Thomas, D.C., J.D. Roberts, and T.A. Kunkel, *Heteroduplex repair in extracts of human HeLa cells.* J Biol Chem, 1991. **266**(6): p. 3744-51.
38. Holmes, J., Jr., S. Clark, and P. Modrich, *Strand-specific mismatch correction in nuclear extracts of human and Drosophila melanogaster cell lines.* Proc Natl Acad Sci U S A, 1990. **87**(15): p. 5837-41.
39. Kadyrov, F.A., et al., *Endonucleolytic function of MutLalpha in human mismatch repair.* Cell, 2006. **126**(2): p. 297-308.
40. Pena-Diaz, J., et al., *Noncanonical mismatch repair as a source of genomic instability in human cells.* Mol Cell, 2012. **47**(5): p. 669-80.
41. Gillespie, P.J., A. Gambus, and J.J. Blow, *Preparation and use of Xenopus egg extracts to study DNA replication and chromatin associated proteins.* Methods, 2012. **57**(2): p. 203-13.
42. Brooks, P., et al., *Mismatch repair involving localized DNA synthesis in extracts of Xenopus eggs.* Proc Natl Acad Sci U S A, 1989. **86**(12): p. 4425-9.
43. Nash, H.M., et al., *Cloning of a yeast 8-oxoguanine DNA glycosylase reveals the existence of a base-excision DNA-repair protein superfamily.* Curr Biol, 1996. **6**(8): p. 968-80.
44. Dherin, C., et al., *Excision of oxidatively damaged DNA bases by the human alpha-hOgg1 protein and the polymorphic alpha-hOgg1(Ser326Cys) protein which is frequently found in human populations.* Nucleic Acids Res, 1999. **27**(20): p. 4001-7.
45. Warren, J.J., et al., *Structure of the human MutSalpha DNA lesion recognition complex.* Mol Cell, 2007. **26**(4): p. 579-92.
46. Schanz, S., et al., *Interference of mismatch and base excision repair during the processing of adjacent U/G mispairs may play a key role in somatic hypermutation.* Proc Natl Acad Sci U S A, 2009. **106**(14): p. 5593-8.
47. Ghodgaonkar, M.M., et al., *Ribonucleotides misincorporated into DNA act as strand-discrimination signals in eukaryotic mismatch repair.* Mol Cell, 2013. **50**(3): p. 323-32.
48. Iaccarino, I., et al., *hMSH2 and hMSH6 play distinct roles in mismatch binding and contribute differently to the ATPase activity of hMutSalpha.* EMBO J, 1998. **17**(9): p. 2677-86.
49. Kubota, Y. and H. Takisawa, *Determination of initiation of DNA replication before and after nuclear formation in Xenopus egg cell free extracts.* J Cell Biol, 1993. **123**(6 Pt 1): p. 1321-31.

50. Koi, M., et al., *Human chromosome 3 corrects mismatch repair deficiency and microsatellite instability and reduces N-methyl-N'-nitro-N-nitrosoguanidine tolerance in colon tumor cells with homozygous hMLH1 mutation.* Cancer Res, 1994. **54**(16): p. 4308-12.
51. Baerenfaller, K., F. Fischer, and J. Jiricny, *Characterization of the "mismatch repairosome" and its role in the processing of modified nucleosides in vitro.* Methods Enzymol, 2006. **408**: p. 285-303.
52. van Loon, B. and U. Hubscher, *An 8-oxo-guanine repair pathway coordinated by MUTYH glycosylase and DNA polymerase lambda.* Proc Natl Acad Sci U S A, 2009. **106**(43): p. 18201-6.
53. Hashimoto, Y., et al., *Rad51 protects nascent DNA from Mre11-dependent degradation and promotes continuous DNA synthesis.* Nat Struct Mol Biol, 2010. **17**(11): p. 1305-11.

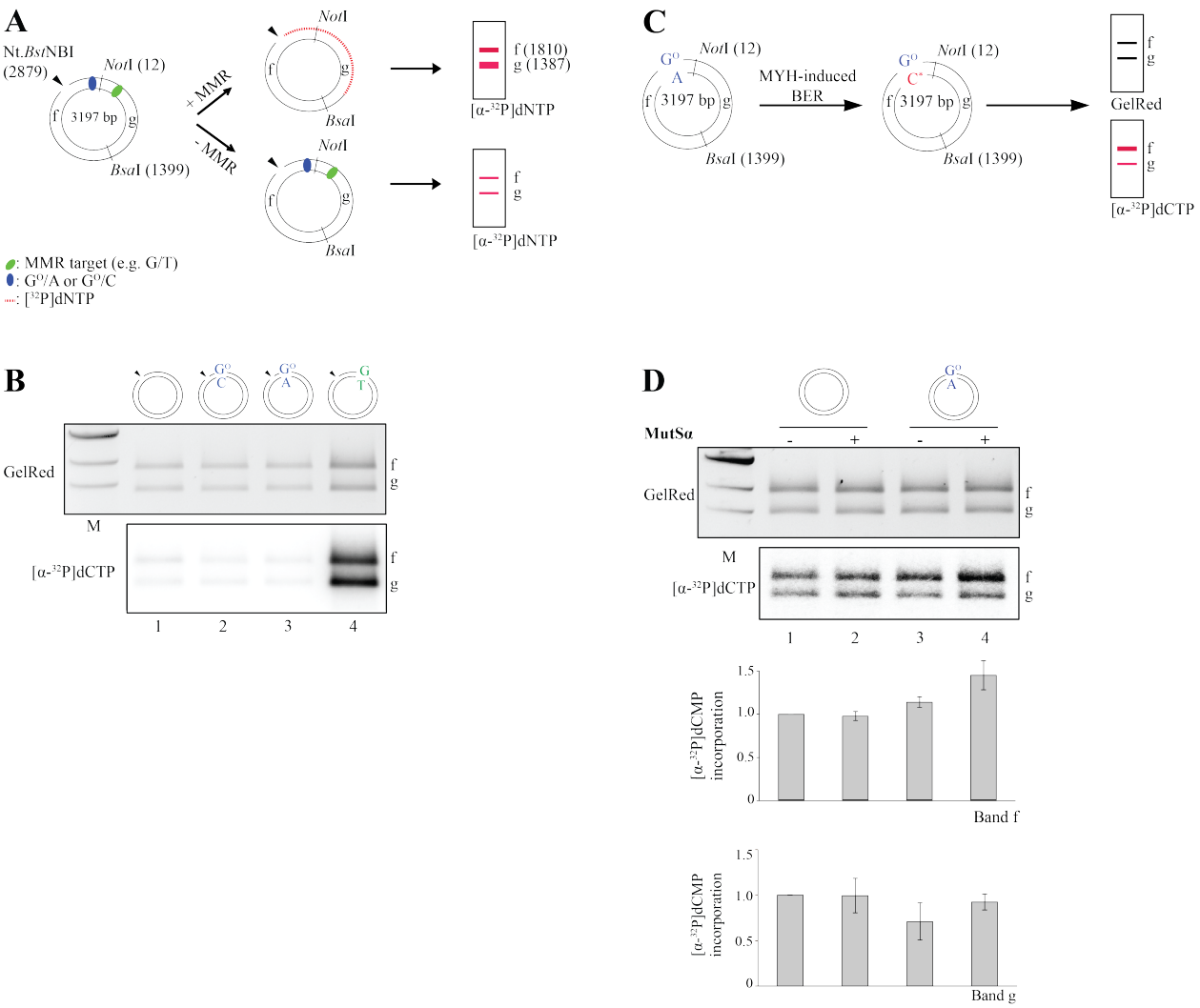

Figure 1. Mismatch repair stimulates MYH activities in human cells. (**A**) Schematic representation of a MMR-dependent nucleotide incorporation assay using 5'-nicked substrates. In the absence of a MMR target (-MMR), very little repair-mediated [^{32}P]dNMP incorporation takes place. In the presence of a MMR target (+MMR), MMR-mediated [^{32}P]dNMP incorporation can be detected upon *Not*I/*Bsa*I digestion of the phagemid DNA in both the 1810 bp **f** and 1387 bp **g** fragments. Locations of the modified base pairs/mispairs: G^{O}/A, 3183; G^{O}/C, 3188; G/T, 45. (**B**) G^{O}/A and G^{O}/C base pairs are not addressed by MMR in a MMR-dependent nucleotide incorporation assay. 5'-nicked substrates containing either no mismatch, or a G^{O}/C, G^{O}/A or G/T mismatch 306-363 nucleotides away from the nick, were incubated with HCT116 nuclear cell extracts supplemented with purified recombinant MutLα and [α-^{32}P]dCTP. Upon *Not*I/*Bsa*I restriction digestion, GelRed-stained DNA served as the DNA loading control, while the autoradiograph visualized MMR-dependent repair tracts in fragments **f** and **g** by means of [^{32}P]dCMP incorporation. M, molecular size marker (1 kb ladder, New England Biolabs). (**C**) Schematic representation of a MYH-dependent nucleotide incorporation assay. Repair of G^{O}/A to G^{O}/C by MYH-mediated BER can be detected primarily by incorporation of [^{32}P]dCMP into the 1810 bp fragment generated by *Not*I/*Bsa*I digestion of the substrate. (**D**) MutSα stimulates MYH activity on G^{O}/A mispairs in a BER-dependent nucleotide incorporation assay. Homoduplex or G^{O}/A-containing closed circular substrates were incubated with HCT116 nuclear cell extracts depleted of MSH6 and supplemented with recombinant purified MutSα where indicated (+). The reactions were supplemented with [α-^{32}P]dCTP to help visualize MYH-induced BER efficiencies, which were quantitated from the intensity ratio between band **f** in the autoradiograph and in the GelRed-stained agarose gel. The value for lane 1 was set to 1. MYH-independent [^{32}P]dCMP incorporation was determined from the relative intensities of band **g** in the autoradiograph and in the GelRed-stained agarose gel. The quantifications represent an average of 3 independent experiments +/- standard deviation (SD).

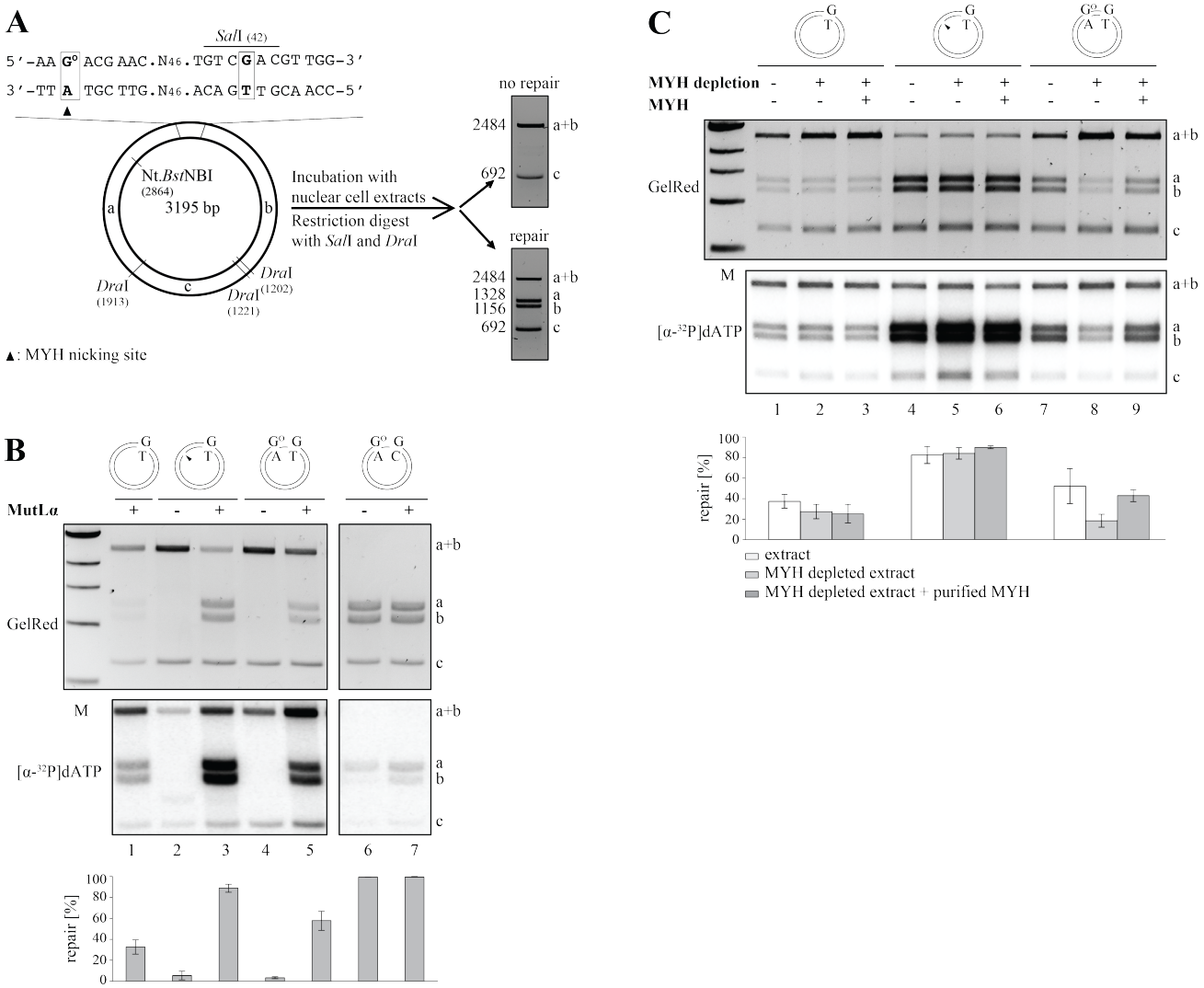

Figure 2. A single G^O/A base pair in a DNA heteroduplex acts as an initiation site for MMR in human nuclear cell extracts. (**A**) Schematic representation of the G^O/A-G/T substrate and the *in vitro* MMR assay. The substrate carries a G^O/A mispair 57 nucleotides away from a G/T mismatch, which is located in a *Sal*I recognition site. The presence of the mismatch makes the phagemid refractory to cleavage with the enzyme, such that incubation with *Sal*I and *Dra*I yields fragments of 2484 (a+b), 692 (c) and 19 bp (the smallest fragment is not detectable on 1% agarose gels strained with GelRed). Introduction of a single nick into the inner strand by Nt.*Bst*NBI and incubation with human nuclear cell extracts results in a repair of the G/T mismatch to G/C, which regenerates the *Sal*I site. Upon incubation with *Sal*I and *Dra*I, the repaired phagemid gives rise to fragments of 1328 (a), 1156 (b), 692 (c) and 19 base pairs. (**B**) G^O/A mispairs serve as initiation sites for MMR. The efficiency of repair of a G/T mismatch in supercoiled G/T (lane 1), nicked G/T (lane 2,3), supercoiled G^O/A-G/T (lanes 4,5,) and supercoiled G^O/A-G/C (lane 6,7) substrates incubated with nuclear extracts of MutLα-deficient HCT116 cells, supplemented where indicated (+) with purified MutLα. (**C**) G/T repair in the G^O/A-G/T substrate is dependent on MYH. The supercoiled G/T (lanes 1-3), nicked G/T (lanes 4-6), and the supercoiled G^O/A-G/T (lanes 7-9) substrates were incubated with extracts of HCT116 cells, which were either mock-depleted (lanes 1, 4, 7), MYH-depleted (lanes 2, 5, 8) or MYH-depleted and supplemented with recombinant MYH (lanes 3, 6, 9). The efficiency of the repair reactions shown in panels **B** and **C** was estimated by ImageQuant from scans of GelRed-stained agarose gels. The indicated MMR efficiencies (%) represent an average of 3 independent experiments +/- standard deviation (SD).

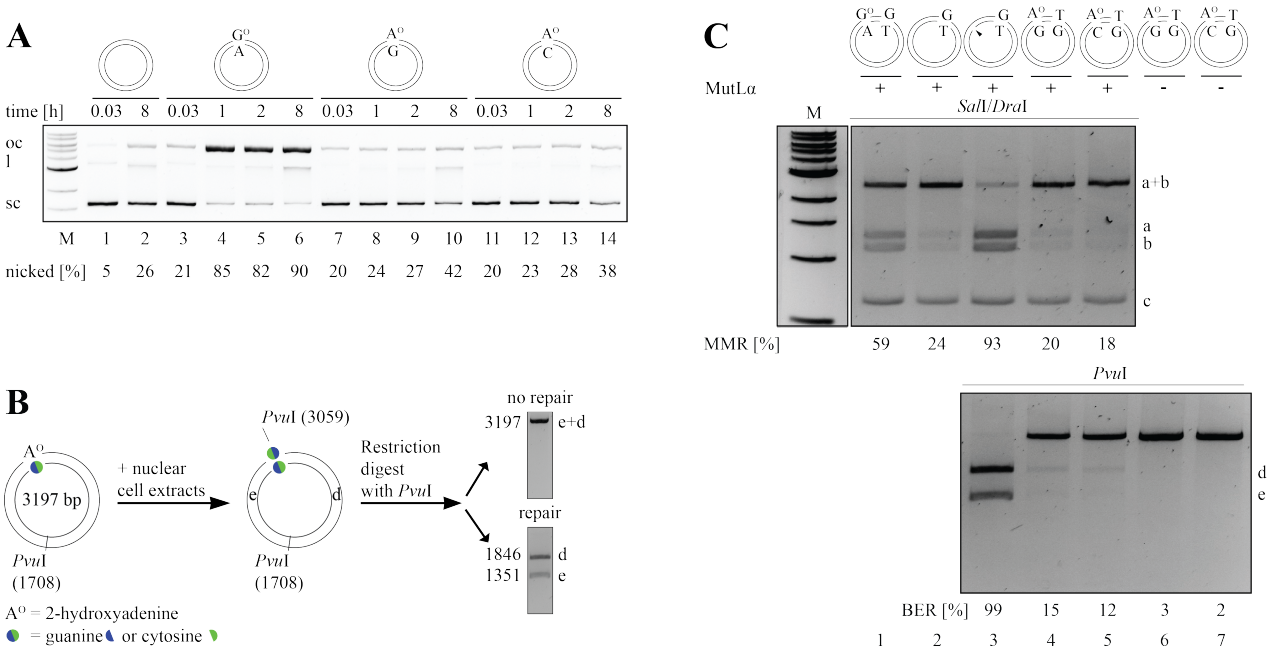

Figure 3. A^O/G and A^O/C mispairs do not act as initiation sites for MMR in human nuclear cell extracts. (**A**) The supercoiled homoduplex, G^O/A, A^O/G or A^O/C substrates were incubated with recombinant, purified MYH and APE1 for the indicated times and analyzed by agarose gel electrophoresis. The quantification shows the percentage of open circular (oc) substrate compared to the total DNA (oc + sc). Only the G^O/A substrate was cleaved with appreciable efficiency. The mobility of the supercoiled (sc), open circular (oc) and linear (l) DNA molecules is indicated on the left. (**B**) Schematic representation of phagemid substrates containing A^O mispaired with guanine or cytosine. The A^O residue is located within a *Pvu*I restriction site, which makes the phagemid refractory to cleavage with this enzyme. A^O/G to C/G, or A^O/C to G/C repair restores the *Pvu*I site. Incubation with the enzyme gives rise to fragments of 1846 bp (d) and 1351 bp (e). Position of A^O/G: 3060, A^O/C: 3057. (**C**) A^O/G and A^O/C mispairs do not serve as MMR initiation sites. The indicated substrates were incubated with MMR-deficient HCT116 extracts supplemented (+) or not (-) with purified MutLα. Upper panel: Efficiency of G/T to G/C repair mediated by MMR was estimated by S*al*I/*Dra*I restriction digests of the recovered substrates: supercoiled G^O/A-G/T (lane 1), supercoiled G/T (lane 2), nicked G/T (lane 3), supercoiled A^O/G-T/G (lane 4) supercoiled A^O/C-T/G (lane 5). Lower panel: Digestion of the shown recovered phagemids with *Pvu*I, which detects MYH-dependent BER of A^O to C in the A^O/G substrate, or A^O to G in the A^O/C substrate. The nicked G/T substrate (lane 3) served as the positive control for *Pvu*I digestion. A^O/G-T/G and A^O/C-T/G substrates that were not incubated with the extracts (lanes 6-7) contain defective *Pvu*I sites and thus served as negative controls. MMR and BER efficiencies (%) are indicated below the panels.

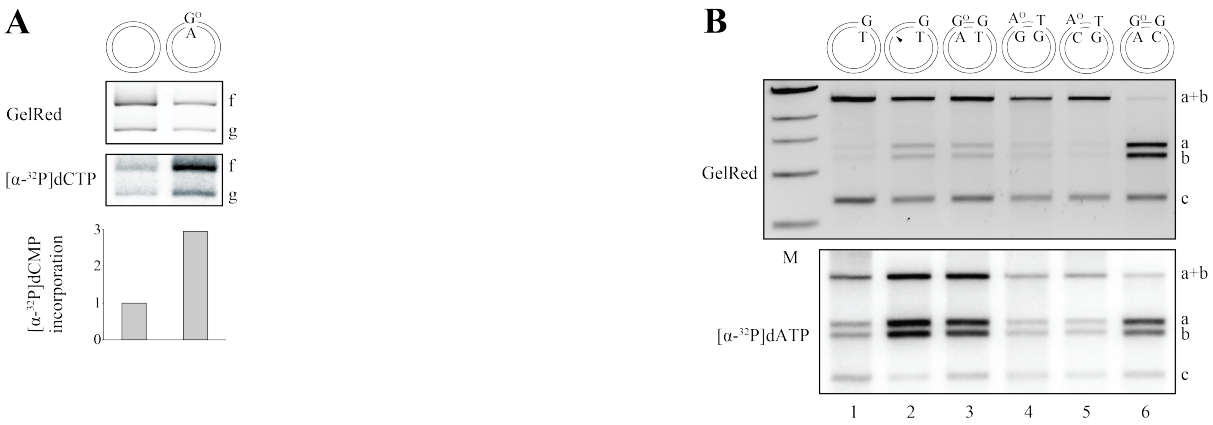

Figure 4. The G^O/A mispair acts as a MMR initiation site in *Xenopus laevis* egg extracts. (**A**) MYH is active in *Xenopus laevis* eggs. Supercoiled homoduplex or G^O/A substrates were incubated with the extracts supplemented with [α-^{32}P]dCTP. While only background levels of [α-^{32}P]dCMP were incorporated into the homoduplex substrate (lane 1), substantial incorporation into the 1810 bp fragment **f** of the G^O/A substrate was detected (lane 2), which is indicative of base excision repair. For quantification, [α-^{32}P]dCMP incorporation into the homoduplex substrate was set to 1. The panels show representative images of two independent experiments. (**B**) G^O/A, but not A^O/G or A^O/C serves as an initiation site for MMR in *Xenopus laevis* egg extracts. G/T (lane 1), nicked G/T (lane 2), G^O/A-G/T (lane 3), A^O/G-T/G (lane 4), A^O/C-T/G (lane 5) or G^O/A-G/C (lane 6) substrates were incubated with *Xenopus laevis* egg extracts. Upon *Sal*I/*Dra*I digestion of the recovered phagemids, MMR efficiencies were estimated from the GelRed-stained agarose gels, while MMR-dependent DNA synthesis was visualized by [α-^{32}P]dATP incorporation seen in the autoradiograph. The panels show representative images of three independent experiments.

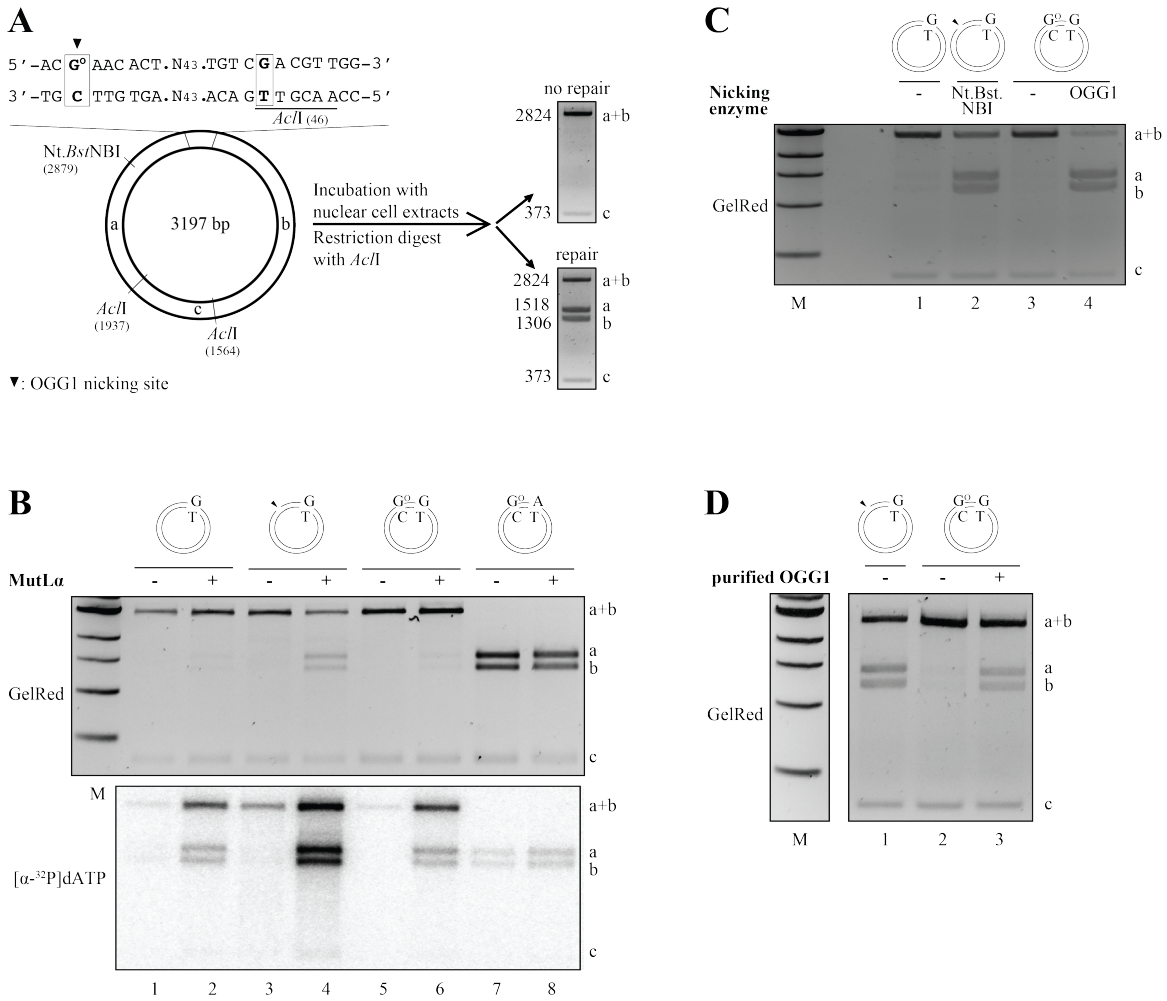

Figure 5. A G^O/C base pair does not act as an initiation site for MMR in nuclear extracts of human cells. (**A**) Schematic representation of the G^O/C-G/T substrate used in the *in vitro* MMR assay. The circular heteroduplex substrate carries a G^O/C base pair 54 nucleotides from a G/T mismatch in the recognition site of *Acl*I endonuclease. The positions of two further *Acl*I cleavage sites and the Nt.*Bst*NBI site, where a nick can be introduced selectively into the outer strand, are indicated. In the absence of repair, digestion of the phagemid with *Acl*I gives rise to fragments of 2824 (**a+b**) and 373 bp (**c**). Repair of the G/T mismatch to A/T regenerates a third *Acl*I restriction site, such that the phagemid DNA is cleaved into 3 fragments of 1518 (**a**), 1306 (**b**), and 373 bp (**c**). (**B**) Substrates G/T (lanes 1, 2), nicked G/T (lanes 2, 3), G^O/C-G/T (lanes 4, 5) and G^O/C-A/T (lanes 7,8) were incubated with extracts of HCT116 cells supplemented (+) or not (-) with purified recombinant MutLα and were analyzed on a GelRed-stained agarose gel. The autoradiographs visualized [α-^{32}P]dAMP incorporation into the different substrate fragments. Only background levels of repair were detected in the G^O/C-G/T substrate. (**C**) OGG1-generated DNA termini at G^O/C sites act as MMR initiation sites. The G^O/C-G/T phagemid substrate was pre-incubated either with Nt.*Bst*NBI (lane 2), or with recombinant, purified OGG1 (lane 4) to generate nicked substrates (see Fig S5B). The substrates were then purified and incubated with LoVo nuclear cell extracts supplemented with purified MutSα (lanes 1-4). Supercoiled G/T (lane 1) and G^O/C-G/T (lane 3) phagemid substrates served as controls. (**D**) A G^O/C base pair activates MMR in extracts supplemented with OGG1. The nicked G/T (lane 1) and the G^O/C-G/T (lanes 2, 3) substrates were incubated with LoVo nuclear cell extracts supplemented with purified MutSα, supplemented (+) or not (-) with 40 ng of purified recombinant OGG1. The panels in **B**, **C** and **D** show representative images of three independent experiments.

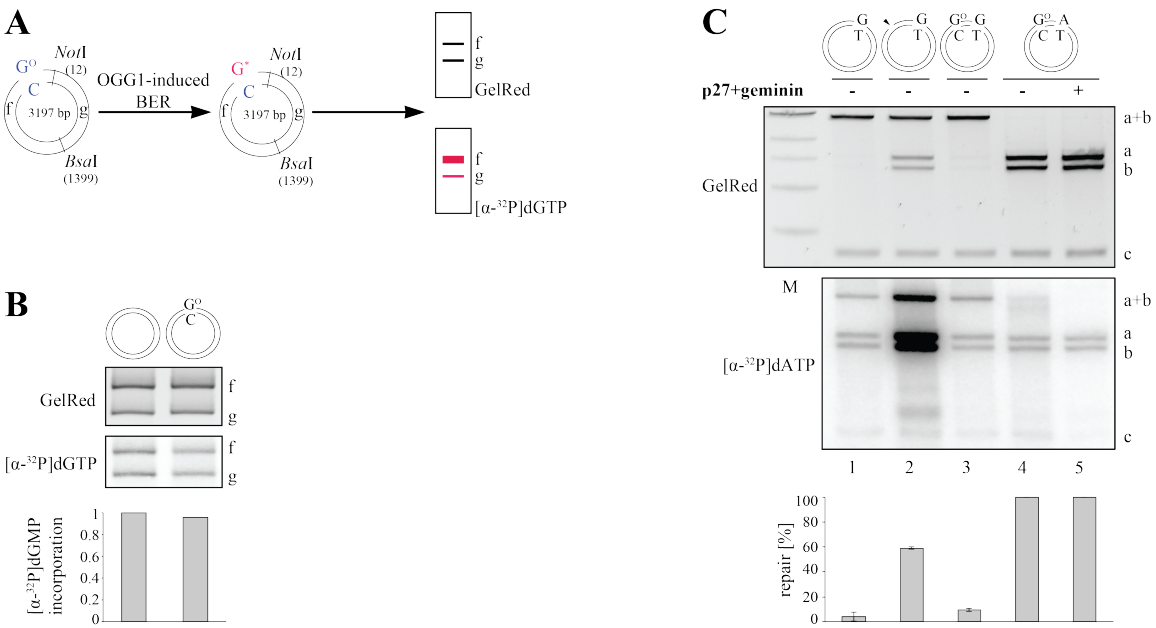

Figure 6. A G^O/C base pair does not act as an initiation site for MMR in *Xenopus laevis* egg extracts. (**A**) Schematic representation of an *in vitro* OGG1-dependent repair synthesis assay. OGG1-initiated BER of G^O/C to G/C should incorporate [α-^{32}P]dGMP into the 1810 bp (**f**) fragment generated by *Not*I/*Bsa*I digestion of the substrate. (**B**) *Xenopus laevis* egg extracts lack OGG1 activity, as only background levels of [α-^{32}P]dGMP were incorporated into the control homoduplex and the G^O/C substrates. OGG1-dependent BER efficiencies were quantified from the intensity ratio between band f in the autoradiograph and the GelRed-stained agarose gel using ImageQuant. The panel shows a representative image of two independent experiments. (**C**) The MMR activity in *Xenopus laevis* egg extracts was determined using supercoiled G/T (lane 1), nicked G/T (lanes 2), G^O/C-G/T (lane 3) and G^O/C-A/T (lanes 4, 5) substrates. That similar background levels of [α-^{32}P]dAMP were incorporated into the control G^O/C-A/T substrate in the absence (lane 4) and presence (lane 5) of the replication inhibitors p27 and geminin demonstrates that the phagemids were not replicated under these conditions [53]. The panel shows representative images of three independent experiments quantitated below.

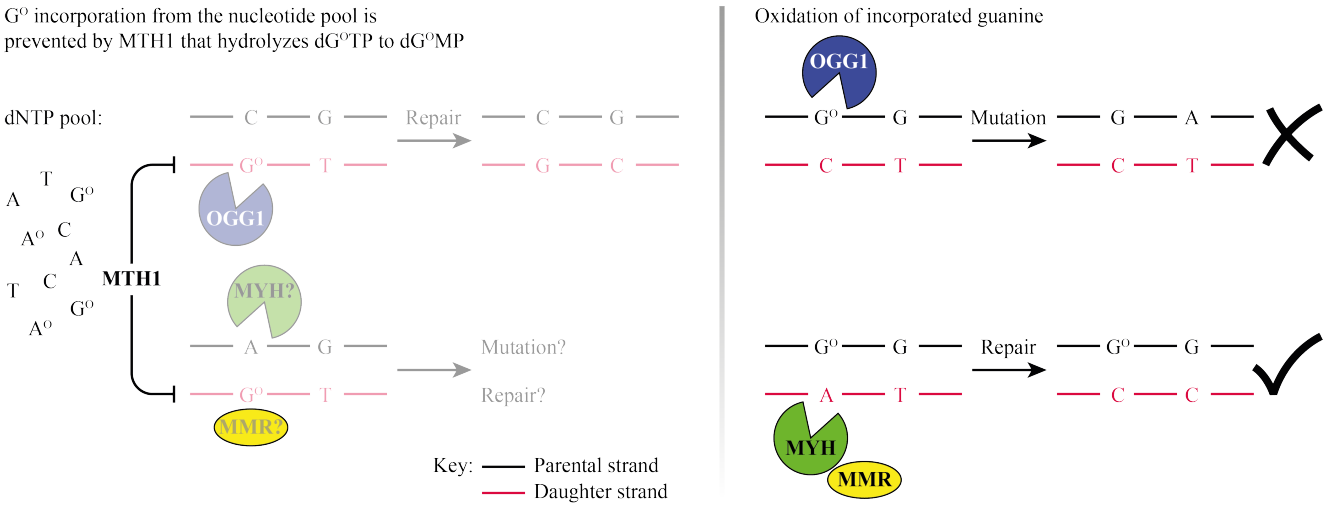

Figure 7. BER-dependent mismatch repair at 8-oxoguanine sites. If MMR recognizes a mismatch (G/T) during replication, it will search for a close-by strand discontinuity in order to induce its repair process by EXOI-loading to the nick. We hypothesized that these strand discontinuities might result from OGG1- or MYH- induced BER-intermediates, but would have different effects on MMR fidelity. **Left panel:** deoxy-8-oxoguanosine triphosphate (dG^{O}TP) in the nucleotide pool is hydrolyzed to its monophosphate (dG^{O}MP) by MTH1, thus preventing G^{O} incorporation into the newly synthesized DNA strand. The occurrence of C/G^{O} and thus OGG1-directed MMR to the daughter strand is therefore unlikely. Also A/G^{O} mispairs will be infrequently generated. It would be inexplicit whether MYH would excise the A from the parental strand or whether MMR would be involved in the removal of G^{O} from the daughter strand. The effect on MMR fidelity at close-by mismatches is therefore unclear. **Right panel:** In contrast, G/C base pairs are frequently oxidized to G^{O}/C in the DNA helix. Thus, G^{O} would be in the parental strand during the next round of replication. If C is incorporated opposite G^{O}, G^{O}/C is repaired by OGG1-induced BER. During S-phase, OGG1-generated nicks would misdirect MMR to the parental strand, so that it could not repair the G/T mismatch to G/C but instead, mutate it to A/T. Indeed, this unfavorable event was suppressed in our *in vitro* studies. If G^{O}/C containing DNA helices replicate, they can also give rise to G^{O}/A mispairs with A in the daughter strand. G^{O}/A is repaired by MYH-induced BER, thereby being stimulated by MMR proteins. MYH-induced nicks at the A-site, would correctly direct MMR to the daughter strand and enable it to repair G/T to G/C. Our studies in human and *Xenopus laevis* cell extracts showed that MYH-directed MMR takes place, suggesting that higher eukaryotes might have adopted G^{O}/A mispairs as strand discrimination signals for MMR.

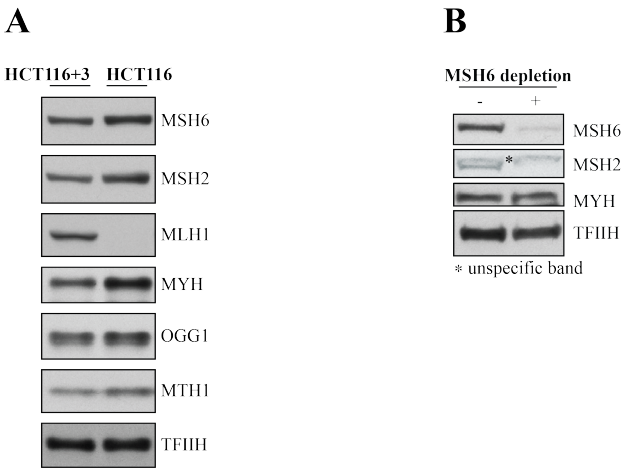

Figure S1. (**A**) Western blot analysis of HCT116 and HCT116 + chromosome 3 nuclear cell extracts to verify the presence and relative abundance of MMR (MSH6, MSH2, MLH1) and BER (MYH, OGG1, MTH1) proteins. The absence of MutLα in HCT116 cells is well documented and was, where indicated, complemented with the purified recombinant protein. (**B**) Western blot showing the efficiency of MSH6 immunodepletion of HCT116 nuclear cell extracts.

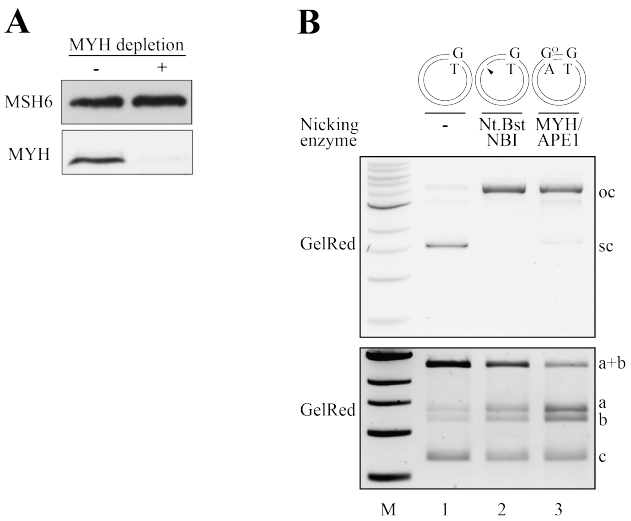

Figure S2. (**A**) Western blot showing MYH immunodepletion efficiency of HCT116 nuclear cell extracts. (**B**) MYH/APE1-generated DNA termini at G^O/A sites are recognized by MMR. Upper panel: The G/T substrate, either supercoiled (lane 1) or pre-nicked with Nt.*Bst*NBI (lane 2), or the G^O/A-G/T phagemid (lane 3) were incubated with purified recombinant MYH-GST and APE1 or mock-incubated under the same experimental conditions. Lower panel: The purified substrates were incubated with HCT116 nuclear extracts supplemented with MutLα, digested with *Sal*I/*Dra*I and analyzed on GelRed stained agarose gels. The G/T mispair in the pre-treated G^O/A-G/T substrate was very efficiently repaired.

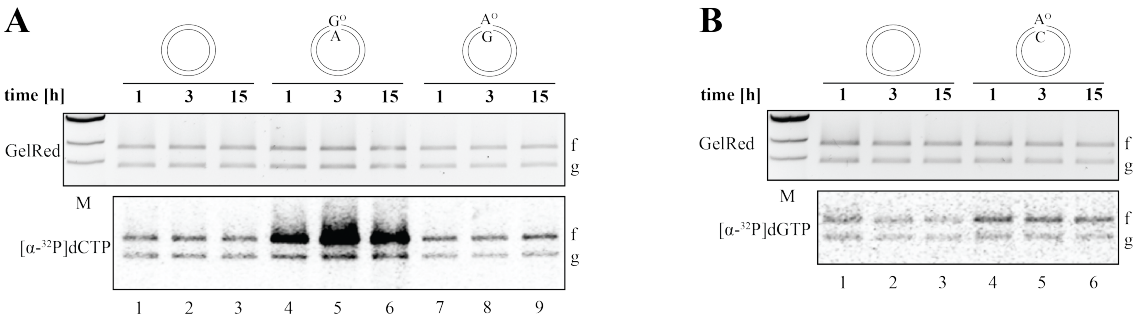

Figure S3. MYH is active in HCT116 extracts and addresses G^O/A but not A^O/G or A^O/C sites. (**A**) The supercoiled homoduplex (lanes 1-3), G^O/A (lanes 4-6) and A^O/G (lanes 7-9) substrates were incubated with the extracts for the indicated time points. The reactions were supplemented with [α-^{32}P]dCTP. As visualized in the autoradiograph, [^{32}P]dCMP incorporation into fragment **f** of a *Not*I/*Bsa*I digested phagemid, indicative of short-patch repair, was detected above background only in the G^O/A substrate. (**B**) The supercoiled homoduplex (lanes 1-3) and A^O/C (lanes 4-6) substrates were incubated with the extracts for the indicated time points, in reactions supplemented with [α-^{32}P]dGTP. Only low levels of radioactive nucleotide were incorporated into the fragment **f** of a *Not*I/*Bsa*I digested A^O/C phagemid, indicative of inefficient BER.

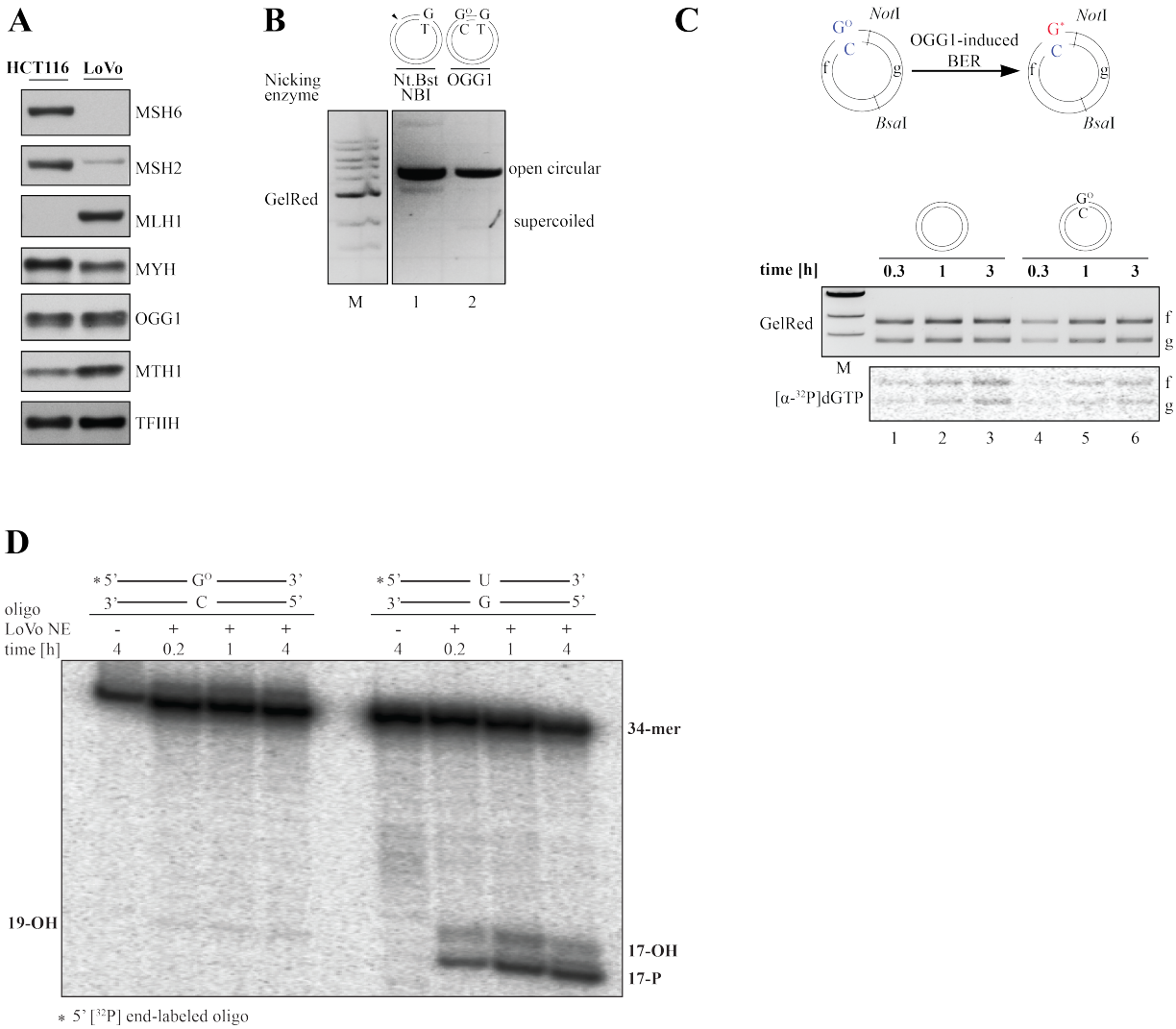

Figure S5. (**A**) Western blot analysis of HCT116 and LoVo nuclear cell extracts to verify the presence and relative abundance of MMR (MSH6, MSH2, MLH1) and BER (MYH, OGG1, MTH1) proteins. The absence of MutLα in HCT116 cells and of MutSα in LoVo cells is evident, and was, where required, compensated by the addition of purified recombinant protein. (**B**) The G^O/C-G/T phagemid substrate was pre-incubated with purified recombinant OGG1 (lane 2), thereby generating a nicked substrate, which migrates in the same position in the 1% agarose gel as the G/T substrate nicked with Nt.*Bst*NBI (lane 1). These pre-nicked substrates were purified and used in the MMR assays (see Figure 5C). (**C**) Absence of OGG1 activity in human nuclear cell extracts. Upper panel: Schematic representation of an OGG1-dependent nucleotide incorporation assay. Repair of G^O/C to G/C by OGG1-mediated BER should result in incorporation of [^{32}P]dGMP into fragment **f** generated by *Not*I/*Bsa*I digestion of the substrate. Lower panel: OGG1-dependent nucleotide incorporation assay. Substrates Homoduplex or G^O/C substrates were incubated with the extracts supplemented with [α-^{32}P]dGTP for the indicated times. As seen in the autoradiograph, both substrates incorporated similar amounts of [^{32}P]dGMP, which were close to background. (**D**) Nuclear extracts of LoVo cells contain extremely low OGG1 activity on a G^O/C oligonucleotide substrate, as compared to UNG activity on a U/G oligonucleotide substrate. The G^O/C- or U/G-containing 34-mer oligonucleotides were [^{32}P]-labeled at the 5' terminus of the G^O or U-containing strand, respectively. 20 fmol oligonucleotide were incubated with 100 µg LoVo nuclear cell extracts (+) at 37°C for the indicated times. The oligonucleotide substrates were loaded in the control lanes (-). The OGG1- or UNG-mediated nicking efficiencies in the cell extracts were analyzed on 20% denaturing polyacrylamide gels. The predicted sites of cleavage are indicated by arrows.

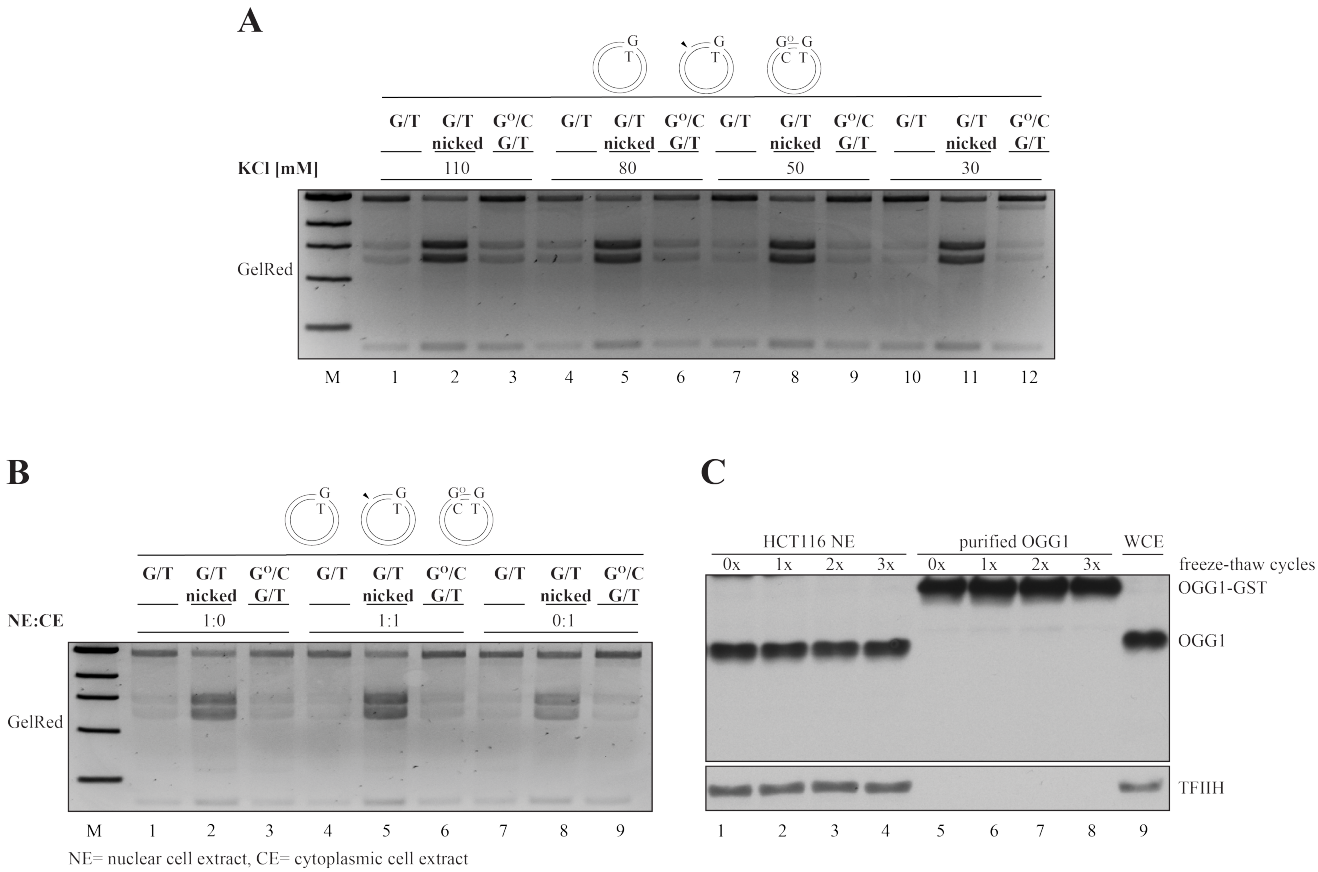

Figure S6. Optimization of experimental conditions for *in vitro* MMR assays with G^{O}/C substrates. (**A**) Effect of salt concentration on MMR efficiency. The G/T, nicked G/T and G^{O}/C-G/T substrates were incubated with HCT116 nuclear cell extracts supplemented with MutLα in buffers containing 110 (lanes 1-3), 80 (lanes 4-6), 50 (lanes 7-9) or 30 (lane 12) mM KCl. Decreasing salt concentrations did not improve OGG1-dependent MMR activity. (**B**) Comparison of MMR activity in nuclear and cytoplasmic cell extracts. The G/T, nicked G/T and G^{O}/C-G/T substrates were incubated in a buffer containing 110 mM KCl and HCT116 cell extracts either nuclear (1:0), nuclear and cytoplasmic (1:1), or only cytoplasmic (0:1). The panels **A** and **B** show UV shadowing of a 1% agarose gel stained with GelRed. (**C**) OGG1 stability in nuclear cell extracts (NE) of HCT116 cells. The extracts were freeze/thawed up to three times and examined for OGG1 degradation by Western blotting (lanes 2-4). The control samples (0x, lanes 1, 5) were not freeze/thawed, which corresponds to conditions used in our *in vitro* MMR assays. Purified recombinant OGG1-GST (Trevigen, lanes 6-8) and OGG1 present in whole cell extracts (WCE) of HCT116 cells (lane 9) served as controls.

3.1.2 Additional data relating to the manuscript

3.1.2.1 Establishment of an in vivo MMR assay

Aim

In the course of my work on the interplay of MMR and BER during the processing of oxidative DNA damage, one of my aims was to test the *in vivo* relevance of the observations that we made in extracts of human cells and in *Xenopus laevis* eggs. Since no adequate method was available at that time, we set out to establish an *in vivo* MMR assay. For this purpose, I designed and set-up a Master project that I supervised during a period of 8 months. The different methods tested, their pros and cons, as well as the results we achieved with the newly-developed method, are summarized below.

Establishment of an *in vivo* MMR assay

The approach we chose was to transfect plasmids containing a G^O/A mismatch in the proximity of a MMR target into cells, recover them after 24 hours and analyze their repair. The MMR target G/T, as also used in the *in vitro* MMR assays (see chapter 3.1.1), is inappropriate for *in vivo* MMR assays. This is because it would be recognized not only by MMR proteins but also by the DNA glycosylases TDG and MBD4, which are only negligibly active in our *in vitro* conditions. To circumvent this problem, we designed substrates that contained a 2 nucleotide loop in their inner strand, and thus represented a target exclusively for MMR. Since the outer strand encodes a *Sal*I restriction site, repair of the loop would make the substrate susceptible to *Sal*I digestion (Figure 3-1).

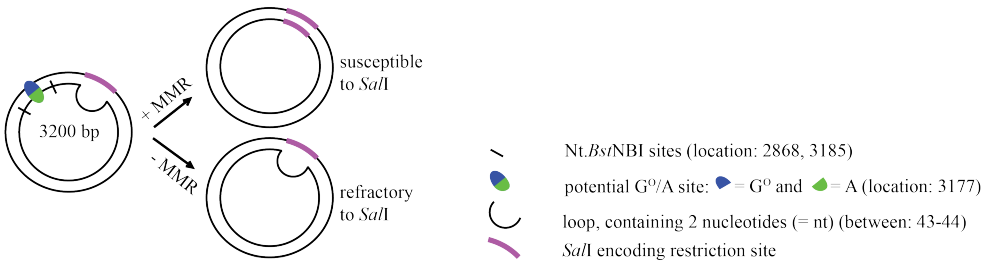

Figure 3-1: Schematic representation of the looped substrate.
A circular substrate contains a 2 nucleotide (GC) loop in the bottom strand. The positions of a potential G^O/A base pair, located 67 nucleotides away from the loop, and of Nt.BstNBI nicking sites are indicated. In the presence of MMR, the loop is repaired and generates a SalI restriction site.

In order to analyze repair of the recovered substrates, we tested and evaluated four different approaches (Figure 3-2).

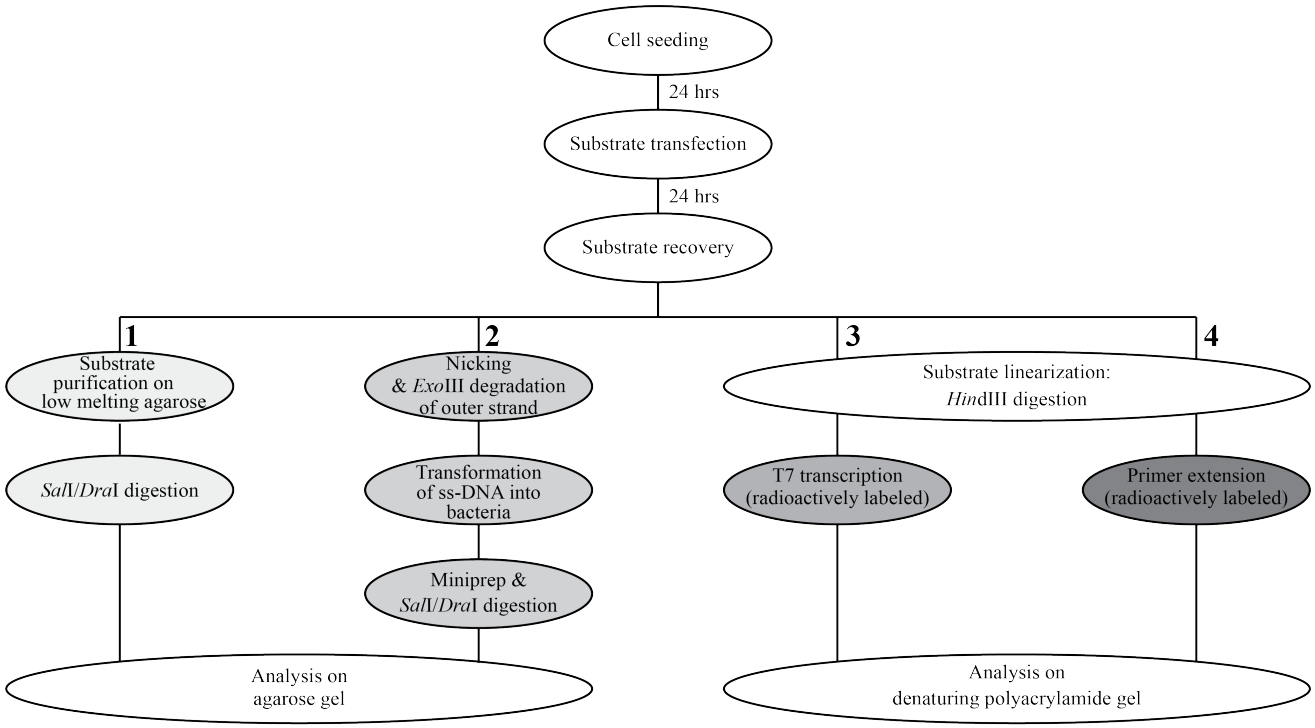

Figure 3-2: Flow chart, illustrating four different (1-4) approaches to analyze the repair of recovered substrates.

Approach 1

In the first approach, we gel-purified the recovered substrate and subsequently digested it with *Sal*I/*Dra*I, either in-gel or upon β-agarase I treatment and ethanol precipitation. Both led to incomplete digestion of the samples, which made quantifications difficult. Furthermore, we recovered only small amounts of DNA, about 1/10 of what we transfected, which were difficult to detect on GelRed-stained agarose gels. The following approaches therefore aimed to increase the signal by either amplification of the recovered DNA (approaches 2+3) or by radioactively-labeling it (approaches 3+4).

Approach 2

The second method involved nicking and ExoIII-mediated degradation of the outer strand, to yield the single-stranded (ss) inner plasmid strand, i.e. the one that MMR should have been directed to. The obtained ss-DNA was transformed into DH10B bacteria, which generated the appropriate complementary strand and amplified it. Subsequent column purification of the plasmid gave rise to sufficient and detectable amounts of plasmid and furthermore allowed complete *Sal*I/*Dra*I digestion. One drawback we encountered here was that we had no possibility to clearly prove that ExoIII completely degraded the outer strand, including the site opposite the loop. Furthermore, a control, Nt.*Bst*NBI pre-nicked substrate recovered from the transfected cells, still contained the nick in the inner strand. ExoIII treatment would have led to its linearization and hence would have prevented its transformation into bacteria. This would falsify the repair ratios amongst the different substrates. The next two approaches were based on the

amplification of the loop-spanning part of the inner strand. Amplicons of repaired substrates would hence appear two nucleotides shorter. This difference can be visualized on 10% polyacrylamide gels.

Approach 3

Upon *Hin*dIII linearization of the plasmid, we amplified the loop-spanning inner strand fragment, using run-off transcription with T7 RNA polymerase and radioactively-labeled NTPs. Although this approach led to a clear increase in sensitivity, it yielded also undefined bands of similar size to the transcript, which could be attributed to transcript slippage during transcription initiation [344].

Approach 4

Our fourth approach was similar, but based on primer extension of the linearized inner-strand fragment. Though starting with small amounts of recovered template DNA, the use of either 5' [^{32}P]-labeled primer, or the addition of radioactively labeled nucleotides, allowed an adequate detection of the primer extension products. Furthermore, this approach is not prone to strand slippage and hence leads to defined bands. Following optimization, we validated this method by applying it to substrates that were repaired within our standard *in vitro* MMR assay. Indeed, the repair percentages of the primer extension assay correlated tightly with those of the *in vitro* assay, thus excluding any bias of this method. Since this approach turned out to be suitable, we applied it to the following *in vivo* MMR assays. For details of the methods of the different approaches, as well as the validation of the primer extension-based method, the reader is referred to the Master thesis of Isabel Wassing. An overview about the different methods as well as their pros and cons is provided in Table 3-1.

Table 3-1: Advantages and disadvantages of different in vivo MMR assay approaches

No.	Method of substrate analysis upon its recovery from cells	Advantages	Disadvantages
1	Direct *Sal*I/*Dra*I digestion	- Quick method	- Incomplete restriction digestion - Little amounts of recovered DNA ➔ hard to detect
2	Amplification of repaired ss-DNA in bacteria & subsequent *Sal*I/*Dra*I digestion	- Amplification of substrate ➔ easy to detect - Complete restriction digestion	- ExoIII degradation past the mismatch is unverifiable - Falsified repair ratios in case of recovery of nicked substrates
3	T7 transcription (length of transcript indicates repair)	- Increased sensitivity due to i) amplification due to multiple transcripts ii) radioactive nucleotide incorporation	- Undefined transcripts - unstable RNA product ➔ degradation
4	Primer extension (length of DNA fragment indicates repair)	- Increased sensitivity due to radioactive nucleotide incorporation - stable DNA product ➔ defined bands	

3.1.2.2 *MYH-dependent mismatch repair in vivo*

MYH-dependent MMR *in vivo*

The validated primer extension-based *in vivo* MMR assay was applied to our substrates of interest. MMR-proficient HCT116 + chromosome 3 cells, either siLUC- or siMYH-treated, were transfected with different substrates (Figure 3-3 B, left panel). Upon recovery, the plasmids were linearized by *Hin*dIII digestion. Primer extension yielded fragments of defined lengths: 83 bp in the absence of repair or 81 bp in case of MMR-catalyzed loop removal (Figure 3-3 A).

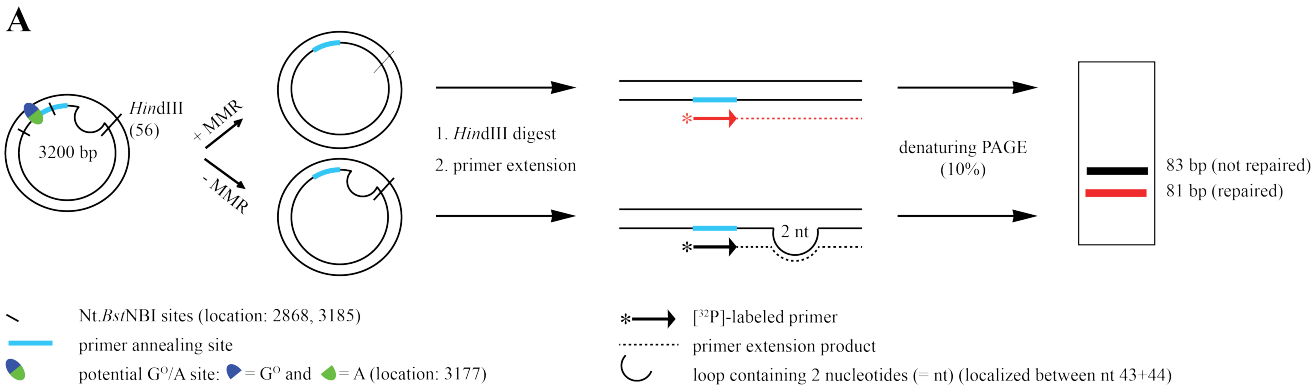

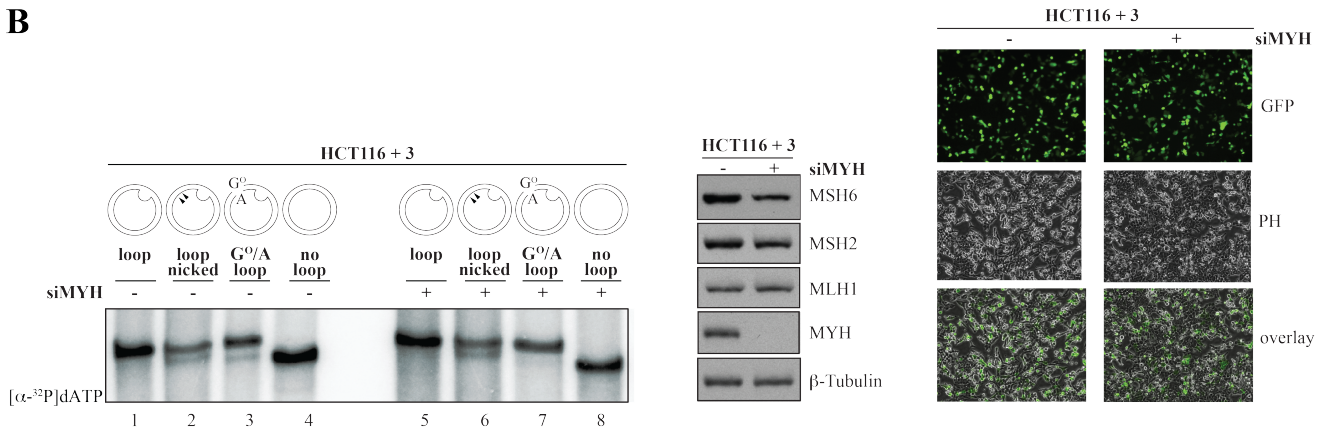

Figure 3-3: MYH-addressed G°/A sites serve as initiation sites for MMR in vivo.
(A) Schematic representation of an in vivo MMR assay. In the presence of MMR, the loop is repaired, which can be visualized by a primer extension assay. After recovery and linearization of the plasmid with HindIII, a [32P]-labeled primer binds to the binding site in the bottom strand (bright blue) and generates an 81 bp product. In the absence of MMR, the loop remains, which results in an 83 bp fragment. (B) In vivo MMR assay in HCT116 + chromosome 3 cells. (Left) Repair of substrates, either containing a loop, a loop and two 3' nicks (loop nicked), a G°/A base pair in the proximity of a loop (G°/A-loop) or a homoduplex (no loop) was analyzed upon recovery from human cells. Primer extension revealed repair of both the loop nicked and the G°/A-loop substrates. Upon siRNA-mediated knockdown of MYH, repair of the G°/A-loop substrate was abolished. (Middle) The MYH knockdown efficiency at the time of substrate transfection is shown on a Western blot. (Right) Transfection of siLUC- and siMYH-treated cells with pEGFP shows comparable transfection efficiencies.

As expected, nicked loop substrates (lanes 2+6) were repaired in the extracts and served as positive control. In addition, we could show that G^O/A sites in the close proximity of the loop served as initiation sites for MMR also *in vivo*, as an 81 bp fragment could be detected on the gel (lane 3). We could furthermore show that knockdown of MYH (Figure 3-3 B, Western blot) abolished MMR on the G^O/A-loop substrate (lane 7), indicating that MMR acted MYH-dependent *in vivo*. As the transfection efficiencies of both siLUC- and siMYH-treated cells were comparable (Figure 3-3 B, right panel), the above observations confirm our *in vitro* data.

3.1.2.3 MYH is physically stabilized by mismatch repair proteins

The effect of a transient MutSα knockdown on MYH levels

In the previous chapter 3.1.1 we described that MMR enhances MYH activity on G^O/A-containing plasmids, thus confirming the data of Gu *et al*. [35] using another experimental approach. They also observed a physical interaction between MutSα and MYH [35], which could not clearly be confirmed in our pulldown experiments (see chapter 3.2.4). However, the data presented below point into the same direction: siRNA-mediated knockdown of MSH6 or MSH2 led to a clear decrease of MYH levels, indicating that MYH is stabilized by MutSα (Figure 3-4). We showed this effect in three different cell lines and used three different siRNA sequences against MSH6 in order to exclude any off-target effects, but the result was the same for all of them. Unexpectedly, MLH1 knockdown brought about the same effect, most noticeably in U2OS cells. Conversely, the presence of MYH seemed not to be required for mismatch repair protein stability).

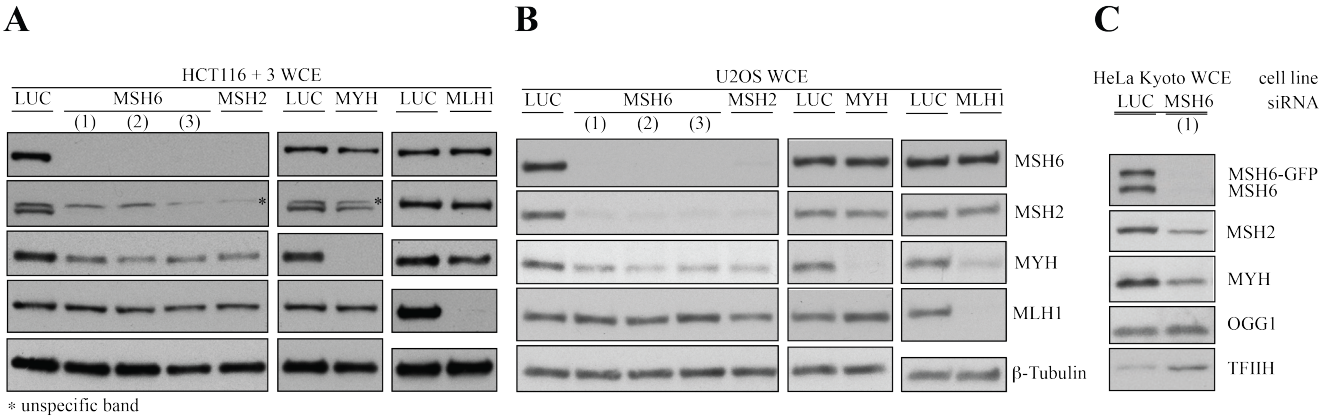

Figure 3-4: MutSα physically stabilizes MYH.
MYH levels in whole cell extracts (WCE) of (A) HCT116 + chromosome 3, (B) U2OS and (C) HeLa Kyoto (stably expressing MSH6-GFP) cells were analyzed by Western blotting. Cells were treated with the indicated siRNAs for 3 days. Three different siRNAs were used against MSH6 (1-3).

The effect of permanent MutSα deficiency on MYH levels

Interestingly, we observed the converse effect in two cell lines that have a permanent defect in MutSα. HEC59 cells, which have two heterozygous *hMSH2* mutations and HCT15 cells, which exhibit two mutations in the *hMSH6* gene, express higher levels of MYH than their chromosome 2 -complemented, repair-proficient counterparts (Figure 3-5). Also the BER enzyme polymerase-β is slightly increased in the MMR-deficient cell lines, as previously observed by Martin *et al*. [285].

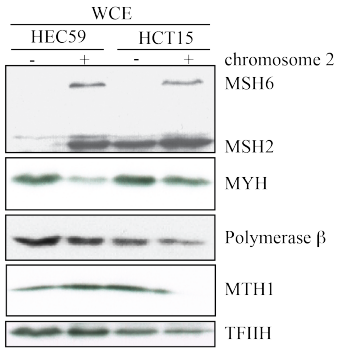

Figure 3-5: MYH is overexpressed in HEC59 and HCT15 cells when compared to their repair proficient counterparts. The Western blot shows expression levels of MutSα, MYH and polymerase-β in whole cell extracts (WCE) of HEC59 and HCT15 cells as well as in cells of their mismatch repair proficient (+ chromosome 2) counterparts [345].

3.1.2.4 Testing the activity of OGG1 in nuclear cell extracts

Time course: activity of MMR proteins in extracts

During our studies on the interplay of MMR and BER at G^O sites, we discovered that MMR cannot initiate at G^O/C sites in extracts. However, addition of recombinant purified OGG1 to the extracts generated entry points that were efficiently used by MMR. The reason why endogenous OGG1 cannot bring about this effect could be traced back to its low activity or low abundance in the extracts (see chapter 3.1.1). Furthermore, we could exclude that this was caused by inappropriate salt concentrations in the reaction buffer, missing co-factors from the cytoplasm or its instability in the extracts (chapter 3.1.1, Figure S6). Another factor that might be responsible for the lack of OGG1-dependent MMR in the extracts could be OGG1's slow kinetics, as described for recombinant OGG1 by several research groups [242, 244]. If this was the case, MMR proteins in the extracts could be inactive by the time that OGG1 has inserted nicks. To test MMR protein activity over time, we incubated HCT116 nuclear cell extracts and MutLα at 37°C. G/T nicked substrate was added either immediately or at the indicated time points to different reactions. Repair efficiencies in each reaction were analyzed by restriction enzyme digestion. Encouragingly, MMR was similarly active up to 3 hours (Figure 3-6 A). Thus, a decrease in its activity could be excluded as a factor restricting OGG1-dependent MMR.

Time course: substrate accessibility in extracts

Since our extracts are capable of performing plasmid supercoiling by nucleosome loading [74], we furthermore asked whether DNA packaging could restrict plasmid accessibility for OGG1. To address this, we incubated the G^O/C-G/T substrate with

HCT116 extracts and MutLα. Recombinant OGG1 was then added at the indicated time points. Since we showed before that MMR proteins are similarly active during the entire incubation period, and since purified OGG1 generates entry points for MMR, any time-dependent change in OGG1-dependent MMR activity would result from supercoiling and inaccessibility of the substrate. After 1 hour of pre-incubation, OGG1-dependent MMR still occurred (Figure 3-6 B). Only longer pre-incubation times abolished repair to background levels (lane 1).

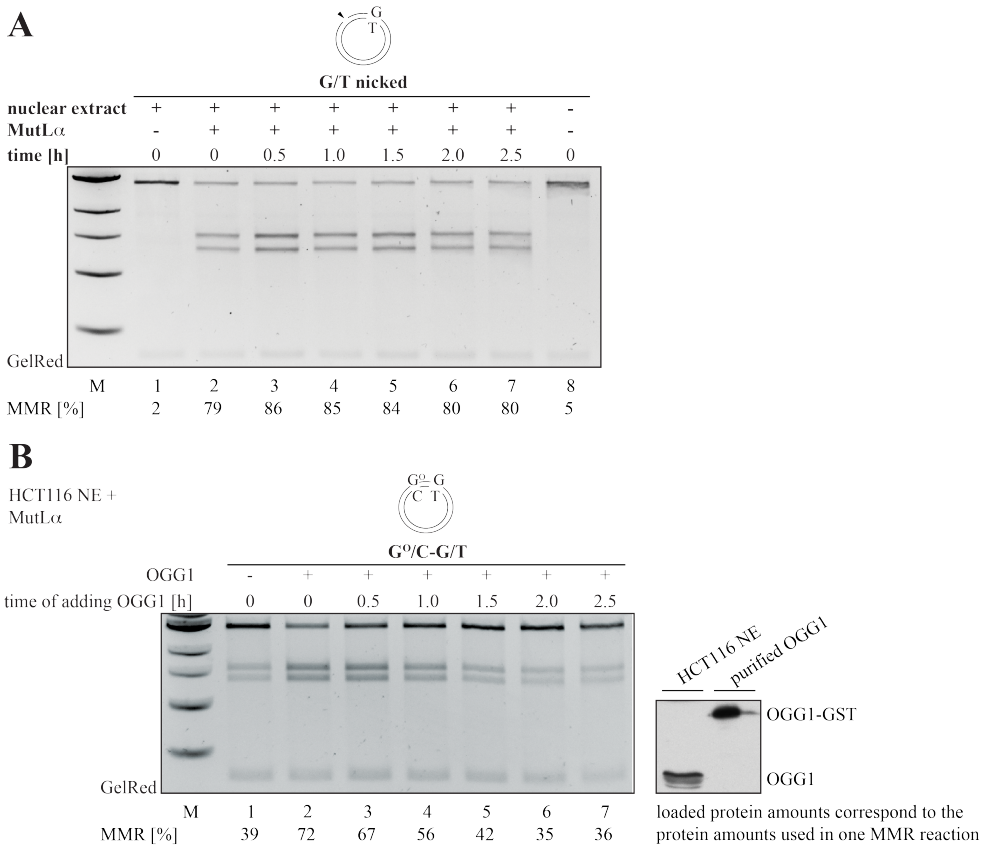

Figure 3-6: Time course: MMR activity & substrate accessibility.
(A) MMR proteins in nuclear cell extracts are active up to 3 hours. MMR assay. To test the activity of MMR factors in nuclear cell extracts over time, HCT116 extracts and MutLα were incubated at 37°C. G/T nicked substrate was added to the extracts at the indicated time points. From the time of adding the substrate, each reaction continued for 30 min. Upon SalI/DraI digestion, repair efficiencies were analyzed on a GelRed-stained 1% agarose gel and quantified (MMR [%]). (B) G^O/C-G/T substrate is accessible for purified OGG1 up to 1 hour. MMR assay. (Left panel) To test accessibility of closed-circular G^O/C-G/T substrate for OGG1, the substrate was incubated with HCT116 nuclear cell extracts and MutLα. 0.03 U purified OGG1 (Trevigen) were added to the mixture at the specified time points. From the time of adding the substrate, each reaction continued for 1 hour. Upon SalI/DraI digestion, repair efficiencies were analyzed on a GelRed-stained agarose gel and quantified. (Right panel) The Western blot shows that the OGG1 amount added to each MMR reaction corresponded to the OGG1 amount present in the volume of nuclear cell extracts usually used for one MMR reaction.

OGG1 activity in MMR buffer

To additionally prove that the used *in vitro* assay conditions are adequate for OGG1 activity, we tested the nicking activity of recombinant OGG1 on G^O/C-G/T substrates. This was performed in a buffer containing no salt (nicking buffer) or in MMR buffer containing 110 mM KCl that was also used for the other *in vitro* MMR experiments (Figure 3-7). Nicking in both buffers worked, but was more efficient in the MMR buffer (compare lanes 2+6). In line with other observations [240], addition of APE1 even increased OGG1 activity in the MMR buffer (lane 8). This proves that the conditions we used are compatible with OGG1 activity).

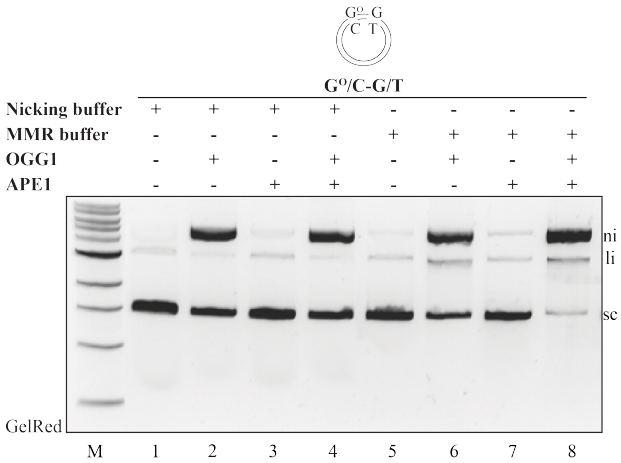

Figure 3-7: Purified OGG1 is active under in vitro MMR assay conditions.
Nicking assay. To prove suitability of the in vitro MMR assay conditions for OGG1, its activity on G^O/C-G/T substrates was tested in MMR buffer (lanes 5-8) and compared to its activity in nicking buffer containing no salt (lanes 1-4). 39 ng OGG1 or 0.05 U APE1 (NEB) were added where indicated (+). Separation of the phagemid substrates on an agarose gel gave rise to nicked (ni) plasmid where OGG1 was active, or to supercoiled (sc) configurations where no OGG1 activity was detected. li, linearized.

3.1.3 The involvement of PARP-1 and PARP inhibition in BER-dependent mismatch repair

Background

Poly(ADP-ribose) polymerase 1 (PARP-1) is an abundant nuclear protein and key regulator of various processes such as DNA damage response. Numerous studies attributed PARP-1 to an involvement in the base excision repair (BER) pathway (see chapter 1.9.3.4), but it was also linked to oxidative DNA damage response. This suggests a role of PARP-1 in BER of oxidative DNA lesions. Based on our previous results that showed that mismatch repair (MMR) initiates at MYH/APE1-generated nicks (see chapter 3.1.1), we became interested to test the effect of PARP inhibition on MYH-dependent MMR *in vitro*. At the same time, these experiments should reveal whether PARP-1 is involved specifically in MYH- or OGG1-induced BER.

Experimental set-up

To elucidate this, we performed biochemical studies, which have the advantage that G^O/A and G^O/C sites can be generated at specific sites in the plasmids, while oxidative stress in cells can lead to various undefined DNA modifications [168]. We took advantage of the previously described *in vitro* MMR assay and incubated nuclear cell extracts with the substrates that contained G^O/A or G^O/C sites in the close proximity of a G/T mismatch. Since MMR activity on G/T mismatches restored a *Sal*I (in G^O/A-G/T substrates) or *Acl*I (in G^O/C-G/T substrates) restriction site (see chapter 3.1.1, Figures 2A + 5A), this served as read-out for the accessibility of MYH- and OGG1-initiated nicks for MutSα-activated EXOI. Addition of Olaparib to the reactions should clarify whether PARP-1 was able to transiently bind MYH- and OGG1-initiated nicks and how this would affect BER-dependent MMR.

Possible outcomes

As discussed in detail in chapter 1.9.4.1, 'trapping' of PARP-1 on DNA breaks upon PARP-1 inhibition is currently the most accepted model. Since MMR is able to displace BER proteins immediately after the glycosylase-mediated nick generation, trapping of PARP-1 on MYH- or OGG1-initiated nicks could have three different outcomes on BER-dependent MMR (Figure 3-8).

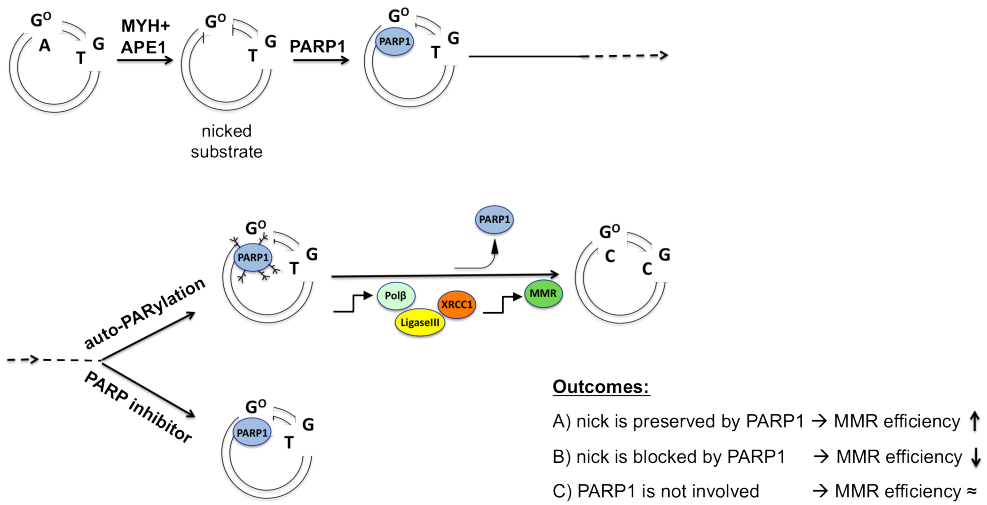

Figure 3-8: Model showing how PARP inhibition could affect MYH-initiated MMR.
The model suggests PARP-1 binding to MYH/APE1-generated nicks. Under normal conditions, PARP-1 would be auto-modied by poly(ADP-ribosyl)ation. This would lead to recruitment of other BER factors and dissociation of PARP-1. If the remaining nick was located in the proximity of a MMR target (G/T), it would serve as an initiation site for MMR proteins, namely EXOI. This would allow MMR to repair the close-by mismatch. In the presence of PARP inhibitors (PARPi), PARP-1 would not be modified, which could lead to several scenarios: PARP-1 could remain bound to the nick thereby a) preserving the nick, which would provide better accessibility for EXOI. b) physically block the nick for other enzymes, including EXOI. A last scenario would suggest that c) PARP-1 is not involved in this process and PARPi would not affect MMR activity at all.

One possible scenario would be that PARP-1 preserved the nick, thereby making it accessible for MMR for a longer time period. This should result in increased MMR activity on the G/T mismatch. Another scenario could be that PARP-1 would physically block the nick, thus making it inaccessible for other enzymes, such as EXOI. A third scenario would be that PARP-1 played no role at MYH- and OGG1-initiated nicks, and PARP inhibition would not affect MMR activity. During the limited time that was available for this project, I gained some interesting results that will be presented below. In chapter 4.2, I will discuss it and provide a detailed outlook on future experiments that could be carried out based on our observations to date.

PAR formation and PARP inhibition in extracts

First, we tested the ability of nuclear cell extracts to perform poly(ADP-ribose) (PAR) formation (Figure 3-9 A). Nuclear cell extracts of HCT116 + chromosome 3 cells were incubated for 1 min either in the absence (lane 1) or presence (lanes 2-3) of activated DNA, which contains a large number of breaks. One sample was additionally supplemented with 50 μM NAD^+ (lane 3). Western blot analysis of PAR levels in the protein samples revealed that our extracts were able to form PAR polymers (lane 2). However, PAR levels were substantially increased upon NAD^+ addition (lane 3). This can be explained by the fact that cell extracts were dialyzed during the preparation procedure, hence most NAD^+ was removed. Although intracellular NAD^+ concentrations are ~500 μM [346, 347], no clear difference in PAR levels was detectable upon addition of 50 or 500 μM NAD^+ on the Western blot (data not shown). To test whether addition of 50 μM NAD^+ affects repair efficiencies on G^O/A-G/T substrates, we performed a MMR assay in HCT116 cell extracts supplemented with MutLα and increasing amounts of NAD^+ (Figure 3-9 B). Quantifications demonstrate that MYH-dependent MMR efficiencies did not change with NAD^+ concentration. This allowed us to perform MMR assays as described in the previous chapter 3.1.1, but in the presence of NAD^+. Furthermore, we defined the Olaparib concentration needed to inhibit PAR formation upon addition of NAD^+ to the extracts (Figure 3-9 C). HCT116 + chromosome 3 cell extracts were incubated in the presence of 500 μM NAD^+, activated DNA and various concentrations of Olaparib. It turned out that already the lowest dose of Olaparib, 500 μM (lane 4), was enough to abolish PAR formation to the same level as in extracts that were not subjected to activated DNA. Thus, all further experiments were performed with 500 μM Olaparib.

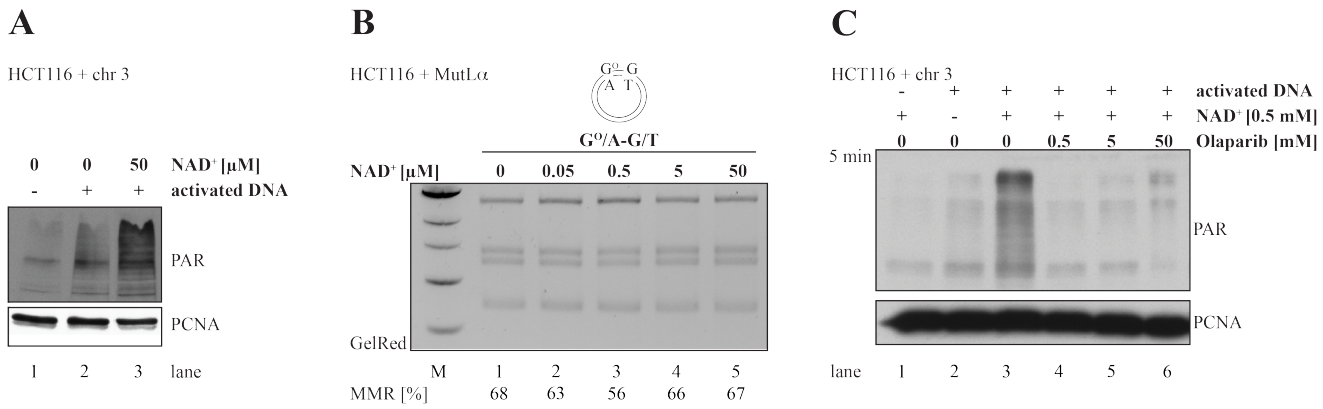

Figure 3-9: PAR formation can be activated and inhibited in nuclear cell extracts.
(A) The ability of HCT116 + chromosome 3 nuclear cell extracts to form PAR was tested by incubation of 50 µg extracts and 100 ng activated/sheared DNA. One reaction was supplemented with 50µM NAD^+ (lane 3) while one reaction was not (lane 2). Extracts in the control reaction (lane 1) were not activated with sheared DNA. Incubations were carried out for 1 min and subsequently prepared for Western blot analysis using anti-PAR and anti-PCNA (= loading control) antibodies. (B) The presence of additional NAD^+ in nuclear cell extracts does not affect MMR or MYH activities. MMR assay using a G^O/A-G/T substrate, HCT116 extracts and MutLα was performed under standard conditions (lane 1) or supplemented with the indicated amounts of NAD^+. MMR efficiencies (%) of each reaction were quantified. (C) Olaparib inhibits PAR formation in nuclear cell extracts. 50 µg HCT116 + chromosome 3 nuclear cell extracts were either incubated with 0.5 mM NAD^+ (lane 1), 100 ng sheared DNA (lane 2) or both (lanes 3-6). Samples 4-6 were additionally treated with 0.5, 5 or 50 mM Olaparib. Reactions were performed for 5 min. Western blot analysis was carried out for PAR detection. PCNA: loading control.

PARP inhibition in MYH-dependent MMR

Our first aim was to elucidate the effect of PARP inhibition by Olaparib on MYH-dependent MMR (Figure 3-10 A). We incubated G^O/A-G/T plasmids with HCT116 nuclear cell extracts and, where indicated, with MutLα. Reactions were either supplemented with NAD^+ or Olaparib. Treatment with Olaparib in the absence of NAD^+ increased chances for efficient PARP inhibition. As expected, no MMR on the G^O/A-G/T substrate was observed in the absence of MutLα (lane 1), while, in the presence of MutLα, it was repaired to 60% (lane 2). Interestingly, PARP inhibition decreased G^O/A-G/T repair 0.7 fold to 43%. A heteroduplex substrate without any nick was repaired to 37%, both in the absence (lane 4) or presence (lane5) of Olaparib. Thus, repair efficiencies of the G^O/A-G/T substrate were 1.6 fold higher than of the G/T substrate in the absence of Olaparib, but only 1.16 fold higher in the presence of Olaparib. Thus MYH-dependent MMR efficiency was almost abolished by PARP inhibition.

PARP inhibition in OGG1-dependent MMR

A similar observation was made for OGG1-dependent MMR (Figure 3-10 B). We had shown before (chapter 3.1.1) that OGG1 activity in extracts is insufficient to provide entry points for MMR at G^O/C sites. Nevertheless, addition of recombinant, purified OGG1 increased its activity, thereby allowing access for MMR at OGG1-generated nicks. To be able to test the effects of PARP-1 inhibition on OGG1-initiated MMR, we had to add additional OGG1 to the reactions (Figure 3-10, lanes 1, 3-6). As previously shown, in the absence of extra OGG1 (lane 2), repair efficiencies on G^O/C-G/T substrates were low compared to G/T control

substrates (lanes 5-6). The presence of purified OGG1 allowed MMR to access the nick and to repair G/T to A/T with an efficiency of 86% (lane 3). Interestingly, in the presence of Olaparib (lane 4), MMR efficiency on G^O/C-G/T substrates dropped down to 71%, thereby decreasing 0.8 fold. The effect on the control G/T plasmid was less, decreasing 0.9 fold from 41% to 37% in the presence of Olaparib. Interestingly, the effect of PARP inhibition on MYH-initiated MMR was stronger than on OGG1-inititated MMR: in the presence of Olaparib, MMR efficiency on the G^O/A-G/T substrate was only 1.16 fold increased compared to the G/T substrate while on the G^O/C-G/T plasmid it was still 1.9 fold more than on the G/T plasmid.

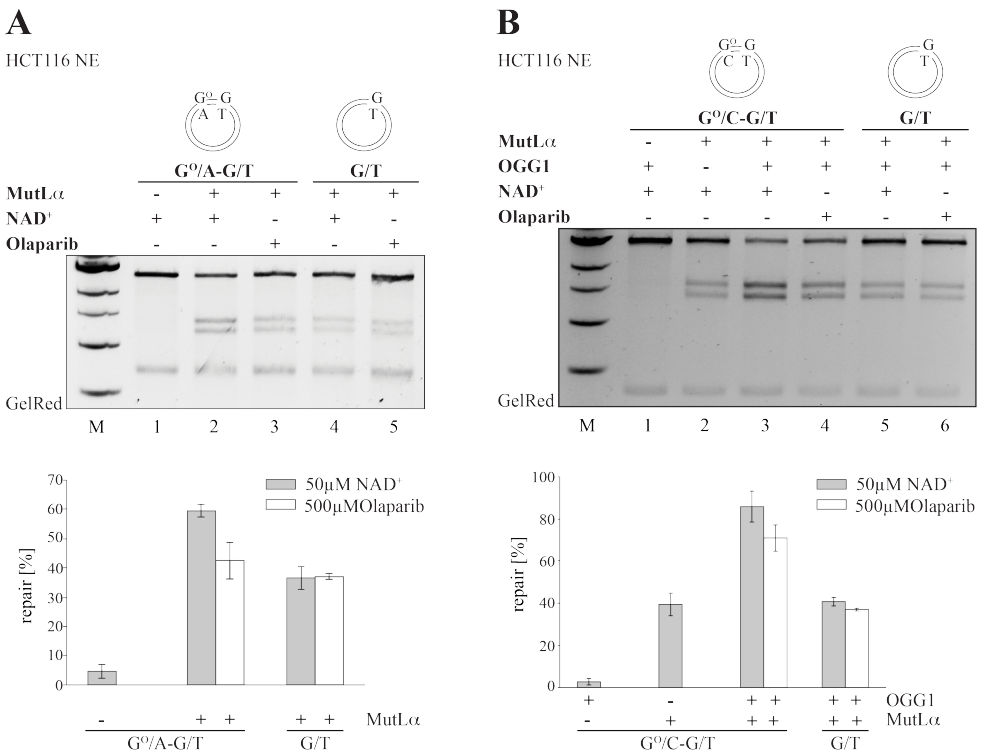

Figure 3-10: Olaparib decreases repair efficiencies on G^O/A-G/T and G^O/C-G/T substrates.
(A) The MMR assay was performed with HCT116 nuclear cell extracts that were incubated with G^O/A-G/T (lanes 1-3) or G/T (lanes 4-5) substrate, either in the presence of 50 µM NAD^+ (lanes 1, 2, 4) or of 800 µM Olaparib (lanes 3+5). MutLα was added where indicated. The quantification represents an average of 3 independent experiments +/- standard deviation. (B) The assay was performed similarly to what is described in (A) but using the G^O/C-G/T substrate (lanes 1-4). Since OGG1 activities were not detectable in extracts (compare lane 2 with negative controls 5+6), purified OGG1 was additionally added to all other reactions (lanes 1, 3-6). The quantification represents an average of 3 independent experiments +/- standard deviation.

3.2 Towards the elucidation of the interactome of MSH6 during oxidative stress

Background

As described in detail in chapter 1.8.1, the role of the mismatch repair (MMR) recognition factor MutSα during the repair of oxidative DNA lesions is poorly understood to date. A promising approach to gain more insights into potential novel roles of MutSα is the performance of interactome studies of its component MSH6. Studying it in the absence or presence of oxidative stress should reveal the relevant interaction partners of MSH6 that are specifically required during oxidative DNA damage response. Besides its essential binding partner MSH2, other MSH6 interaction partners have been described, such as PCNA, MYH, CAF1, H3K36me3, 9-9-1 complex, BRCA1, BARD1, BLM, ATM, ATR and CHEK1 [35, 47, 73, 74, 348-353]. The interaction with ATM/ATR/CHEK1 suggests a role for MSH6 in signaling [353], but might not necessarily be linked to oxidative DNA damage response. Hence, among the proteins listed above only the interaction with MYH points towards a direct involvement of MSH6 in oxidative DNA damage processing. This limited information reflects the need for further insights into this enigmatic role of MutSα. My contribution to the elucidation of the MSH6 interactome during oxidative DNA damage response was the generation and evaluation of tools needed for successful MSH6 pulldowns. My achievements are summarized below.

3.2.1 Generation of a destination vector that allows inducible gene replacement

Generation of the 'pTO+AIO CSH GW FRT' destination vector

In order to circumvent antibody-mediated blockage of potential interaction sites on the MSH6 protein during immunoprecipitation, we decided to work with a C-terminally tagged version of MSH6. The location of the tag was determined by the nature of the MSH6 structure. Since it contains a multifunctional N-terminal domain including an essential PCNA interaction site between amino acids 4 and 11 (see Figure 1-5), tagging the N-terminus might impair some of those functions. When we started this project, no mammalian cell line expressing exogenous tagged MSH6 existed. The probable reason for that was that indeed, technical difficulties in expressing exogenous MSH6 have been reported previously [79] and have also been observed in our laboratory. The reason for that is currently unclear (see chapter 4.3). To try to overcome this obstacle, we chose to work with a system and tag that was previously validated to be suitable for Mass Spectrometry [354]. This system is based on the Gateway® technology (Invitrogen) and allows doxycycline-(Dox-) inducible expression of a protein of interest, tagged with streptavidin binding peptide and a hemagglutinin epitope (Strep/HA), under the regulation of a CMV promoter. Vector integration occurs *via* FRT recombination in Flp-In T-REx cell lines. Since our long-term goal was not only the expression of tagged wild type

MSH6 but also of its mutants, we modified the vector in the way that it additionally allowed simultaneous knockdown of the endogenous protein of interest, thus resulting in inducible gene replacement. The different cloning steps are listed under material and methods (chapter 6.2, Table 6-3). A schematic illustration of the functional elements of the final destination vector named 'pTO+AIO CSH GW FRT' is presented in Figure 3-11.

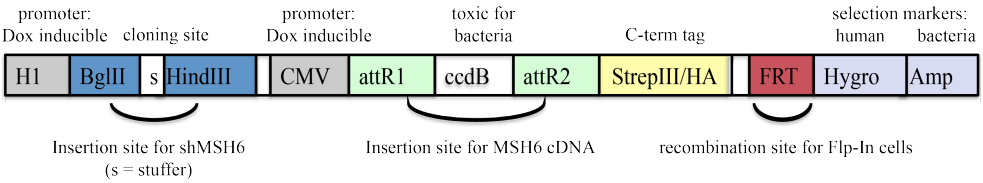

Figure 3-11: Scheme showing crucial elements in the pTO+AIO CSH GW FRT vector. ***H1*** *= Doxycycline- (Dox-) inducible promoter (containing a Tet repressor binding site) for the regulation of shRNA expression.* ***CMV*** *= Dox-inducible promoter (containing a Tet repressor binding site) for the regulation of Strep/HA-tagged protein expression.* ***BglII-stuffer-HindIII site****: shRNA can be cloned between the BglII and HindIII site, thereby destroying the BglII site. The stuffer allows improved accessibility of the restriction enzymes to the BglII and HindIII sites and its excision serves as control for successful double restriction digestion.* ***StrepIII/HA*** *= Strep/HA = SH = C-terminal tag of the protein of interest. The tag consists of a streptavidin-tag III and a hemagglutinin epitope.* ***Hygro*** *= hygromycin B resistance gene. Selection marker in mammalian cells.* ***Amp*** *= ampicillin resistance gene. Selection marker in bacteria.* ***FRT*** *= recombination site. It serves as binding and cleavage site for the Flp recombinase, leading to site-specific integration of the vector into a single FRT site in the Flp-In cell line.* ***ccdB*** *= gene, encoding a toxic product for bacteria. Selection marker for successful integration of the cDNA of interest into the vector.* ***attR1/attR2 sites****: recombination site, allowing the recombination of an ENTRY and a destination vector.*

Table 3-2: Features and corresponding advantages of the 'pTO+AIO CSH GW FRT' vector when recombined with a protein of interest containing entry vector.

Feature	Advantage
Simultaneous Dox-inducible	1. Gene replacement:
a) expression of C-terminal Strep/HA-tagged protein and	- decreased risk of losing interaction partners that bind to the endogenous protein
b) knockdown of endogenous protein	- suitable for mutant studies - counteracting protein overexpression
	2. isogenic cell system
	3. prevention of mutations caused by stable knockdown or stable expression of (mutant) exogenous proteins
Strep/HA tag	1. Efficient two-step pulldown of the protein of interest
FRT recombination site allows vector insertion into Flp-In cell lines at only one specific gene locus	1. Fast generation of stable cell lines 2. No variations amongst different clones
Stuffer	Allows efficient *Bgl*II/*Hin*dIII digestion, hence facilitating shRNA insertion

The color code clarifies interrelated features and advantages.

While a shRNA targeting a non-coding mRNA region is inserted between the *Bgl*II and *Hin*dIII site of the destination vector, the gene of interest is inserted from an

entry vector *via* attR-mediated LR recombination. The shRNA and tagged protein will be expressed under an inducible H1 and CMV promoter, respectively. The advantages of the 'pTO+AIO CSH GW FRT' destination vector are summarized in Table 3-2. This vector can be used for expression and knockdown of any protein of interest. Furthermore, it can be used for just one of both purposes.

3.2.2 Generation of a vector that allows simultaneous induction of MSH6-Strep/HA expression and shRNA-mediated knockdown of endogenous MSH6

Generation of 'pTO+AIO hMSH6-SH GW FRT + shMSH6' vector

In this project, MSH6 represented our protein of interest. The different cloning steps are schematically shown in Figure 3-12 and the corresponding vector maps of vectors A-D (Figure 3-12) are shown in appendices A1-A4. In the first instance, shRNA targeting the 3' UTR region of MSH6 mRNA was inserted into the 'pTO+AIO CSH GW FRT' vector generated earlier. In parallel, MSH6 A116G cDNA was amplified from a pcDNA3-hMSH6 vector and inserted into the pENTR3C vector. Subsequently, the MSH6 mutation was corrected using PCR site-directed mutagenesis, and both entry and destination vectors were recombined in a LR-reaction. The detailed cloning methods are described under material and methods (see chapter 6.2, pages 131-132).

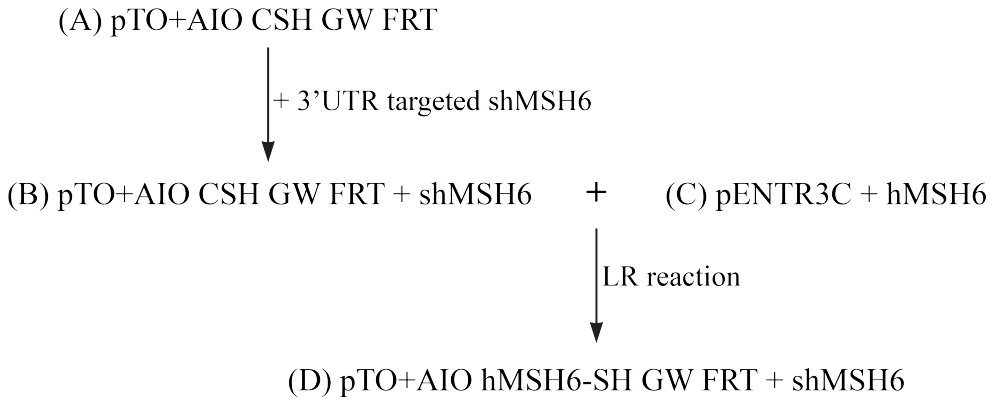

Figure 3-12: Generation of 'pTO+AIO hMSH6-SH FRT + shMSH6' vector.
The generation of the 'pTO+AIO hMSH6-SH FRT + shMSH6' vector (= D) required previous construction of the vectors A), B) and C). The 'pTO+AIO CSH GW FRT' vector (= A) served as starting vector into which the shRNA, targeting MSH6 mRNA, was inserted, resulting in vector (B). In parallel, the hMSH6 cDNA sequence was integrated into the entry vector pENTR3C (= C). Both vector B) and C) were recombined using an LR-reaction, giving rise to the final 'pTO+AIO hMSH6-SH FRT + shMSH6' vector (= D). The corresponding vector maps are presented in appendices A1-A4 and show all crucial vector elements.

3.2.3 Generation of stable Flp-In T-REx cell lines

Inducible isogenic cell line expressing shMSH6

The resultant 'pTO+AIO hMSH6-SH GW FRT + shMSH6' and 'pTO+AIO CSH GW FRT + shMSH6' vectors were used for the generation of stable Hek293 (data not shown) and U2OS Flp-In T-REx cell lines (Figure 3-13). Although generation of cell clones was, in theory, not necessary, FRT-independent vector integration into the cells genome had previously been observed in our laboratory. Thus, upon 3 days of doxycycline treatment, different clones were tested for MSH6 knockdown and exogenous protein expression levels (Figure 3-13). 'pTO+AIO CSH GW FRT + shMSH6' based cell lines express only 3' UTR shMSH6 (Figure 3-13 A). Four of those, especially clone 8, showed efficient MSH6 knockdown and thus represented a useful isogenic and inducible system that can be used to study MutSα-dependent phenotypes in future.

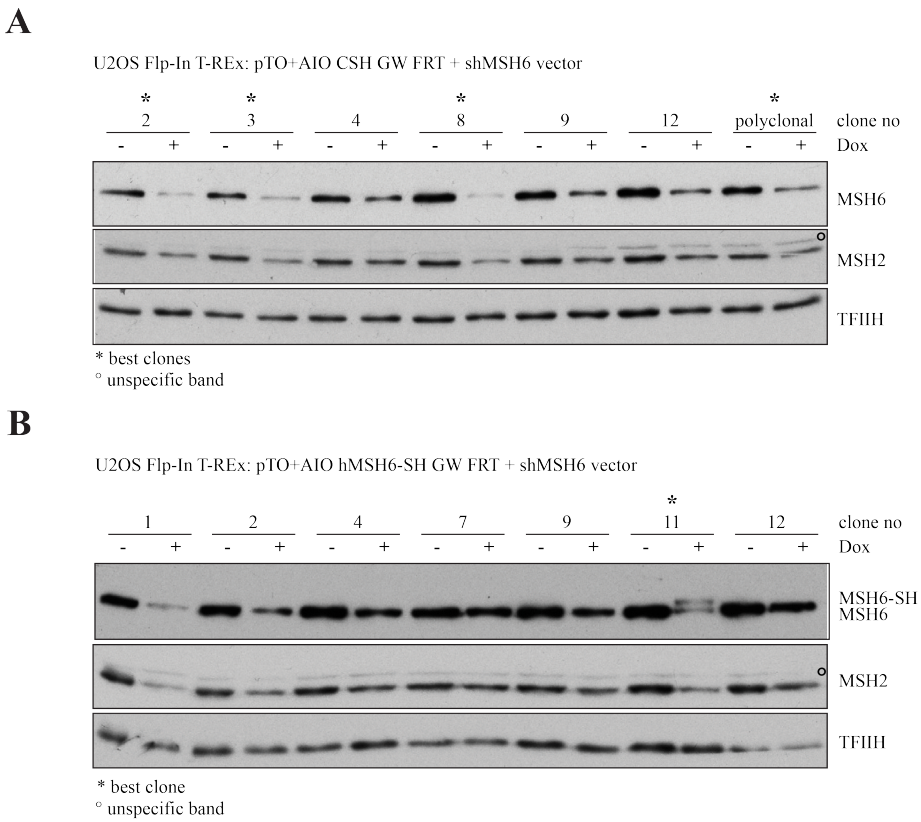

Figure 3-13: Screening stable U2OS Flp-In T-REx clones for suitability.
A) U2OS Flp-In T-REx clones, stably expressing the 'pTO+AIO CSH GW FRT + shMSH6' vector, were screened for efficient MSH6 knockdown. Cells were treated with 10 µg/ml Dox, which was replenished every 2 days. After 3 days, the cells were harvested in Lämmli buffer and MutSα protein levels were analyzed by Western blotting. B) U2OS Flp-In T-REx clones stably expressing the 'pTO+AIO hMSH6-SH GW FRT + shMSH6' vector were screened for efficient expression of exogenous hMSH6-Strep/HA and simultaneous knockdown of endogenous MSH6, following the procedure described in A).

Inducible isogenic cell line expressing shMSH6 and MSH6-Strep/HA

'pTO+AIO hMSH6-SH GW FRT + shMSH6' based cell lines expressed both 3'UTR shMSH6 and exogenous MSH6-Strep/HA (Figure 3-13 B). Only clone 11 expressed the tagged version of MSH6, but only at low levels, resulting in a 1:1 ratio of endogenous to exogenous MSH6 levels. This low MSH6-Strep/HA expression indicates that our system is suboptimal since normally CMV-controlled gene expression leads to substantial overexpression of the protein or, in case of MSH6 which gets stabilized by MSH2, at least comparable expression levels to endogenous MSH6. All in all, clone 11 failed to show complete gene replacement, which makes the cell line inappropriate for prospective mutant studies. A prolonged period of doxycycline treatment did not induce substantial changes in protein levels (Figure 3-14).

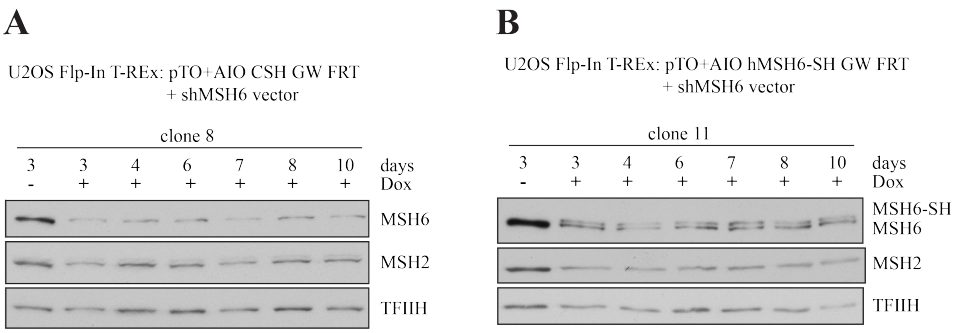

Figure 3-14: Testing MSH6-Strep/HA expression and MSH6 knockdown levels of the most suitable U2OS Flp-In T-REx clones over time.
U2OS Flp-In T-REx cells either expressing the 'pTO+AIO CSH GW FRT + shMSH6' (clone 8, panel A) or 'pTO+AIO hMSH6-SH GW FRT + shMSH6' (clone 11, panel B) vector were treated with 10 µg/ml Dox for 3 to 10 days. Endogenous MSH6 and exogenous MSH6-Strep/HA levels of whole cell extracts were analyzed by Western blotting.

3.2.4 HeLa Kyoto MSH6-LAP cell line: Characterization & MSH6 pulldown

BAC TransgeneOmics

In 2008, the laboratory of Anthony Hyman published a novel high-throughput technique for the generation of stable BAC transgenic mammalian cell lines in which transgenes are tagged with a 'localization and affinity purification' (LAP) tag [355].

HeLa Kyoto MSH6-LAP cell line

Amongst others, they generated a HeLa Kyoto cell line stably expressing C-terminally LAP-tagged MSH6. To our knowledge, this BACmid based approach is the first that succeeded in stably expressing exogenous tagged MSH6. The LAP tag allows GFP based localization of the tagged protein within the cell, as well as a two-step purification of the protein *via* GFP and, upon pre-scission protease cleavage, S-protein. The scheme of the C-terminal tagging cassette including the structure of the LAP tag is presented in Figure 3-15.

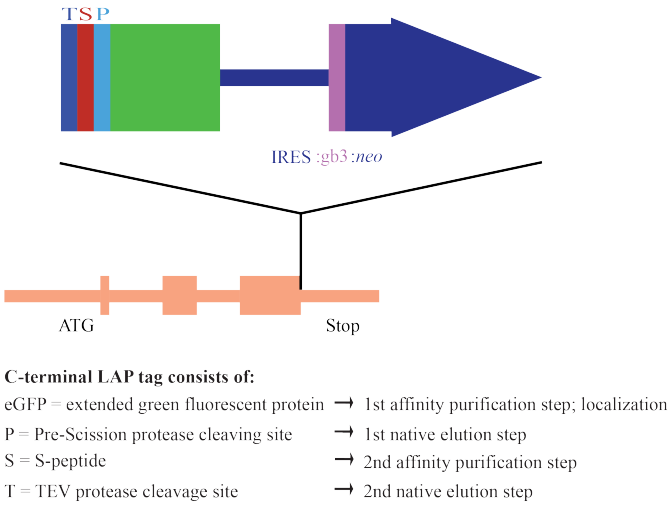

Figure 3-15: Tagging cassette for C-terminal LAP-tagging.
Schematic representation of a genomic region that contains the gene of interest (orange) and the cassette for tagging it at the C-terminus. The tag is inserted as a cassette with a neomycin resistance gene downstream of an internal ribosome entry site (IRES:neo). gb3, bacterial promoter. The LAP tag consists of the following elements: extended green fluorescent protein (EGFP), Pre-Scission protease cleavage site (P), S-peptide (S) and tobacco etch virus protease cleavage site (T). Adapted from [355].

Cell line characterization

We characterized the HeLa Kyoto MSH6-LAP cell line in terms of growth, GFP expression and functionality of the exogenous protein. FACS and immunofluorescence analysis revealed GFP expression localized to the nucleus (Figure 3-16 A-B). Cells exhibited a normal growth behavior with a doubling time of 24 hours (Figure 3-16 D). More importantly, we could show that the tagged MSH6 version was functional: Upon MNNG treatment, both endogenous and exogenous MSH6 were recruited to the chromatin accompanied by mono-ubiquitylated PCNA, a MMR-dependent event occurring in response to MNNG treatment [94] (Figure 3-16 C).

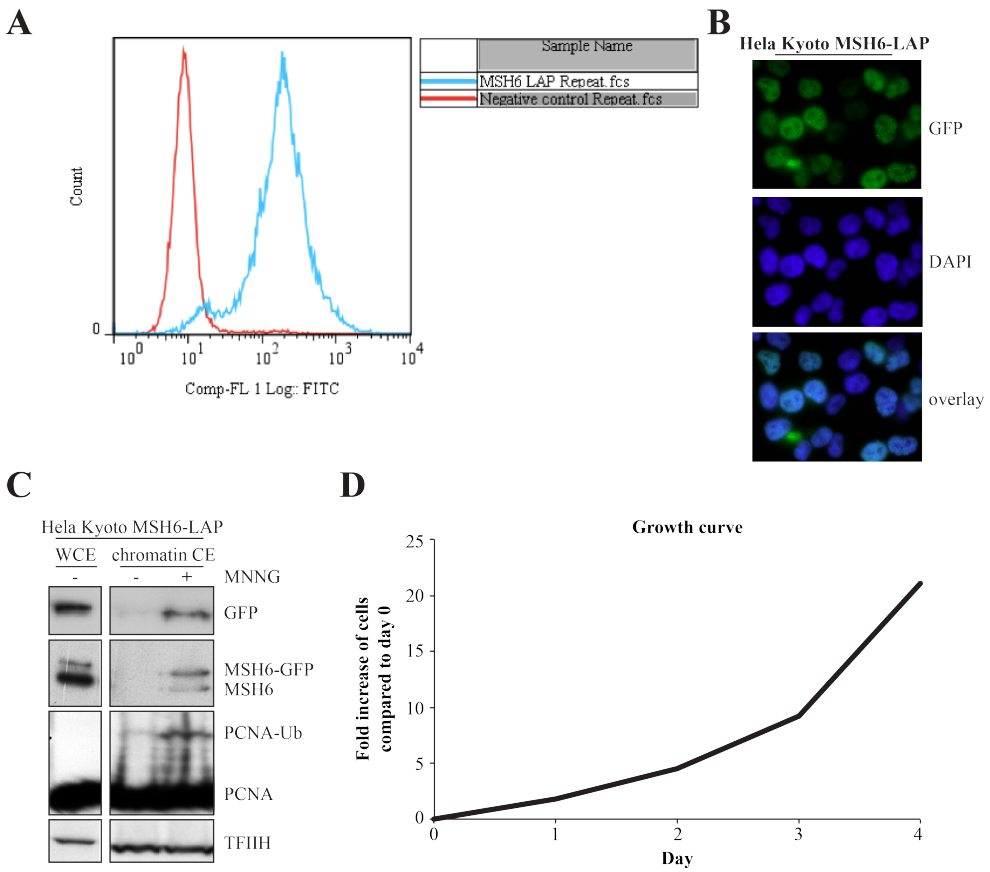

Figure 3-16: Characterization of a HeLa Kyoto MSH6-LAP cell line.
This HeLa Kyoto cell line contains a stably integrated BACmid vector encoding C-terminally LAP-tagged MSH6. The cell line was a kind gift of Anthony A. Hyman, MPI, Dresden, Germany. A) Flow cytometry analysis of GFP expression in HeLa Kyoto MSH6-LAP cells (blue) and HeLa Kyoto wild type cells (red). B) Immunofluorescence analysis of GFP expression in HeLa Kyoto MSH6-LAP cells. Cells were fixed in 3.7% formaldehyde, permeabilized with 0.2% Triton X-100 and stained with DAPI. C) The functionality of LAP-tagged MSH6 was tested in cells by pretreating them with 10 µM O6-benzylguanine for 1 hour and subsequently with 5 µM MNNG for 6 hours. At this time point, chromatin-enriched cell extracts, as well as whole cell extracts, were prepared and MSH6-GFP recruitment to the chromatin upon MNNG treatment was analyzed by Western blotting. D) A growth curve was generated by seeding 50'000 HeLa Kyoto MSH6-LAP cells into four 6-well dishes, respectively. After 1, 2, 3 and 4 days, cell numbers were counted.

Furthermore, we wanted to ensure that the MMR-dependent behavior of HeLa Kyoto MSH6-LAP cells towards oxidative stress corresponded to the behavior of previously tested cell lines [260]. Indeed, knockdown of both endogenous and exogenous MSH6 (Figure 3-18, right panel) brought about sensitivity to $KBrO_3$ (Figure 3-18, left panel). Additional cell cycle studies revealed an accumulation of cells in G_2/M phase 4 to 8 hours post $KBrO_3$ treatment. In agreement with the cell survival data, 24 hours post $KBrO_3$ treatment, control cells (siLUC) had recovered, while the number of siMSH6-treated cells that were arrested in G_2/M had even increased (Figure 3-17). Even though this cell line does not allow *MSH6* gene

replacement, based on its characterization, it represents a suitable tool for MSH6 pulldowns.

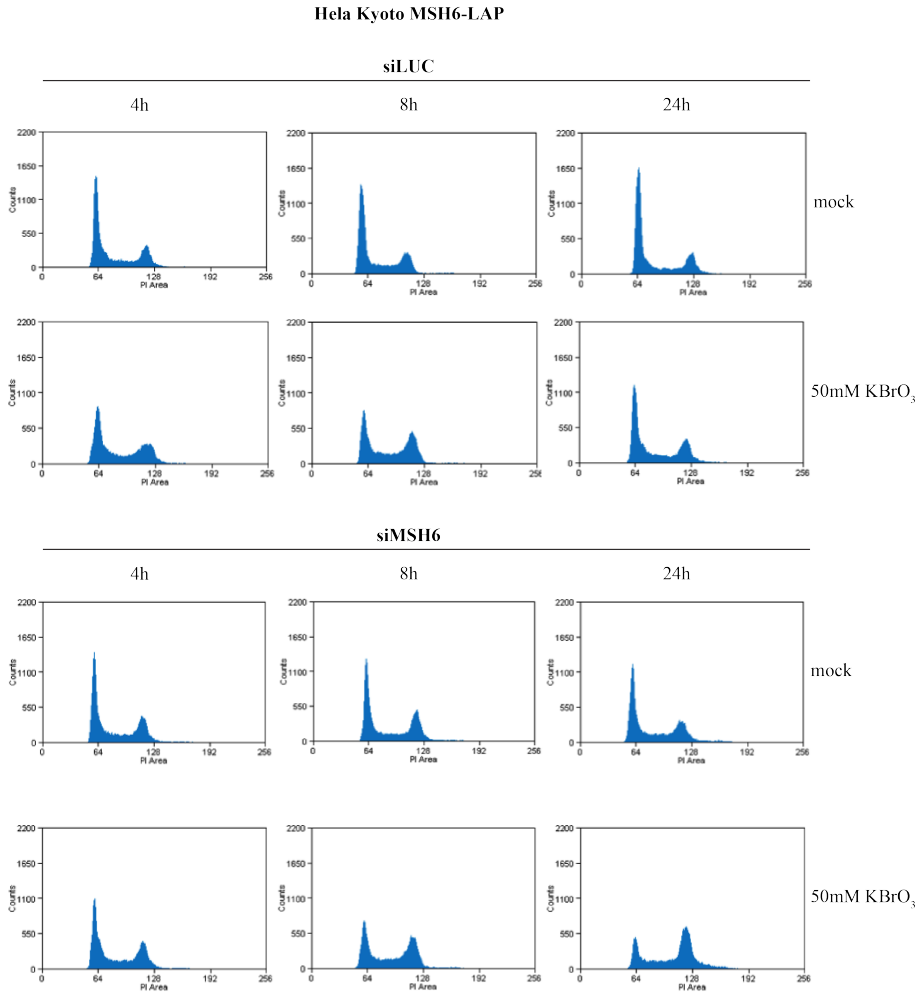

Figure 3-17: MutSα-deficient cells show prolonged G_2/M arrest upon oxidative stress.
Cell cycle analysis. HeLa Kyoto MSH6-LAP cells, either treated with siLUC or siMSH6, were exposed to 50 mM $KBrO_3$ or to PBS/Hepes (mock) for 30min. 4, 8 and 24 hours after treatment, the cells were harvested and fixed in 70% ethanol. The DNA was stained with propidium iodide (PI) and the cell cycle stages were analyzed by flow cytometry.

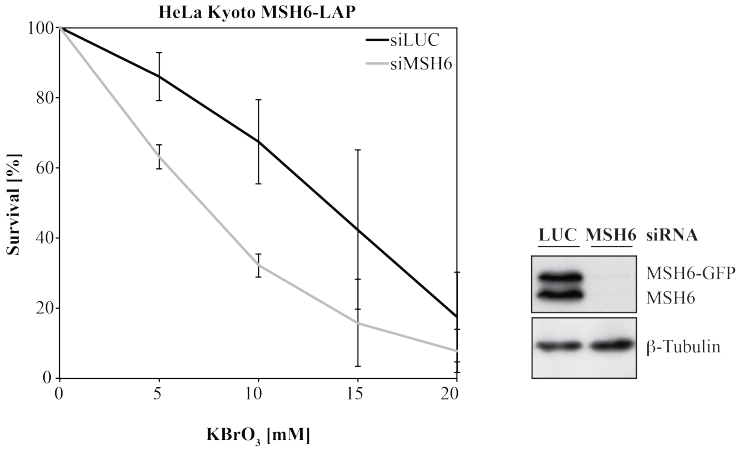

Figure 3-18: MutSα deficiency sensitizes cells towards oxidative stress.
HeLa Kyoto MSH6-LAP cells, either treated with siLUC or siMSH6, were exposed to different concentrations of $KBrO_3$. 72 hrs after treatment, the cells' survival was measured in terms of their metabolic activity, using a CellTiter-Blue cell viability assay. The graph represents the results of five independent experiments, each carried out in triplicate. Each data point represents an average +/- standard deviation. The Western blot shows MSH6 knockdown efficiency of one representative experiment at the time of the drug treatment.

MSH6 pulldown

Since proteins that are involved in oxidative DNA damage repair should be recruited to the DNA in this process, we performed pulldown experiments in chromatin-enriched cell extracts. This should allow enrichment of potential proteins of interest. The p150 subunit of chromatin assembly factor 1 (CAF-1) served as 'quality control' of these extracts, since it should only be present in the chromatin fraction. First pulldown experiments, carried out as one-step purification using GFP-Trap_A beads in untreated chromatin-enriched cell extracts, were extremely efficient in terms of MSH6-LAP and MSH2 enrichment (Figure 3-19). A problem we encountered was inconsistence with regard to detection of expected interaction partners such as MYH, PCNA or CAF-1. As ascertained by Western blotting, most pulldown experiments revealed low presence of known interaction partners (data not shown), while in others they could be detected but at the cost of a high non-specific background (Figure 3-19, see Western blot). Possible strategies for pulldown optimization, as well as prospective experiments that can be carried out based on the hitherto-generated and evaluated tools will be discussed in chapter 4.3.

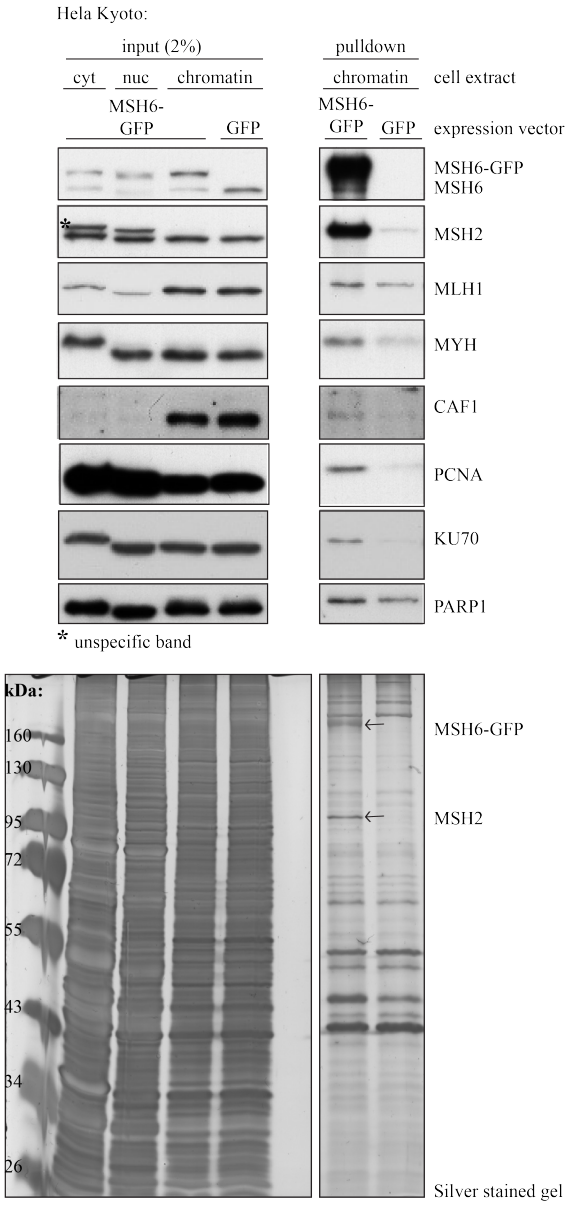

Figure 3-19: GFP-pulldown in chromatin-enriched cell extracts of HeLa Kyoto MSH6-LAP cells. A GFP-pulldown, usingGFP-Trap_A beads, was performed in chromatin-enriched cell extracts of HeLa Kyoto cells expressing either C-terminally LAP-tagged MSH6 or only GFP (= control reaction). Upper panel: Analysis of the pulldown reaction was performed by Western blotting, which was used to detect known and expected MSH6-binding partners. 2% input of chromatin-enriched cell extracts (chromatin) served as control for the efficiency of protein enrichment after the pulldown. 2% input of the cytoplasmic (cyt) and nuclear soluble (nuc) fraction served as quality control for chromatin-enriched cell extracts (quality marker: CAF1). Lower panel: Silver staining of the same pulldown reaction was performed for visualization of all present proteins. Pictures from the input and the pulldown, which are presented in separate pictures here, derive from the same gels with the same exposure times.

3.3 MYH-induced oxidative DNA damage repair partially contributes to PARP inhibitor sensitivity in BRCA1-deficient cells

Background

We hypothesized that MYH and/or OGG1 induced base excision repair (BER) intermediates of oxidative DNA lesions would contribute to PARP inhibitor sensitivity in the absence of homologous recombination (HR). To test this we performed survival studies with BRCA1-deficient cells that were treated with the PARP inhibitor Olaparib. If the hypothesis was true, knockdown of MYH and/or OGG1 should overcome sensitivity to Olaparib, leading to increased survival rates. Since siRNA-mediated knockdown of OGG1 protein levels was inefficient even 6 days after treatment, and even though mRNA levels were downregulated by 80% (data not shown), we turned our experimental focus on MYH.

Testing Olaparib

Before we started the survival assays, we validated the potency of Olaparib, which is a selective inhibitor of mammalian PARP-1, PARP-2 and PARP-3, thus one of the most specific inhibitors on the market. Nevertheless, since PARP-1 and -2 were reported to have overlapping functions, inhibition of both might be even beneficial. Since H_2O_2 is known to lead to nuclear poly(ADP-ribose) (PAR) formation, SUM149PT and HeLa cells were treated with 1 mM H_2O_2 for 10 minutes. To validate the effect of Olaparib, other cells were pretreated with 0.1 µM Olaparib (= evaluated IC_{50} value of Olaparib in SUM149 PT cells) for one hour, following a short 1 mM H_2O_2/0.1 µM Olaparib combination treatment. Mock-treated cells served as control. Immunofluorescence staining of PAR revealed efficient inhibition of PARP-mediated poly(ADP-ribose) formation in the cells that were pretreated with Olaparib (Figure 3-20). We therefore continued with the survival studies.

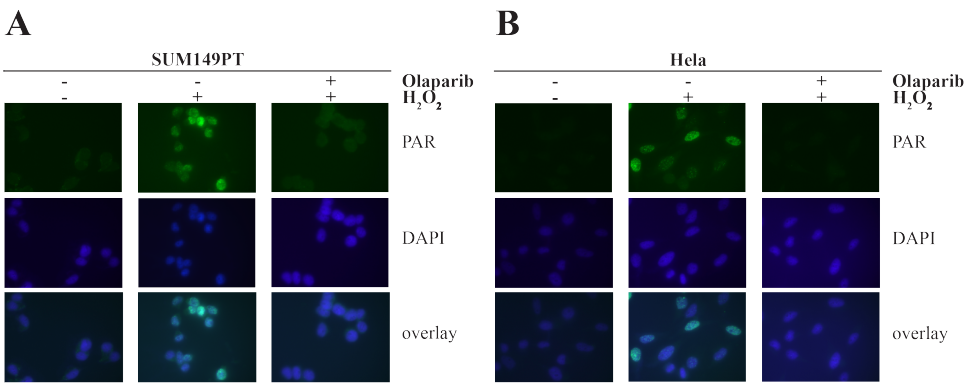

Figure 3-20: Olaparib inhibits PAR formation in cells upon H_2O_2 treatment.
SUM149PT (A) and HeLa (B) cells were either mock-treated (PBS) or treated with 0.125 µM or 50 µM Olaparib for 1 hour. After 1 hour, the medium was replaced by 1 mM H_2O_2 and the corresponding amount of PBS or Olaparib for 10 min. Cells were fixed immediately with methanol/acetic acid and stained with anti-PAR 10H antibody (GFP) and DAPI.

Cell lines

In this study we made use of two BRCA1-deficient breast cancer cell lines. The SUM149PT cell line contains a 2288delT mutation in exon 11 of the BRCA1 gene and shows low BRCA1 transcript levels [356]. Similar BRCA1 transcript levels were observed in SUM1315MO2 cells, which have a 185delAG mutation in exon 2 of the BRCA1 gene [356]. Ovcar-8 cells, deriving from ovarian adenocarcinoma tissue, and U2OS osteosarcoma cells exhibit a wild type BRCA1/-2 status and were, where required, treated with siRNA against BRCA1.

Long-term survival studies: continuous PARPi treatment

To evaluate our hypothesis, SUM149PT and SUM1315MO2 cells were transfected with siRNA against luciferase (= control) or MYH. Three days after siRNA transfection, when MYH knockdown was complete (data not shown), cells were subjected to a continuous Olaparib treatment with various doses. 10 days posttreatment, cells were fixed and stained with 0.5% crystal violet / 20% ethanol and colonies were counted (Figure 3-21 A-B). A similar assay was performed in Ovcar-8 cells (Figure 3-21 C), but since they exhibit a BRCA1/-2 wild type phenotype, they were treated with siRNA against luciferase (= control), MYH, BRCA1, or BRCA1 and MYH together. In these experiments we did not observe any differences in colony survival when comparing siLUC- with siMYH- (SUM149PT, SUM1315MO2) or siBRCA1- with siBRCA1/siMYH-treated cells (Ovcar-8). Nevertheless, BRCA1 knockdown in Ovcar-8 cells brought about the expected Olaparib sensitivity, proving that PARP inhibition worked. Equal survival of the control and MYH knockdown cells could be explained by the fact that siRNA-mediated knockdown of MYH is only transient and protein expression will recur about 2 days posttreatment. The clonogenic survival assay, in contrast, was performed until 10 days posttreatment. If Olaparib were stable in the medium over several days and was not washed out, this would result in a continuous exposure of the cells to the drug. Any effect of MYH knockdown on cell survival would hence be masked as soon as MYH is expressed again. However, if oxidative DNA lesions were the source of PARP inhibitor toxicity in HR-deficient cells, the effect of Olaparib should be enhanced upon additional DNA oxidation. Two possibilities would be to either additionally expose cells to reactive oxygen species (ROS), such as H_2O_2, or to co-downregulate the hydrolase MTH1, which hydrolyzes oxidized purine nucleoside triphosphates to monophosphates, thereby preventing their incorporation from the deoxynucleotide pool into newly-synthesized DNA. However, a higher number of oxidized bases in the DNA would be expected from exposure to ROS, since this would not only increase incorporation of oxidized deoxynucleotides from the pool but also oxidize non-replicating DNA.

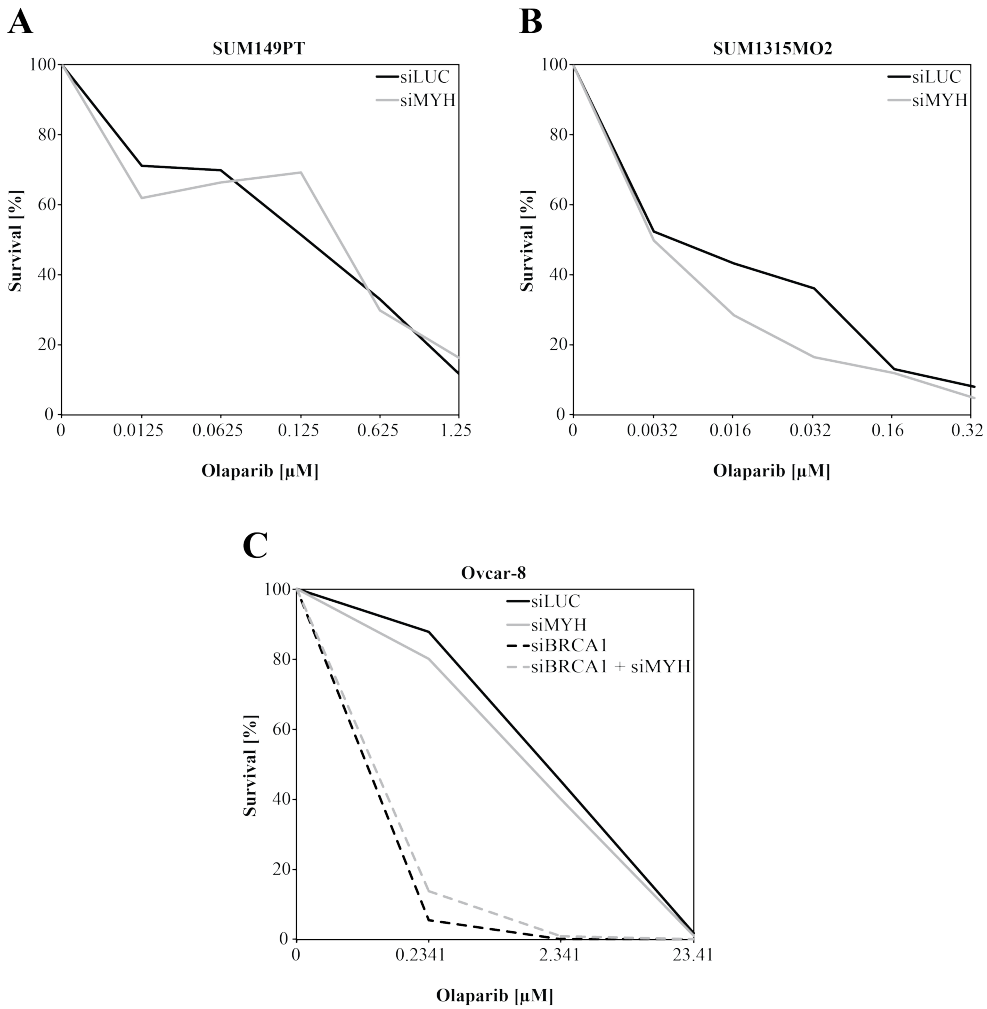

Figure 3-21: In long-term survival studies, a transient MYH knockdown has no effect on cell survival in BRCA1-deficient cells upon continuous Olaparib treatment.
Clonogenic survival assay of BRCA1-deficient (A) SUM149PT, (B) SUM1315MO2 and BRCA1-proficient (C) Ovcar-8 cells upon continuous treatment with various concentrations of Olaparib. Three days before treatment, cells were either treated with siLUC or siMYH. Since the BRCA1 status is crucial for the cells' response to Olaparib, Ovcar-8 cells (C) were additionally treated with siBRCA1.

Long-term survival studies: continuous PARPi treatment & H_2O_2

We performed clonogenic survival assays with SUM149PT cells that were treated with either 50 or 100 µM H_2O_2 for 1 hour, or continuously with 0.065 µM Olaparib. A combination treatment involved preincubation of the cells with Olaparib for one hour and subsequent addition of H_2O_2 for another hour. In this case, the drugs were washed off and replaced with Olaparib-containing medium for continuous treatment (Figure 3-22). The Western blot shows MYH knockdown efficiency at the day of treatment. Despite only a transient siRNA-mediated knockdown of MYH, the additional exposure to H_2O_2 brought about differences in cell survival of siLUC- or siMYH-treated cells. Monotreatment with H_2O_2 resulted

in a dose-dependent response of control cells (siLUC), while MYH knockdown cells were 1.5 (50 µM H_2O_2) and 1.7 fold (100 µM H_2O_2) more resistant as compared to control cells. Reduced DNA damage recognition in the absence of MYH, can explain the observed resistance to H_2O_2 in those cells. As already observed in the previous experiment (Figure 3-21), Olaparib monotreatment did not lead to any differences in colony survival. However, similar to H_2O_2 treatment alone, a combination treatment of H_2O_2 and Olaparib resulted in 1.9 (50 µM H_2O_2) and 1.4 fold (100 µM H_2O_2) increased survival of MYH knockdown cells when compared to the control cells. Overall, toxicity in H_2O_2 + Olaparib-treated cells was increased compared to single treatments. These results show that Olaparib activity is enhanced in the presence of oxidative stress, supporting the idea that PARP inhibitor sensitivity in HR-deficient cells depends on oxidized DNA products. Furthermore, since MYH knockdown led to tolerance of the combination treatment, this experiment suggests that the oxidized DNA was, at least partially, addressed by MYH.

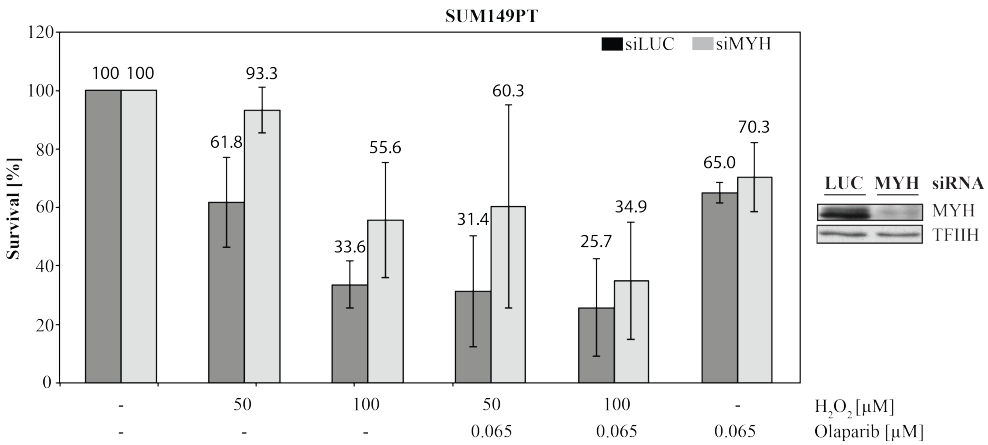

Figure 3-22: In long-term survival studies, a transient MYH knockdown in BRCA1-deficient cells leads to increased cell survival upon H_2O_2 / Olaparib combination treatment.
Clonogenic survival assay of BRCA1-deficient SUM149PT cells either treated with siRNA against luciferase (siLUC) or MYH (siMYH). Cells were treated with either H_2O_2 or Olaparib alone, or with Olaparib and H_2O_2 together. In the last case, cells were treated with 0.065 µM Olaparib for 1 hour, and then H_2O_2 was added for another hour. After that, the medium was removed, cells were washed with PBS and new medium supplemented with 0.065 µM Olaparib (= continuous treatment) was added. The graph represents the results of two independent experiments, each carried out in triplicate. Each data point represents an average +/- standard deviation. Whole cell extracts (WCE) were prepared at the day of treatment and used for Western blot analysis of the MYH knockdown efficiency.

Long-term survival studies: acute Olaparib treatment

In the next step, we aimed to work under natural conditions, i.e. in the absence of H_2O_2. In order to avoid possible masking of MYH knockdown-dependent changes in cell survival, we performed a clonogenic survival assay in SUM149PT cells, but this time using an acute 1 day Olaparib treatment (Figure 3-23). Consequently,

cells were only exposed to Olaparib at the day of complete MYH knockdown (Figure 3-23, Western blot). Any masking effects were herewith excluded. Indeed, under those assay conditions, MYH knockdown cells were more tolerant to Olaparib than the control cells.

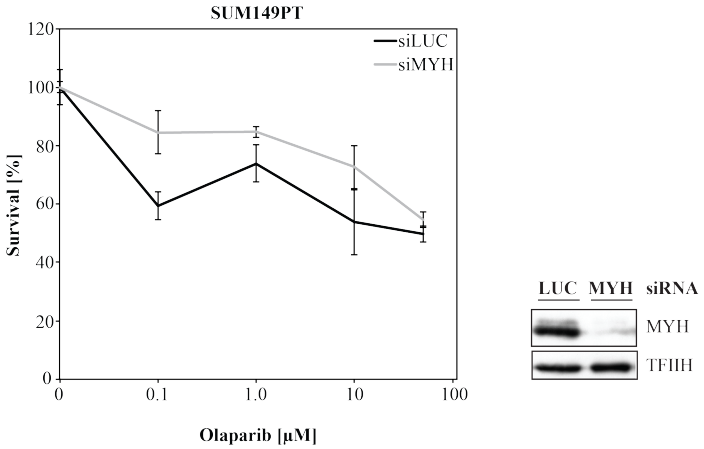

Figure 3-23: In long-term survival studies, a transient MYH knockdown in BRCA1-deficient cells leads to increased cell survival upon acute Olaparib treatment.
Clonogenic survival assay of BRCA1-deficient SUM149PT cells, either treated with siRNA against luciferase (siLUC) or MYH (siMYH), upon acute Olaparib treatment. Cells were treated with the indicated concentrations of Olaparib. 24 hours later, Olaparib was washed off and fresh medium was added to the cells. Standard deviations were calculated from triplicates within one experiment. Whole cell extracts were prepared on the day of Olaparib treatment and were used for Western blot analysis of the MYH knockdown efficiency.

Short-term survival studies in SUM149PT cells

Another approach to circumvent that MYH knockdown-dependent changes in cell survival might be masked, was to use short-term survival assays. We took advantage of a CellTiter-Blue cell viability assay (Promega) and measured cells' survival in terms of their metabolic activity, already 3 days after Olaparib treatment. For this purpose, at the day of measurement, Resazurin was applied to the cells, which then reduced it to Resorufin, a fluorescent substance with an emission wavelength of 590 nm. Since this assay lasted much shorter, MYH knockdown should be complete over the majority of the time. Again, SUM149PT cells were treated with siRNA against luciferase (= control) or MYH. The Western blot presents MYH protein levels at the time of Olaparib treatment. We observed that at doses of 0.1 - 10 µM Olaparib, MYH knockdown resulted in about 1.4 fold increased survival compared to control cells (Figure 3-24). Thus, those data were in agreement with the previous results shown in Figure 3-23.

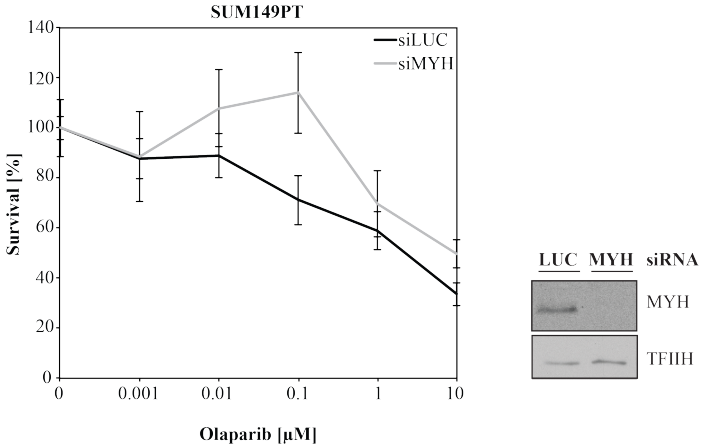

Figure 3-24: In short-term cell survival studies, a transient MYH knockdown leads to increased cell survival upon continuous Olaparib treatment in BRCA1-deficient SUM149PT cells.
CellTiter-Blue cell viability assay of BRCA1-deficient SUM149PT cells, either treated with siRNA against luciferase (siLUC) or MYH (siMYH), upon continuous Olaparib treatment. 72 hours after treatment, the cells' survival was measured in terms of their metabolic activity using a CellTiter-Blue cell viability assay. Standard deviations were calculated from triplicates within one experiment. Whole cell extracts for Western blot analysis of MYH knockdown efficiency were prepared on the day of Olaparib treatment.

Short-term survival studies in U2OS cells

We finally decided to confirm those results in another cell line, using the same short-term survival assay. U2OS cells are BRCA1 wild type, hence cells were treated with siRNA against luciferase (= control), BRCA1, or BRCA1 and MYH (Figure 3-25, A). As expected, BRCA1 knockdown resulted in PARP inhibitor sensitivity, proving efficient Olaparib treatment. In line with the previous experiment (Figure 3-24), additional MYH knockdown lead to 1.3 fold more survival when compared to BRCA1-deficient cells. An advantage of the U2OS cell system is that it allows the comparison of different survival curves with that of 'wild type'/BRCA1-proficient cells. Therefore, this was the first experiment that revealed that MYH deficiency does not fully rescue the BRCA1-deficient phenotype in the presence of Olaparib, but at least by 50%. In chapter 3.1.1, we provided *in vitro* evidence that MutSα enhances MYH activity. In this regard, we made an interesting side observation. Similar to MYH, a MSH6 knockdown in BRCA1 deficient cells resulted in slight tolerance to Olaparib. A triple knockdown of BRCA1, MYH and MSH6 even increased the tolerance to the same level than in BRCA1/MYH double knockdown cells (Figure 3-25, B). This suggests that MYH and MSH6 act in the same pathway during oxidative DNA damage repair, as observed *in vitro*. The data described here, will be discussed in chapter 4.4.

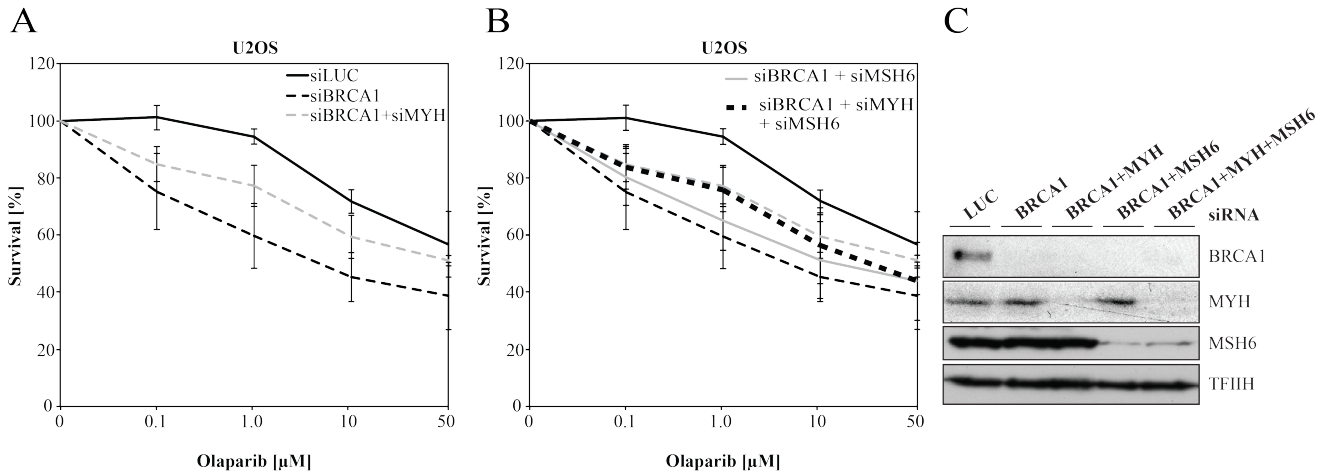

Figure 3-25: In short-term survival studies, a transient MYH knockdown partially rescues BRCA1 deficiency-mediated cell sensitivity towards Olaparib.

CellTiter-Blue cell viability assay of U2OS cells upon continuous Olaparib treatment. Cells were either treated with siRNA against luciferase (siLUC), BRCA1 (siBRCA1) or BRCA1 and MYH (siBRCA1 + siMYH) (panels A+B). Panel B additionally represents results for siBRCA1 + siMSH6 as well as siBRCA1 + siMYH + siMSH6 combination knockdowns. 72 hours after treatment, the cells' survival was measured in terms of their metabolic activity using a CellTiter-Blue cell viability assay. The graph represents the results of four independent experiments each carried out in triplicate. Each data point represents an average +/- standard deviation. (C) Whole cell extracts for Western blot analysis of the knockdown efficiencies were prepared on the day of Olaparib treatment.

4 Discussion & Outlook

4.1 The interdependence of base excision repair and mismatch repair during the processing of 8-oxoguanine

MMR activity on the leading strand

The principle mechanism of eukaryotic mismatch repair (MMR) during replication is well documented [40, 41] and its key players have been identified [357]. Nevertheless, some key mechanistic details of this pathway are still not clearly understood. One of these concerns the question how is MMR directed to the daughter strand in order to increase replication fidelity. On the lagging strand, this can be explained by preexisting, transient nicks between Okazaki fragments that occur every ~200 base pairs [358]. In contrast, the only preexisting strand discontinuity on the leading strand is its 3'-terminus. It was unclear for many years how 3' nicks could serve as entry-sites for 3'-5' strand degradation, given that the only nuclease implicated in MMR to date, EXOI, has an obligate 5'-3' polarity. This mystery was resolved by the finding of an intrinsic endonuclease activity of the MutLα subunit PMS2 [67], which was shown to be able to incise the daughter strand in the vicinity of the mismatch, thereby creating 5' nicks that can be used for EXOI-catalyzed degradation. A remaining question was how MutLα might be able to incise the strand that contained the preexisting 3' strand discontinuity. This was first proposed to be regulated by signaling between the MutSα/MutLα complex and the nick [67]. Later, however, Pluciennik *et al*. showed that this strand directionality is determined by an interaction of MutLα with PCNA [68]. MutSα would replace the polymerase at the 3'-terminus of the leading strand, recruit MutLα and form a PCNA/MutSα/MutLα complex that slides back to the mismatch in 3'-5' direction (see Figure 1-4). The assumption that MutLα can only cleave 5'-3'-oriented phosphodiester linkages could explain its strand bias for the primer strand [69]. However, strand discontinuities should not be more than 1000 base pairs away from the mismatch to allow efficient MMR [63]. Since the leading strand seems to lack sufficient amounts of nicks or gaps, this raised the question whether it might contain other strand discontinuities that might be used by the MMR system for the purpose of strand discrimination.

The mutual dependence of MutSα & MYH

We shed light onto this issue by showing that MMR can "hijack" MYH/APE1-generated breaks at G^O/A sites, allowing it to initiate its repair process (see chapter 3.1.1). Since G^O/A sites are frequently generated by polymerases [179, 182] but not recognized by their proofreading activity [184], each should be addressed by MYH and converted into a transient nick by the downstream-acting AP endonuclease. We also observed that MMR stimulates the activity of MYH, as described previously [35], but found an additional explanation how this might be achieved. Since siRNA-mediated knockdown of MMR proteins led to decreased MYH levels, this indicated that the former proteins stabilized MYH (see chapter 3.1.2.3). This

furthermore showed that MMR proteins indirectly enhance the activity of the MMR pathway by stabilizing their own nick-generator. In contrast, HEC59 and HCT15 cells, which have mutations in the *MSH2* or *MSH6* gene, respectively, showed higher levels of MYH than their undepleted controls. This scenario differs from that above, in that the MMR-deficient cell lines permanently lack MutSα expression. Therefore, they might have developed mechanisms to overexpress or stabilize MYH, possibly through enhanced transcription. The need for MYH in the absence of MMR can be explained by the synthetic lethality of MMR and the BER polymerase-β [285]. Both pathways are involved in the processing of oxidative damage [246], but if one is defective, the other can compensate for its absence. However, since MMR defects are the result of mutagenesis rather than evolution, MYH instability associated with transient knockdowns of MutSα/MutLα is most likely caused by the loss of interacting partners.

The meaning of low OGG1 activity

We furthermore observed that OGG1 was almost inactive in the cell extracts, which prevented "hijacking" of OGG1-generated nicks by MMR. Assuming that this low OGG1 activity reflects the *in vivo* situation, it can be explained by the fact that G^O/C sites are not directly mutagenic and therefore do not need to be repaired efficiently. This would also explain why OGG1-deficient mice do not develop tumors [245] and why OGG1 defects in humans have not been reported to cause cancer. In contrast, the efficient removal of mutagenic G^O/A sites by MYH is much more important, as reflected by the development of colorectal cancer when *MYH* is mutated.

Reasons of low OGG1 activity in extracts

However, we had to demonstrate that the lack of OGG1 activity in the extracts was not caused by our extract preparation or assay conditions (see chapters 3.1.1 + 3.1.2.4). We therefore first confirmed the presence of the protein in the extracts by Western blotting, and tested its stability by several freeze-thaw cycles. The protein appeared to be relatively abundant and stable. We next combined nuclear and cytoplasmic extracts in order to eliminate the possibility that OGG1 is inactive due to a lack of an activator protein. This assay also yielded no explanation for OGG1 inactivity. Another possibility is that the sluggish mode of action of OGG1 *in vitro* [240, 242] would preclude it from competing with MMR proteins or nucleosome loading. This scenario was also discarded, because substrate accessibility was observed to be diminished only after 1.5 hours of plasmid incubation, and MMR proteins were still active after 3 hours. One crucial factor that could affect OGG1 activity might be inappropriate salt concentration. Since the assay is performed under physiological salt concentration (110 mM KCl) that favors MMR, MYH and recombinant OGG1, this explanation can also be ruled out. The protein extraction from the nuclei was also performed at low salt concentration (150 mM NaCl), which is rather unlikely to cause inactivition of the protein. Another possibility could be that we did not extract an active form of OGG1, in that it might lack

essential posttranslational modifications (PTMs). The only reported PTM of OGG1 is phosphorylation [243], but an *in vivo* experiment showed that serine phosphorylation of OGG1 seems to rather determine its cellular localization to the chromatin than affect its activity [244]. However, given that the recombinant OGG1 used in our experiments was active despite having been purified from bacteria, which lack serine, threonine and tyrosine kinases [359], the lack of phosphorylation is unlikely to be the reason for OGG1 inactivity in the extracts. Taken together, our data suggest that what we observed *in vitro* reflects the situation *in vivo*. The most likely scenario would therefore be that OGG1 is inhibited in the extracts by other proteins such as chaperones. This would also explain why we observe OGG1-dependent MMR upon addition of recombinant OGG1 to the extracts. The latter would cause an imbalance in the ratio of OGG1 and its inhibitor; no inhibitor would be available for the extra OGG1, which would then be functional.

In vivo MMR studies

To test this assumption, our next goal is to study BER-dependent MMR *in vivo*. For this purpose, we developed an *in vivo* MMR assay and we could confirm that MMR also "hijacks" MYH-initiated nicks on substrates transfected into human cells (see chapters 3.1.2.1 + 3.1.2.2). To entirely clarify the issue discussed above, one main focus of future studies will be to study OGG1-dependent MMR *in vivo*. This could be achieved with the described assay or, since its sensitivity is limited due to co-recovery of plasmids that were not available for repair, using a fluorescence-based approach. This would have the advantage that only substrates that reached the nucleus would be analyzed, thus reducing background levels of unrepaired plasmids.

Impact of the study

We should point out that G^{O}/A intermediates are unlikely to be the only strand discontinuities besides Okazaki fragments and 3' termini of the leading strand. Their limited contribution is apparent from the fact that MAP-tumors rarely exhibit microsatellite instability (MSI), a hallmark of MMR-deficiency. In tumours displaying MSI, MMR deficiency was caused either by biallelic promoter silencing of the *MLH1* gene [221] or by G to T transversion mutations in *MMR* genes, resulting from MYH dysfunction [222, 224]. However, our laboratory has shown that also RNaseH2-induced nicks can be "hijacked" by MMR. We therefore propose that many different kinds of repair intermediates could be "hijacked" by MMR, and hence collectively contribute to MMR directionality and efficiency, and thus also to replication fidelity. A future challenge is to identify the nature of all these intermediates. The ability of MMR to use breaks generated by other pathways of DNA metabolism as strand discrimination signals represents a perfect back-up system for MutLα, ensuring that the loss of one nick-generator would not impair MMR function and hence its role in cancer prevention.

4.2 The involvement of PARP-1 and PARP inhibition in BER-dependent mismatch repair

Achievements

We extended the study described above and asked whether PARP-1, which was previously linked to oxidative DNA damage response and base excision repair (BER), might play a role during MYH- and OGG1-directed mismatch repair (MMR). As described in chapter 3.1.3 (Figure 3-8), trapping of PARP-1 on DNA glycosylase-generated nicks by PARP inhibition, could affect MMR in different ways: it could preserve the nick thereby increasing its accessibility for MutSα-activated EXOI, or it could block the single-strand break. In this case, EXOI would not have access to the nick and MMR activity would decrease. Our data point towards the last scenario, thereby giving insights into possible effects of PARP inhibition on MMR activity. Furthermore, these experiments implicate that PARP-1 binds to MYH/APE1- and OGG1-generated nicks *in vitro*. We made several observations during this study, which are discussed in the following sections.

PARP inhibition in 3'- and 5'-directed BER-dependent MMR

Interestingly, MYH-dependent MMR was more affected by Olaparib than OGG1-dependent MMR (Figure 3-10). This might be due to a more prominent role of PARP-1 at MYH/APE1-generated nicks, but it might also be a result of the position of the nick relative to the mismatch. While MYH generates 3' nicks at G^O/A-G/T substrates, OGG1 generates 5' nicks at G^O/C-G/T plasmids. Since EXOI acts in a 5'-3' direction, MMR on 3' nicked substrates depends on the intrinsic endonucleolytic activity of MutLα (see chapter 1.3.2.2) [67]. MutLα will generate various nicks in the proximity of the initial nick and the mismatch, thus generating 5' nicks that can be used by exonuclease EXOI. This increased number of nicks, representing potential binding sites for PARP-1, might also explain the stronger effect of PARP inhibition on G^O/A-G/T substrates. Whether this assumption is correct could be clarified with experiments using G/T-G^O/A and G/T-G^O/C substrates, leading to MYH/APE1-induced 5' and OGG1-induced 3' nicks, respectively.

NAD^+ and PARP inhibitors in chromatin packaging

In order to exclude any unspecific, PARP-1-independent, inhibitory effects of Olaparib on the MMR machinery or other factors involved in this process, PARP-1-depleted cell extracts could serve as control. Furthermore, removal of histones from the extracts could exclude any NAD^+ or PARP inhibitor-dependent effects on chromatin packaging, thus influencing repair-processes. Such effects cannot be fully excluded in our experiments. However, we showed that the NAD^+ concentrations that were used in our assays did not affect G^O/A-G/T repair (Figure 3-9 B). Furthermore, G/T unnicked control plasmids also exhibited background levels of MutLα-dependent MMR (Figure 3-10). Since those repair levels did not change upon Olaparib addition, we can assume that the MMR machinery itself and chromatin packaging was, at least not significantly, affected by Olaparib.

PARP inhibition in 3' and 5' directed MMR

In order to distinguish the effects of Olaparib on BER from its effects on MMR, future experiments should involve 5' and 3' Nt.*Bst*NBI prenicked G/T substrates. This would allow studying the effect of Olaparib exclusively on MMR and should indicate whether PARP-1 exhibits different binding affinities to nicks introduced by MYH/APE1, OGG1 or a nickase. In fact, reconstituted systems, involving all enzymes that are required for efficient 3'- or 5'-directed MMR, were defined [62, 63, 66, 357] and did not include PARP-1. It therefore does not play an essential role during this process, but this does not exclude transient protection of the nicks by PARP-1. If the latter was indeed the case, PARP-1 inhibition on Nt.*Bst*NBI nicked heteroduplex substrates should also affect MMR. Indeed, a study of Liu *et al*. showed that increasing amounts of PARP-1 in the absence of NAD^+, thus imitating a PARP inhibition situation, to a 4- (MutSα, MutLα, EXOI, RPA) or 6- (+PCNA, RFC) protein system, decreased 5' and 3' excision by EXOI on nicked heteroduplex substrates [308]. PARP inhibition might therefore not only affect BER-dependent MMR as shown in our study, but also BER-independent MMR processes as shown by Liu *et al* [308].

Impact of the study

Taken together, the effect of PARP inhibition on DNA repair that we describe here could represent possible side effects of PARP inhibition in non-cancerous cells. However, even if PARP inhibition would affect MYH-dependent MMR processes, in terms of clinical application the number of G^O/A mispairs in cells might not be enough to give rise to a MMR-deficient phenotype upon PARP inhibition. But if this observation could be extrapolated to other MMR events, such as MMR initiating at Okazaki fragments or RNaseH2-generated nicks [72], PARP inhibition could seriously affect the overall MMR efficiency. A consequence could be an altered response to other treatments, since a lack of MMR leads to resistance of various kinds of drugs (see chapter 1.8.2). Although we also showed an effect of PARP inhibition on OGG1-dependent MMR, this finding is expected to be less relevant, since OGG1-dependent MMR does not occur in cell extracts (see chapter 3.1.1). Thus far, we have not questioned how it is possible at all that the well coordinated BER pathway can be interrupted by MMR and enable it to displace BER proteins from the DNA prior to completion of repair. It is likely that this process is coordinated by other factors and it will be a future challenge to test if PARP-1 might be one of those by controlling access of the different repair enzymes to the nick.

4.3 Towards the elucidation of the interactome of MSH6 during oxidative stress

Achievements

As described in detail in chapter 1.8.1, there is emerging evidence that mismatch repair (MMR) is involved during oxidative DNA damage repair, but its precise role in this process is poorly understood. Our long-term aim is thus to get more insights into potential novel roles of the mismatch recognition factor MutSα during

oxidative DNA damage response. This should be achieved by studying the interactome of the MutSα heterodimer component MSH6 using mass spectrometry. As mentioned in chapter 3.2, my goal was to establish and evaluate the required tools for efficient MutSα pulldowns. For this purpose I modified a destination vector that was provided by Matthias Gstaiger, according to our needs. The resultant 'pTO+AIO CSH GW FRT' vector (see Figure 3-11, Table 3-2) can be used for either i) isogenic inducible gene replacement or for ii) inducible knockdown, of any protein of interest. In the former case, it allows C-terminal Strep/HA tagging of the protein, making it suitable for pulldown experiments. Though MSH6 expression in this vector was not sufficient, I succeeded in the generation of an isogenic inducible MSH6 knockdown cell line, which can be used for future MutSα studies (Figure 3-14 A). Due to the vector's universal applicability, it could in future also be tested for MSH2 gene replacement, and in case of success be used for MutSα/β interactome studies. In a second step, I characterized a HeLa Kyoto MSH6-LAP cell line in terms of exogenous MSH6 expression, functionality, its behavior towards oxidative stress and its suitability for GFP pulldowns (Figure 3-18, Figure 3-17, Figure 3-19). In fact, to our knowledge, this is the first cell line that successfully expresses exogenous tagged MSH6. As expected, MSH6 knockdown in this cell line lead to increased sensitivity and G_2/M arrest upon $KBrO_3$ treatment. Furthermore, I could show that GFP pulldowns of LAP-tagged MSH6 were extremely efficient, a prerequisite for future interactome studies (Figure 3-19). In the following two sections, the reasons for successful MSH6 expression from BACmids, as well as various other approaches for interactome studies that can be done based on my work, will be discussed.

MSH6 expression

We showed that MSH6 expression from bacterial artificial chromosomes (BACmids) was much more efficient than from cDNA vectors. In general, there are various reasons that can underlie low protein expression levels in mammalian cell lines. One possibility is an impairment of protein folding or function due to the tag, which could block active sites or interactions with other proteins. In the case of MSH6, it would thus be illogical to tag the N-terminal domain, since this possesses multifunctionality and a PIP domain at its extreme N-terminus (see chapter 1.3.2.2). The C-terminus in contrast is part of the ATPase containing domain. Whether its linkage to a tag affects MSH6 activity is difficult to anticipate, but it seems unlikely, since C-terminal LAP-tagged MSH6 in HeLa Kyoto cells was functional. Besides the location of the tag, its size could also influence the protein's function. For instance, bulky tags bring about greater chances of impairing proteins' functionality. However, it seems that the rather big (≈ 29 kDa) S-protein/GFP containing tag does not negatively influence MSH6 activity. Though it is not proven, it is likely that also the comparably small (≈ 5 kDa) Strep/HA tag would not affect MSH6 activity. It should also be considered that overexpression

of proteins that are involved in signaling processes as might be the case for MSH6 [80, 82], can be 'toxic' for the cell. This might protect itself by enhanced degradation of the protein or its mRNA. However, although controlled by a strong CMV promoter, overexpression of MSH6-Strep/HA in U2OS Flp-In T-REx cells should not present a problem, as MSH6 protein levels should be self-limiting when not accompanied by a concomitant rise in MSH2 [56, 360]. Based on our observation, low MSH6 protein expression from the 'pTO+AIO hMSH6-SH GW FRT + shMSH6' vector may more likely be caused by problems in the MSH6 expression itself than by post-expressional influences. Like in our approach, expression of tagged proteins in mammalian cells is typically performed with cDNA-based transgenes that lack the normal endogenous regulatory information and are driven by unrelated promoters. This approach led however to unsuccessful attempts of our and probably other laboratories in expressing tagged versions of MSH6. The first success was achieved recently by the laboratory of Anthony Hyman that expressed tagged MSH6 from a BACmid [355], which has the advantage that it allows insertions with more than 300 kilobases. BACmids therefore contain complete genes with all their endogenous regulatory sequences, such as introns or untranslated regions (UTRs), and furthermore allow protein expression under the control of its natural promoter, thereby ensuring normal expression levels. Our observations indicate that some of those natural regulatory sequences might be essential for successful MSH6 expression. This assumption would moreover be supported by the fact that MutSα activity could be restored in the MSH6-mutated HCT15 cell line by introducing chromosome 2 [345]. In this case, comparable to expression from a BACmid, MSH6 expression occurs from its entire gene including its own promoter and regulatory sequences.

Outlook

Based on the high pulldown efficiency of exogenous MSH6 and its binding partner MSH2 from HeLa Kyoto cell extracts, the specificity of co-precipitated interaction partners of MSH6-LAP could be enhanced in various ways, each bringing along advantages and disadvantages. Co-precipitation of expected interaction partners in GFP control cells points towards insufficient purification of the beads (Figure 3-19), which might be achieved by more stringent washing or a second purification step *via* S-protein. Both approaches however could be at the cost of losing interaction partners of the actual protein of interest. Those were, apart from MSH2, already only rarely detectable and, if so, only in little amounts. This could be explained by non-functionality of the exogenous protein, but is unlikely, since we showed that it is recruited to chromatin upon MNNG treatment (Figure 3-16 C). It might well be that only in the presence of DNA damage, such as oxidative stress, interaction partners increase their binding affinity to MSH6, which would then facilitate their detection. MSH6 might also bind weakly or only transiently to many of its interaction partners. In this case, protein crosslinking in cells could increase their detection. In fact, another possibility would be to use BirA or ascorbate

peroxidase (APEX) tags. An engineered form of the 35 kDa biotin protein ligase BirA has promiscuous properties and thus biotinylates all proximate proteins, which can subsequently be purified in a streptavidin-dependent manner [361, 362]. Also an engineered variant of APEX biotinylates proximate proteins (< 20 nm) in an APEX- and H_2O_2-dependent manner [363]. Since this approach is inducible by H_2O_2, it even allows for snapshots of 'interacting' complexes. Regarding the available tools that were developed and evaluated during this project, future pulldown and interactome studies might make use of the following approaches. The hitherto lack of inducible gene replacement in the otherwise suitable HeLa Kyoto MSH6-LAP cell line could be resolved by engineering of the BACmid. Furthermore, future studies could be done based on the generated 'pTO+AIO hMSH6-SH GW FRT + shMSH6' vector. One approach would be the replacement of the Strep/HA tag on this vector by GFP. Although, as discussed above, a negative effect of the Strep/HA tag on MSH6 functionality is rather unlikely, replacement with a GFP tag could be tested, since this worked in the BACmid approach. Additionally, if expression of tagged MSH2 from cDNA turns out to be efficient, a cell line allowing for inducible gene replacement with MSH2-Strep/HA could be generated based on the 'pTO+AIO CSH GW FRT' vector and be used for MutSα/β interactome studies.

4.4 The underlying sources of DNA damage and repair that mediate PARP inhibitor sensitivity in HR-deficient cells

Achievements

Although the potency of PARP inhibitors in homologous recombination (HR)-deficient tumors can plausibly be explained by the 'concept of synthetic lethality' [328, 329] (chapter 1.9.4.1), the underlying sources of DNA damage that lead to single-strand breaks (SSBs), and thus to PARP inhibitor sensitivity, have not been examined yet. Since PARP inhibitors work as monotherapies in the described genetic background, it is likely that SSBs arise from endogenous sources of DNA damage. It is assumed that, since oxidation is a main source of endogenous DNA damage [169], it could be a main contributor to PARP inhibitor sensitivity. However, this had not been proven to date. Using survival studies, we showed that MYH knockdown in BRCA1-deficient cells gave rise to increased survival upon Olaparib treatment, suggesting that MYH-generated nicks can contribute to Olaparib sensitivity. These data represent first *in vivo* evidence that oxidation indeed contributes to PARP inhibitor sensitivity in HR-deficient cells. Furthermore, they prove that PARP-1 is involved in MYH-mediated BER *in vivo*.

Impact of the study

These observations might have clinical relevance. In the described genetic background, the effect of PARP inhibitors could be potentiated with additional oxidizing agents, such as Methotrexate. This drug is already used for treatment of various kinds of cancers and was furthermore shown to lead to accumulation of 8-

oxoguanine [284]. In terms of personalized medicine, it might be beneficial to apply PARP inhibitors to tumors that exhibit high MYH and/or low MTH1 protein levels. Another possibility would be a simultaneous inhibition of MTH1. In fact, an important step in the direction of such a clinical application was achieved recently, since selective and potent MTH1 inhibitors have been developed and validated in human cells and mice [256, 257]. Overall, our observations are in line with other studies that also described MYH to induce lethal SSBs. Oka *et al*. showed that accumulation of MYH-generated SSBs in either mitochondria or in the nucleus upon oxidative stress, activated two distinct cell death pathways [364]. Knockdown of MYH suppressed both kinds of cell death. This suggested that MYH induces cell death under oxidative stress in order to prevent mutagenesis [365], as happens for example in *APC* or *KRAS* genes of MAP patients. Those and our studies imply that MYH can introduce SSBs that lead to cell death. The mechanisms of cell death will be different, however. During our study, we made several observations that are discussed in the following sections.

Olaparib stability

Since little information about Olaparib stability under culture conditions is publically available, except sensitivity to temperature and light (material safety data sheet, Olaparib), we initially assumed Olaparib to be unstable in cell culture medium at 37°C over a long period of time. Thus, first experiments (Figure 3-21) were carried out with a continuous Olaparib treatment in long-term clonogenic survival assays. Here, we did not observe any differences in colony survival between control and MYH knockdown cells. We thereupon performed similar assays, but using acute Olaparib treatment (Figure 3-23) or short-term survival assays (Figure 3-24 + Figure 3-25). Under those conditions, MYH knockdown cells exhibited resistance to the drug. Contrary to what we assumed, these different outcomes can be explained with long-term stability of Olaparib under culture conditions. Since in all experiments MYH knockdown was transient, re-expression of the protein would mask any effect of PARP inhibition on cell survival.

Role of MYH in response to oxidative stress

Furthermore, we showed that MYH knockdown in SUM149PT cells led to H_2O_2 tolerance (Figure 3-22). We observed this effect also in other, HR-proficient cell lines such as Hek293 or HeLa Kyoto MSH6-LAP (data not shown). Due to the enhanced oxidative DNA damage tolerance in MYH knockdown cells, this observation can be well explained. Those data are in line with studies of Yusaku Nakabeppu and colleagues. Here, they showed that accumulation of 8-oxoguanine led to cell death, which was triggered by MYH-induced single-strand breaks. Knockdown of MYH reduced the number of SSBs and thus led to 8-oxoguanine tolerance and better cell survival [364, 365]. By contrast, other studies demonstrated that MYH knockdown in HeLa cells [366] or in cells carrying mutated MYH [216, 367] brought about more sensitivity to oxidative stress. Further studies are required to evaluate those discrepancies.

Other contributors to PARPi sensitivity in HR-deficient cells

Experiments with siBRCA1-treated Ovcar-8 cells showed that additional knockdown of MYH brought about Olaparib resistance (Figure 3-25). However, survival was only restored by 50% when compared to BRCA1-proficient Ovcar-8 cells. This means that MYH is a contributor to Olaparib sensitivity in this genetic background, but apparently other factors also play a role here. Assuming that PARP inhibitor sensitivity could be entirely attributed to intermediates of the BER pathway, glycosylases that address endogenous DNA damages, such as OGG1, UNG, SMUG1, TDG, MBD4, MPG, NTH1 or NEILs, could also play a role here. How efficiently they could contribute to such effect would depend on the incidence of the respective lesions and the effect of PARP-1 upon their activities. In fact, oxidative DNA lesions are more abundant in cells than other endogenous DNA damages [169]. This would suggest that glycosylases such as MBD4, MPG, UNG or TDG might play more minor roles in PARP inhibitor toxicity than oxidative DNA damage specific glycosylases such as OGG1, NTH1, NEIL1, NEIL2 or NEIL3. Amongst those, OGG1 might be a main contributor to PARP inhibitor sensitivity in HR-deficient cells, given that its substrate 8-oxoguanine is a predominant modification amongst oxidative DNA lesions. Furthermore, it should be considered that also spontaneous depurination represents a main threat to genomic integrity [169], leading to the loss of about 5000 purine bases and thus apurinic sites per cell per day. This means that if APE1 incised AP-sites were also recognized by PARP-1, its inhibition could have significant effects on cells' fates even in the absence of any glycosylase.

Outlook

Due to time constraints, this project had to be stopped at this point, but our findings represent a promising starting point to extend the project in various directions. Future experiments should validate our findings in SUM149PT cells using CellTiter-Blue and clonogenic survival assays. To further evaluate the contribution of oxidative stress to PARP inhibitor sensitivity, survival studies with Olaparib-treated BRCA1/-2 deficient cells should be performed under hypoxic or hyperoxic conditions. In line with our findings, hypoxia would be expected to increase cell survival. As discussed in the previous section, it would be interesting to use similar experiments to elucidate the contributions of other glycosylases to Olaparib sensitivity. Overall, such extension of the project should provide fundamental evidence for the origin of PARP inhibitor toxicity in HR-deficient cells.

5 Conclusions

The correct propagation of genetic information is indispensable for the maintenance and proper function of cells and organisms. However, faithful replication depends on various factors and multiple DNA repair mechanisms that contribute to its high fidelity. The work of this PhD thesis concentrated on two of those repair mechanisms, mismatch repair (MMR) and base excision repair (BER), as well as on the protein PARP-1 in the context of oxidative DNA damage.

Postreplicative MMR increases replication fidelity by several orders of magnitude, but to do so it needs to be directed to the newly-synthesized daughter strand. How this is regulated *in vivo* is still poorly understood, but it is assumed that strand discrimination signals primarily derive from gaps between Okazaki fragments on the lagging strand and from 3' termini of the leading strand. The imbalance in the abundance of strand discontinuities between the two strands is obvious and begs the question how accessibility of the leading strand for MMR is ensured. In this work we show that MMR can "hijack" breaks generated as intermediates of MYH-initiated BER of G^O/A mispairs and use them as strand discrimination signals. This we showed in human nuclear extracts as well as in extracts of *Xenopus laevis* eggs, and we are currently extending these studies also to human cells *in vivo*.

Taken together with recent findings from our laboratory, which demonstrated that ribonucleotides misincorporated into the nascent DNA strand during replication can also be "hijacked" by the MMR system as strand discrimination signals, it might be expected that MMR deploys breaks generated during all base excision repair events in this manner. However, only the "hijacking" of breaks in nascent DNA strands would contribute to increased replication fidelity, whereas breaks in the parental strand would provide the system with the wrong strand directionality, as well as possibly bringing about a collapse of the replication forks. Interestingly, G^O/C pairs in which the oxidized guanine would be in the parental strand do not appear to be processed by BER during the time course of the MMR reactions in the cell extracts. This suggests that MMR and BER are highly regulated as to which lesions may serve as strand discrimination signals at replication forks and which cannot. How such ingenious fine-tuning of strand accessibility is regulated and whether it takes place also *in vivo* needs further detailed investigation. Does it involve active inhibition of certain BER glycosylases? Or is the regulation simply the result of the different abundances of certain DNA lesions, the individual repair enzymes or the different kinetics of the respective repair processes? It would also be useful to gain more insights into how ongoing BER is displaced by MMR proteins, as exemplified at sites of G^O/A processing. Does it involve inhibition of the downstream BER enzymes such as polymerase β/λ, or is the exchange regulated by other nick binding enzymes, such as PARP-1? This remains to be

tested. Also interactome studies of MMR proteins could help to identify such 'regulator'. However, our preliminary data point towards an involvement of PARP-1 in BER-dependent MMR and this topic is the subject of future studies.

PARP inhibitors are currently in Phase III clinical trials for the treatment of BRCA-deficient breast and ovarian cancer. Surprisingly, the biological role of the main target of these inhibitors, PARP-1, is not fully understood. In the current age of “personalized medicine”, full understanding of the mode of action of all cancer chemotherapeutics is required if we are to predict the response of individual patients to combination cancer therapy and also avoid deleterious side effects. During the course of this work, we took a small step towards identifying the source of spontaneous DNA damage that leads to the death of BRCA-deficient cells. By demonstrating that the effect of PARP inhibition was reduced by the downregulation of MYH activity in human cell lines, we implicated oxidative DNA damage as one of the underlying sources of strand breaks that feed into the homologous recombination pathway inactivated by BRCA malfunction. Other sources of endogenous DNA damage involved in the sensitivity of BRCA-deficient cells to PARP inhibitors remain to be identified, and the involvement of repair mechanisms responsible for their processing must be closely studied. The putative involvement of PARP-1 in MMR represents one such example. Should PARP-1 inhibition indeed affect MMR efficiency, as indicated in our preliminary *in vitro* experiments, this could have deleterious consequences, given that MMR dysfunction leads to DNA damage tolerance, which represents a serious problem in cancer therapy. The experiments described in this thesis address only a small fraction of the questions that remain to be answered in the future. If we are to develop more efficient ways of treating cancer, we must gain detailed understanding of the mechanisms of action of cancer therapeutics and of the biological pathways involved in their metabolism. In this way, we should be able to use the differences between tumor types and individuals in the design of therapeutic strategies that would optimize the patient response to this important class of substances.

6 Materials & Methods

6.1 Studies relating to the manuscript

In vivo MMR assay

In vivo MMR assay

HCT116 + chromosome 3 cells were transfected with siRNA against luciferase or MYH using RNaiMax (Invitrogen) as per manufacturer's protocol. 48 hours later, the cells were seeded in 6-well plates at a density of 500'000 cells per well and in triplicates. The following description refers to the treatment of a single well. 24 hours after seeding, the cells were transfected with 500 ng G^O/A-loop, loop, or homoduplex substrate or with 1 µg nicked loop substrate using Lipofectamine 2000 (Invitrogen) as per manufacturer's protocol. Transfection of 500 ng EGFP expression plasmid in a separate well served as control for transfection efficiency. The substrates were recovered 24 h later, EGFP expression was recorded by immunofluorescence (Olympus IX81) and whole cell extracts were prepared from separate wells for western blot analysis of knockdown efficiencies. The recovery process was performed as follows: cells were washed twice with PBS, trypsinized and transferred to 1.5 ml tubes. They were then pelleted at 1'000 rpm for 2 min, washed once with PBS and resuspended in P1 buffer (Qiagen). SDS and Proteinase K (AppliChem) were added to final concentrations of 0.6% (w/v) and 2.4 mg/ml, respectively. After incubation at 55°C for 1 hour, NaOH was added to a final concentration of 45.5 mM and incubation continued for 5 min at room temperature. Buffer A3 (Macherey Nagel) was added to a final concentration of 0.23% (v/v) and incubated for 5 min on ice. The mix was loaded on NucleoSpin®Plasmid columns (Macherey Nagel) the substrates were recovered according to the manufacturer's protocol and eluted in water. Contaminating linear genomic DNA was removed by Plasmid-Safe™ ATP-dependent DNase (Epicentre) treatment as per manufacturer's protocol. Substrates from three 6-well plates were pooled, concentrated by ethanol precipitation and digested with *Hin*dIII-HF (NEB) in 1x NEBuffer 2 (NEB). The substrate amounts were estimated on a GelRed- stained 1% agarose gel and equal amounts of substrate were used for primer extension. A 30 µl mix containing 1x NEBuffer 25 ng recovered substrate, 0.67 mM dNTPs and 4 nM [γ-^{32}P]ATP 5'-labeled primer (5'-GAATTGTAATACGACTCACTATAGGGCGAATTGGCGG-3') was heated at 95°C for 10 min. Primer annealing to the denatured substrate was performed at 50°C for 15 min. 1 U DNA polymerase I, Large Klenow fragment (NEB) was added and elongation performed at 37°C for 30min. After heat inactivation at 75°C for 20 min, the samples were concentrated by ethanol precipitation and resolved in 10 µl loading dye (80% formamide, 1 mM EDTA, 50 mM Tris-HCl pH 8.3). To visualize repair efficiencies, 2µl of each primer extension product were separated on a 10% denaturing polyacrylamide gel and analyzed with a Typhoon scanner (FLA 9500, GE Healthcare).

Primers for substrate production

Substrates for the *in vivo* MMR assay were produced as described in chapter 3.1.1. The oligonucleotides listed below served as primers and the single-stranded phagemid DNA listed in brackets, served as template. The *Sal*I (**GTCGAC**) restriction site is highlighted in bold and mispaired residues are underlined. Primer sequences correspond to the outer strand sequence of the substrate.

- loop (pRichi-2850bot*Sal*I(+2)):
  5'-CCAGACGTCT**GTCGAC**GTTGGGAAGCTTGA-3'
- G^O/A-loop (pRichi-2850bot*Sal*I(+2)):
  5'-GACGGCCAGG^OGAATTGTAATACGACTCACTATAGGGCGAATTGGC GGCCGCGATCTGATCAGATCCAGACGTCT**GTCGAC**GTTGGGAAGCTT GAG-3'
- no loop (pRichi-2850bot*Sal*I):
  5'-CCAGACGTCT**GTCGAC**GTTGGGAAGCTTGA-3'

Cell culture, Transfection, Western blot

Cell lines

HCT116 (MutLα-) and HCT116 + chromosome 3 (MutLα+) cells were obtained from Richard Boland and were cultured in McCoy's 5a medium (GIBCO) supplemented with 10% FBS (GIBCO). HCT15 and HCT15 + chromosome 2 cells [345] were cultured in RPMI medium (GIBCO) and 20% FBS (GIBCO). Hec59 and Hec59 + chromosome 2 cells [1] were grown in 50% Ham's F12 and 50% DMEM medium (GIBCO) supplemented with 10% FBS. The medium for the chromosome 2 or 3 complemented cell lines was supplemented with 400 µg/ml G418. U2OS cells were grown in DMEM (GIBCO) supplemented with 10% FBS. All media additionally contained 1% penicillin/streptomycin.

siRNA treatment & Western blot

Cells were transfected with siRNA
siMSH6 (1): 5'-CGCCAUUGUUCGAGAUUUA-3' (Microsynth);
siMSH6 (2): 5'-AUCGCCAUUGUUCGAGAUUUA-3' (Qiagen);
siMSH6 (3): 5'-UUCUGACAAAGGUGGUAAAUU-3' (Microsynth);
siMSH2: 5'-UCCAGGCAUGCUUGUGUUGAA-3' (Qiagen);
siMLH1 (ON-TARGETplus human MLH1 siRNA-SMARTpool, Dharmacon);
siMYH: 5'-UCACAUCAAGCUGACAUAUCAAGUA-3' (Microsynth);
siLUC: 5'-CGUACGCGGAAUACUUCGA-3' (Microsynth) using Lipofectamine RNAiMAX (Invitrogen) as per manufacturer's protocol. 3 days after transfection, whole cell extracts were prepared using 2 x Lämmli buffer (120 mM Tris-HCl pH 6.8, 4% SDS, 20% glycerol). Upon determination of the protein concentration by Lowry assay, proteins were analyzed with SDS-PAGE and Western blot.

***In vitro* OGG1 nicking assay**

In vitro OGG1 nicking assay

100 ng of supercoiled G^O/C-G/T substrate was, where indicated, incubated with 39 ng recombinant, purified OGG1 (gift from Dr. Barbara van Loon) and 0.05 U of APE1 (New England Biolabs), in either 1x nicking buffer (20mM Tris-HCl pH8

1 mM DTT, 1 mM EDTA pH 8, 0.1mg/ml BSA) or 1x MMR buffer (20 mM Tris-HCl pH 7.6, 110 mM KCl, 5 mM $MgCl_2$, 1 mM Glutathione, 50 µg/ml BSA, 0.1 mM dNTPs, 1.5 mM ATP) for 30 min at 37°C. The reactions were stopped by adding 2 µl of 6x loading dye (37.5 mg/ml Ficoll 400, 23% glycerol, 0.03% bromophenol blue) and subsequent heat inactivation. Samples were separated on a 1% agarose gel and visualized with GelRed.

6.2 Studies on the interactome of MSH6

Cell survival assays

siRNA treatment and CellTiter-Blue® cell viability assay

HeLa Kyoto MSH6-LAP cells were seeded at a density of 200'000 cells per dish (Ø = 6 cm). The next day, they were treated with siRNA against luciferase or MSH6. 48 hours posttransfection, cells were re-seeded in triplicates in 96-well plates at a density of 1500 cells/well (siLUC) and 4500 cells/well (siMSH6), respectively. 24 hours after seeding, cells were treated with the indicated concentrations of $KBrO_3$ (see: $KBrO_3$ treatment of cells). 72 hours after drug treatment, cell viability was measured with the CellTiter-Blue® Cell Viability Assay (Promega) according to the manufacturer's protocol. Fluorescence ($560_{Ex}/590_{Em}$ nm), an indicator of metabolic activity, was measured 4 hours after addition of Resazurin.

$KBrO_3$ treatment of cells

A 500 mM $KBrO_3$ stock was prepared in water and was stored in aliquots at -20°C. For treatment purposes, the $KBrO_3$ stock was diluted to the desired concentrations in PBS containing 20 mM Hepes (pH 7.5). The cells were washed once with PBS and subsequently treated with the appropriate $KBrO_3$ dilution for 30 min in the dark. To stop the treatment, the $KBrO_3$ solution was removed and replaced by medium.

Cloning

E. coli strains

DH10B

genotype: F^- endA1 recA1 galE15 galK16 nupG rpsL ΔlacX74 Φ80lacZΔM15 araD139 Δ(ara,leu)7697 mcrA Δ(mrr-hsdRMS-mcrBC) λ^- [368, 369]. Unless otherwise specified, transformations were performed with this *E.coli* strain.

One Shot® *ccdB* Survival ™ 2 $T1^R$

genotype: F-*mcr*A Δ(*mrr-hsd*RMS-*mcr*BC) Φ80*lac*ZΔM15 Δ*lac*X74 *rec*A1 *ara*Δ139 Δ(*ara-leu*)7697 *gal*U *gal*K *rps*L (StrR) *end*A1 *nup*G *fhu*A::*IS2* (Invitrogen™ Life Technologies). Feature: resistant to the *ccdB* gene product.

Vectors

Table 6-1: List of vectors

Name	Purpose	Reference / Supplier
pTO CSH GW FRT	Empty Gateway Destination vector: Tet-inducible CMV promoter for C-term Strep/Strep/HA-tagged protein expression.	Matthias Gstaiger, IMSB, ETHZ
pTO+AIO NSH GW FRT	Empty Gateway Destination vector: Tet-inducible H1 and CMV promoter for shRNA and N-term Strep/HA-tagged protein expression, respectively.	Svenja Kaden, IMCR
pFastBac1 hMLH1	Provides 486 bp stuffer sequence upon *Hin*dIII digest	Margaret Fäsi, IMCR
pcDNA3-hMSH6	Template for PCR amplification of MSH6 (pSR6-FW+pSR6-RV)	Nina Mojas, IMCR
pENTR3C	Empty Gateway Entry vector. Harbors attL1 and attL2 sites to allow LR recombination with destination vector	Invitrogen™
pENTR3C + hMSH6	Gateway Entry vector containing the MSH6 wild type ORF	This study
pTO+AIO CSH GW FRT	Empty Gateway Destination vector: Tet-inducible H1 and CMV promoter for shRNA and C-term Strep/HA-tagged protein expression, respectively.	This study
pTO+AIO CSH GW FRT + shMSH6	Gateway Destination vector: Tet-inducible H1 promoter for shMSH6 expression.	This study
pTO+AIO hMSH6-SH GW FRT + shMSH6	Gateway Destination vector: Tet-inducible H1 and CMV promoter for shMSH6 and C-term MSH6-Strep/HA expression, respectively.	This study

shRNA targeting MSH6

3'UTR targeted shMSH6 sequence:

```
(P)5'-GATCCCTTCTGACAAAGGTGGTAAATTTCAAGAGAAATTTACCACCTTTGTCAGAATTTTTA-3'
       3'-GGAAGACTGTTTCCACCATTTAAAGTTCTCTTTAAATGGTGGAAACAGTCTTAAAAATTCGA-5'(P)
```

shRNA sequence

hairpin

*Bgl*II restriction site

*Hin*dIII restriction site

Primers

Table 6-2: Primer sequences for MSH6 amplification and sequence correction

Name	Sequence 5'-3'	Purpose
pSR6-FW	TCGAAATTAATACGACTCACTATAG	Forward amplification of MSH6 A116G from pcDNA3-hMSH6
pSR6-RV	ATATCTCGAGCATAATTCCTTAATCAAAG TCAGCA	Reverse amplification of MSH6 A116G from pcDNA3-hMSH6
FW-MSH6 A116G	GGGCCTCACGCGAAGGCGGCCGTGCCGC CGCTGCCCCCG**G**GGCCTCTCCTTCCCC [1)]	Correction of MSH6 A116G to MSH6 wild type (forward)
RV-MSH6 A116G	GGCCACCAGGGGTAACCCTCCATCTTGGC CC [2)]	Correction of MSH6 A116G to MSH6 wild type (reverse)

[1)] *Eag*I restriction site, **corrected base**

[2)] *Bst*EII restriction site

Generation of 'pTO+AIO CSH GW FRT' vector

Table 6-3: Cloning steps and corresponding methods for generating the 'pTO+AIO CSH GW FRT' vector

Cloning step	Method	Resulting vector
1. Removal of an interfering *Bgl*II site	Digestion of pTO+AIO NSH GW FRT (E) and pTO CSH GW FRT (F) vectors with *Not*I/*Xma*I. Insertion of the 1189 bp fragment of vector (E) into the 5857 bp fragment of vector (F).	(G)
2. Insertion of an element, containing a H1 promoter and a downstream integration site (*Bgl*II/*Hin*dIII) for shRNA	Digestion of pTO+AIO NSH GW FRT (E) and pTO CSH GW FRT (G) vectors with *Pci*I/*Kpn*I. Insertion of the 3258 bp fragment of vector (E) into the 4215 bp fragment of vector (G).	(H)
3. Insertion of a stuffer sequence between the *Bgl*II and *Hin*dIII sites	Digestion of vector (H) and the pFastBacI hMlhI vector with *Hin*dIII. Insertion of a 486 bp fragment (= stuffer) of pFastBacI hMlhI between the *Bgl*II/*Hin*dIII sites *via Hin*dIII.	pTO+AIO CSH GW FRT vector (= A)

Insertion of shMSH6 into pTO+AIO CSH GW FRT vector

1 µg pTO+AIO CSH GW FRT vector was digested with 20 U *Bgl*II for 5 hours at 37°C and subsequently with 40 U *Hin*dIII for another hour. The stuffer that was cloned between both restriction sites brings about the advantage that successful digestion by both enzymes gives rise to a 486 bp fragment that can be detected on a 1% GelRed-stained agarose gel. shMSH6 and the *Bgl*II/*Hin*dIII digested pTO+AIO CSH GW FRT vector were mixed in a 4:1 ratio and were ligated by T4 DNA ligase (New England Biolabs) overnight at 16°C. Since successful insertion of shMSH6 into the destination vector destroys the *Bgl*II restriction site, the ligation product was purified using an ethanol precipitation, dissolved in water and subsequently subjected to a second *Bgl*II digestion for 3hrs at 37°C. Subsequent transformation into a *ccdB*-resistant *E. coli* strain gave rise to bacterial colonies that were analyzed by restriction enzyme digestion and sequencing.

PCR amplification of MSH6 A116G

PCR-amplification of the MSH6 A116G sequence from the pcDNA3-hMSH6 vector was performed according to the following protocol:

Temperature [°C]	Time	Cycles
98	30 sec	1x
98	10 sec	20x
60	20 sec	
72	5 min	
72	10 min	1x
4	∞	1x

For the generation of sufficient amounts of PCR product, the described PCR reaction was performed 8x in parallel and in separate tubes. One PCR reaction was performed in 1x Phusion buffer (New England Biolabs), 0.2 mM dNTPs, 0.5 µM pSR6-FW and pSR6-RV primers, 10 ng pcDNA3-hMSH6 vector and 0.4 U of

Phusion polymerase (New England Biolabs) according to the thermocycling conditions stated above. The PCR products were purified by ethanol precipitation, pooled and the DNA concentration was measured with a DNA standard on a 1% GelRed-stained agarose gel.

Insertion of MSH6 A116G into the pENTR3C vector

2 µg of both purified PCR product and pENTR3C vector were digested in 1x NEB1 buffer, 1x BSA (NEB), 40 U *Kpn*I-HF (NEB) and 30 U *Xho*I (Roche) in a total volume of 50 µl for 15 h at 16°C. Following gel purification, the insert and the pENTR3C vector were ligated by T4 DNA ligase in a 2:1 ratio overnight at 16°C.

PCR-site directed mutagenesis of MSH6 A116G to wild type

For correction of the MSH6 A116G sequence to MSH6 wild type, PCR-site directed mutagenesis was performed according to the following protocol:

Temperature [°C]	Time	Cycles
98	30 sec	1x
98	10 sec	20x
60	30 sec	
72	15 sec	
72	10 min	1x
4	∞	1x

For the generation of sufficient amounts of the PCR product, the described PCR reaction was performed 6x in parallel and in separate tubes. One PCR reaction was performed in 1x Phusion buffer, 0.2 mM dNTPs, 0.5 µM FW-MSH6 A116G and RV-MSH6 A116G primers, 10 ng pENTR3C + hMSH6(G116A) vector and 0.4 U Phusion polymerase-HF (New England Biolabs) according to the thermocycling conditions stated above. After gel purification, both 2 µg of PCR product and pENTR3C + hMSH6(G116A) vector were digested with 25 U *Eag*I overnight at 37°C and subsequently 25 U *BstE*II were added and the temperature was increased to 60°C for another hour. The desired DNA fragments were again purified by gel extraction. The digested 211 bp PCR fragment containing the corrected MSH6 sequence was inserted into the digested pENTR3C + hMSH6(G116A) vector in a 1:1 ratio by T4 DNA ligase overnight at 16 °C, thereby replacing the MSH6 mutated part in the pENTR3C vector.

pTO+AIO hMSH6-SH GW FRT + shMSH6 vector

Insertion of the MSH6 wild type ORF into the destination vector was achieved by LR recombination of the *att*L and *att*R sites of the pENTR3C + hMSH6 vector and the pTO+AIO CSH GW FRT + shMSH6 destination vector. The LR-reaction was performed according to the "*Gateway™ Cloning Technology*" manual (GibcoBRL® Life Technologies) using the Gateway® LR Clonase® enzyme mix, Invitrogen.

Generation of stable cell lines

Cell lines

U2OS Flp-In T-REx (generated by Daniel Durocher) and Hek293 Flp-In T-REx (Invitrogen) cells were cultured in DMEM (GIBCO), supplemented with 10 % Tet System approved FBS (GIBCO), 100 ug/ml Zeocin (Invitrogen) and 15 ug/mL Blasticidin (Invitrogen).

Generation & Screening of stable Flp-In T-REx cell lines

Four different stable cell lines were generated. U2OS and Hek293 Flp-In T-REx cells were transfected with the pTO+AIO hMSH6-SH GW FRT + shMSH6 or the pTO+AIO CSH GW FRT + shMSH6 vector using X-tremeGENE 9 DNA Transfection Reagent (Roche), 0.2 µg destination vector and 1.8 µg pOG44 vector. Mock-treated cells served as control during the selection process. Furthermore, the generation of the cell lines was performed according to the *"Flp-In system - for generating stable mammalian expression cell lines by Flp recombinase-mediated integration"* manual, Invitrogen. The selection procedure was initiated two days after transfection using a concentration of 50 µg/ml Hygromycin B, which was increased to 250 µg/ml on day 3. After approximately 2 weeks, single clones as well as one bulk culture from several clones were picked, expanded and screened for suitability: $2x10^5$ cells were seeded in a dish (Ø = 6 cm) and were immediately treated with 10 µg/ml doxycycline (Dox). At day 2, Dox was replenished and at day 3, whole cell extracts were prepared with 2x Laemmli buffer (120 mM Tris-HCl [pH 6.8], 4% SDS, 20% glycerol). Endogenous MSH6 as well as MSH6-GFP protein levels were analyzed by Western blotting.

MSH6-LAP pulldown

Cell lines

HeLa Kyoto MSH6-LAP and HeLa Kyoto GFP cell lines were obtained from Prof. Anthony A. Hyman (MPI-CBG, Dresden, DE). Both cell lines were grown in DMEM (GIBCO) supplemented with 10% FBS, 1% penicillin and streptomycin and in case of HeLa Kyoto MSH6-LAP cells additionally with 500 µg/ml G418.

Preparation of chromatin-enriched cell extracts for immunoprecipitation

Extracts were prepared from two different cell lines: HeLa Kyoto MSH6-LAP (= cell line of interest) and HeLa Kyoto GFP (= control cell line). For each cell line, extracts were prepared from six 80% confluent cell culture dishes (Ø = 15 cm). All following steps were performed in the cold room. Each dish was washed with 20 ml PBS and then with 20 ml buffer A (10 mM Hepes pH 7.9, 100 mM KCl, 1.5 mM $MgCl_2$, 0.34 M sucrose, 10% glycerol, 1 mM DTT, 1mM PMSF, 1 EDTA-free protease inhibitor cocktail tablet (Roche) per 100 ml). The buffer was removed completely and 800 µl of the same buffer were added back. Cells were scraped from the dish and transferred to a 1.5 ml Eppendorf tube. The cell membrane was disrupted, by 8 passages through a syringe needle (size: Ø = 0.5 mm). Disrupted cells were incubated on ice for 5 min and spun at 1700 rcf for 5 min to pellet the nuclei (P1). Nuclei were lysed by adding 800 µl of buffer B (3 mM EDTA, 0.2 mM EGTA, 1mM DTT, 1 mM PMSF, 1 EDTA-free protease inhibitor cocktail tablet (Roche) per 100 ml) and rotating the mixture for 10 min. The insoluble chromatin

(P2) was collected by centrifugation at 2000 rcf for 5 min. Fraction P2 was resuspended in 400 µl NP40 buffer (50 mM Tris-HCl pH 8, 150 mM NaCl, 0.5 % NP40, 1 mM EDTA), sonicated briefly (puls: 30%, 15 pulses) and spun at 20 000 rcf for 5 min. The protein concentration of the supernatant containing the chromatin-enriched protein fraction was estimated with a Bradford protein assay.

Pulldown of MSH6-LAP

All following procedures were performed in the cold room. Preclearing of the cell extracts: 40 µl blocked agarose beads (bab-20, Chromotek) were equilibrated by 3 washes with 500 µl ice cold dilution buffer (50 mM Tris-HCl pH8, 150 mM NaCl, 1 mM EDTA, 1 mM PMSF, 1 EDTA-free protease inhibitor cocktail tablet (Roche) per 30 ml). Centrifugation steps were performed at 2700 rcf for 2 min. Beads were then mixed with 2.5 mg chromatin-enriched cell extracts, NP40 buffer and dilution buffer so that a final concentration of 0.2 % NP40 and a total volume of 500 µl was reached. After 1 hr of rotation, beads were centrifuged and the pre-cleared cell extracts (= supernatant) were transferred to 30 µl new, equilibrated GFP-Trap®_A beads (Chromotek). Pulldown: Binding of the proteins to the GFP beads was performed for 2 hr during rotation at 4 °C. Beads were then washed thrice with 500 µl NP40 buffer (50 mM Tris-HCl pH 8, 150 mM NaCl, 0.5 % NP40, 1 mM EDTA). Each washing step included 5 min of rotation and subsequent centrifugation at 2000 rcf for 2min. Subsequently, the beads were resuspended in 30 µl 2x SDS buffer and boiled for 10 min at 95°C. Samples were spun at 2700 rcf for 2 min. The supernatant containing the dissociated immunocomplexes was analyzed by Western blotting.

6.3 Studies on PARP-1 and PARP inhibition

***In vivo* studies**

Cell lines

SUM149PT, SUM1315MO2 and Ovcar-8 cell lines were obtained from KuDOS Pharmaceuticals, UK. SUM149PT cells were cultured in Ham's F12 medium (GIBCO) supplemented with 5% FBS (GIBCO), 5 µg/ml insulin (Sigma-Aldrich), 1 µg/ml hydrocortisone (Sigma-Aldrich) and 10 mM Hepes (GIBCO). SUM1315MO2 cells were grown in the same medium without hydrocortisone but 10 ng/ml EGF (Sigma-Aldrich) instead. Ovcar-8 cells were cultured in RPMI medium (GIBCO) supplemented with 10% FBS (GIBCO). All media additionally contained 1% penicillin and streptomycin.

Immunofluorescence for PAR detection

Cells were seeded at a density of $2x10^6$ cells per dish (Ø = 10 cm) containing a cover slip. 24 hours later, SUM149PT and HeLa cells were either mock-treated (PBS) or treated with 0.125 µM and 50 µM Olaparib, respectively. After 1 hour, the medium was replaced by PBS containing 1 mM H_2O_2 for 10 min. After 10 min, H_2O_2/PBS was removed, cells were washed once with PBS and immediately fixed with methanol/acetic acid (3:1) on ice for 1 hour. Cells were blocked with PBSMT

(5% (w/v) milk powder, 0.05% (v/v) Tween20 in PBS) for 30 min, incubated with anti-PAR 10H antibody (1:500 dilution in PBSMT) overnight at 4°C, subsequently washed with PBS and incubated with the secondary antibody FITC-goat-anti-mouse (Sigma) (1:700 dilution in PBSMT) for 1 hour at room temperature. Cover slips were washed with PBS, fixed with DAPI-containing mounting medium (Vector Laboratories) and analyzed by microscopy (Olympus IX81).

siRNA treatment and clonogenic survival assay

Cells were seeded at a density of 500'000 cells per dish (Ø = 6 cm). 24 hours later, cells were transfected with 40 pmol siRNA against luciferase (siLUC), MYH or BRCA1 or a combination of them, using RNaiMax (Invitrogen) as per the manufacturer's protocol. 15 hours posttransfection, the medium was replaced and, in order to increase the knockdown period of time, 8 hours later a second transfection was performed similarly to the first. For survival assays, 48 hours after the first transfection, cells were seeded in triplicates in 6-well plates at a density of 500 (Ovcar-8), 1000 (SUM149PT) or 2000 cells (SUM1315MO2) per well. 24 hours after seeding, the cells were treated with the indicated concentrations of Olaparib, H_2O_2 or both. Olaparib treatment was performed either continuous or acute (see Olaparib treatment of cells). 8 days (Ovcar-8) or 10 days (SUM149PT, SUM1315MO2) after treatment, the cells were fixed and stained with 0.5% crystal violet in 20% ethanol and colonies containing more than 30 cells were counted. Whole cell extracts for Western blot analysis of the transfection efficiencies were prepared on the day of the drug treatment, using 2x Laemmli buffer (120 mM Tris-HCl [pH 6.8], 4% SDS, 20% glycerol).

siRNA treatment and CellTiter-Blue® cell viability assay

U2OS or SUM149PT cells were seeded at a density of 100'000 or 180'000 cells per 6-well, respectively. 24 hours later, cells were transfected with 40 pmol siRNA against luciferase, MYH, BRCA1 or MSH6 or their combination, using RNaiMax (Invitrogen) as per the manufacturer's protocol. 15 hours posttransfection, the medium was replaced and, in order to increase the knockdown period of time, 8 hours later a second transfection was performed as described before. For survival assays, 48 hours after the first transfection, cells were re-seeded in triplicates in 96-well plates at a density of 1000 cells/well. 24 hours after seeding, cells were treated with the indicated concentrations of Olaparib (see: Olaparib treatment of cells). 72 hours after continuous drug treatment, cell viability was measured with the CellTiter-Blue® Cell Viability Assay (Promega) according to the manufacturer's protocol. Fluorescence ($560_{Ex}/590_{Em}$ nm), an indicator of metabolic activity, was measured 4 hours after the addition of Resazurin.

siRNA sequences

siLUC: 5'-CGUACGCGGAAUACUUCGA-3'
siMYH: 5'-UCACAUCAAGCUGACAUAUCAAGUA-3'
siBRCA1: 5'-ACCAUACAGCUUCAUAAAUAA-3'
siMSH6: 5'-CGCCAUUGUUCGAGAUUUA-3'

Olaparib treatment of cells

For acute treatment, Olaparib (Seleckchem) was directly added to the culture medium. 24 hours posttreatment, cells were washed once with PBS and fresh medium was added. For continuous treatment, cells were not washed and Olaparib remained in the medium. Mock cells were treated with an appropriate amount of DMSO.

Olaparib/H_2O_2 combination treatment of cells

Olaparib (Seleckchem) was directly added to the culture medium. After 1 hour, H_2O_2 was diluted in PBS and was immediately added to the Olaparib-containing medium. 1 hour post H_2O_2 treatment, cells were washed once with PBS, and Olaparib containing medium was added back for continuous treatment. Mock cells were treated with appropriate amounts of DMSO and PBS.

***In vitro* studies**

Preparation of whole cell extracts for PAR detection

The MMR assay was performed as described in chapter 3.1.1, but with slight alterations: 100 ng activated DNA (Amsbio) and 50 µg HCT116 + chromosome 3 nuclear cell extract were incubated in a total volume of 12.5 µl in a buffer containing 20 mM Tris-HCl pH7.6, 5 mM $MgCl_2$, 1 mM Glutathione, 50 µg/ml BSA, 0.1 mM dNTPs, 1.5 mM ATP, 80 mM KCl and the indicated concentrations of NAD^+ or Olaparib. The reaction was incubated at 37°C for max 5 min, stopped by the addition of 5 µl 5x loading dye (0.25 M Tris pH 6.8, 50% glycerol, 8% SDS, 0.5 M DTT, 0.1% Bromphenol Blue), heated at 95°C for 5 min and analyzed by Western blotting. The anti-Poly(ADP-ribose) antibody (rabbit, polyclonal, BD Pharmingen, cat: 551813) was used at a dilution of 1:1000.

In vitro MMR assay with Olaparib or NAD^+

To investigate the role of PARP-mediated PAR formation during MMR processes, *in vitro* MMR assays (see chapter 3.1.1) were performed in the presence of either 500 µM Olaparib (Selleckchem) or 50 µM NAD^+ (New England Biolabs).

7 References

1. Watson, J.D. and F.H. Crick, *The structure of DNA.* Cold Spring Harb Symp Quant Biol, 1953. **18**: p. 123-31.
2. Hoeijmakers, J.H., *Genome maintenance mechanisms for preventing cancer.* Nature, 2001. **411**(6835): p. 366-74.
3. Wogan, G.N., et al., *Environmental and chemical carcinogenesis.* Semin Cancer Biol, 2004. **14**(6): p. 473-86.
4. Alberts, B., J.H. Wilson, and T. Hunt, *Molecular biology of the cell*. 5th ed. 2008, New York: Garland Science. xxxiii, 1601, 90 p.
5. Lindahl, T., *Instability and decay of the primary structure of DNA.* Nature, 1993. **362**(6422): p. 709-15.
6. Ames, B.N., M.K. Shigenaga, and T.M. Hagen, *Oxidants, antioxidants, and the degenerative diseases of aging.* Proc Natl Acad Sci U S A, 1993. **90**(17): p. 7915-22.
7. Helbock, H.J., et al., *DNA oxidation matters: the HPLC-electrochemical detection assay of 8-oxo-deoxyguanosine and 8-oxo-guanine.* Proc Natl Acad Sci U S A, 1998. **95**(1): p. 288-93.
8. Eker, A.P., et al., *DNA repair in mammalian cells: Direct DNA damage reversal: elegant solutions for nasty problems.* Cell Mol Life Sci, 2009. **66**(6): p. 968-80.
9. Daniels, D.S., et al., *DNA binding and nucleotide flipping by the human DNA repair protein AGT.* Nat Struct Mol Biol, 2004. **11**(8): p. 714-20.
10. Srivenugopal, K.S., et al., *Ubiquitination-dependent proteolysis of O6-methylguanine-DNA methyltransferase in human and murine tumor cells following inactivation with O6-benzylguanine or 1,3-bis(2-chloroethyl)-1-nitrosourea.* Biochemistry, 1996. **35**(4): p. 1328-34.
11. Sancar, A., *Structure and function of photolyase and in vivo enzymology: 50th anniversary.* J Biol Chem, 2008. **283**(47): p. 32153-7.
12. Lindahl, T., *An N-glycosidase from Escherichia coli that releases free uracil from DNA containing deaminated cytosine residues.* Proc Natl Acad Sci U S A, 1974. **71**(9): p. 3649-53.
13. Jacobs, A.L. and P. Schar, *DNA glycosylases: in DNA repair and beyond.* Chromosoma, 2012. **121**(1): p. 1-20.
14. Friedberg, E.C. and L.B. Meira, *Database of mouse strains carrying targeted mutations in genes affecting biological responses to DNA damage Version 7.* DNA Repair (Amst), 2006. **5**(2): p. 189-209.
15. Cortazar, D., et al., *Embryonic lethal phenotype reveals a function of TDG in maintaining epigenetic stability.* Nature, 2011. **470**(7334): p. 419-23.
16. Cortellino, S., et al., *Thymine DNA glycosylase is essential for active DNA demethylation by linked deamination-base excision repair.* Cell, 2011. **146**(1): p. 67-79.
17. Xie, Y., et al., *Deficiencies in mouse Myh and Ogg1 result in tumor predisposition and G to T mutations in codon 12 of the K-ras oncogene in lung tumors.* Cancer Res, 2004. **64**(9): p. 3096-102.
18. David, S.S., V.L. O'Shea, and S. Kundu, *Base-excision repair of oxidative DNA damage.* Nature, 2007. **447**(7147): p. 941-50.

19. Jiricny, J., *DNA repair: how MutM finds the needle in a haystack.* Curr Biol, 2010. **20**(4): p. R145-7.
20. Matsumoto, Y. and K. Kim, *Excision of deoxyribose phosphate residues by DNA polymerase beta during DNA repair.* Science, 1995. **269**(5224): p. 699-702.
21. Hegde, M.L., T.K. Hazra, and S. Mitra, *Early steps in the DNA base excision/single-strand interruption repair pathway in mammalian cells.* Cell Res, 2008. **18**(1): p. 27-47.
22. Krokan, H.E. and M. Bjoras, *Base excision repair.* Cold Spring Harb Perspect Biol, 2013. **5**(4): p. a012583.
23. Marintchev, A., et al., *Solution structure of the single-strand break repair protein XRCC1 N-terminal domain.* Nat Struct Biol, 1999. **6**(9): p. 884-93.
24. Caldecott, K.W., et al., *XRCC1 polypeptide interacts with DNA polymerase beta and possibly poly (ADP-ribose) polymerase, and DNA ligase III is a novel molecular 'nick-sensor' in vitro.* Nucleic Acids Res, 1996. **24**(22): p. 4387-94.
25. Caldecott, K.W., *XRCC1 and DNA strand break repair.* DNA Repair (Amst), 2003. **2**(9): p. 955-69.
26. Pascucci, B., et al., *Long patch base excision repair with purified human proteins. DNA ligase I as patch size mediator for DNA polymerases delta and epsilon.* J Biol Chem, 1999. **274**(47): p. 33696-702.
27. Podlutsky, A.J., et al., *Human DNA polymerase beta initiates DNA synthesis during long-patch repair of reduced AP sites in DNA.* EMBO J, 2001. **20**(6): p. 1477-82.
28. Sleeth, K.M., R.L. Robson, and G.L. Dianov, *Exchangeability of mammalian DNA ligases between base excision repair pathways.* Biochemistry, 2004. **43**(40): p. 12924-30.
29. Fortini, P. and E. Dogliotti, *Base damage and single-strand break repair: mechanisms and functional significance of short- and long-patch repair subpathways.* DNA Repair (Amst), 2007. **6**(4): p. 398-409.
30. Petermann, E., C. Keil, and S.L. Oei, *Roles of DNA ligase III and XRCC1 in regulating the switch between short patch and long patch BER.* DNA Repair (Amst), 2006. **5**(5): p. 544-55.
31. Klungland, A. and T. Lindahl, *Second pathway for completion of human DNA base excision-repair: reconstitution with purified proteins and requirement for DNase IV (FEN1).* EMBO J, 1997. **16**(11): p. 3341-8.
32. Otterlei, M., et al., *Post-replicative base excision repair in replication foci.* EMBO J, 1999. **18**(13): p. 3834-44.
33. Boldogh, I., et al., *hMYH cell cycle-dependent expression, subcellular localization and association with replication foci: evidence suggesting replication-coupled repair of adenine:8-oxoguanine mispairs.* Nucleic Acids Res, 2001. **29**(13): p. 2802-9.
34. Parker, A., et al., *Human homolog of the MutY repair protein (hMYH) physically interacts with proteins involved in long patch DNA base excision repair.* J Biol Chem, 2001. **276**(8): p. 5547-55.
35. Gu, Y., et al., *Human MutY homolog, a DNA glycosylase involved in base excision repair, physically and functionally interacts with mismatch repair*

proteins human MutS homolog 2/human MutS homolog 6. J Biol Chem, 2002. **277**(13): p. 11135-42.
36. Parlanti, E., et al., *Base excision repair of adenine/8-oxoguanine mispairs by an aphidicolin-sensitive DNA polymerase in human cell extracts.* Oncogene, 2002. **21**(34): p. 5204-12.
37. Dou, H., S. Mitra, and T.K. Hazra, *Repair of oxidized bases in DNA bubble structures by human DNA glycosylases NEIL1 and NEIL2.* J Biol Chem, 2003. **278**(50): p. 49679-84.
38. Dianov, G., et al., *Repair pathways for processing of 8-oxoguanine in DNA by mammalian cell extracts.* J Biol Chem, 1998. **273**(50): p. 33811-6.
39. Pascucci, B., et al., *Reconstitution of the base excision repair pathway for 7,8-dihydro-8-oxoguanine with purified human proteins.* Nucleic Acids Res, 2002. **30**(10): p. 2124-30.
40. Jiricny, J., *The multifaceted mismatch-repair system.* Nat Rev Mol Cell Biol, 2006. **7**(5): p. 335-46.
41. Modrich, P., *Mechanisms in eukaryotic mismatch repair.* J Biol Chem, 2006. **281**(41): p. 30305-9.
42. Arana, M.E. and T.A. Kunkel, *Mutator phenotypes due to DNA replication infidelity.* Semin Cancer Biol, 2010. **20**(5): p. 304-11.
43. Loeb, L.A. and R.J. Monnat, Jr., *DNA polymerases and human disease.* Nat Rev Genet, 2008. **9**(8): p. 594-604.
44. Jiricny, J., *Postreplicative mismatch repair.* Cold Spring Harb Perspect Biol, 2013. **5**(4): p. a012633.
45. Iyer, R.R., et al., *The MutSalpha-proliferating cell nuclear antigen interaction in human DNA mismatch repair.* J Biol Chem, 2008. **283**(19): p. 13310-9.
46. Masih, P.J., D. Kunnev, and T. Melendy, *Mismatch Repair proteins are recruited to replicating DNA through interaction with Proliferating Cell Nuclear Antigen (PCNA).* Nucleic Acids Res, 2008. **36**(1): p. 67-75.
47. Kleczkowska, H.E., et al., *hMSH3 and hMSH6 interact with PCNA and colocalize with it to replication foci.* Genes Dev, 2001. **15**(6): p. 724-36.
48. Lahue, R.S., K.G. Au, and P. Modrich, *DNA mismatch correction in a defined system.* Science, 1989. **245**(4914): p. 160-4.
49. Langle-Rouault, F., G. Maenhaut-Michel, and M. Radman, *GATC sequences, DNA nicks and the MutH function in Escherichia coli mismatch repair.* EMBO J, 1987. **6**(4): p. 1121-7.
50. Modrich, P., *Methyl-directed DNA mismatch correction.* J Biol Chem, 1989. **264**(12): p. 6597-600.
51. Mechanic, L.E., B.A. Frankel, and S.W. Matson, *Escherichia coli MutL loads DNA helicase II onto DNA.* J Biol Chem, 2000. **275**(49): p. 38337-46.
52. Dao, V. and P. Modrich, *Mismatch-, MutS-, MutL-, and helicase II-dependent unwinding from the single-strand break of an incised heteroduplex.* J Biol Chem, 1998. **273**(15): p. 9202-7.
53. Viswanathan, M., et al., *Redundant exonuclease involvement in Escherichia coli methyl-directed mismatch repair.* J Biol Chem, 2001. **276**(33): p. 31053-8.

54. Burdett, V., et al., *In vivo requirement for RecJ, ExoVII, ExoI, and ExoX in methyl-directed mismatch repair.* Proc Natl Acad Sci U S A, 2001. **98**(12): p. 6765-70.
55. Acharya, S., et al., *hMSH2 forms specific mispair-binding complexes with hMSH3 and hMSH6.* Proc Natl Acad Sci U S A, 1996. **93**(24): p. 13629-34.
56. Palombo, F., et al., *GTBP, a 160-kilodalton protein essential for mismatch-binding activity in human cells.* Science, 1995. **268**(5219): p. 1912-4.
57. de Wind, N., et al., *Inactivation of the mouse Msh2 gene results in mismatch repair deficiency, methylation tolerance, hyperrecombination, and predisposition to cancer.* Cell, 1995. **82**(2): p. 321-30.
58. de Wind, N., et al., *HNPCC-like cancer predisposition in mice through simultaneous loss of Msh3 and Msh6 mismatch-repair protein functions.* Nat Genet, 1999. **23**(3): p. 359-62.
59. Edelmann, W., et al., *The DNA mismatch repair genes Msh3 and Msh6 cooperate in intestinal tumor suppression.* Cancer Res, 2000. **60**(4): p. 803-7.
60. Raschle, M., et al., *Identification of hMutLbeta, a heterodimer of hMLH1 and hPMS1.* J Biol Chem, 1999. **274**(45): p. 32368-75.
61. Cannavo, E., et al., *Expression of the MutL homologue hMLH3 in human cells and its role in DNA mismatch repair.* Cancer Res, 2005. **65**(23): p. 10759-66.
62. Zhang, Y., et al., *Reconstitution of 5'-directed human mismatch repair in a purified system.* Cell, 2005. **122**(5): p. 693-705.
63. Constantin, N., et al., *Human mismatch repair: reconstitution of a nick-directed bidirectional reaction.* J Biol Chem, 2005. **280**(48): p. 39752-61.
64. Holmes, J., Jr., S. Clark, and P. Modrich, *Strand-specific mismatch correction in nuclear extracts of human and Drosophila melanogaster cell lines.* Proc Natl Acad Sci U S A, 1990. **87**(15): p. 5837-41.
65. Jiricny, J., *MutLalpha: at the cutting edge of mismatch repair.* Cell, 2006. **126**(2): p. 239-41.
66. Genschel, J. and P. Modrich, *Mechanism of 5'-directed excision in human mismatch repair.* Mol Cell, 2003. **12**(5): p. 1077-86.
67. Kadyrov, F.A., et al., *Endonucleolytic function of MutLalpha in human mismatch repair.* Cell, 2006. **126**(2): p. 297-308.
68. Pluciennik, A., et al., *PCNA function in the activation and strand direction of MutLalpha endonuclease in mismatch repair.* Proc Natl Acad Sci U S A, 2010. **107**(37): p. 16066-71.
69. Pena-Diaz, J. and J. Jiricny, *PCNA and MutLalpha: partners in crime in triplet repeat expansion?* Proc Natl Acad Sci U S A, 2010. **107**(38): p. 16409-10.
70. Nick McElhinny, S.A., et al., *Genome instability due to ribonucleotide incorporation into DNA.* Nat Chem Biol, 2010. **6**(10): p. 774-81.
71. Nick McElhinny, S.A., et al., *Abundant ribonucleotide incorporation into DNA by yeast replicative polymerases.* Proc Natl Acad Sci U S A, 2010. **107**(11): p. 4949-54.

72. Ghodgaonkar, M.M., et al., *Ribonucleotides misincorporated into DNA act as strand-discrimination signals in eukaryotic mismatch repair.* Mol Cell, 2013. **50**(3): p. 323-32.
73. Li, F., et al., *The histone mark H3K36me3 regulates human DNA mismatch repair through its interaction with MutSalpha.* Cell, 2013. **153**(3): p. 590-600.
74. Schopf, B., et al., *Interplay between mismatch repair and chromatin assembly.* Proc Natl Acad Sci U S A, 2012. **109**(6): p. 1895-900.
75. Malkov, V.A., et al., *Photocross-linking of the NH2-terminal region of Taq MutS protein to the major groove of a heteroduplex DNA.* J Biol Chem, 1997. **272**(38): p. 23811-7.
76. Lamers, M.H., et al., *The crystal structure of DNA mismatch repair protein MutS binding to a G x T mismatch.* Nature, 2000. **407**(6805): p. 711-7.
77. Obmolova, G., et al., *Crystal structures of mismatch repair protein MutS and its complex with a substrate DNA.* Nature, 2000. **407**(6805): p. 703-10.
78. Warren, J.J., et al., *Structure of the human MutSalpha DNA lesion recognition complex.* Mol Cell, 2007. **26**(4): p. 579-92.
79. Edelbrock, M.A., S. Kaliyaperumal, and K.J. Williams, *Structural, molecular and cellular functions of MSH2 and MSH6 during DNA mismatch repair, damage signaling and other noncanonical activities.* Mutat Res, 2013. **743-744**: p. 53-66.
80. Kaliyaperumal, S., S.M. Patrick, and K.J. Williams, *Phosphorylated hMSH6: DNA mismatch versus DNA damage recognition.* Mutat Res, 2011. **706**(1-2): p. 36-45.
81. Pleschke, J.M., et al., *Poly(ADP-ribose) binds to specific domains in DNA damage checkpoint proteins.* J Biol Chem, 2000. **275**(52): p. 40974-80.
82. Matsuoka, S., et al., *ATM and ATR substrate analysis reveals extensive protein networks responsive to DNA damage.* Science, 2007. **316**(5828): p. 1160-6.
83. Gu, L., et al., *ATP-dependent interaction of human mismatch repair proteins and dual role of PCNA in mismatch repair.* Nucleic Acids Res, 1998. **26**(5): p. 1173-8.
84. Lau, P.J. and R.D. Kolodner, *Transfer of the MSH2.MSH6 complex from proliferating cell nuclear antigen to mispaired bases in DNA.* J Biol Chem, 2003. **278**(1): p. 14-7.
85. Pena-Diaz, J. and J. Jiricny, *Mammalian mismatch repair: error-free or error-prone?* Trends Biochem Sci, 2012. **37**(5): p. 206-14.
86. Lipkin, S.M., et al., *Meiotic arrest and aneuploidy in MLH3-deficient mice.* Nat Genet, 2002. **31**(4): p. 385-90.
87. Nishant, K.T., A.J. Plys, and E. Alani, *A mutation in the putative MLH3 endonuclease domain confers a defect in both mismatch repair and meiosis in Saccharomyces cerevisiae.* Genetics, 2008. **179**(2): p. 747-55.
88. Baker, S.M., et al., *Male mice defective in the DNA mismatch repair gene PMS2 exhibit abnormal chromosome synapsis in meiosis.* Cell, 1995. **82**(2): p. 309-19.
89. Harfe, B.D. and S. Jinks-Robertson, *DNA mismatch repair and genetic instability.* Annu Rev Genet, 2000. **34**: p. 359-399.
90. Harfe, B.D. and S. Jinks-Robertson, *Mismatch repair proteins and mitotic genome stability.* Mutat Res, 2000. **451**(1-2): p. 151-67.

91. McMurray, C.T., *Hijacking of the mismatch repair system to cause CAG expansion and cell death in neurodegenerative disease.* DNA Repair (Amst), 2008. **7**(7): p. 1121-34.
92. Peng, M., et al., *The FANCJ/MutLalpha interaction is required for correction of the cross-link response in FA-J cells.* EMBO J, 2007. **26**(13): p. 3238-49.
93. Zhang, N., et al., *hMutSbeta is required for the recognition and uncoupling of psoralen interstrand cross-links in vitro.* Mol Cell Biol, 2002. **22**(7): p. 2388-97.
94. Pena-Diaz, J., et al., *Noncanonical mismatch repair as a source of genomic instability in human cells.* Mol Cell, 2012. **47**(5): p. 669-80.
95. Schanz, S., et al., *Interference of mismatch and base excision repair during the processing of adjacent U/G mispairs may play a key role in somatic hypermutation.* Proc Natl Acad Sci U S A, 2009. **106**(14): p. 5593-8.
96. Stavnezer, J. and C.E. Schrader, *Mismatch repair converts AID-instigated nicks to double-strand breaks for antibody class-switch recombination.* Trends Genet, 2006. **22**(1): p. 23-8.
97. Chahwan, R., et al., *The ATPase activity of MLH1 is required to orchestrate DNA double-strand breaks and end processing during class switch recombination.* J Exp Med, 2012. **209**(4): p. 671-8.
98. Gillet, L.C. and O.D. Scharer, *Molecular mechanisms of mammalian global genome nucleotide excision repair.* Chem Rev, 2006. **106**(2): p. 253-76.
99. Sancar, A., et al., *Molecular mechanisms of mammalian DNA repair and the DNA damage checkpoints.* Annu Rev Biochem, 2004. **73**: p. 39-85.
100. Lehmann, A.R., *The xeroderma pigmentosum group D (XPD) gene: one gene, two functions, three diseases.* Genes Dev, 2001. **15**(1): p. 15-23.
101. de Laat, W.L., N.G. Jaspers, and J.H. Hoeijmakers, *Molecular mechanism of nucleotide excision repair.* Genes Dev, 1999. **13**(7): p. 768-85.
102. Aboussekhra, A., et al., *Mammalian DNA nucleotide excision repair reconstituted with purified protein components.* Cell, 1995. **80**(6): p. 859-68.
103. Araujo, S.J., et al., *Nucleotide excision repair of DNA with recombinant human proteins: definition of the minimal set of factors, active forms of TFIIH, and modulation by CAK.* Genes Dev, 2000. **14**(3): p. 349-59.
104. Mu, D., et al., *Reconstitution of human DNA repair excision nuclease in a highly defined system.* J Biol Chem, 1995. **270**(6): p. 2415-8.
105. Hanawalt, P.C. and G. Spivak, *Transcription-coupled DNA repair: two decades of progress and surprises.* Nat Rev Mol Cell Biol, 2008. **9**(12): p. 958-70.
106. Huang, J.C., et al., *Human nucleotide excision nuclease removes thymine dimers from DNA by incising the 22nd phosphodiester bond 5' and the 6th phosphodiester bond 3' to the photodimer.* Proc Natl Acad Sci U S A, 1992. **89**(8): p. 3664-8.
107. Scharer, O.D., *Nucleotide excision repair in eukaryotes.* Cold Spring Harb Perspect Biol, 2013. **5**(10): p. a012609.

108. Chiruvella, K.K., Z. Liang, and T.E. Wilson, *Repair of double-strand breaks by end joining.* Cold Spring Harb Perspect Biol, 2013. **5**(5): p. a012757.
109. Jasin, M. and R. Rothstein, *Repair of strand breaks by homologous recombination.* Cold Spring Harb Perspect Biol, 2013. **5**(11): p. a012740.
110. Sartori, A.A., et al., *Human CtIP promotes DNA end resection.* Nature, 2007. **450**(7169): p. 509-14.
111. Garcia, V., et al., *Bidirectional resection of DNA double-strand breaks by Mre11 and Exo1.* Nature, 2011. **479**(7372): p. 241-4.
112. Moynahan, M.E., et al., *Brca1 controls homology-directed DNA repair.* Mol Cell, 1999. **4**(4): p. 511-8.
113. Zhong, Q., et al., *Association of BRCA1 with the hRad50-hMre11-p95 complex and the DNA damage response.* Science, 1999. **285**(5428): p. 747-50.
114. Yu, X., et al., *The C-terminal (BRCT) domains of BRCA1 interact in vivo with CtIP, a protein implicated in the CtBP pathway of transcriptional repression.* J Biol Chem, 1998. **273**(39): p. 25388-92.
115. San Filippo, J., P. Sung, and H. Klein, *Mechanism of eukaryotic homologous recombination.* Annu Rev Biochem, 2008. **77**: p. 229-57.
116. Yuan, S.S., et al., *BRCA2 is required for ionizing radiation-induced assembly of Rad51 complex in vivo.* Cancer Res, 1999. **59**(15): p. 3547-51.
117. Tarsounas, M., D. Davies, and S.C. West, *BRCA2-dependent and independent formation of RAD51 nuclear foci.* Oncogene, 2003. **22**(8): p. 1115-23.
118. Liu, Y., et al., *RAD51C is required for Holliday junction processing in mammalian cells.* Science, 2004. **303**(5655): p. 243-6.
119. Ristic, D., et al., *Human Rad51 filaments on double- and single-stranded DNA: correlating regular and irregular forms with recombination function.* Nucleic Acids Res, 2005. **33**(10): p. 3292-302.
120. Chen, X.B., et al., *Human Mus81-associated endonuclease cleaves Holliday junctions in vitro.* Mol Cell, 2001. **8**(5): p. 1117-27.
121. Boddy, M.N., et al., *Mus81-Eme1 are essential components of a Holliday junction resolvase.* Cell, 2001. **107**(4): p. 537-48.
122. Ogrunc, M. and A. Sancar, *Identification and characterization of human MUS81-MMS4 structure-specific endonuclease.* J Biol Chem, 2003. **278**(24): p. 21715-20.
123. Stark, J.M., et al., *Genetic steps of mammalian homologous repair with distinct mutagenic consequences.* Mol Cell Biol, 2004. **24**(21): p. 9305-16.
124. Tutt, A., et al., *Mutation in Brca2 stimulates error-prone homology-directed repair of DNA double-strand breaks occurring between repeated sequences.* EMBO J, 2001. **20**(17): p. 4704-16.
125. Gottlieb, T.M. and S.P. Jackson, *The DNA-dependent protein kinase: requirement for DNA ends and association with Ku antigen.* Cell, 1993. **72**(1): p. 131-42.
126. Chan, D.W., et al., *Autophosphorylation of the DNA-dependent protein kinase catalytic subunit is required for rejoining of DNA double-strand breaks.* Genes Dev, 2002. **16**(18): p. 2333-8.

127. Wang, Y.G., et al., *Phosphorylation and regulation of DNA ligase IV stability by DNA-dependent protein kinase.* J Biol Chem, 2004. **279**(36): p. 37282-90.
128. Chan, D.W., et al., *DNA-dependent protein kinase phosphorylation sites in Ku 70/80 heterodimer.* Biochemistry, 1999. **38**(6): p. 1819-28.
129. Lees-Miller, S.P. and K. Meek, *Repair of DNA double strand breaks by non-homologous end joining.* Biochimie, 2003. **85**(11): p. 1161-73.
130. Boulton, S.J. and S.P. Jackson, *Saccharomyces cerevisiae Ku70 potentiates illegitimate DNA double-strand break repair and serves as a barrier to error-prone DNA repair pathways.* EMBO J, 1996. **15**(18): p. 5093-103.
131. Decottignies, A., *Alternative end-joining mechanisms: a historical perspective.* Front Genet, 2013. **4**: p. 48.
132. Pierce, A.J., et al., *Ku DNA end-binding protein modulates homologous repair of double-strand breaks in mammalian cells.* Genes Dev, 2001. **15**(24): p. 3237-42.
133. Allen, C., et al., *DNA-dependent protein kinase suppresses double-strand break-induced and spontaneous homologous recombination.* Proc Natl Acad Sci U S A, 2002. **99**(6): p. 3758-63.
134. Zimmermann, M., et al., *53BP1 regulates DSB repair using Rif1 to control 5' end resection.* Science, 2013. **339**(6120): p. 700-4.
135. Di Virgilio, M., et al., *Rif1 prevents resection of DNA breaks and promotes immunoglobulin class switching.* Science, 2013. **339**(6120): p. 711-5.
136. Chapman, J.R., et al., *RIF1 is essential for 53BP1-dependent nonhomologous end joining and suppression of DNA double-strand break resection.* Mol Cell, 2013. **49**(5): p. 858-71.
137. Escribano-Diaz, C., et al., *A cell cycle-dependent regulatory circuit composed of 53BP1-RIF1 and BRCA1-CtIP controls DNA repair pathway choice.* Mol Cell, 2013. **49**(5): p. 872-83.
138. Xie, A., et al., *Distinct roles of chromatin-associated proteins MDC1 and 53BP1 in mammalian double-strand break repair.* Mol Cell, 2007. **28**(6): p. 1045-57.
139. Cao, L., et al., *A selective requirement for 53BP1 in the biological response to genomic instability induced by Brca1 deficiency.* Mol Cell, 2009. **35**(4): p. 534-41.
140. Pichierri, P., A. Franchitto, and F. Palitti, *Predisposition to cancer and radio sensitivity.* Genetics and Molecular Biology, 2000. **23**(4): p. 1101-1105.
141. Stone, M.P., et al., *Interstrand DNA cross-links induced by alpha,beta-unsaturated aldehydes derived from lipid peroxidation and environmental sources.* Acc Chem Res, 2008. **41**(7): p. 793-804.
142. Kim, J.M., et al., *Cell cycle-dependent chromatin loading of the Fanconi anemia core complex by FANCM/FAAP24.* Blood, 2008. **111**(10): p. 5215-22.
143. Longerich, S., et al., *FANCI binds branched DNA and is monoubiquitinated by UBE2T-FANCL.* J Biol Chem, 2009. **284**(35): p. 23182-6.

144. Smogorzewska, A., et al., *Identification of the FANCI protein, a monoubiquitinated FANCD2 paralog required for DNA repair.* Cell, 2007. **129**(2): p. 289-301.
145. Kratz, K., et al., *Deficiency of FANCD2-associated nuclease KIAA1018/FAN1 sensitizes cells to interstrand crosslinking agents.* Cell, 2010. **142**(1): p. 77-88.
146. Deans, A.J. and S.C. West, *DNA interstrand crosslink repair and cancer.* Nat Rev Cancer, 2011. **11**(7): p. 467-80.
147. Xia, F., et al., *Deficiency of human BRCA2 leads to impaired homologous recombination but maintains normal nonhomologous end joining.* Proc Natl Acad Sci U S A, 2001. **98**(15): p. 8644-9.
148. Howlett, N.G., et al., *Biallelic inactivation of BRCA2 in Fanconi anemia.* Science, 2002. **297**(5581): p. 606-9.
149. West, S.C., *Molecular views of recombination proteins and their control.* Nat Rev Mol Cell Biol, 2003. **4**(6): p. 435-45.
150. Garcia-Higuera, I., et al., *Interaction of the Fanconi anemia proteins and BRCA1 in a common pathway.* Mol Cell, 2001. **7**(2): p. 249-62.
151. Biertumpfel, C., et al., *Structure and mechanism of human DNA polymerase eta.* Nature, 2010. **465**(7301): p. 1044-8.
152. Silverstein, T.D., et al., *Structural basis for the suppression of skin cancers by DNA polymerase eta.* Nature, 2010. **465**(7301): p. 1039-43.
153. Masutani, C., et al., *The XPV (xeroderma pigmentosum variant) gene encodes human DNA polymerase eta.* Nature, 1999. **399**(6737): p. 700-4.
154. Cleaver, J.E., *Xeroderma pigmentosum: variants with normal DNA repair and normal sensitivity to ultraviolet light.* J Invest Dermatol, 1972. **58**(3): p. 124-8.
155. Hoege, C., et al., *RAD6-dependent DNA repair is linked to modification of PCNA by ubiquitin and SUMO.* Nature, 2002. **419**(6903): p. 135-41.
156. Bienko, M., et al., *Ubiquitin-binding domains in Y-family polymerases regulate translesion synthesis.* Science, 2005. **310**(5755): p. 1821-4.
157. Kannouche, P.L., J. Wing, and A.R. Lehmann, *Interaction of human DNA polymerase eta with monoubiquitinated PCNA: a possible mechanism for the polymerase switch in response to DNA damage.* Mol Cell, 2004. **14**(4): p. 491-500.
158. Sabbioneda, S., et al., *Yeast Rev1 is cell cycle regulated, phosphorylated in response to DNA damage and its binding to chromosomes is dependent upon MEC1.* DNA Repair (Amst), 2007. **6**(1): p. 121-7.
159. Gohler, T., et al., *ATR-mediated phosphorylation of DNA polymerase eta is needed for efficient recovery from UV damage.* J Cell Biol, 2011. **192**(2): p. 219-27.
160. Bienko, M., et al., *Regulation of translesion synthesis DNA polymerase eta by monoubiquitination.* Mol Cell, 2010. **37**(3): p. 396-407.
161. Wimmer, U., et al., *Control of DNA polymerase lambda stability by phosphorylation and ubiquitination during the cell cycle.* EMBO Rep, 2008. **9**(10): p. 1027-33.
162. Jung, Y.S., G. Liu, and X. Chen, *Pirh2 E3 ubiquitin ligase targets DNA polymerase eta for 20S proteasomal degradation.* Mol Cell Biol, 2010. **30**(4): p. 1041-8.

163. Chance, B., H. Sies, and A. Boveris, *Hydroperoxide metabolism in mammalian organs.* Physiol Rev, 1979. **59**(3): p. 527-605.
164. Monsalve, M., et al., *Mitochondrial dysfunction in human pathologies.* Front Biosci, 2007. **12**: p. 1131-53.
165. Inoue, M., et al., *Mitochondrial generation of reactive oxygen species and its role in aerobic life.* Curr Med Chem, 2003. **10**(23): p. 2495-505.
166. Jackson, A.L. and L.A. Loeb, *The contribution of endogenous sources of DNA damage to the multiple mutations in cancer.* Mutat Res, 2001. **477**(1-2): p. 7-21.
167. Valko, M., et al., *Free radicals, metals and antioxidants in oxidative stress-induced cancer.* Chem Biol Interact, 2006. **160**(1): p. 1-40.
168. Cooke, M.S., et al., *Oxidative DNA damage: mechanisms, mutation, and disease.* FASEB J, 2003. **17**(10): p. 1195-214.
169. De Bont, R. and N. van Larebeke, *Endogenous DNA damage in humans: a review of quantitative data.* Mutagenesis, 2004. **19**(3): p. 169-85.
170. van Loon, B., E. Markkanen, and U. Hubscher, *Oxygen as a friend and enemy: How to combat the mutational potential of 8-oxo-guanine.* DNA Repair (Amst), 2010. **9**(6): p. 604-16.
171. Gough, D.R. and T.G. Cotter, *Hydrogen peroxide: a Jekyll and Hyde signalling molecule.* Cell Death Dis, 2011. **2**: p. e213.
172. Klaunig, J.E. and L.M. Kamendulis, *The role of oxidative stress in carcinogenesis.* Annu Rev Pharmacol Toxicol, 2004. **44**: p. 239-67.
173. Carocho, M. and I.C. Ferreira, *A review on antioxidants, prooxidants and related controversy: natural and synthetic compounds, screening and analysis methodologies and future perspectives.* Food Chem Toxicol, 2013. **51**: p. 15-25.
174. Boveris, A., et al., *Mitochondrial metabolic states regulate nitric oxide and hydrogen peroxide diffusion to the cytosol.* Biochim Biophys Acta, 2006. **1757**(5-6): p. 535-42.
175. Neeley, W.L. and J.M. Essigmann, *Mechanisms of formation, genotoxicity, and mutation of guanine oxidation products.* Chem Res Toxicol, 2006. **19**(4): p. 491-505.
176. Burrows, C.J. and J.G. Muller, *Oxidative Nucleobase Modifications Leading to Strand Scission.* Chem Rev, 1998. **98**(3): p. 1109-1152.
177. Gedik, C.M., A. Collins, and Escodd, *Establishing the background level of base oxidation in human lymphocyte DNA: results of an interlaboratory validation study.* FASEB J, 2005. **19**(1): p. 82-4.
178. Collins, A.R., *Oxidative DNA damage, antioxidants, and cancer.* Bioessays, 1999. **21**(3): p. 238-46.
179. Shibutani, S., M. Takeshita, and A.P. Grollman, *Insertion of specific bases during DNA synthesis past the oxidation-damaged base 8-oxodG.* Nature, 1991. **349**(6308): p. 431-4.
180. Lowe, L.G. and F.P. Guengerich, *Steady-state and pre-steady-state kinetic analysis of dNTP insertion opposite 8-oxo-7,8-dihydroguanine by Escherichia coli polymerases I exo- and II exo.* Biochemistry, 1996. **35**(30): p. 9840-9.
181. Furge, L.L. and F.P. Guengerich, *Analysis of nucleotide insertion and extension at 8-oxo-7,8-dihydroguanine by replicative T7 polymerase exo-*

and human immunodeficiency virus-1 reverse transcriptase using steady-state and pre-steady-state kinetics. Biochemistry, 1997. **36**(21): p. 6475-87.

182. Einolf, H.J. and F.P. Guengerich, *Fidelity of nucleotide insertion at 8-oxo-7,8-dihydroguanine by mammalian DNA polymerase delta. Steady-state and pre-steady-state kinetic analysis.* J Biol Chem, 2001. **276**(6): p. 3764-71.
183. Avkin, S. and Z. Livneh, *Efficiency, specificity and DNA polymerase-dependence of translesion replication across the oxidative DNA lesion 8-oxoguanine in human cells.* Mutat Res, 2002. **510**(1-2): p. 81-90.
184. Hsu, G.W., et al., *Error-prone replication of oxidatively damaged DNA by a high-fidelity DNA polymerase.* Nature, 2004. **431**(7005): p. 217-21.
185. Zhuang, Z., et al., *Regulation of polymerase exchange between Poleta and Poldelta by monoubiquitination of PCNA and the movement of DNA polymerase holoenzyme.* Proc Natl Acad Sci U S A, 2008. **105**(14): p. 5361-6.
186. Haracska, L., et al., *Efficient and accurate replication in the presence of 7,8-dihydro-8-oxoguanine by DNA polymerase eta.* Nat Genet, 2000. **25**(4): p. 458-61.
187. Lee, D.H. and G.P. Pfeifer, *Translesion synthesis of 7,8-dihydro-8-oxo-2'-deoxyguanosine by DNA polymerase eta in vivo.* Mutat Res, 2008. **641**(1-2): p. 19-26.
188. McCulloch, S.D., et al., *The efficiency and fidelity of 8-oxo-guanine bypass by DNA polymerases delta and eta.* Nucleic Acids Res, 2009. **37**(9): p. 2830-40.
189. Maga, G., et al., *8-oxo-guanine bypass by human DNA polymerases in the presence of auxiliary proteins.* Nature, 2007. **447**(7144): p. 606-8.
190. Markkanen, E., et al., *A switch between DNA polymerases delta and lambda promotes error-free bypass of 8-oxo-G lesions.* Proc Natl Acad Sci U S A, 2012. **109**(50): p. 20401-6.
191. Al-Tassan, N., et al., *Inherited variants of MYH associated with somatic G:C-->T:A mutations in colorectal tumors.* Nat Genet, 2002. **30**(2): p. 227-32.
192. Jones, S., et al., *Biallelic germline mutations in MYH predispose to multiple colorectal adenoma and somatic G:C-->T:A mutations.* Hum Mol Genet, 2002. **11**(23): p. 2961-7.
193. Sieber, O.M., et al., *Multiple colorectal adenomas, classic adenomatous polyposis, and germ-line mutations in MYH.* N Engl J Med, 2003. **348**(9): p. 791-9.
194. Nghiem, Y., et al., *The mutY gene: a mutator locus in Escherichia coli that generates G.C----T.A transversions.* Proc Natl Acad Sci U S A, 1988. **85**(8): p. 2709-13.
195. Michaels, M.L. and J.H. Miller, *The GO system protects organisms from the mutagenic effect of the spontaneous lesion 8-hydroxyguanine (7,8-dihydro-8-oxoguanine).* J Bacteriol, 1992. **174**(20): p. 6321-5.
196. Fortini, P., et al., *8-Oxoguanine DNA damage: at the crossroad of alternative repair pathways.* Mutat Res, 2003. **531**(1-2): p. 127-39.

197. Sakumi, K., et al., *Cloning and expression of cDNA for a human enzyme that hydrolyzes 8-oxo-dGTP, a mutagenic substrate for DNA synthesis.* J Biol Chem, 1993. **268**(31): p. 23524-30.
198. Fortini, P., et al., *The type of DNA glycosylase determines the base excision repair pathway in mammalian cells.* J Biol Chem, 1999. **274**(21): p. 15230-6.
199. McAuley-Hecht, K.E., et al., *Crystal structure of a DNA duplex containing 8-hydroxydeoxyguanine-adenine base pairs.* Biochemistry, 1994. **33**(34): p. 10266-70.
200. van Loon, B. and U. Hubscher, *An 8-oxo-guanine repair pathway coordinated by MUTYH glycosylase and DNA polymerase lambda.* Proc Natl Acad Sci U S A, 2009. **106**(43): p. 18201-6.
201. Sobol, R.W., et al., *Requirement of mammalian DNA polymerase-beta in base-excision repair.* Nature, 1996. **379**(6561): p. 183-6.
202. Dianov, G.L., et al., *Role of DNA polymerase beta in the excision step of long patch mammalian base excision repair.* J Biol Chem, 1999. **274**(20): p. 13741-3.
203. Allinson, S.L., Dianova, II, and G.L. Dianov, *DNA polymerase beta is the major dRP lyase involved in repair of oxidative base lesions in DNA by mammalian cell extracts.* EMBO J, 2001. **20**(23): p. 6919-26.
204. Stucki, M., et al., *Mammalian base excision repair by DNA polymerases delta and epsilon.* Oncogene, 1998. **17**(7): p. 835-43.
205. Maga, G., et al., *Replication protein A and proliferating cell nuclear antigen coordinate DNA polymerase selection in 8-oxo-guanine repair.* Proc Natl Acad Sci U S A, 2008. **105**(52): p. 20689-94.
206. Markkanen, E., J. Dorn, and U. Hubscher, *MUTYH DNA glycosylase: the rationale for removing undamaged bases from the DNA.* Front Genet, 2013. **4**: p. 18.
207. Hirano, S., et al., *Mutator phenotype of MUTYH-null mouse embryonic stem cells.* J Biol Chem, 2003. **278**(40): p. 38121-4.
208. Russo, M.T., et al., *Role of MUTYH and MSH2 in the control of oxidative DNA damage, genetic instability, and tumorigenesis.* Cancer Res, 2009. **69**(10): p. 4372-9.
209. Russo, M.T., et al., *Accumulation of the oxidative base lesion 8-hydroxyguanine in DNA of tumor-prone mice defective in both the Myh and Ogg1 DNA glycosylases.* Cancer Res, 2004. **64**(13): p. 4411-4.
210. Sakamoto, K., et al., *MUTYH-null mice are susceptible to spontaneous and oxidative stress induced intestinal tumorigenesis.* Cancer Res, 2007. **67**(14): p. 6599-604.
211. Cheadle, J.P. and J.R. Sampson, *MUTYH-associated polyposis--from defect in base excision repair to clinical genetic testing.* DNA Repair (Amst), 2007. **6**(3): p. 274-9.
212. Aretz, S., et al., *MUTYH-associated polyposis (MAP): evidence for the origin of the common European mutations p.Tyr179Cys and p.Gly396Asp by founder events.* Eur J Hum Genet, 2013.
213. Nielsen, M., et al., *MUTYH-associated polyposis (MAP).* Crit Rev Oncol Hematol, 2011. **79**(1): p. 1-16.

214. Bai, H., et al., *Functional characterization of two human MutY homolog (hMYH) missense mutations (R227W and V232F) that lie within the putative hMSH6 binding domain and are associated with hMYH polyposis.* Nucleic Acids Res, 2005. **33**(2): p. 597-604.
215. Bai, H., et al., *Functional characterization of human MutY homolog (hMYH) missense mutation (R231L) that is linked with hMYH-associated polyposis.* Cancer Lett, 2007. **250**(1): p. 74-81.
216. Ruggieri, V., et al., *Loss of MUTYH function in human cells leads to accumulation of oxidative damage and genetic instability.* Oncogene, 2013. **32**(38): p. 4500-8.
217. Molatore, S., et al., *MUTYH mutations associated with familial adenomatous polyposis: functional characterization by a mammalian cell-based assay.* Hum Mutat, 2010. **31**(2): p. 159-66.
218. Grasso, F., et al., *Genetic instability in lymphoblastoid cell lines expressing biallelic and monoallelic variants in the human MUTYH gene.* Hum Mol Genet, 2014.
219. O'Shea, A.M., et al., *Pathological features of colorectal carcinomas in MYH-associated polyposis.* Histopathology, 2008. **53**(2): p. 184-94.
220. Kambara, T., et al., *Role of inherited defects of MYH in the development of sporadic colorectal cancer.* Genes Chromosomes Cancer, 2004. **40**(1): p. 1-9.
221. Colebatch, A., et al., *The role of MYH and microsatellite instability in the development of sporadic colorectal cancer.* Br J Cancer, 2006. **95**(9): p. 1239-43.
222. Lefevre, J.H., et al., *MYH biallelic mutation can inactivate the two genetic pathways of colorectal cancer by APC or MLH1 transversions.* Fam Cancer, 2010. **9**(4): p. 589-94.
223. Cleary, S.P., et al., *Germline MutY human homologue mutations and colorectal cancer: a multisite case-control study.* Gastroenterology, 2009. **136**(4): p. 1251-60.
224. Morak, M., et al., *Biallelic MUTYH mutations can mimic Lynch syndrome.* Eur J Hum Genet, 2014.
225. van Puijenbroek, M., et al., *The natural history of a combined defect in MSH6 and MUTYH in a HNPCC family.* Fam Cancer, 2007. **6**(1): p. 43-51.
226. Gu, Y. and A.L. Lu, *Differential DNA recognition and glycosylase activity of the native human MutY homolog (hMYH) and recombinant hMYH expressed in bacteria.* Nucleic Acids Res, 2001. **29**(12): p. 2666-74.
227. Kundu, S., et al., *Ser 524 is a phosphorylation site in MUTYH and Ser 524 mutations alter 8-oxoguanine (OG): a mismatch recognition.* DNA Repair (Amst), 2010. **9**(10): p. 1026-37.
228. Parker, A.R., et al., *Defective human MutY phosphorylation exists in colorectal cancer cell lines with wild-type MutY alleles.* J Biol Chem, 2003. **278**(48): p. 47937-45.
229. Dorn, J., et al., *Regulation of Human MutYH DNA Glycosylase by the E3 Ubiquitin Ligase Mule.* J Biol Chem, 2014. **289**(10): p. 7049-58.
230. van der Kemp, P.A., et al., *Cloning and expression in Escherichia coli of the OGG1 gene of Saccharomyces cerevisiae, which codes for a DNA glycosylase that excises 7,8-dihydro-8-oxoguanine and 2,6-diamino-4-*

hydroxy-5-N-methylformamidopyrimidine. Proc Natl Acad Sci U S A, 1996. **93**(11): p. 5197-202.

231. Nash, H.M., et al., *Cloning of a yeast 8-oxoguanine DNA glycosylase reveals the existence of a base-excision DNA-repair protein superfamily.* Curr Biol, 1996. **6**(8): p. 968-80.
232. Lu, R., H.M. Nash, and G.L. Verdine, *A mammalian DNA repair enzyme that excises oxidatively damaged guanines maps to a locus frequently lost in lung cancer.* Curr Biol, 1997. **7**(6): p. 397-407.
233. Radicella, J.P., et al., *Cloning and characterization of hOGG1, a human homolog of the OGG1 gene of Saccharomyces cerevisiae.* Proc Natl Acad Sci U S A, 1997. **94**(15): p. 8010-5.
234. Denver, D.R., S.L. Swenson, and M. Lynch, *An evolutionary analysis of the helix-hairpin-helix superfamily of DNA repair glycosylases.* Mol Biol Evol, 2003. **20**(10): p. 1603-11.
235. Karahalil, B., et al., *Substrate specificity of the Ogg1 protein of Saccharomyces cerevisiae: excision of guanine lesions produced in DNA by ionizing radiation- or hydrogen peroxide/metal ion-generated free radicals.* Nucleic Acids Res, 1998. **26**(5): p. 1228-33.
236. Dherin, C., et al., *Excision of oxidatively damaged DNA bases by the human alpha-hOgg1 protein and the polymorphic alpha-hOgg1(Ser326Cys) protein which is frequently found in human populations.* Nucleic Acids Res, 1999. **27**(20): p. 4001-7.
237. Waters, T.R., et al., *Human thymine DNA glycosylase binds to apurinic sites in DNA but is displaced by human apurinic endonuclease 1.* J Biol Chem, 1999. **274**(1): p. 67-74.
238. Pope, M.A., S.L. Porello, and S.S. David, *Escherichia coli apurinic-apyrimidinic endonucleases enhance the turnover of the adenine glycosylase MutY with G:A substrates.* J Biol Chem, 2002. **277**(25): p. 22605-15.
239. Parikh, S.S., et al., *Base excision repair initiation revealed by crystal structures and binding kinetics of human uracil-DNA glycosylase with DNA.* EMBO J, 1998. **17**(17): p. 5214-26.
240. Hill, J.W., et al., *Stimulation of human 8-oxoguanine-DNA glycosylase by AP-endonuclease: potential coordination of the initial steps in base excision repair.* Nucleic Acids Res, 2001. **29**(2): p. 430-8.
241. Yang, H., et al., *Enhanced activity of adenine-DNA glycosylase (Myh) by apurinic/apyrimidinic endonuclease (Ape1) in mammalian base excision repair of an A/GO mismatch.* Nucleic Acids Res, 2001. **29**(3): p. 743-52.
242. Zharkov, D.O., et al., *Substrate specificity and reaction mechanism of murine 8-oxoguanine-DNA glycosylase.* J Biol Chem, 2000. **275**(37): p. 28607-17.
243. Hu, J., et al., *Phosphorylation of human oxoguanine DNA glycosylase (alpha-OGG1) modulates its function.* Nucleic Acids Res, 2005. **33**(10): p. 3271-82.
244. Dantzer, F., et al., *Human OGG1 undergoes serine phosphorylation and associates with the nuclear matrix and mitotic chromatin in vivo.* Nucleic Acids Res, 2002. **30**(11): p. 2349-57.

245. Klungland, A., et al., *Accumulation of premutagenic DNA lesions in mice defective in removal of oxidative base damage.* Proc Natl Acad Sci U S A, 1999. **96**(23): p. 13300-5.
246. Colussi, C., et al., *The mammalian mismatch repair pathway removes DNA 8-oxodGMP incorporated from the oxidized dNTP pool.* Curr Biol, 2002. **12**(11): p. 912-8.
247. Janik, J., et al., *8-Oxoguanine incision activity is impaired in lung tissues of NSCLC patients with the polymorphism of OGG1 and XRCC1 genes.* Mutat Res, 2011. **709-710**: p. 21-31.
248. Naylor, S.L., et al., *Loss of heterozygosity of chromosome 3p markers in small-cell lung cancer.* Nature, 1987. **329**(6138): p. 451-4.
249. Chevillard, S., et al., *Mutations in OGG1, a gene involved in the repair of oxidative DNA damage, are found in human lung and kidney tumours.* Oncogene, 1998. **16**(23): p. 3083-6.
250. Kohno, T., et al., *Genetic polymorphisms and alternative splicing of the hOGG1 gene, that is involved in the repair of 8-hydroxyguanine in damaged DNA.* Oncogene, 1998. **16**(25): p. 3219-25.
251. Audebert, M., et al., *Alterations of the DNA repair gene OGG1 in human clear cell carcinomas of the kidney.* Cancer Res, 2000. **60**(17): p. 4740-4.
252. Fujikawa, K., et al., *The oxidized forms of dATP are substrates for the human MutT homologue, the hMTH1 protein.* J Biol Chem, 1999. **274**(26): p. 18201-5.
253. Nakabeppu, Y., *Molecular genetics and structural biology of human MutT homolog, MTH1.* Mutat Res, 2001. **477**(1-2): p. 59-70.
254. Kang, D., et al., *Intracellular localization of 8-oxo-dGTPase in human cells, with special reference to the role of the enzyme in mitochondria.* J Biol Chem, 1995. **270**(24): p. 14659-65.
255. Maki, H. and M. Sekiguchi, *MutT protein specifically hydrolyses a potent mutagenic substrate for DNA synthesis.* Nature, 1992. **355**(6357): p. 273-5.
256. Gad, H., et al., *MTH1 inhibition eradicates cancer by preventing sanitation of the dNTP pool.* Nature, 2014. **508**(7495): p. 215-21.
257. Huber, K.V., et al., *Stereospecific targeting of MTH1 by (S)-crizotinib as an anticancer strategy.* Nature, 2014. **508**(7495): p. 222-7.
258. Earley, M.C. and G.F. Crouse, *The role of mismatch repair in the prevention of base pair mutations in Saccharomyces cerevisiae.* Proc Natl Acad Sci U S A, 1998. **95**(26): p. 15487-91.
259. Ni, T.T., G.T. Marsischky, and R.D. Kolodner, *MSH2 and MSH6 are required for removal of adenine misincorporated opposite 8-oxo-guanine in S. cerevisiae.* Mol Cell, 1999. **4**(3): p. 439-44.
260. Chang, D.K., et al., *Effect of H(2)O(2) on cell cycle and survival in DNA mismatch repair-deficient and -proficient cell lines.* Cancer Lett, 2003. **195**(2): p. 243-51.
261. Russo, M.T., et al., *The oxidized deoxynucleoside triphosphate pool is a significant contributor to genetic instability in mismatch repair-deficient cells.* Mol Cell Biol, 2004. **24**(1): p. 465-74.
262. Larson, E.D., K. Iams, and J.T. Drummond, *Strand-specific processing of 8-oxoguanine by the human mismatch repair pathway: inefficient removal of 8-oxoguanine paired with adenine or cytosine.* DNA Repair (Amst), 2003. **2**(11): p. 1199-210.

263. Macpherson, P., et al., *8-oxoguanine incorporation into DNA repeats in vitro and mismatch recognition by MutSalpha.* Nucleic Acids Res, 2005. **33**(16): p. 5094-105.
264. Mazurek, A., M. Berardini, and R. Fishel, *Activation of human MutS homologs by 8-oxo-guanine DNA damage.* J Biol Chem, 2002. **277**(10): p. 8260-6.
265. Zlatanou, A., et al., *The hMsh2-hMsh6 complex acts in concert with monoubiquitinated PCNA and Pol eta in response to oxidative DNA damage in human cells.* Mol Cell, 2011. **43**(4): p. 649-62.
266. Niessen, R.C., et al., *MUTYH and the mismatch repair system: partners in crime?* Hum Genet, 2006. **119**(1-2): p. 206-11.
267. Lynch, H.T., et al., *Review of the Lynch syndrome: history, molecular genetics, screening, differential diagnosis, and medicolegal ramifications.* Clin Genet, 2009. **76**(1): p. 1-18.
268. Peltomaki, P., *Role of DNA mismatch repair defects in the pathogenesis of human cancer.* J Clin Oncol, 2003. **21**(6): p. 1174-9.
269. Papadopoulos, N. and A. Lindblom, *Molecular basis of HNPCC: mutations of MMR genes.* Hum Mutat, 1997. **10**(2): p. 89-99.
270. Bronner, C.E., et al., *Mutation in the DNA mismatch repair gene homologue hMLH1 is associated with hereditary non-polyposis colon cancer.* Nature, 1994. **368**(6468): p. 258-61.
271. Li, G.M., *Mechanisms and functions of DNA mismatch repair.* Cell Res, 2008. **18**(1): p. 85-98.
272. Fink, D., S. Aebi, and S.B. Howell, *The role of DNA mismatch repair in drug resistance.* Clin Cancer Res, 1998. **4**(1): p. 1-6.
273. Beranek, D.T., *Distribution of methyl and ethyl adducts following alkylation with monofunctional alkylating agents.* Mutat Res, 1990. **231**(1): p. 11-30.
274. Duckett, D.R., et al., *Human MutSalpha recognizes damaged DNA base pairs containing O6-methylguanine, O4-methylthymine, or the cisplatin-d(GpG) adduct.* Proc Natl Acad Sci U S A, 1996. **93**(13): p. 6443-7.
275. Karran, P., *Mechanisms of tolerance to DNA damaging therapeutic drugs.* Carcinogenesis, 2001. **22**(12): p. 1931-7.
276. Curtin, N.J., et al., *Novel poly(ADP-ribose) polymerase-1 inhibitor, AG14361, restores sensitivity to temozolomide in mismatch repair-deficient cells.* Clin Cancer Res, 2004. **10**(3): p. 881-9.
277. Papouli, E., P. Cejka, and J. Jiricny, *Dependence of the cytotoxicity of DNA-damaging agents on the mismatch repair status of human cells.* Cancer Res, 2004. **64**(10): p. 3391-4.
278. McNeill, D.R., et al., *Impairment of APE1 function enhances cellular sensitivity to clinically relevant alkylators and antimetabolites.* Mol Cancer Res, 2009. **7**(6): p. 897-906.
279. Aebi, S., et al., *Loss of DNA mismatch repair in acquired resistance to cisplatin.* Cancer Res, 1996. **56**(13): p. 3087-90.
280. Fink, D., et al., *The role of DNA mismatch repair in platinum drug resistance.* Cancer Res, 1996. **56**(21): p. 4881-6.

281. Fiumicino, S., et al., *Sensitivity to DNA cross-linking chemotherapeutic agents in mismatch repair-defective cells in vitro and in xenografts.* Int J Cancer, 2000. **85**(4): p. 590-6.
282. Wu, Q., et al., *Mismatch repair participates in error-free processing of DNA interstrand crosslinks in human cells.* EMBO Rep, 2005. **6**(6): p. 551-7.
283. Aquilina, G., et al., *N-(2-chloroethyl)-N'-cyclohexyl-N-nitrosourea sensitivity in mismatch repair-defective human cells.* Cancer Res, 1998. **58**(1): p. 135-41.
284. Martin, S.A., et al., *Methotrexate induces oxidative DNA damage and is selectively lethal to tumour cells with defects in the DNA mismatch repair gene MSH2.* EMBO Mol Med, 2009. **1**(6-7): p. 323-37.
285. Martin, S.A., et al., *DNA polymerases as potential therapeutic targets for cancers deficient in the DNA mismatch repair proteins MSH2 or MLH1.* Cancer Cell, 2010. **17**(3): p. 235-48.
286. Martin, S.A., et al., *Parallel high-throughput RNA interference screens identify PINK1 as a potential therapeutic target for the treatment of DNA mismatch repair-deficient cancers.* Cancer Res, 2011. **71**(5): p. 1836-48.
287. Pridgeon, J.W., et al., *PINK1 protects against oxidative stress by phosphorylating mitochondrial chaperone TRAP1.* PLoS Biol, 2007. **5**(7): p. e172.
288. Chambon, P., J.D. Weill, and P. Mandel, *Nicotinamide mononucleotide activation of new DNA-dependent polyadenylic acid synthesizing nuclear enzyme.* Biochem Biophys Res Commun, 1963. **11**: p. 39-43.
289. Hottiger, M.O., et al., *Toward a unified nomenclature for mammalian ADP-ribosyltransferases.* Trends Biochem Sci, 2010. **35**(4): p. 208-19.
290. Kraus, W.L. and M.O. Hottiger, *PARP-1 and gene regulation: progress and puzzles.* Mol Aspects Med, 2013. **34**(6): p. 1109-23.
291. Woodhouse, B.C. and G.L. Dianov, *Poly ADP-ribose polymerase-1: an international molecule of mystery.* DNA Repair (Amst), 2008. **7**(7): p. 1077-86.
292. Krishnakumar, R. and W.L. Kraus, *The PARP side of the nucleus: molecular actions, physiological outcomes, and clinical targets.* Mol Cell, 2010. **39**(1): p. 8-24.
293. Poirier, G.G., et al., *Poly(ADP-ribosyl)ation of polynucleosomes causes relaxation of chromatin structure.* Proc Natl Acad Sci U S A, 1982. **79**(11): p. 3423-7.
294. Ahel, D., et al., *Poly(ADP-ribose)-dependent regulation of DNA repair by the chromatin remodeling enzyme ALC1.* Science, 2009. **325**(5945): p. 1240-3.
295. Timinszky, G., et al., *A macrodomain-containing histone rearranges chromatin upon sensing PARP1 activation.* Nat Struct Mol Biol, 2009. **16**(9): p. 923-9.
296. Reale, A., et al., *Modulation of DNMT1 activity by ADP-ribose polymers.* Oncogene, 2005. **24**(1): p. 13-9.
297. Schultz, N., et al., *Poly(ADP-ribose) polymerase (PARP-1) has a controlling role in homologous recombination.* Nucleic Acids Res, 2003. **31**(17): p. 4959-64.

298. Yang, Y.G., et al., *Ablation of PARP-1 does not interfere with the repair of DNA double-strand breaks, but compromises the reactivation of stalled replication forks.* Oncogene, 2004. **23**(21): p. 3872-82.
299. Meyer, R., et al., *Negative regulation of alkylation-induced sister-chromatid exchange by poly(ADP-ribose) polymerase-1 activity.* Int J Cancer, 2000. **88**(3): p. 351-5.
300. Bryant, H.E., et al., *PARP is activated at stalled forks to mediate Mre11-dependent replication restart and recombination.* EMBO J, 2009. **28**(17): p. 2601-15.
301. Gagne, J.P., et al., *Proteome-wide identification of poly(ADP-ribose) binding proteins and poly(ADP-ribose)-associated protein complexes.* Nucleic Acids Res, 2008. **36**(22): p. 6959-76.
302. Ruscetti, T., et al., *Stimulation of the DNA-dependent protein kinase by poly(ADP-ribose) polymerase.* J Biol Chem, 1998. **273**(23): p. 14461-7.
303. Spagnolo, L., et al., *Visualization of a DNA-PK/PARP1 complex.* Nucleic Acids Res, 2012. **40**(9): p. 4168-77.
304. Lieber, M.R., *The mechanism of double-strand DNA break repair by the nonhomologous DNA end-joining pathway.* Annu Rev Biochem, 2010. **79**: p. 181-211.
305. Audebert, M., B. Salles, and P. Calsou, *Involvement of poly(ADP-ribose) polymerase-1 and XRCC1/DNA ligase III in an alternative route for DNA double-strand breaks rejoining.* J Biol Chem, 2004. **279**(53): p. 55117-26.
306. Wang, M., et al., *PARP-1 and Ku compete for repair of DNA double strand breaks by distinct NHEJ pathways.* Nucleic Acids Res, 2006. **34**(21): p. 6170-82.
307. Tong, W.M., et al., *Synergistic role of Ku80 and poly(ADP-ribose) polymerase in suppressing chromosomal aberrations and liver cancer formation.* Cancer Res, 2002. **62**(23): p. 6990-6.
308. Liu, Y., F.A. Kadyrov, and P. Modrich, *PARP-1 enhances the mismatch-dependence of 5'-directed excision in human mismatch repair in vitro.* DNA Repair (Amst), 2011. **10**(11): p. 1145-53.
309. Wilson, S.H. and T.A. Kunkel, *Passing the baton in base excision repair.* Nat Struct Biol, 2000. **7**(3): p. 176-8.
310. de Murcia, J.M., et al., *Requirement of poly(ADP-ribose) polymerase in recovery from DNA damage in mice and in cells.* Proc Natl Acad Sci U S A, 1997. **94**(14): p. 7303-7.
311. Wang, Z.Q., et al., *Mice lacking ADPRT and poly(ADP-ribosyl)ation develop normally but are susceptible to skin disease.* Genes Dev, 1995. **9**(5): p. 509-20.
312. Luo, X. and W.L. Kraus, *On PAR with PARP: cellular stress signaling through poly(ADP-ribose) and PARP-1.* Genes Dev, 2012. **26**(5): p. 417-32.
313. Fisher, A.E., et al., *Poly(ADP-ribose) polymerase 1 accelerates single-strand break repair in concert with poly(ADP-ribose) glycohydrolase.* Mol Cell Biol, 2007. **27**(15): p. 5597-605.
314. Noren Hooten, N., et al., *Poly(ADP-ribose) polymerase 1 (PARP-1) binds to 8-oxoguanine-DNA glycosylase (OGG1).* J Biol Chem, 2011. **286**(52): p. 44679-90.

315. Masson, M., et al., *XRCC1 is specifically associated with poly(ADP-ribose) polymerase and negatively regulates its activity following DNA damage.* Mol Cell Biol, 1998. **18**(6): p. 3563-71.
316. Dantzer, F., et al., *Involvement of poly(ADP-ribose) polymerase in base excision repair.* Biochimie, 1999. **81**(1-2): p. 69-75.
317. Dantzer, F., et al., *Base excision repair is impaired in mammalian cells lacking Poly(ADP-ribose) polymerase-1.* Biochemistry, 2000. **39**(25): p. 7559-69.
318. Khodyreva, S.N., et al., *Apurinic/apyrimidinic (AP) site recognition by the 5'-dRP/AP lyase in poly(ADP-ribose) polymerase-1 (PARP-1).* Proc Natl Acad Sci U S A, 2010. **107**(51): p. 22090-5.
319. Helleday, T., *The underlying mechanism for the PARP and BRCA synthetic lethality: clearing up the misunderstandings.* Mol Oncol, 2011. **5**(4): p. 387-93.
320. Woodhouse, B.C., et al., *Poly(ADP-ribose) polymerase-1 modulates DNA repair capacity and prevents formation of DNA double strand breaks.* DNA Repair (Amst), 2008. **7**(6): p. 932-40.
321. Parsons, J.L., et al., *Poly(ADP-ribose) polymerase-1 protects excessive DNA strand breaks from deterioration during repair in human cell extracts.* FEBS J, 2005. **272**(8): p. 2012-21.
322. Xanthoudakis, S., et al., *The redox/DNA repair protein, Ref-1, is essential for early embryonic development in mice.* Proc Natl Acad Sci U S A, 1996. **93**(17): p. 8919-23.
323. Gu, H., et al., *Deletion of a DNA polymerase beta gene segment in T cells using cell type-specific gene targeting.* Science, 1994. **265**(5168): p. 103-6.
324. Tebbs, R.S., L.H. Thompson, and J.E. Cleaver, *Rescue of Xrcc1 knockout mouse embryo lethality by transgene-complementation.* DNA Repair (Amst), 2003. **2**(12): p. 1405-17.
325. Satoh, M.S. and T. Lindahl, *Role of poly(ADP-ribose) formation in DNA repair.* Nature, 1992. **356**(6367): p. 356-8.
326. Strom, C.E., et al., *Poly (ADP-ribose) polymerase (PARP) is not involved in base excision repair but PARP inhibition traps a single-strand intermediate.* Nucleic Acids Res, 2011. **39**(8): p. 3166-75.
327. Clark, J.B., G.M. Ferris, and S. Pinder, *Inhibition of nuclear NAD nucleosidase and poly ADP-ribose polymerase activity from rat liver by nicotinamide and 5'-methyl nicotinamide.* Biochim Biophys Acta, 1971. **238**(1): p. 82-5.
328. Bryant, H.E., et al., *Specific killing of BRCA2-deficient tumours with inhibitors of poly(ADP-ribose) polymerase.* Nature, 2005. **434**(7035): p. 913-7.
329. Farmer, H., et al., *Targeting the DNA repair defect in BRCA mutant cells as a therapeutic strategy.* Nature, 2005. **434**(7035): p. 917-21.
330. Papeo, G., et al., *PARP inhibitors in cancer therapy: an update.* Expert Opin Ther Pat, 2013. **23**(4): p. 503-14.
331. Patel, A.G., J.N. Sarkaria, and S.H. Kaufmann, *Nonhomologous end joining drives poly(ADP-ribose) polymerase (PARP) inhibitor lethality in homologous recombination-deficient cells.* Proc Natl Acad Sci U S A, 2011. **108**(8): p. 3406-11.

332. Peralta-Leal, A., et al., *PARP inhibitors: new partners in the therapy of cancer and inflammatory diseases.* Free Radic Biol Med, 2009. **47**(1): p. 13-26.
333. Plummer, R., et al., *Phase I study of the poly(ADP-ribose) polymerase inhibitor, AG014699, in combination with temozolomide in patients with advanced solid tumors.* Clin Cancer Res, 2008. **14**(23): p. 7917-23.
334. Fong, P.C., et al., *Poly(ADP)-ribose polymerase inhibition: frequent durable responses in BRCA carrier ovarian cancer correlating with platinum-free interval.* J Clin Oncol, 2010. **28**(15): p. 2512-9.
335. Mendes-Pereira, A.M., et al., *Synthetic lethal targeting of PTEN mutant cells with PARP inhibitors.* EMBO Mol Med, 2009. **1**(6-7): p. 315-22.
336. Giannini, G., et al., *Human MRE11 is inactivated in mismatch repair-deficient cancers.* EMBO Rep, 2002. **3**(3): p. 248-54.
337. Vilar, E., et al., *MRE11 deficiency increases sensitivity to poly(ADP-ribose) polymerase inhibition in microsatellite unstable colorectal cancers.* Cancer Res, 2011. **71**(7): p. 2632-42.
338. Williamson, C.T., et al., *ATM deficiency sensitizes mantle cell lymphoma cells to poly(ADP-ribose) polymerase-1 inhibitors.* Mol Cancer Ther, 2010. **9**(2): p. 347-57.
339. Horton, T.M., et al., *Poly(ADP-ribose) polymerase inhibitor ABT-888 potentiates the cytotoxic activity of temozolomide in leukemia cells: influence of mismatch repair status and O6-methylguanine-DNA methyltransferase activity.* Mol Cancer Ther, 2009. **8**(8): p. 2232-42.
340. Edwards, S.L., et al., *Resistance to therapy caused by intragenic deletion in BRCA2.* Nature, 2008. **451**(7182): p. 1111-5.
341. Rottenberg, S., et al., *High sensitivity of BRCA1-deficient mammary tumors to the PARP inhibitor AZD2281 alone and in combination with platinum drugs.* Proc Natl Acad Sci U S A, 2008. **105**(44): p. 17079-84.
342. Chiarugi, A., *A snapshot of chemoresistance to PARP inhibitors.* Trends Pharmacol Sci, 2012. **33**(1): p. 42-8.
343. Dumitriu, I.E., et al., *UV irradiation inhibits ABC transporters via generation of ADP-ribose by concerted action of poly(ADP-ribose) polymerase-1 and glycohydrolase.* Cell Death Differ, 2004. **11**(3): p. 314-20.
344. Imburgio, D., et al., *Studies of promoter recognition and start site selection by T7 RNA polymerase using a comprehensive collection of promoter variants.* Biochemistry, 2000. **39**(34): p. 10419-30.
345. Umar, A., et al., *Correction of hypermutability, N-methyl-N'-nitro-N-nitrosoguanidine resistance, and defective DNA mismatch repair by introducing chromosome 2 into human tumor cells with mutations in MSH2 and MSH6.* Cancer Res, 1997. **57**(18): p. 3949-55.
346. Williams, G.T., et al., *NAD metabolism and mitogen stimulation of human lymphocytes.* Exp Cell Res, 1985. **160**(2): p. 419-26.
347. Loetscher, P., R. Alvarez-Gonzalez, and F.R. Althaus, *Poly(ADP-ribose) may signal changing metabolic conditions to the chromatin of mammalian cells.* Proc Natl Acad Sci U S A, 1987. **84**(5): p. 1286-9.

348. Clark, A.B., et al., *Functional interaction of proliferating cell nuclear antigen with MSH2-MSH6 and MSH2-MSH3 complexes.* J Biol Chem, 2000. **275**(47): p. 36498-501.
349. Bai, H., et al., *Interaction between human mismatch repair recognition proteins and checkpoint sensor Rad9-Rad1-Hus1.* DNA Repair (Amst), 2010. **9**(5): p. 478-87.
350. Wang, Q., et al., *Adenosine nucleotide modulates the physical interaction between hMSH2 and BRCA1.* Oncogene, 2001. **20**(34): p. 4640-9.
351. Yang, Q., et al., *The mismatch DNA repair heterodimer, hMSH2/6, regulates BLM helicase.* Oncogene, 2004. **23**(21): p. 3749-56.
352. Wang, Y., et al., *BASC, a super complex of BRCA1-associated proteins involved in the recognition and repair of aberrant DNA structures.* Genes Dev, 2000. **14**(8): p. 927-39.
353. Liu, Y., et al., *Interactions of human mismatch repair proteins MutSalpha and MutLalpha with proteins of the ATR-Chk1 pathway.* J Biol Chem, 2010. **285**(8): p. 5974-82.
354. Wepf, A., et al., *Quantitative interaction proteomics using mass spectrometry.* Nat Methods, 2009. **6**(3): p. 203-5.
355. Poser, I., et al., *BAC TransgeneOmics: a high-throughput method for exploration of protein function in mammals.* Nat Methods, 2008. **5**(5): p. 409-15.
356. Elstrodt, F., et al., *BRCA1 mutation analysis of 41 human breast cancer cell lines reveals three new deleterious mutants.* Cancer Res, 2006. **66**(1): p. 41-5.
357. Dzantiev, L., et al., *A defined human system that supports bidirectional mismatch-provoked excision.* Mol Cell, 2004. **15**(1): p. 31-41.
358. Ogawa, T. and T. Okazaki, *Discontinuous DNA replication.* Annu Rev Biochem, 1980. **49**: p. 421-57.
359. Sahdev, S., S.K. Khattar, and K.S. Saini, *Production of active eukaryotic proteins through bacterial expression systems: a review of the existing biotechnology strategies.* Mol Cell Biochem, 2008. **307**(1-2): p. 249-64.
360. Marra, G., et al., *Mismatch repair deficiency associated with overexpression of the MSH3 gene.* Proc Natl Acad Sci U S A, 1998. **95**(15): p. 8568-73.
361. Roux, K.J., et al., *A promiscuous biotin ligase fusion protein identifies proximal and interacting proteins in mammalian cells.* J Cell Biol, 2012. **196**(6): p. 801-10.
362. Choi-Rhee, E., H. Schulman, and J.E. Cronan, *Promiscuous protein biotinylation by Escherichia coli biotin protein ligase.* Protein Sci, 2004. **13**(11): p. 3043-50.
363. Rhee, H.W., et al., *Proteomic mapping of mitochondria in living cells via spatially restricted enzymatic tagging.* Science, 2013. **339**(6125): p. 1328-31.
364. Oka, S., et al., *Two distinct pathways of cell death triggered by oxidative damage to nuclear and mitochondrial DNAs.* EMBO J, 2008. **27**(2): p. 421-32.
365. Oka, S. and Y. Nakabeppu, *DNA glycosylase encoded by MUTYH functions as a molecular switch for programmed cell death under oxidative stress to suppress tumorigenesis.* Cancer Sci, 2011. **102**(4): p. 677-82.

366. Hwang, B.J., G. Shi, and A.L. Lu, *Mammalian MutY homolog (MYH or MUTYH) protects cells from oxidative DNA damage.* DNA Repair (Amst), 2014. **13**: p. 10-21.
367. Turco, E., et al., *Understanding the role of the Q338H MUTYH variant in oxidative damage repair.* Nucleic Acids Res, 2013. **41**(7): p. 4093-103.
368. Casadaban, M.J. and S.N. Cohen, *Analysis of gene control signals by DNA fusion and cloning in Escherichia coli.* J Mol Biol, 1980. **138**(2): p. 179-207.
369. Grant, S.G., et al., *Differential plasmid rescue from transgenic mouse DNAs into Escherichia coli methylation-restriction mutants.* Proc Natl Acad Sci U S A, 1990. **87**(12): p. 4645-9.
370. Barbara Schöpf., *DNA mismatch repair and chromatin & Functional characterization of the zinc finger of KIAA1018*. Dissertation DISS. ETH NO. 18996. 2010

8 Appendices

Appendix 1: Vector map of pTO+AIO CSH GW FRT

(A) pTO+AIO CSH GW FRT

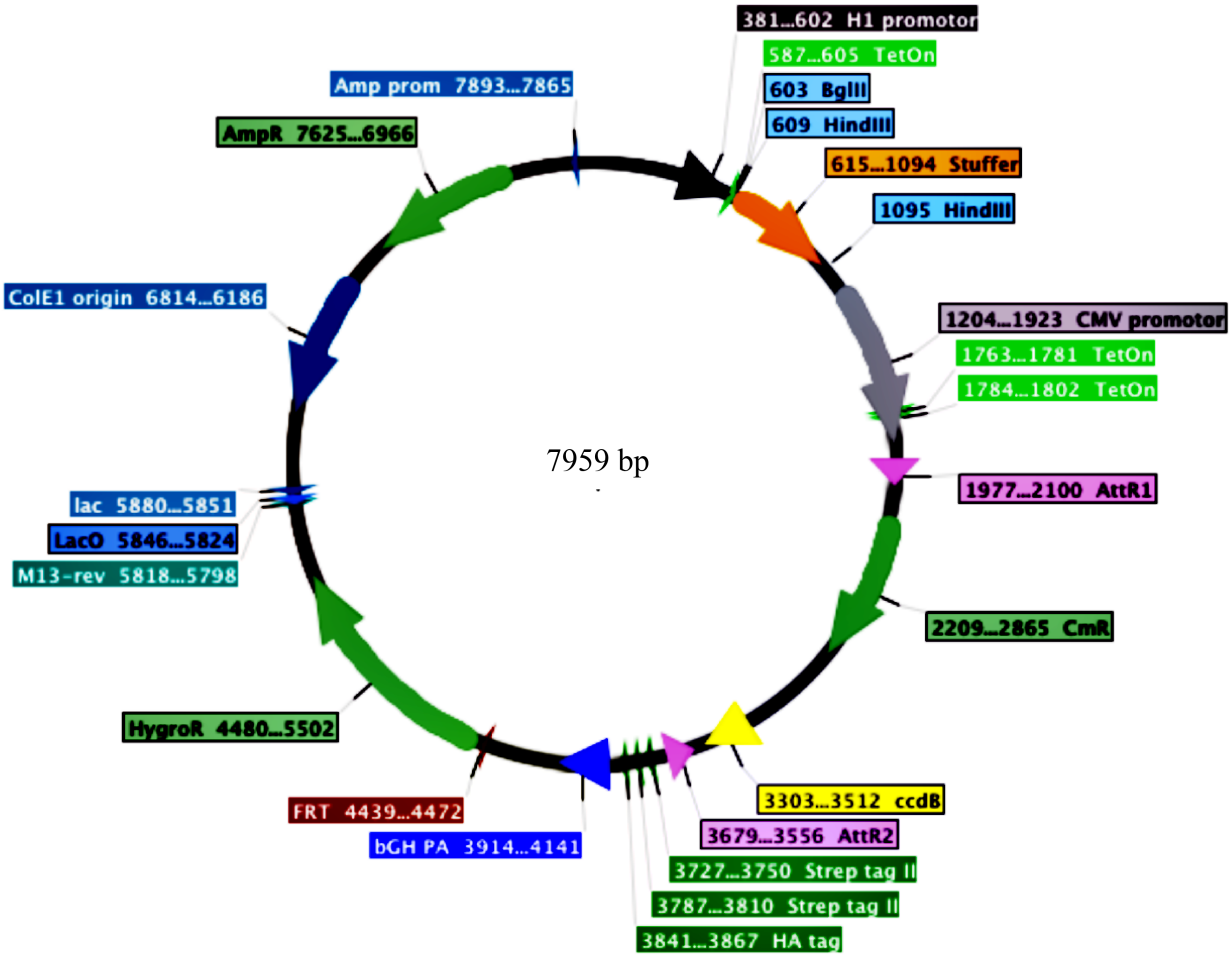

Appendix 2: Vector map of pTO+AIO CSH GW FRT + shMSH6

(B) pTO+AIO CSH GW FRT + shMSH6

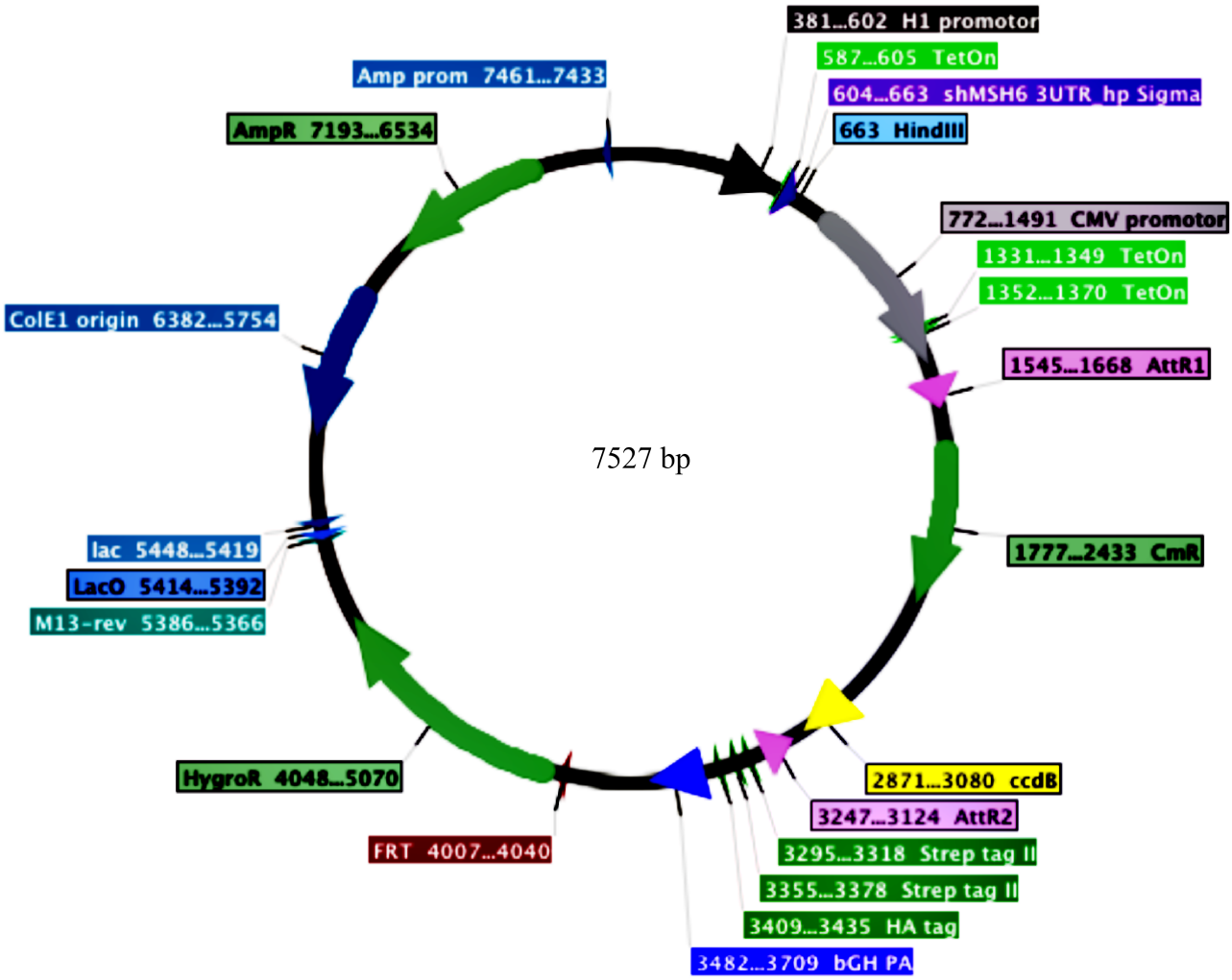

Appendix 3: Vector map of pENTR3C + hMSH6

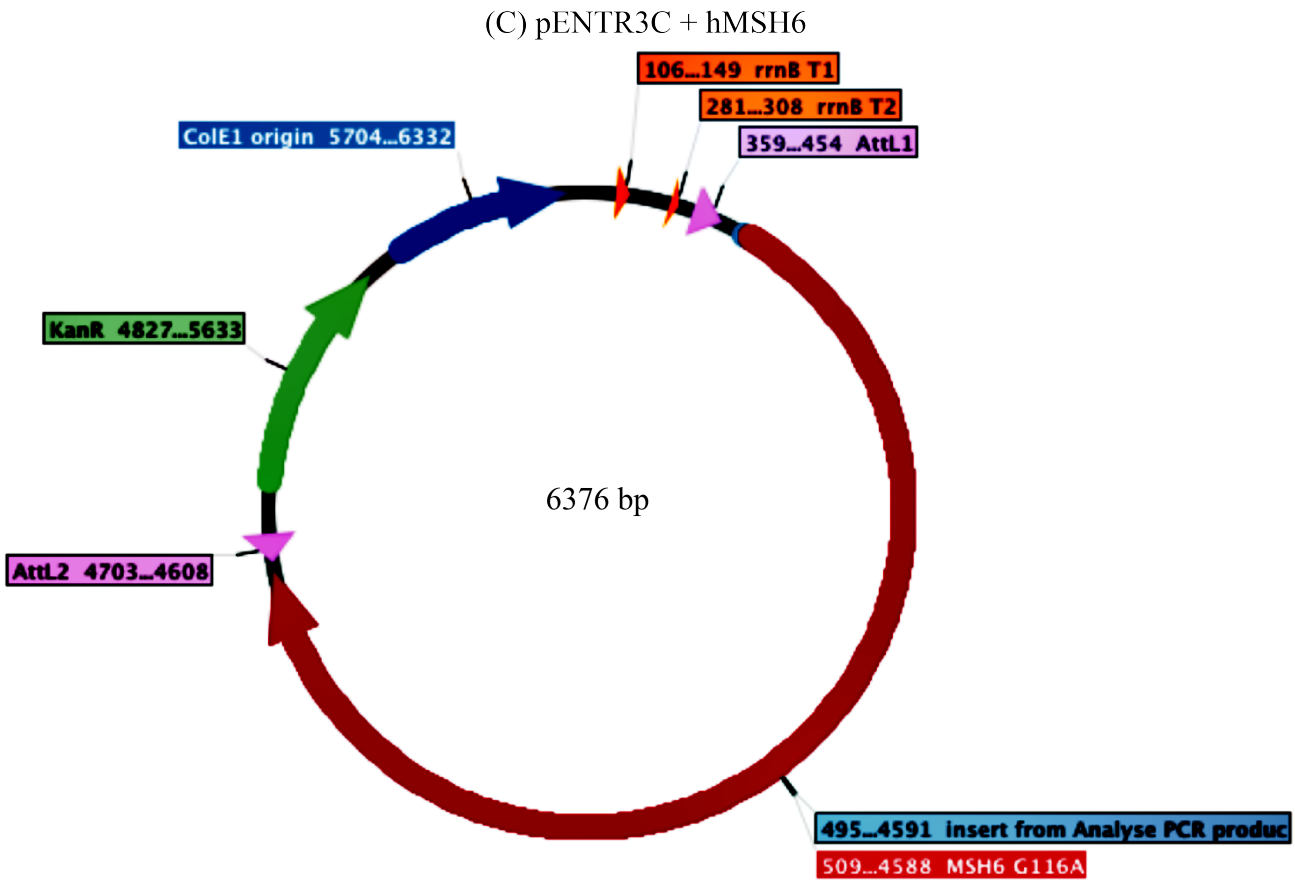

Appendix 4: Vector map of pTO+AIO hMSH6-SH GW FRT + shMSH6

(D) pTO+AIO hMSH6-SH GW FRT + shMSH6